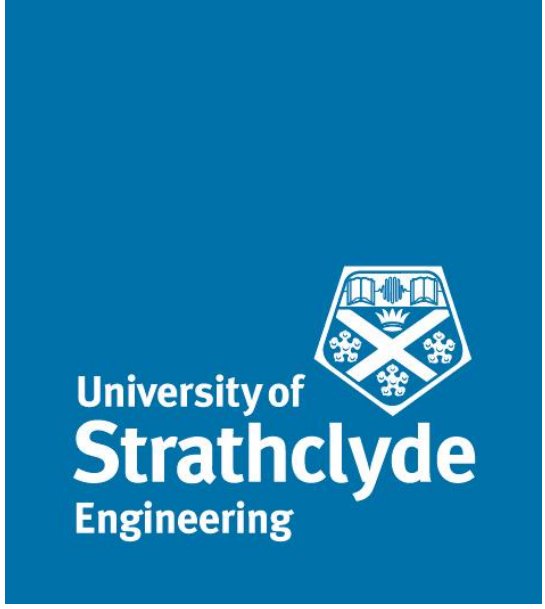

Wind farm control and modelling to provide grid primary response and meet O&M requirements

Velissarios Kourkoulis

A thesis submitted for the degree of Doctor of Philosophy

Wind Energy Systems Centre for Doctoral Training

Department of Electronic and Electrical Engineering

University of Strathclyde

2019

This thesis is the result of the author's original research. It has been composed by the author and has not been previously submitted for examination which has led to the award of a degree.

Velissarios Kourkoulis

January 2019

Dedicated to my Dora

"If we knew what it was we were doing, it would not be called research, would it?" – *Albert Einstein*

Acknowledgements

As with all acknowledgement lists there will be people not listed who should be, but there is definitely no one mentioned here who does not thoroughly deserve it.

First and foremost, I would like to express my sincere gratitude to my supervisor, professor William Leithead. His help and guidance kept me motivated and without him, this work would not have been possible.

I will also like to express my gratitude to my good friends and colleagues Alex Giles and Eddie Corr. They have been of great help to me.

Thank you to all my colleagues at the University of Strathclyde, particularly James Carroll, Adam Stock, Saman Poushpas, Hamish MacDonald, Pablo Jaen Sola, Shona Pennock, Kamyab Givaki, David Hamilton and Drew Smith. A lot of thanks to all my friends and colleagues, whose help was really important for completing this project.

I am truly grateful to my family; my parents and sister, who have supported me through my whole life. Finally, I owe a great debt of appreciation to my wife Dora. She is a real treasure for me. She is my success and inspiration. She has helped me become the man I am today, and I am really grateful for that.

Abstract

In the past years, investing in wind industry has been of a great interest. In all future energy scenarios regarding GB power generation, a substantial penetration of wind energy is envisaged. However, at present, except for occasional curtailment of generation, wind farms simply output all the power that can be extracted from the wind at any given time. By increasing the proportion of energy production from wind farms, and especially offshore wind farms, it is of great importance not to operate wind farms in such a simple manner. There is a need of allowing wind farms to operate in a far more flexible way. Regarding the viewpoint of the grid operators, wind farms will need to provide services such as frequency support to match supply and demand. From the viewpoint of the wind farm operators, wind farms will need to be operated in such a manner as to maximise the return of investment. To meet these grid and operator requirements a wind farm controller is developed.

The main goal of this thesis is to create a complete power system model to explore whether a wind farm level controller can be utilised to provide ancillary services to the transmission system operator, whilst safe-guarding the wind farm assets. Results from each chapter are novel and provide some new insight towards reducing O&M costs for wind farm operators, while providing advanced flexibility and frequency stability services to the transmission system operator. The thesis concludes that the wind farm controller would be essential for increasing controllability and flexibility of wind farms and improve power system frequency stability.

Contents

List of Figures

List of Tables

Abbreviations

AC	Alternating Current
AEP	Average Annual Energy Production
AGS	Accelerated Growth Scenario
ARPS	Advanced Regional Prediction System
BEM	Blade Element Momentum
CAPEX	Capital Expenditure
CFD	Computational Fluid Dynamics
CSC	Current Source Converter
CSP	Concentrated Solar Power
DAWM	Deep Array Wake Model
DC	Direct Current
DFIG	Doubly-Fed Induction Generator
DSOGI	Dual Second Order Generalized Integrator
ELV	Emission Limit Values
EU	European Union
EV	Eddy Viscosity
FCR	Fixed Charge Rate
FFT	Fast Fourier Transform
GB	Great Britain
GGS	Gone Green Scenario
GHG	Greenhouse Gases
GTO	Gate Turn-off Thyristor
HAWT	Horizontal Axis Wind Turbine
HVDC	High Voltage Direct Current
IBL	Internal Boundary Layer
IED	Industrial Emission Directive
IGBT	Insulated Gate Bipolar Transistor
LCoE	Levelized Cost of Energy
LCPD	Large Combustion Plant Directive
LES	Large Eddy Simulation
LWFM	Large Wind Farm Model
MFR	Mandatory Frequency Response

MIMO	Multiple Input-Multiple Output
MPC	Model Predictive Control
NGET	National Grid Electricity Transmission
NWP	Numerical Weather Prediction
O&M	Operation and Maintenance
OPEX	Operational Expenditure
PAC	Power Adjusting Controller
PBL	Planetary Boundary Layer
PCC	Point of Common Coupling
PI	Proportional – Integral
PLL	Phase-Locked Loop
PMU	Phasor Measurement Unit
PSC	Positive-Sequence Calculator
PSD	Power Spectral Density
PSS	Power System Stabilizer
PSS/E	Power Transmission System Planning Software
PWM	Pulse Width Modulation
RGBN	Reduced Great British Network
SPS	Slow Progression Scenario
SPWM	Sinusoidal Pulse Width Modulation
SRF	Synchronous Reference Frame
TKE	Turbulent Kinetic Energy
UK	United Kingdom
VAWT	Vertical Axis Wind Turbine
VSC	Voltage Source Converters

C_P	Coefficient of Power
C_T	Coefficient of Thrust
$\hat{C}_T$	Coefficient of Thrust local to the rotor
R	Rotor radius
V_∞	Wind speed far upstream from the rotor
V_A	Wind speed at the position of the rotor in its absence
V_R	Wind speed at the rotor
$\dot{V}_A$	Rate of change of the wind speed at the position of the rotor in its absence

$\dot{V}_R$	Rate of change of wind velocity at the rotor
α	Induction factor
$\dot{\alpha}$	Rate of change of the induction factor
α_s	Steady state induction factor
β	Blade pitch angle
ΔP	Increment in power
ΔT	Increment in torque
$\Delta \beta$	Increment in pitch angle
$\Delta \omega$	Increment in generator speed
λ_R	Tip speed ratio relative to the wind velocity at the rotor

Chapter 1 – Introduction

This thesis details the development of a wind farm controller that allows for flexible operation of wind farms by using the Power Adjusting Controller (PAC) [1]. The wind farm controller receives signals from the grid and wind farm operator and reacts in such way as to provide ancillary services to the grid and, at the same time, ensures that the turbines operate within pre-defined safety boundaries. The interaction of the effect of the altered power from the wind farm and the grid is assessed.

1.1 Thesis Objectives

Based on the need for more flexible operation of wind farms and improved power system stability, the objective of this thesis is to answer the following research question:

"Can we operate (offshore) wind farms flexibly under all operational conditions to provide ancillary services to the grid operator, thus improving power system stability whilst ensuring reduced Operation & Maintenance (O&M) costs?"

The development of a wind farm controller to be used to trade-off the grid requirements against the operators need for optimal utilisation of their assets is key to answer the aforementioned research question. To achieve this, a wind farm model able to provide a good approximation of the wind field and wake interactions between the turbines has been developed. The model is capable of simulating wind farms consisting of 100 wind turbines in reasonable time periods, allowing for an investigation of the dynamics of a wind farm across an extensive set of operating points as would be required for the evaluation of a control system.

The wind farm controller is able to alter the power output of the wind farm by the use of the PAC. Each wind turbine has a PAC which augments the full-envelope controller, in so doing providing increased flexibility of operation. It enables the generated power to be modified, by regulating the difference between the generated power and the power available from the wind to track an externally provided set point (ΔP). By adjusting this set point ($\pm\Delta P$), the wind

turbine can be operated in the required manner. The PAC is generic and can be applied to a large range of turbines.

The wind farm controller allows for flexible operation of the wind farm. It allows the wind farm operator to decrease the power output if needed, and ensures that the wind turbines are used in such way as to avoid failures. In order to achieve this, an O&M analysis of real offshore wind farm data has been carried out. This analysis has provided a strategy for turbine prioritization for the controller, as it includes the consideration of site conditions in the choice of the wind turbines to be utilized by the wind farm controller.

The development of a network wind farm controller which evaluates the grid frequency and reacts to grid events by generating signals for the wind farm controller to improve grid stability is also presented. This controller makes sure that the wind farm responds to grid events, such as loss of load or generation, and requests changes in the wind farm power output to improve grid stability. In order to demonstrate this, network models with increased complexity have been developed. For any type of grid event, i.e. loss of generation/load or a fault, the network wind farm controller evaluates the system conditions at the point of connection of the wind farm and sends signals to the wind farm controller to request grid support. The wind farm model is connected to the grid model via a VSC-HVDC link. This is because VSC-HVDC systems are expected to be the default means of connection for large offshore wind farms to the network.

1.2 Thesis Overview

In chapter 1, a brief introduction to the thesis is provided.

In chapter 2, an overview of the wind industry and the power system is provided. This chapter includes the synopsis of the difference between conventional power generators and wind energy sources, and an examination of the effect of the introduction of wind farms on the existing power system. An overview of the evolution of wind turbines and wind farms is also included in this chapter. This chapter concludes by introducing the limitations of the power system, and how wind farm level controllers can ensure power system stability.

Chapter 3 details the analysis of O&M data from large offshore wind farms. This analysis is used to ensure that the wind turbines are safely utilised; this is done according to probability of failure for the wind turbines for given operating conditions. The offshore wind farm data is used to investigate the effect of the following environmental conditions on wind turbine reliability: wind speed, turbulence intensity and wind direction. The wind farm controller will use the outcome of this analysis to increase turbine reliability.

In chapter 4, the development of a small wind farm model comprising 10 wind turbines is presented. The wind turbine model and wind and wake model used to represent the wind field and the wake interactions between the turbines are discussed. The approach taken for the design of the wind farm controller is provided.

Chapter 5 provides the evaluation of a large wind farm model consisting of 100 wind turbines. The analysis includes the assessment of the capabilities of the wind farm controller to respond to signals from the operator and the grid and provide the requested power output. The simulation results are used to evaluate the effect of the wind farm controller prioritisation on the individual turbine loads.

Chapter 6 describes the power system model, the VSC-HVDC link between the wind farm and the grid and the development of the network wind farm controller. An overview of the synchronous machine model and grid frequency measurement strategies is provided. The development of the VSC-HVDC model is presented. This model is used to connect the wind farm with the grid. A literature review of the different HVDC strategies is provided and the basic operational principles and control of the VSC-HVDC systems is discussed. Finally, the concept of the network wind farm controller, which is used to provide grid information to the wind farm controller, is introduced.

Chapter 7 evaluates the dynamic interaction between the wind farm, the VSC-HVDC link and the power system. The complete integrated model of the wind farm, HVDC link and power network is presented. The effect of the wind farm controller capabilities to provide ancillary services to the grid is assessed through simulations of the integrated model.

Chapter 8 summarises the results of the work presented in this thesis, draws conclusions and discusses the future work that may be undertaken in this area of research.

Chapter 9 contains a list of references and is followed by the appendices.

1.3 Contribution to Knowledge

The contributions of this work are listed below:

- The development of a dynamic wind farm model capable of representing large offshore wind farms, included in which is a wind farm controller. Operating in conjunction with the PAC, the wind farm controller permits flexible operation of the wind farm, in doing so potentially becoming similar to a conventional power plant.
- O&M analysis of offshore wind farm data which allows for the investigation of the effect of site conditions on offshore wind turbine failures. The novelty of this analysis is in the offshore population of modern multi-megawatt turbines. Furthermore, failure rates of this type of population have been investigated in the past, but never in terms of how failure rates are affected by site conditions.
- The development of a network wind farm controller which assesses the grid status and provides signals to the wind farm controller to improve grid stability. The combination of the network wind farm controller and the PAC makes it possible for the wind farm to mimic the response of a synchronous machine in order to ameliorate grid stability.
- The development of an integrated power system model which comprises the following elements: the wind farm model, the grid system model and the VSC-HVDC link between the wind farm and the grid. This model is used to investigate the effect of the wind farm controller on the power system stability.

1.4 Publications

- V. Kourkoulis and W. Leithead, *Applying a power adjusting controller for a 2MW wind turbine,* in 9th EAWE PhD Seminar on Wind Energy in Europe, Visby, 2013.
- V. Kourkoulis and W. Leithead, *Wind farm control to meet grid and O&M requirements,* in International Conference on Offshore Renewable Energy, Glasgow, 2014.
- V. Kourkoulis and W. Leithead, *Wind farm control to meet grid requirements,* in EWEA Offshore, Copenhagen, 2015.

- V. Kourkoulis, J. Carroll and W. Leithead, *Effect of site conditions on offshore wind turbine failures,* in IET International Conference on Renewable Power Generation, Beijing, 2015.
- V. Kourkoulis and W. Leithead, *Wind farm modelling and control to meet grid and O&M requirements,* in 12th EAWE PhD Seminar on Wind Energy in Europe, Copenhagen, 2016.

Chapter 2 – Wind Energy Technology Overview

The wind industry has seen rapid growth in recent decades, in so doing becoming a mature and competitive industry. This chapter provides an overview of the power system and the development of wind energy technology over the years, along with the challenges of integrating high volumes of wind energy into the power system.

2.1 Conventional Power System

The conventional power system comprised large synchronous generators, potentially in remote areas, which supplied power to consumers all over the power system through transmission and distribution systems. A simplified overview of a conventional power system is illustrated in Figure 2-1 [2].

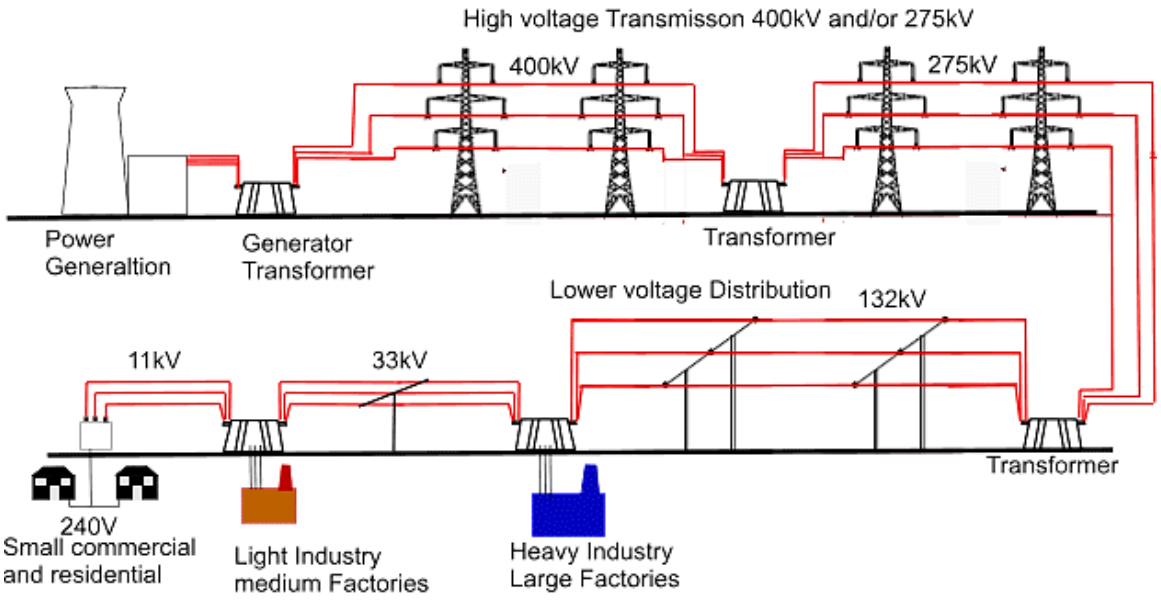

Figure 2-1: Conventional electricity system [2]

As can be seen in Figure 2-1, a transformer is used to step up the voltage to transfer the power via the high voltage transmission system. The voltage increase allows for decreased resistive losses in the transmission lines. The Great British (GB) transmission lines operate at 400kV and 275kV.

The role of the transmission system is to interconnect many generator units and loads across different parts of a country, or even between countries. Due to its ability to transfer electricity over long distances, the transmission system allows integration of remote generation. It allows loads to be supplied by the most economical power plants and, additionally, provides flexible operation for all generating units, allowing for optimised maintenance schedules and increased system stability [3].

As the power is transferred closer to the demand centres, the electricity voltage is stepped down at a distribution substation to transfer the power to the loads. The UK distribution lines are operating at 132kV, 33kV and 11kV. The distribution system includes all the infrastructure that is needed to bring the electricity to the end user and is generally unidirectional [3].

In a conventional power system, most generating units are large synchronous machines, directly connected to the grid. Each unit converts energy from a source to produce electricity. The generation units may be categorised according to their fuel source: coal, gas, nuclear, oil, hydro and others. There are also some asynchronous generators connected to the grid such as wind, PV, marine and others.

2.2 Wind Energy

This section focuses on the presentation of the development of the wind industry. An overview of how the wind industry started, progressed and has grown through time, and the challenges of wind integration into the power system is provided.

Climate change has significantly affected the future of the energy industry. As can be seen in Figure 2-2 [4], the energy sector contributes 25% of the global greenhouse gas emissions,

which makes the decarbonization of the sector a key requirement to achieve of a low carbon future.

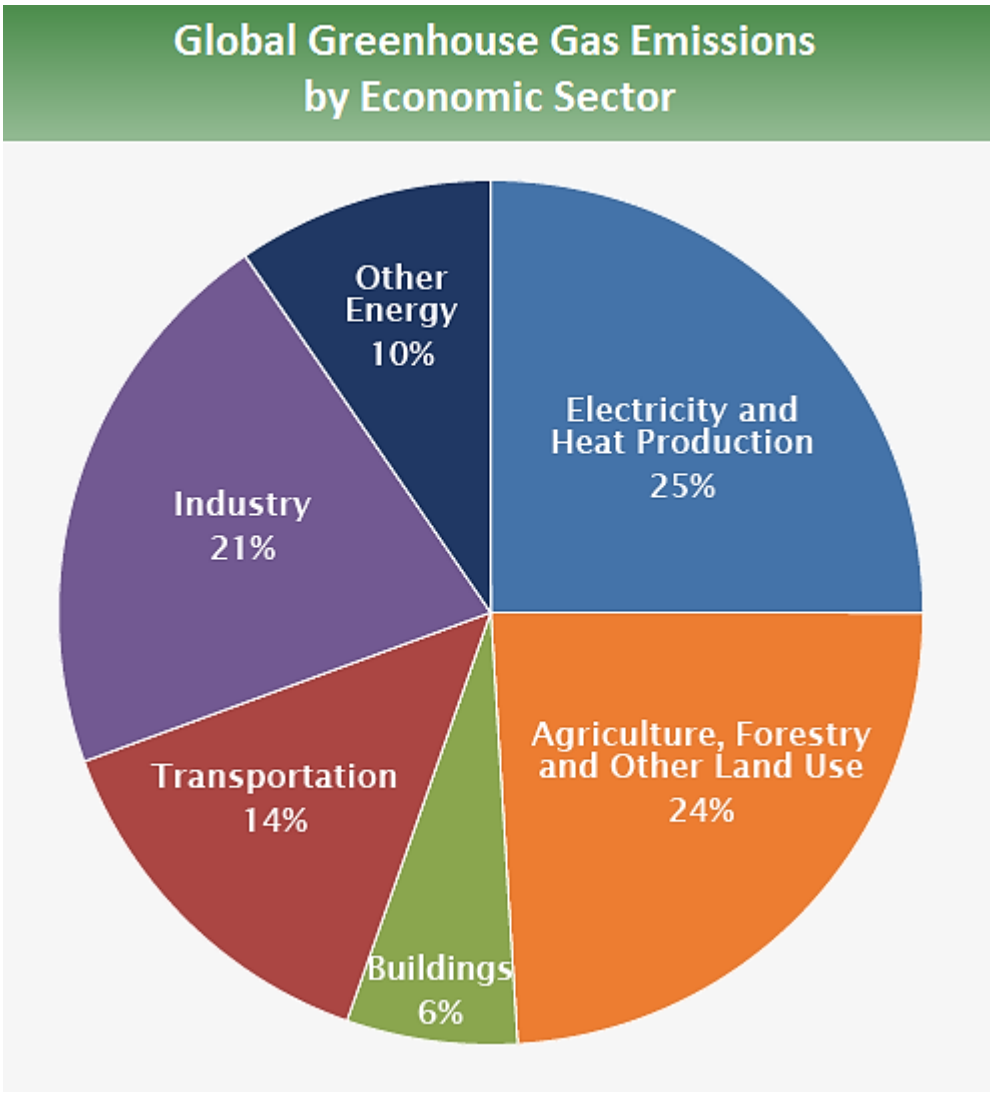

Figure 2-2: Global greenhouse gas emissions by economic sector (based on global emissions from 2010) [4]

The reduction regarding the carbon footprint of all the EU nations, has driven the countries to set targets for the decrease of CO_2 emissions. The UK has committed to the reduction of its carbon footprint by setting a target that 15% of its energy will be produced by renewable sources, while the Scottish government have chosen to implement a target of 20% of energy to be produced using renewable sources by 2020 [5].

2.2.1 Early Challenges of Wind Industry

Wind energy has been harnessed for over four thousand years. It was one of the first non-animal sources of energy to be used by humans. It was initially used for sailing boats, but it was also used by wind mills mainly in China, Persia and the Middle East. Wind mills were later introduced in Europe and were improved initially by the Dutch and later by the English. Eventually, wind mills were unable to compete with the low cost and reliable fossil fuel energy production machines.

Since the late 19th century, there have been several attempts to produce electricity using the wind. These types of machines are known as wind generators, aero-generators, or nowadays commonly wind turbines. The first wind turbines were simple power production units which used small DC machines. Larger wind turbines, able to provide large scale power production were first introduced in the USA, with the installation of the 1.25 MW two bladed Smith-Putnam wind turbine in the late 1930's.

In Europe, research continued after World War II in Denmark, France, the UK and Germany. Since the late 1980's, the technology became sufficiently mature to enable the Wind Industry to continue growing and evolving. An extensive range of commercial wind turbines is currently available from various manufacturers around the world. The cost of power production from wind turbines has decreased significantly with the maturation of the industry, allowing wind to be a competitive power production source.

Today, wind energy has been established as the most important renewable energy source which is economically stable when compared to conventional power production methods [6].

2.2.2 Evolution of Wind Turbines

Wind energy is the most widely used renewable energy source in the world. It can now economically compete with conventional power production methods, such as coal, natural gas, oil and nuclear. The available energy in the wind is harnessed using wind turbines. There are two main types of wind turbines, HAWTs and VAWTs.

The main difference between these two types of wind turbines is the axis of rotation of the rotor. For HAWTs, the axis of rotation is horizontal with respect to the ground; conversely, for VAWTs, the axis of rotation of the rotor is perpendicular to the ground. The clear majority of wind turbines are HAWTs. The basic components of a wind turbine are listed below:

- Rotor blades
- Hub
- Nacelle
- Gearbox (if applicable)
- Generator
- Power converter.

Wind turbines have been increasing in size and capacity, as illustrated in Figure 2-3 [7]. The largest commercial HAWT to date is the Vestas V164 which has a rated capacity of 8 MW; however, the industry is now moving towards the development of larger machines, mainly for the offshore wind industry.

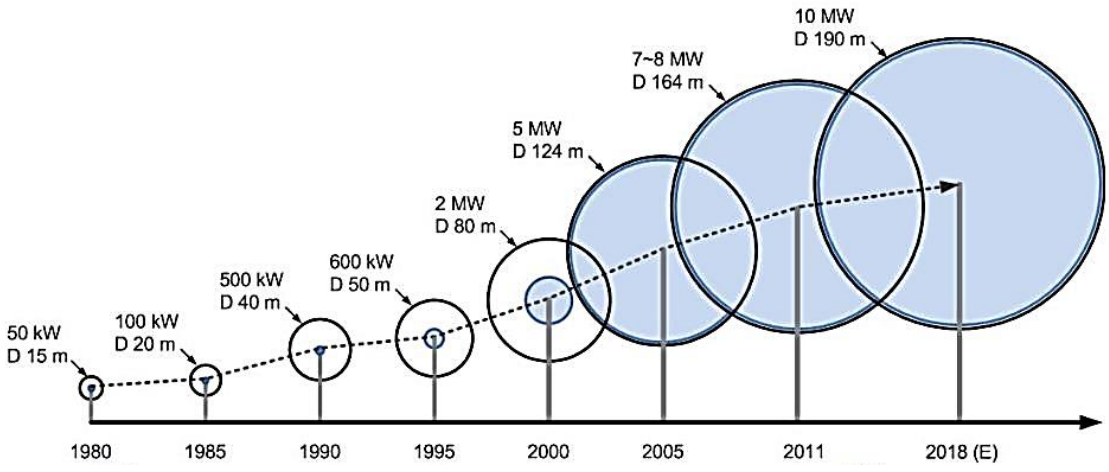

Figure 2-3: Commercial HAWT size development [7]

To date, there have been other types of wind turbines under development. These turbines have not matured enough to be used for mass production, but some types show promise. The most important wind turbine trends are listed below [8]:

- Ducted turbines,
- Airborne turbines and
- Multi-rotor turbines.

2.2.3 Evolution of Wind Farms

Wind farms have developed along with the wind turbines over the years. We can divide wind farms into two major categories:

- Onshore wind farms and
- Offshore wind farms.

Onshore wind energy is one of the most mature and cost-competitive type of renewable technologies. The first commercial wind farm which was developed in southern New Hampshire in 1980 and had a total rated capacity of 0.6MW, comprising 20 wind turbines rated at 30kW each [9]. The largest onshore wind farm to date is the Gansu wind farm project, which is a group of large wind farms and currently has total rated capacity of 6800MW [10].

The lack of available space and the desire for increased power production has pushed wind industry towards offshore wind. Offshore wind farms have increased infrastructure and maintenance costs due to the need for turbine foundations, offshore substations, subsea cabling and transporting vessels, all of which increases the cost of energy. There are also advantages of offshore wind farms: the potential for increased turbine size; higher wind speeds due to reduced surface roughness; and higher capacity factors. The largest offshore wind farm to date is the London Array, comprising 175 3.6 MW wind turbines, with a total rated capacity of 630MW [11].

2.3 Wind Integration in Power Systems

As explained in section 2.1, the concept of a unified power system was developed at a time when the clear majority of generation were directly-coupled synchronous generators. The fact that these machines were, and still are, directly-coupled to the power network meant that they provided the system with inertia, which provides a temporary short-term power balancing mechanism when the demand and generation are unequal. In addition to that, the power production of synchronous generators can be controlled directly from the fuel consumption (i.e. gas, coal, nuclear, oil).

Most modern turbines tend to be decoupled from the grid and use power converters to supply energy to the grid. As wind turbines displace conventional, directly-coupled generators, the grid inertia is decreased, leading to reduced system stability. Moreover, due to wind intermittency, wind farms cannot regulate their power production in the same manner as conventional generation, and they simply output power according to a predefined operating strategy which does not take the dynamics of the power system into account. Studies have predicted that approximately 20% of wind energy can be accommodated on power grids, if power systems remain unchanged [12].

However, future scenarios for UK power generation envisage a substantial penetration of wind energy. It will then no longer be appropriate to operate wind farms in this simple manner. From the viewpoint of the grid operators, these wind farms will need to provide services such as voltage and frequency support (i.e. synthetic inertia and droop control), spinning reserve and support to matching of supply to demand. From the viewpoint of the operators, the wind farms will need to be operated in such a manner as to maximise the return on investment. To meet these requirements will require the wind farms to be operated more flexibly. This allows the development of a wind farm level controller which will exploit all the available information from the turbines and will allow for improved wind farm utilization and will ultimately allow wind farms to be operated as conventional power plants.

Chapter 3 - O&M Data Analysis

Wind turbine availability and Operation & Maintenance (O&M) costs are two of the largest contributors to the cost of energy for wind farms. For offshore wind projects in particular, increased wind turbine availability is a key factor for cost reduction due to the cost of service vessels along with the uncertain and harsh weather conditions increased. Consequently, it is believed that a wind farm controller should consider O&M data to prevent or postpone future expected wind turbine failures.

3.1 Introduction

In the past few years there has been an increased interest in offshore wind. As more offshore wind farms are developed, improved turbine reliability is necessary. Wind turbine or wind farm availability is defined as the ratio of the time that the wind turbine/farm is available and ready to operate, over the total time in the period, as can be seen in Equation 3-1 [13].

$$Availability = \frac{Time\ that\ the\ turbine/farm\ is\ available\ and\ ready\ to\ operate}{Total\ time\ in\ the\ period} \quad [3\text{-}1]$$

It is clear that the reliability of a wind turbine influences its availability; that is, reducing a wind turbine's downtime increases its availability. Increased availability is key to reduce operational costs, and consequently the cost of energy. For the wind industry, the levelized cost of energy can be calculated by using Equation 3-2 [14].

$$LCoE = \frac{(CAPEX \times FCR) + OPEX}{(AEP/1000)} \quad [3\text{-}2]$$

where LCoE is the levelized cost of energy, CAPEX is the capital expenditure, FCR is the fixed charge rate, OPEX is the operational expenditure and AEP is the net average annual energy

production. The OPEX includes all expenditure occurring after the point of issue of a takeover certificate. Such expenditures are the wind farm operation, maintenance, the port activities (i.e. cost of service vessel), licence fees and other costs [15]. For offshore wind, the OPEX accounts for approximately 33% of the total cost of energy [16]. Furthermore, for offshore wind farms the O&M costs account for approximately 53% of the total OPEX, and this is without considering vessel costs [15].

The maintenance costs can be divided into scheduled maintenance and unscheduled maintenance. Scheduled maintenance includes all the periodic checks and preventive maintenance actions of all the aspects of the wind turbine. Unscheduled maintenance includes the corrective maintenance actions taken due to an unforeseen failure of a wind turbine component. Many published papers suggest that unscheduled maintenance accounts for a greater proportion of the overall maintenance costs than does scheduled maintenance [16] [17]. The need for the reduction of unscheduled maintenance is obvious and the analysis of offshore wind farm SCADA data performed in this chapter aims to the prevention of future wind turbine corrective maintenance actions.

3.2 Literature Review

In the past, there has been an increased interest in offshore wind. However, even though there are studies of the effect of weather conditions on turbine availability for onshore wind farms, there is little-to-no published research investigating how weather conditions affect offshore wind turbines.

A study by Faulstich *et al.* examined the effect of wind speed dependent failure rates on energy production [18]. The analysis was based on data from modern onshore wind turbines. Because of the wind speed characteristics, this research was based on onshore turbine failures; in any case, the effects of other site conditions, such as turbulence intensity and/or yaw error, were not considered. However, Faulstich does not investigate the correlation of wind speed to the wind turbine failures but is mainly focused on the correlation between the wind speeds prior to the turbine failure and the follow-up wind speeds. This study compares time-based availability and energy-based availability models to check the differences between these two models, based on the definition of minor failures (i.e. up to 4 hours downtime) and major

failures (i.e. over 4 hours downtime). The results have shown that for minor failures there is a strong correlation between pre and post failure wind speeds, while for major failures the correlation between pre and post failure wind speeds reduces with increasing interval.

A study by Tavner *et al.* investigated the effects of weather conditions and location on onshore wind turbine failure rate and downtime [19]. Data comprising the failures and weather conditions from 3 different sites based in Germany (i.e. Ormont, Fehmarn and Krummhörn) were used. This research did not consider the effects of site conditions other than wind speed. The analysis was based on small onshore turbines; this can be deduced by noting that the rated power of the wind turbines considered ranged from 300kW to 330kW. Given that modern offshore wind turbines have rated powers of several megawatts, these machines cannot be considered a representative sample for investigating offshore wind farms. This study investigated daily and monthly correlation periods, to investigate the fact that wind turbine failures sometimes might take place after the event that causes them has occurred. The results show strong correlation between wind speed and turbine failures for monthly periods (i.e. 55% - 75%) and weak correlation for daily periods (i.e. 10% -23%).

Another study by Tavner *et al.* investigated the influence of the weather on the reliability of wind turbines [20]. The study mainly focused on the effect of wind speed on reliability; a clear relationship between the failure rate of onshore wind turbines and the averaged wind energy index was demonstrated. The data, covering a period of 10 years (1994-2004), used for this study was collected from Windstats, including historic, maintained, Danish wind turbines and online data collected for the Danish weather. The size of the population of turbines reporting to Windstats varied from 2086 machines in 1994, to 904 machines in 2004. The data set covered a large variety of wind turbines, but the vast majority were 3-bladed HAWTs. Within the population analysed, the following variations were present:

- Variations in size (from 100kW to 2.5MW),
- Variations in blade aerodynamics and structural designs,
- Variations in mechanical architecture (i.e. direct drive, indirect drive) and
- Variations in controls (i.e. stall regulated, pitch regulated).

Research carried out by the EU FP7 Reliawind project was mainly interested in identifying and understanding the critical failures and their mechanisms for onshore wind turbines; this was achieved through quantitative studies of detailed wind farm data [21]. Initially, the reliability of operational turbines at different sites was measured. This analysis was used to calculate the time to failure and downtime for the different components of the turbines. All wind turbines used in this analysis had a rated power above 850kW; in addition, this analysis was based on 10-minute SCADA data, fault/alarm logs, service reports and O&M contractor reports.

An analysis by Wilson *et al.* involved the modelling of the effects of the environment on offshore wind turbine failures [22]. Environmental conditions included maximum daily gust speed, average daily wind speed and ambient temperature. The weather data used in this analysis originated from the UK Met Office. The turbine data used in this analysis came from a set of maintenance records used as part of an onshore wind turbine management system. The results indicate that high gusts (i.e. maximum daily gusts) have been identified as a key parameter for wind turbine failures.

There have also been various publications which have investigated offshore wind turbine availability [23] [24] [25] [26]; however, these studies did not consider the correlation between the turbine failures and the effect of weather conditions.

3.3 Research Opportunities

Most papers encountered in literature that investigated the effect of weather conditions on wind turbine failures used data from onshore wind turbines. Most of these onshore machines are significantly smaller than the modern multi-megawatt offshore machines. Some researchers focused mainly on wind speed, while others, even though their analysis included more environmental conditions, used weather data taken from UK Met offices, corresponding to sites which are far from the locations of both existing and proposed offshore wind farms. The studies which have investigated offshore wind turbine failure data did not consider the correlation between the turbine failures and the effect of weather conditions, and mainly focused on how condition monitoring could improve wind turbine availability.

It was decided that this is an area for further research. The novelty of this work is in the data set, which comprises a wealth of data for modern multi-megawatt offshore wind turbines. The failure data and weather data were directly provided by the wind turbine manufacturer. Failure rates of this type of population have been investigated in the past [27], but never in terms of how they are affected by site conditions. This analysis will be used directly by the wind farm controller, described in Chapter 4, to prevent wind turbine failures and protect the machines which are more likely to fail.

3.4 Offshore Wind Turbine Reliability

Unscheduled offshore wind turbine failures, as explained in Section 3.1, collectively represent one of the main contributors to the increased O&M cost. Increasing wind turbine availability will contribute to lowering the cost of energy. To achieve that, a clear understanding of what drives these failures must be obtained. This is particularly true for offshore wind farms, where transfer vessels and harsh weather conditions can directly influence turbine availability.

3.4.1 Population Analysis

The population analysed in this research consists of between 40-100 wind turbines from 2 different offshore wind farms, which have been operational for more than 5 years. The turbines analysed are all identical, indirect drive, modern multi-megawatt offshore turbines with rated powers of between 2 - 5MW and rotor diameter between 80m and 120m. In total, this population has provided data covering approximately 270 turbine years or approximately 2.4 million hours of turbine operation. Exact turbine model, number of failures, wind farm locations, rated power and blade size cannot be provided for confidentiality reasons.

3.4.2 Cost Categorization of Failures

The analysis of failures can be categorized into three groups, as shown in Table 3-1. The categorization is based on the cost of the repair:

Category	Cost
Minor Repair	Below €1000
Major Repair	Between €1000 and €10000
Major Replacement	Above €10000

Table 3-1: Failure Categorization

As can be seen in Table 3-1, the unscheduled failures can be divided in three categories: the first category is the “minor repairs” category, where the cost of the repair is less than €1000; the second category is the “major repairs”, where the cost of the repair is between €1000 and €10000; finally, the third category is the “major replacements” category, where the cost of the repair exceeds €10000.

It should be noted that this cost categorization description only reflects the cost of the repair (i.e. workhours and spare part costs) and does not account for any other additional costs (e.g. the cost of a crane vessel, loss due to downtime of turbine, etc.).

3.4.3 Reliability Analysis Methodology

The wind turbine manufacturer provided access to their database. The data analysed included the following detailed information: turbine locations (i.e. longitude, latitude), important dates (e.g. start-up dates, failure dates), costs (i.e. component costs), type of maintenance (i.e. scheduled, non-scheduled), component failed (e.g. gearbox, generator), turbine downtimes due to failure, average wind speed, wind speed standard deviation, absolute wind direction and complete alarm logs. Turbulence intensity was calculated from the database using Equation 3-3 [28].

$$I = \frac{\sigma}{\bar{u}} \qquad [3\text{-}3]$$

where I is the turbulence intensity, σ is the standard deviation of wind speed variations and $\bar{u}$ is the mean wind speed.

The in-depth analysis of the data was initiated once the database was filtered. Filtering included the identification of operational wind turbines, excluding from the analysis the turbines that experienced failures within the time period under consideration. The filtering was based on the analysis of the wind farm alarm logs, which were available for all the wind turbines over the total operational period. In this research, the analysis focused on the "major replacements" cost category failure type. This choice is related to the significance of the "major replacements" cost category compared to the total cost of all unscheduled maintenance, as will be later explained thoroughly in Section 3.5.2. The analysis includes the categorization of failure rates, the categorization of failure rate costs, the effect of wind speed on unscheduled wind turbine failures, the effect of turbulence intensity on unscheduled wind turbine failures and the effect of wind direction on unscheduled wind turbine failures.

It should be noted that for all the environmental effects that were considered in this research, each wind turbine that experienced a "major replacement" category unscheduled failure was not only compared against the mean environmental conditions of the wind farm, but it was also compared against the mean weather conditions of the neighbouring wind turbines, which have been located within 12 rotor diameters from the turbine that experienced the failure. The same analysis procedure was carried out for both wind farms.

All the analysis results have been normalised to allow the investigation of potential relationships between the weather conditions and the wind turbine failures for both sites. Since the number of failures experienced by the two wind farms and the number of turbines per wind farm are not identical (i.e. different populations with different sizes), the normalisation allows the comparison and assessment of the influence of the inputs (i.e. weather conditions) to the outputs (i.e. "major replacement" failures). The normalisation process can be described as follows [29]: the turbine that experienced the failure is used as the control unit and its variables (i.e. weather data) are used as the control variables, while the other turbines in the farm, or the vicinity, are normalised based on the mean of the control variable values for all available turbines in the wind farm.

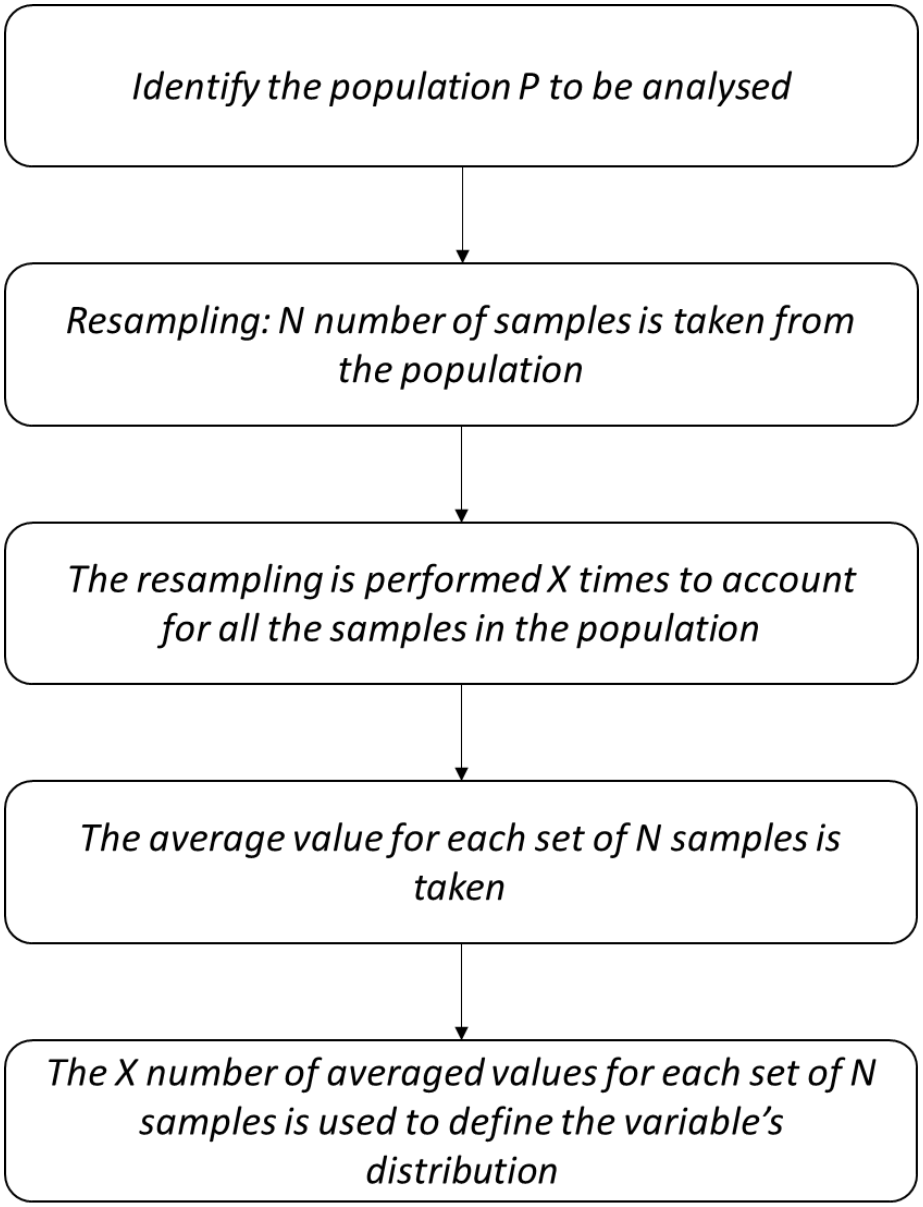

Figure 3-1: Bootstrapping process overview

To statistically estimate the confidence of our analysis, the bootstrapping technique is used [30]. In bootstrapping, the basic principle is that inference about a population from sample data can be modelled by resampling the sample data and performing inference about a sample from resampled data [30]. Initially, the population (P) is defined. The population consists of the weather data under consideration (i.e. wind speed, turbulence intensity or wind direction) for

a monthly period prior to the “major replacement” failure occurring. It also includes all the identified “major replacement” failures experienced by the turbines in the specific wind farm over the total operational period. A resampling is then performed, with N number of samples taken from the population P, where N is the total number of “major replacement” failures. This resampling is performed X times, where X corresponds to the total number of samples in the population P. The mean of each set of N samples is calculated. The total number X of the mean calculated samples of each dataset is then used for the distribution of the analysed variable (i.e. wind speed, turbulence intensity or wind direction). Because of the resample averaging, the distribution is close to a normal distribution by the central limit theorem [31]. The steps for the bootstrapping technique used in this research are illustrated in Figure 3-1.

3.5 Wind Turbine O&M Data Analysis

In this section, the results of the analysis of the “major replacement” category failures are presented. For both offshore sites failure data for the entire lifetime of each wind farm has been included in the analysis. The failure and weather data provided by the turbine manufacturer are three-day averaged data. The research included the examination of data not only from the month that the unscheduled failure occurred, but also from the month before the failure occurred. Hence, for each “major replacement” failure the analysis of weather related reasons for failure have been investigated. The site conditions investigated are wind speed, turbulence intensity and wind direction. All the data used in Figures have been normalised to ensure data confidentiality.

3.5.1 Site Conditions

The wind data was provided directly from the wind turbines. For both wind farms, weather data for the entire lifetime of each site has been analysed.

3.5.1.1 Site 1

The analysis of the wind speed and direction for the first offshore wind farm can be seen in Figure 3-2. This wind rose shows the average wind speeds, in m/s, and directions of all the turbines in the farm over their operational lifetime.

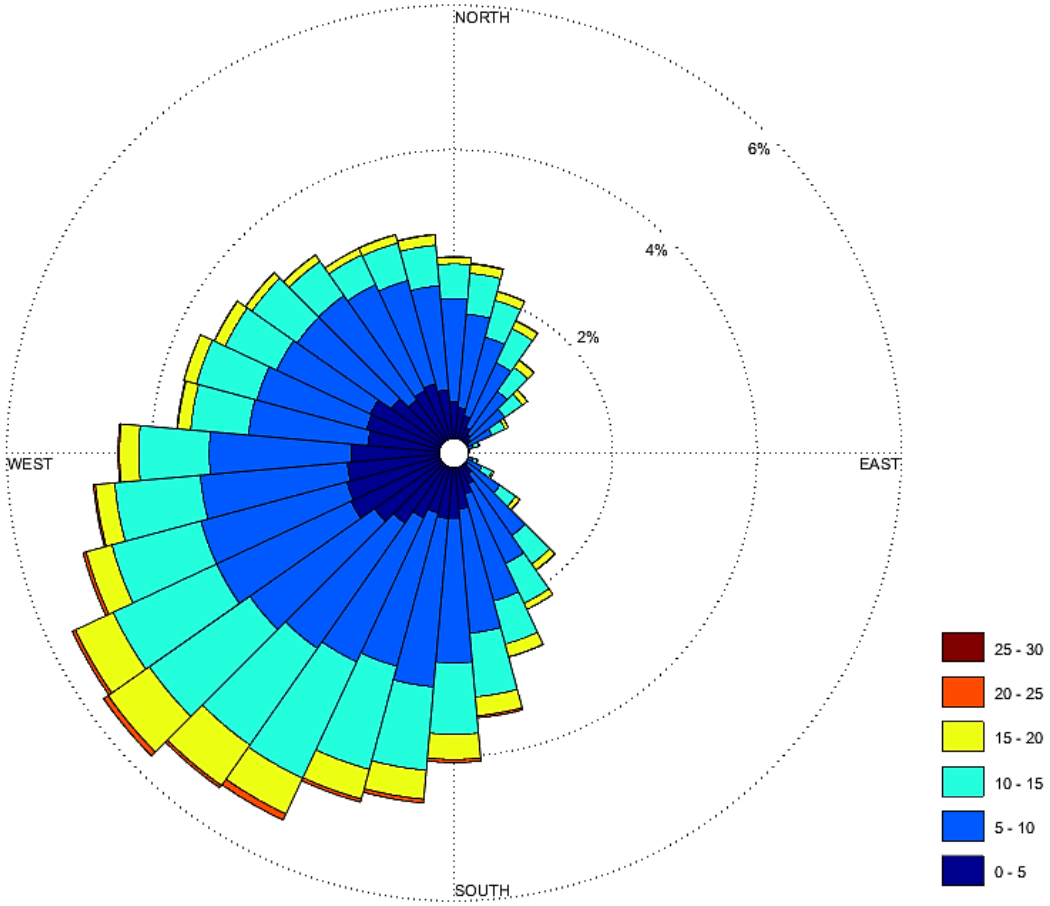

Figure 3-2: Wind Rose for Wind Farm 1

The mean wind direction for this wind farm is approximately 190° and the mean wind speed is approximately 8.6m/s.

3.5.1.2 Site 2

The analysis of the wind speed and direction for the second offshore wind farm can be seen in Figure 3-3. This wind rose shows the average wind speeds, in m/s, and directions of all the turbines in the farm over their operational lifetime.

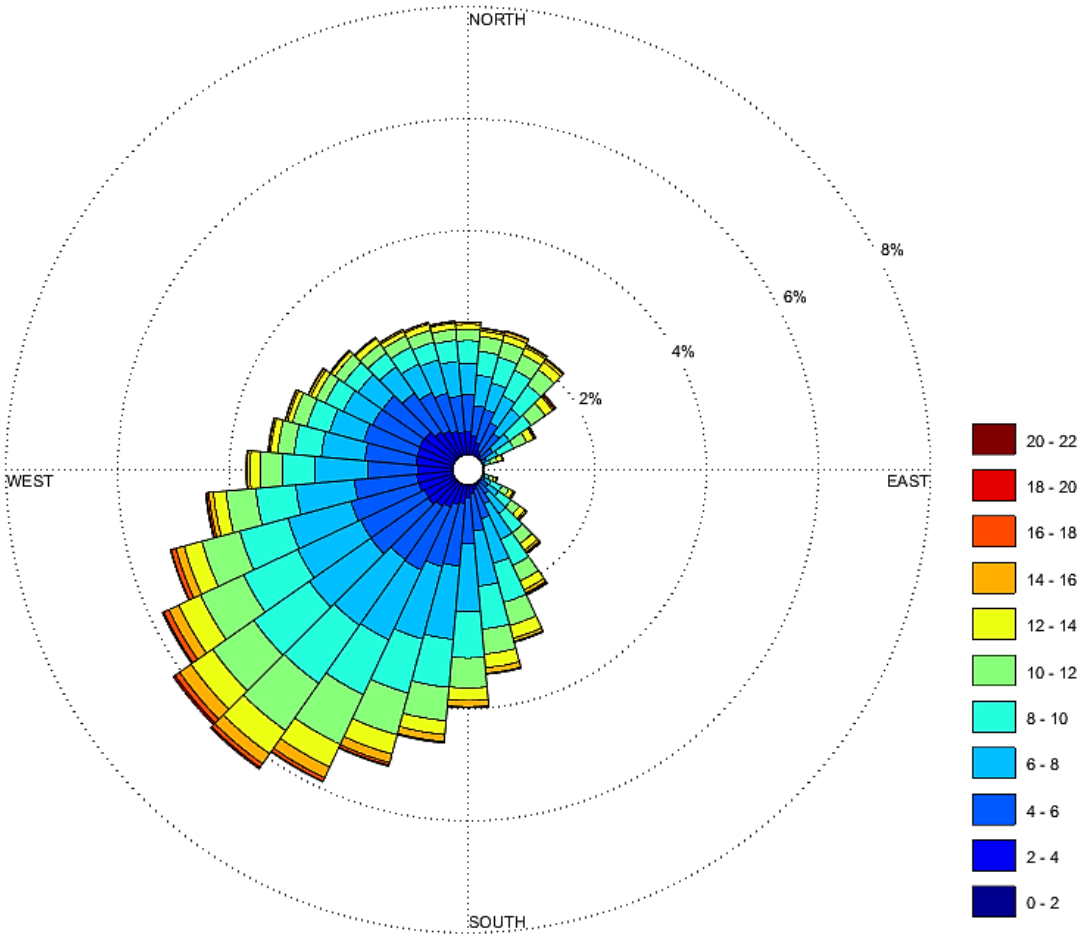

Figure 3-3: Wind Rose for Wind Farm 2

The mean wind direction for this wind farm is approximately 192° and the mean wind speed is approximately 7.7m/s.

3.5.2 Failure Rate and Cost Analysis

In this section, the results of the analysis of failures rates and costs are presented. For both sites, failure and cost data for the entire lifetime of each wind farm has been analysed.

3.5.2.1 Site 1

The failure rate analysis for the first wind farm has been broken down into three failure categories, as described in section 3.4.2. The results can be seen in Figure 3-4:

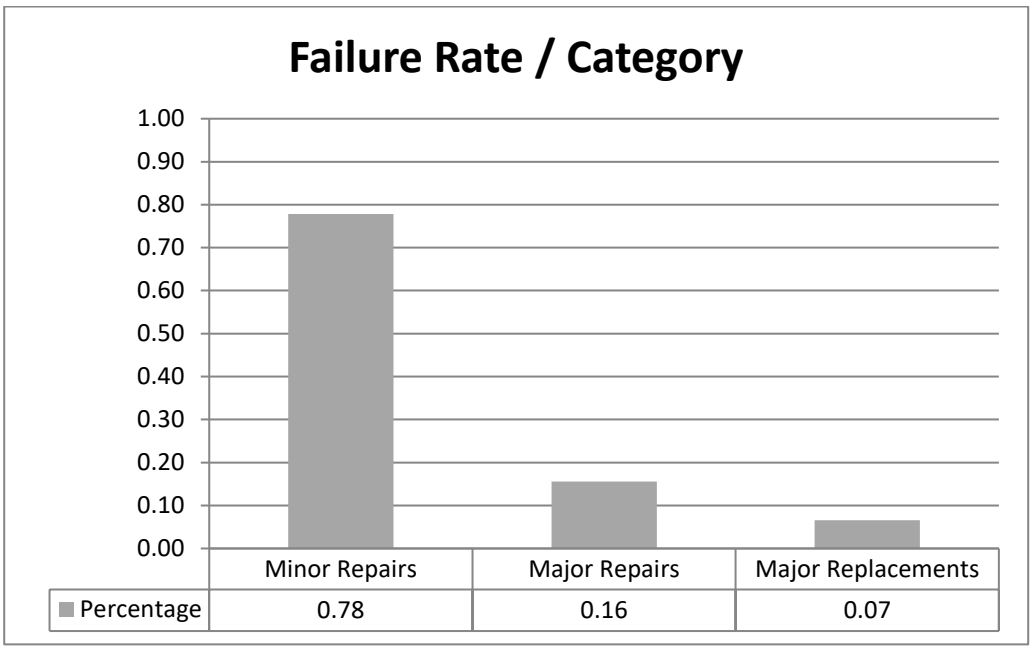

Figure 3-4: Failure rate analysis per category for Wind Farm 1

As expected, most of the failures that occur in wind farm 1 are minor repairs. The number of failures for major repairs and major replacements are significantly less.

The cost analysis for unscheduled failures for site 1 can be seen in Figure 3-5. As can be seen in Figure 3-5, major replacements are responsible for the majority of the cost of unscheduled maintenance. This is the main incentive for the choice of “major replacements” type of failures as the basis of this research. Minor and major repairs correspond to a small portion of the unscheduled maintenance cost.

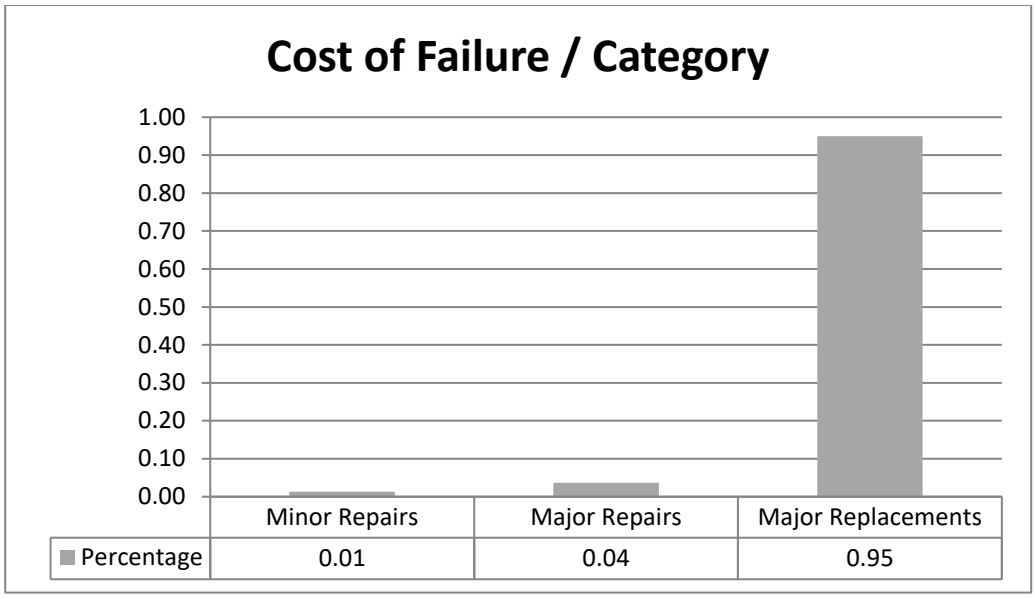

Figure 3-5: Cost analysis per category for Wind Farm 1

3.5.2.2 Site 2

The failure rate analysis for the second wind farm has been broken down into three failure categories, as described in section 3.4.2. The results are shown in Figure 3-6:

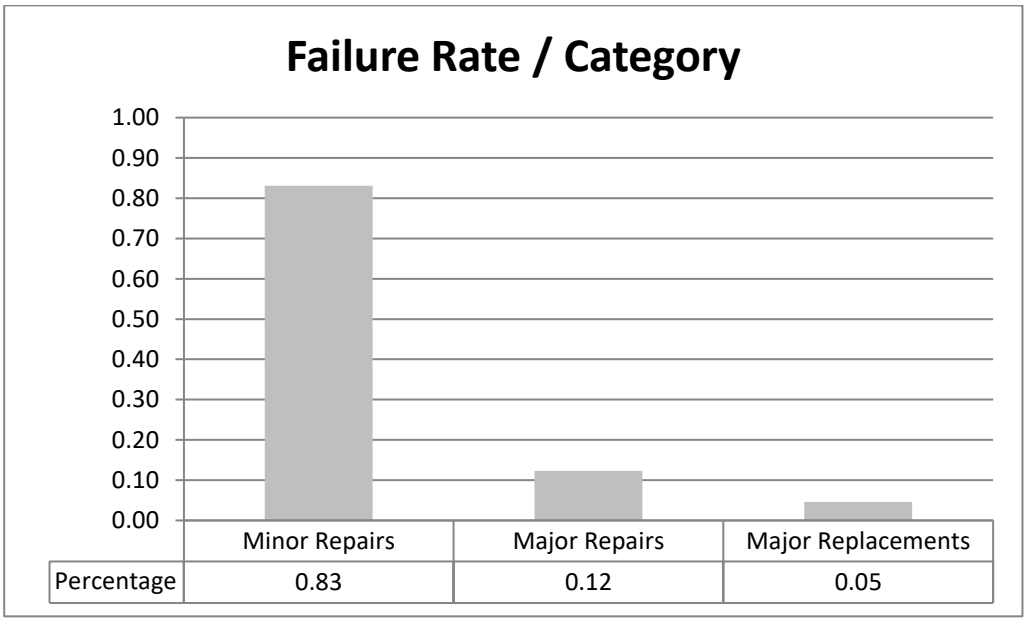

Figure 3-6: Failure rate analysis per category for Wind Farm 2

As expected, most of the failures that occur in wind farm 2 are minor repairs, with the remaining two categories constituting only a small proportion of the total failures. The cost analysis for unscheduled failures for site 2 is shown in Figure 3-7:

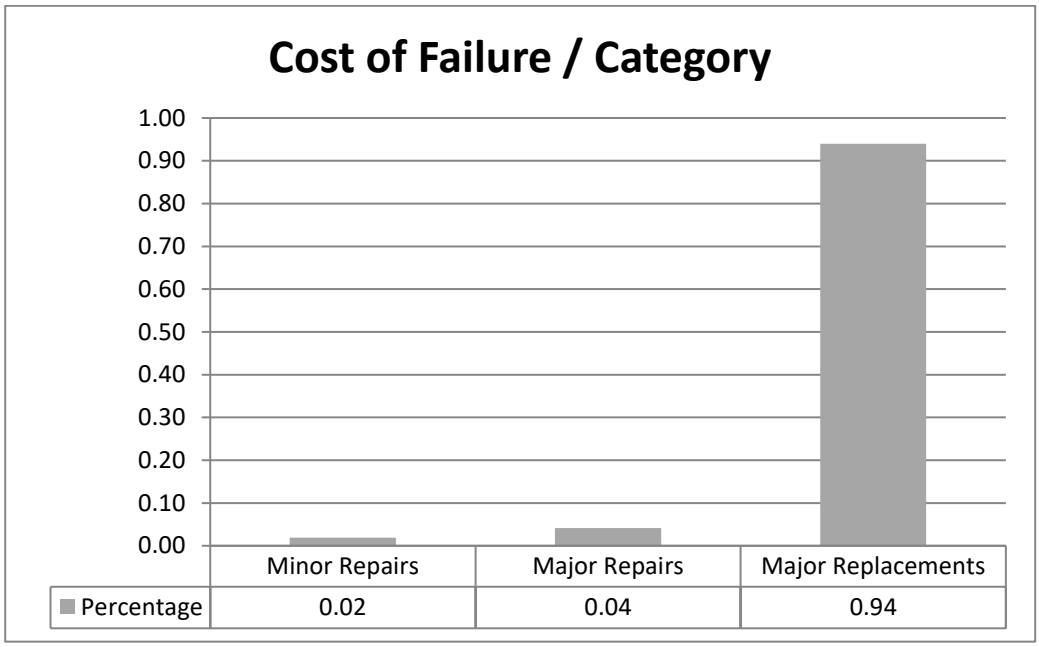

Figure 3-7: Cost analysis per category for Wind Farm 2

As can be seen in Figure 3-7, major replacements are responsible for the majority of the cost of unscheduled maintenance. This is the main incentive for the choice of “major replacements” type of failures as the basis of this research. Minor and major repairs correspond to a small portion of the unscheduled maintenance cost.

3.5.3 Wind Speed Analysis

In this section, the results of the analysis of the wind speed effect over unscheduled “major replacement” type of failures is presented. The wind speed data for the entire lifetime of each wind farm has been analysed.

3.5.3.1 Site 1

Wind speed, whether below or above farm mean wind speed on “major replacement” type of failures for wind farm 1 is shown in Figure 3-8:

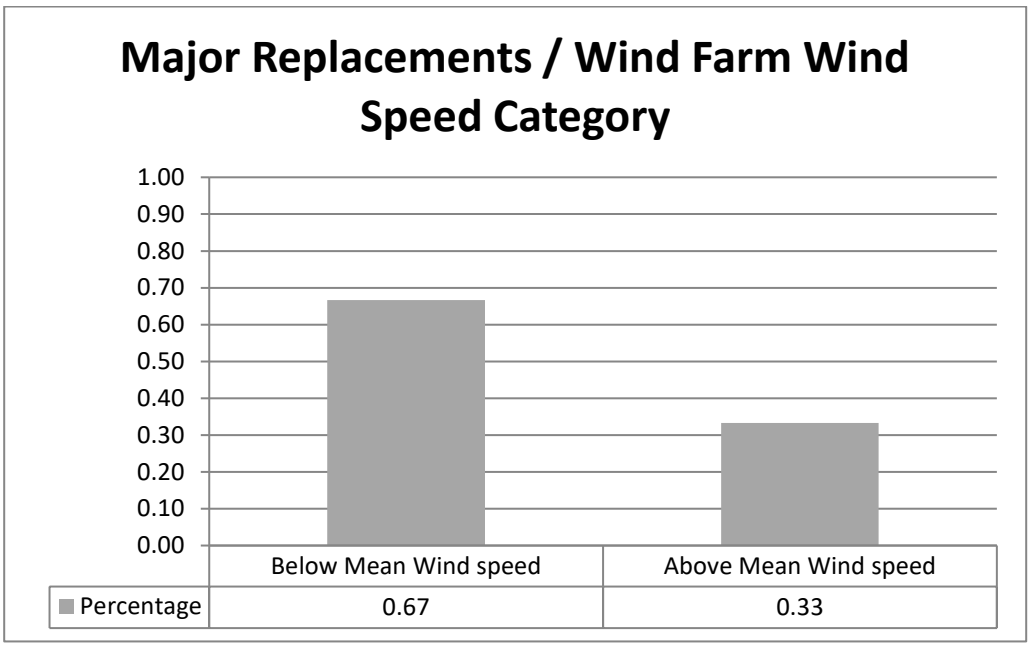

Figure 3-8: Effect of wind speed over Wind Farm 1 on major replacement failures

As can be seen in Figure 3-8, the majority of turbines that experienced a “major replacement” type of failure were experiencing lower wind speeds than the mean wind speed of wind farm 1. Only a few of the turbines that had a major replacement were experiencing higher wind speeds that the average wind speed of the wind farm.

Figure 3-9 depicts the normalised average wind speed spread for wind farm 1. As can be seen, the average wind speed spread of the healthy wind turbines operating below and above the wind speed conditions of the turbines that experienced the major replacement failures is approximately ±4%. This variation is within the expected wind speed range for offshore wind farms [32] [33].

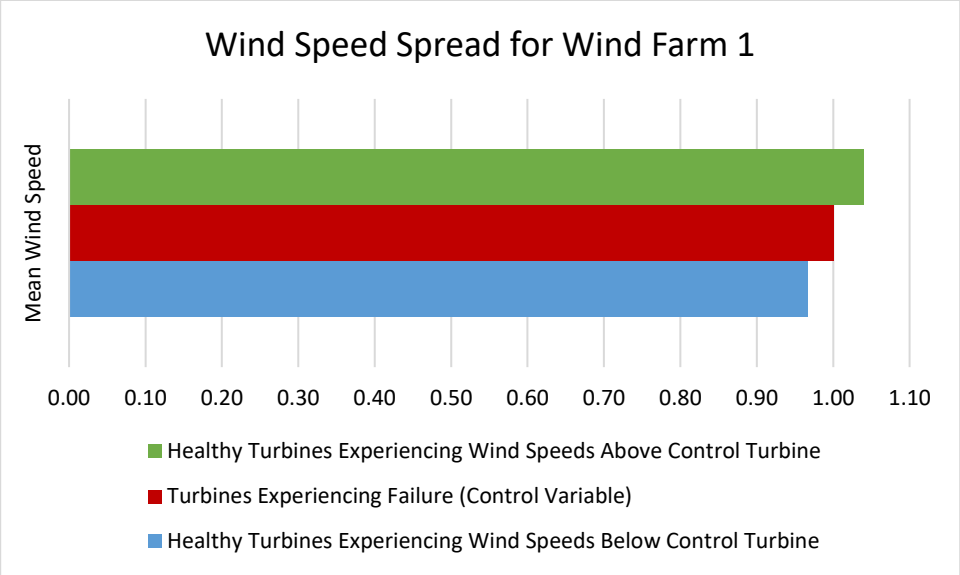

Figure 3-9: Mean wind speed spread for wind farm 1

To statistically estimate the confidence of our analysis, the bootstrapping technique is used [30]. In bootstrapping, samples on N mean wind speeds is taken from the whole population of turbine mean wind speeds, where N is the number of turbines with failure. The mean of each sample of N mean wind speeds is calculated. The averaging of N number of samples is performed by resampling as many times as the observed dataset (i.e. size equal to the observed dataset). In this way a probability distribution for the mean of the mean wind speeds can be estimated. Because of the averaging, it will be close to a normal distribution by the central limit theorem [31]. Figure 3-10 depicts the 95% confidence interval for wind farm 1.

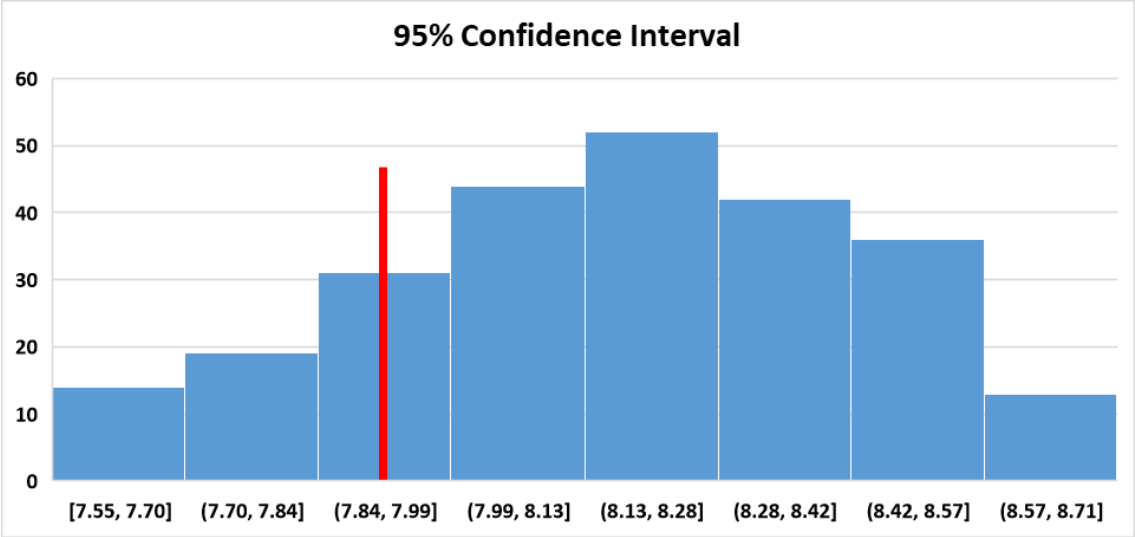

Figure 3-10: 95% confidence interval for mean wind speed of wind farm 1

As can be seen in Figure 3-10, by using bootstrapping to a value of N equal to the number of major replacement failures for wind farm 1, the 95% confidence interval for the mean wind speed is $7.55\,{}^{m}/_{s} < mean < 8.72\,{}^{m}/_{s}$. The mean wind speed for the turbines that experienced a "major replacement" failure for wind farm 1 is $7.89\,{}^{m}/_{s}$, which is within the 95% confidence interval.

The analysis is repeated, but this time only the neighbouring turbines to the wind turbines that experienced a "major replacement" type of failure have been considered. The results are shown in Figure 3-11. As can be seen in Figure 3-11, the majority of turbines that experienced a "major replacement" type of failure were experiencing lower wind speeds than the mean wind speed of their neighbouring turbines. Only a few of the turbines that had a major replacement were experiencing higher wind speeds that the average wind speed of the neighbouring turbines.

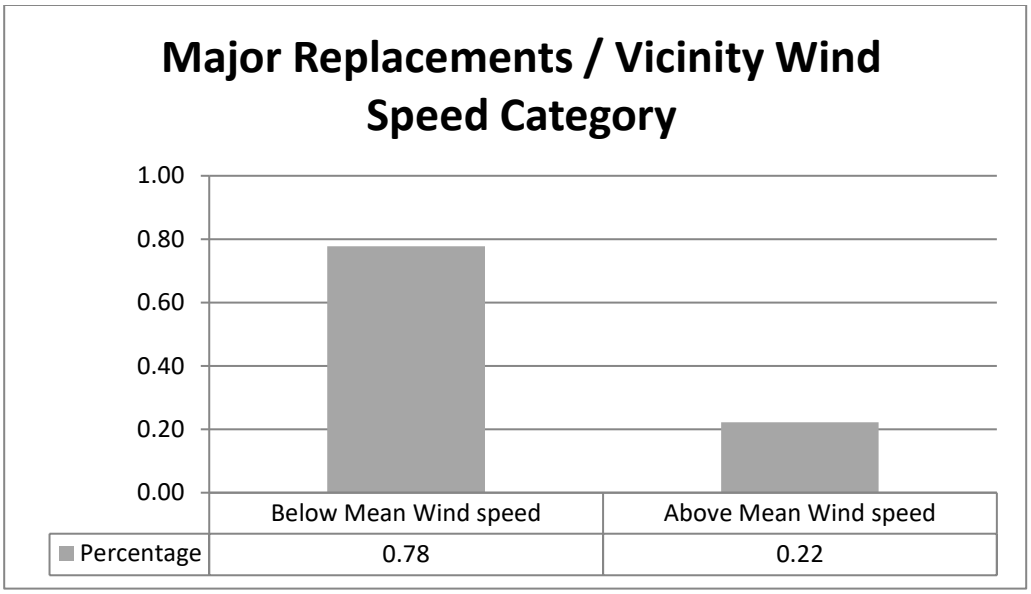

Figure 3-11: Effect of wind speed over neighbouring turbines on major replacement failures

Figure 3-12 depicts the 95% confidence interval for wind farm 1, regarding the analysis of the effect of local wind speed conditions on “major replacement” failures.

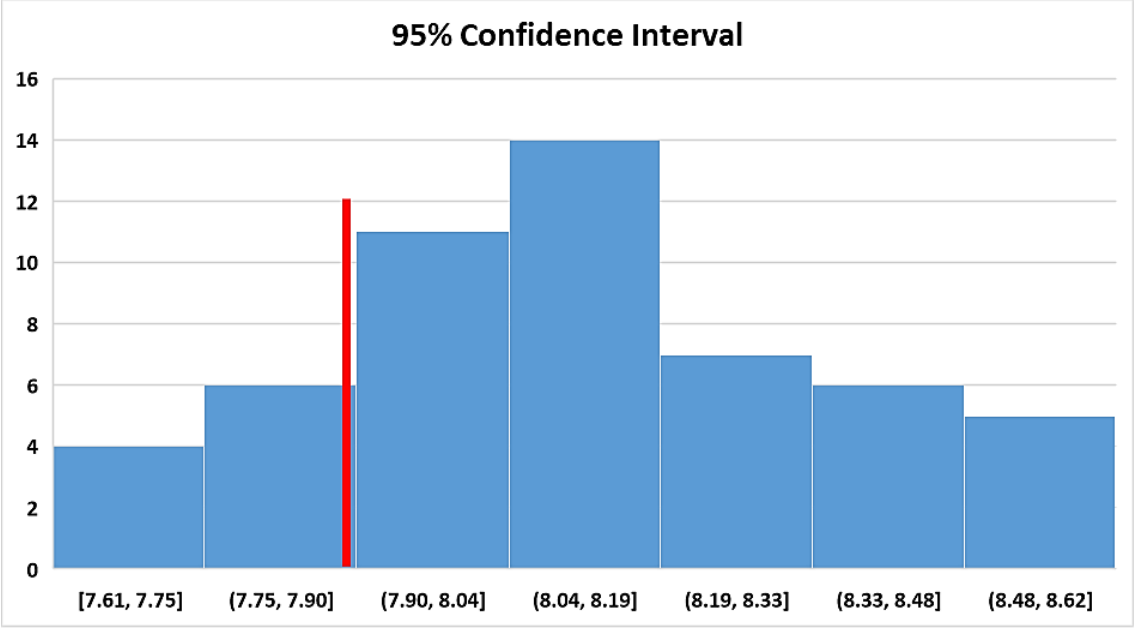

Figure 3-12: 95% confidence interval for neighbouring turbine wind speed of wind farm 1

As can be seen in Figure 3-12, by using bootstrapping to a value of N equal to the number of major replacement failures for wind farm 1, the 95% confidence interval for the mean wind speed of neighbouring turbines is $7.61\,{}^{m}/_{s} < mean < 8.57\,{}^{m}/_{s}$. The mean wind speed for the turbines that experienced a "major replacement" failure for wind farm 1 is $7.89\,{}^{m}/_{s}$, which is within the 95% confidence interval.

For both wind speed conditions under investigation, namely wind farm average wind speed and local average wind speed, the mean wind speed of the wind turbines having experienced "major replacement" failures was below the average "healthy" wind turbine wind speed values, as was also shown in Figures 3-7 and 3-10.

3.5.3.2 Site 2

The effect of wind speed on "major replacement" type of failures for wind farm 2 is shown in Figure 3-13. As can be seen in Figure 3-13, the majority of turbines that experienced a "major replacement" type of failure were experiencing lower wind speeds than the mean wind speed of wind farm 2. Only some of the turbines that had a major replacement were experiencing higher wind speeds that the average wind speed of the wind farm.

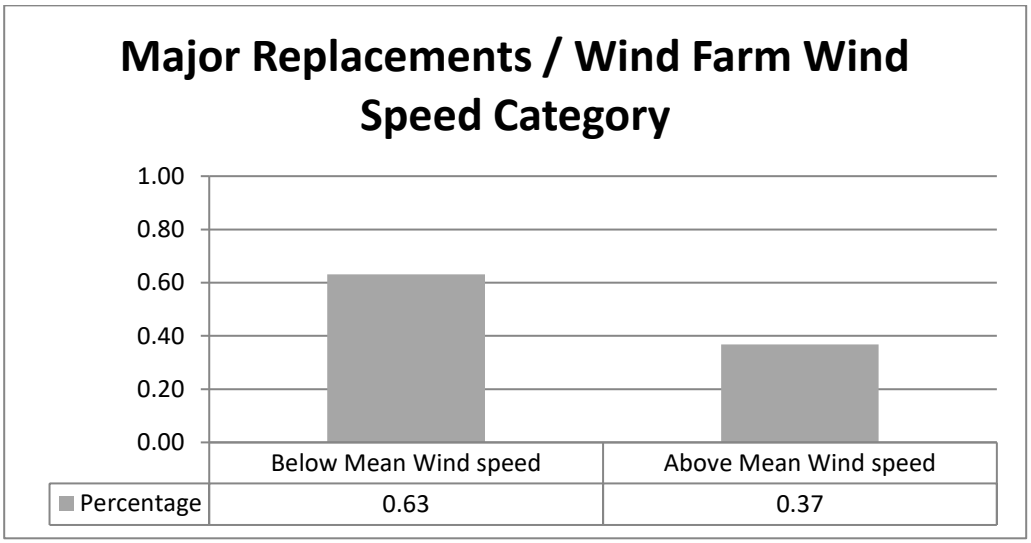

Figure 3-13: Effect of wind speed over Wind Farm 2 on major replacement failures

The spread of the mean wind speed for wind farm 2 is shown in Figure 3-14. As depicted in Figure 3-14, the average wind speed spread of the healthy wind turbines is approximately ±5%, which does not correspond to a significant variation relative to the wind speed conditions experienced by the turbines that failed [32] [33].

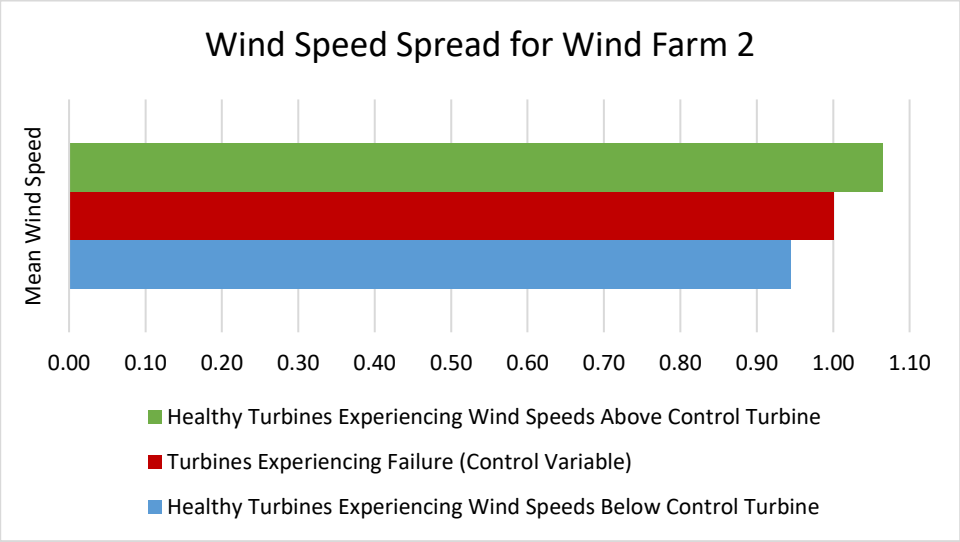

Figure 3-14: Mean wind speed spread for wind farm 2

By using bootstrapping, Figure 3-15 depicts the 95% confidence interval for the average wind speed of wind farm 2. The approach is identical to that used for wind farm 1.

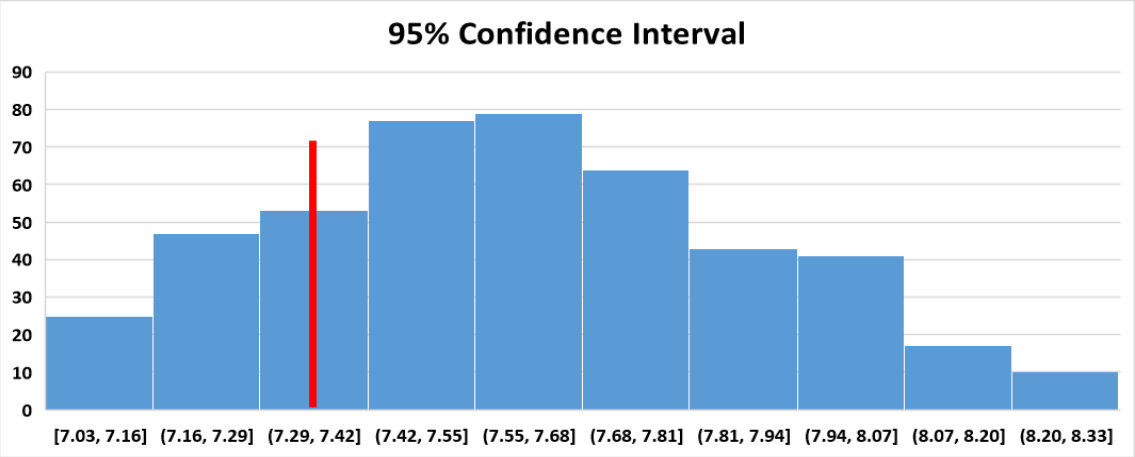

Figure 3-15: 95% confidence interval for mean wind speed of wind farm 2

As can be seen in Figure 3-15, by using bootstrapping to a value of N equal to the number of major replacement failures for wind farm 2, the 95% confidence interval for the mean wind speed is $7.02\,^{m}/_{s} < mean < 8.26\,^{m}/_{s}$. The mean wind speed for the turbines that experienced a "major replacement" failure for wind farm 2 is $7.36\,^{m}/_{s}$, which is within the 95% confidence interval.

The same type of analysis has been performed, but this time only the neighbouring turbines to the wind turbines that experienced a "major replacement" type of failure have been considered. The results are shown in Figure 3-16:

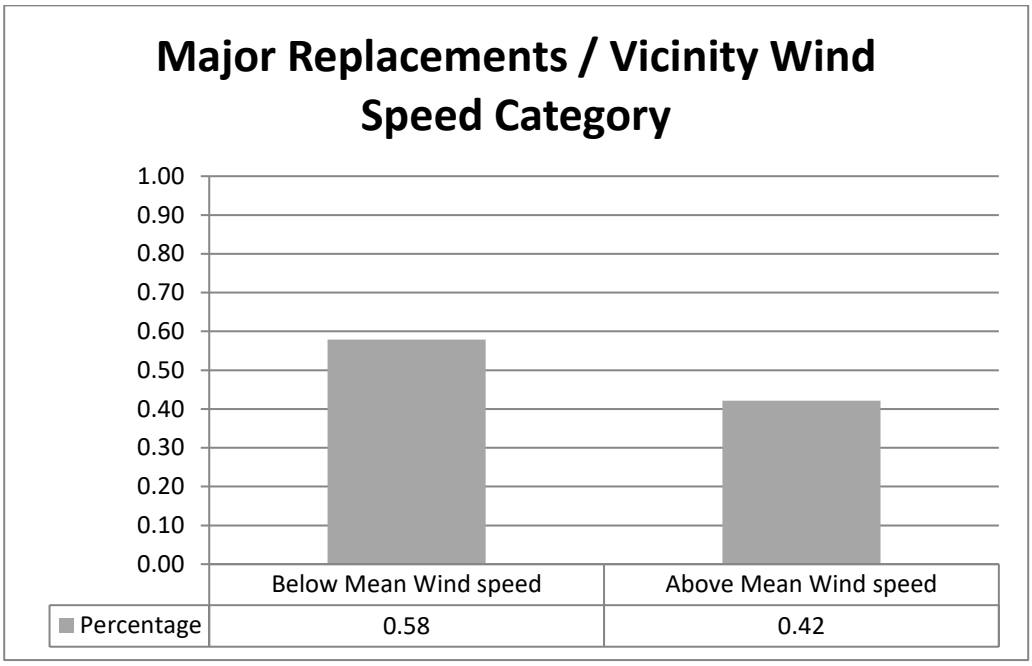

Figure 3-16: Effect of wind speed over neighbouring turbines on major replacement failures

As can be seen in Figure 3-16, most of the turbines that experienced a "major replacement" type of failure were experiencing lower wind speeds than the mean wind speed of their neighbouring turbines. Only some of the turbines that had a major replacement were experiencing higher wind speeds that the average wind speed of the neighbouring turbines.

Figure 3-17 depicts the 95% confidence interval of the local wind speed conditions for wind farm 2.

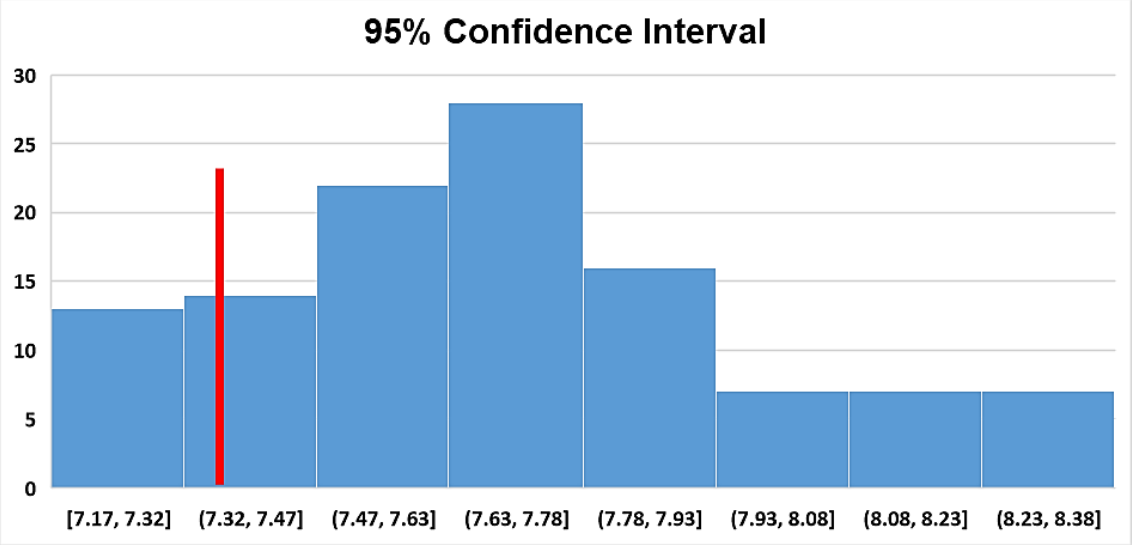

Figure 3-17: 95% confidence interval for neighbouring turbine wind speed of wind farm 2

As can be seen in Figure 3-17, by using bootstrapping to a value of N equal to the number of major replacement failures for wind farm 2, the 95% confidence interval for the mean wind speed of neighbouring turbines is $7.17\,^{m}/_{s} < mean < 8.38\,^{m}/_{s}$. The mean wind speed for the turbines that experienced a "major replacement" failure for wind farm 2 is $7.36\,^{m}/_{s}$, which is within the 95% confidence interval.

For both wind speed conditions under investigation, namely wind farm average wind speed and local average wind speed, the mean wind speed of the wind turbines having experienced "major replacement" failures was below the average "healthy" wind turbine wind speed values, as was also shown in Figures 3-12 and 3-15.

3.5.4 Turbulence Intensity Analysis

In this section, the results of the analysis of turbulence intensity effect over unscheduled "major replacement" type of failures is presented. The turbulence intensity data for the entire lifetime of each wind farm has been analysed.

3.5.4.1 Site 1

Intensity category, whether below or above mean turbulence intensity, on “major replacement” type of failures for wind farm 1 is shown in Figure 3-18:

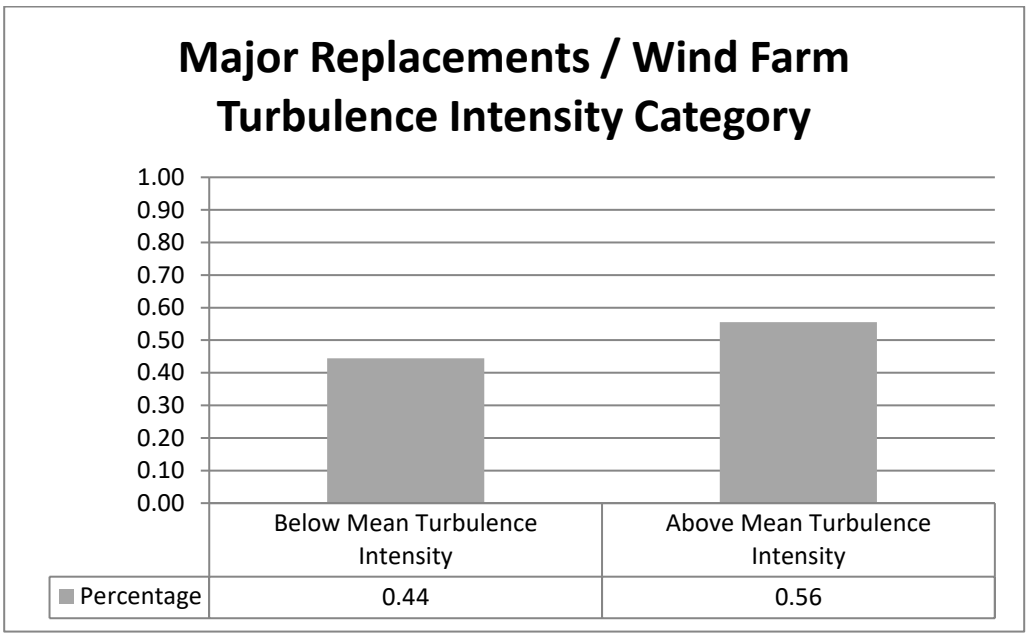

Figure 3-18: Effect of turbulence intensity of Wind Farm 1 on major replacement failures

As can be seen in Figure 3-18, the majority of turbines that experienced a “major replacement” type of failure were experiencing higher turbulence intensity than the mean turbulence intensity of wind farm 1.

Figure 3-19 depicts the average turbulence intensity spread for wind farm 1. As can be seen, the average turbulence intensity variation of the healthy wind turbines is approximately ±6%, relative to the turbulence intensity experienced by the turbines that failed. This variation is within the expected turbulence intensity range for offshore wind farms [34].

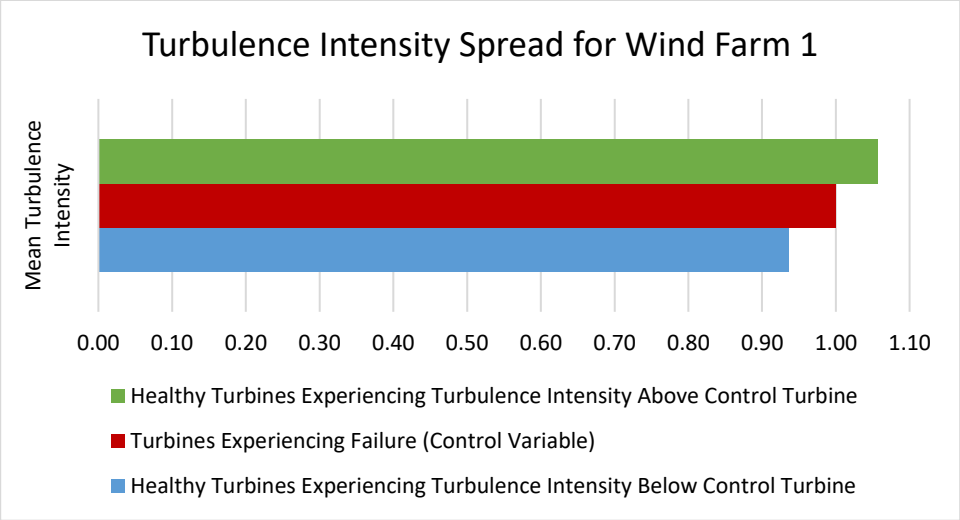

Figure 3-19: Mean turbulence intensity spread for wind farm 1

To statistically estimate the confidence of our analysis, the bootstrapping technique is used [30]. In bootstrapping, samples on N mean turbulence intensity values is taken from the whole population of turbine mean turbulence intensity values, where N is the number of turbines with failure. The mean of each sample of N mean turbulence intensity is calculated. The averaging of N number of samples is performed by resampling as many times as the observed dataset (i.e. size equal to the observed dataset). In this way a probability distribution for the mean of the mean turbulence intensity values can be estimated. Because of the averaging, it will be close to a normal distribution by the central limit theorem [31]. Figure 3-20 depicts the 95% confidence interval for wind farm 1.

As can be seen in Figure 3-20, by using bootstrapping to a value of N equal to the number of major replacement failures for wind farm 1, the 95% confidence interval for the mean turbulence intensity is $10.72\% < mean < 12.00\%$. The mean turbulence intensity for the turbines that experienced a “major replacement” failure for wind farm 1 is 11.53%, which is within the 95% confidence interval.

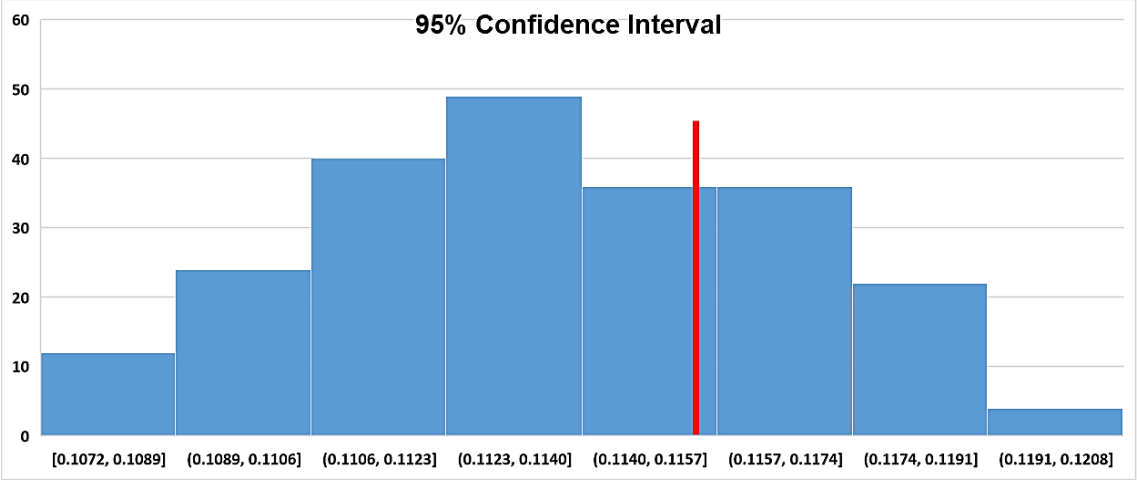

Figure 3-20: 95% confidence interval for mean turbulence intensity of wind farm 1

The results of the effect of turbulence intensity with regards to neighbouring turbines are shown in Figure 3-21. As can be seen in Figure 3-21, most of the turbines that experienced a "major replacement" type of failure were experiencing lower turbulence intensity than the mean turbulence intensity of neighbouring wind turbines.

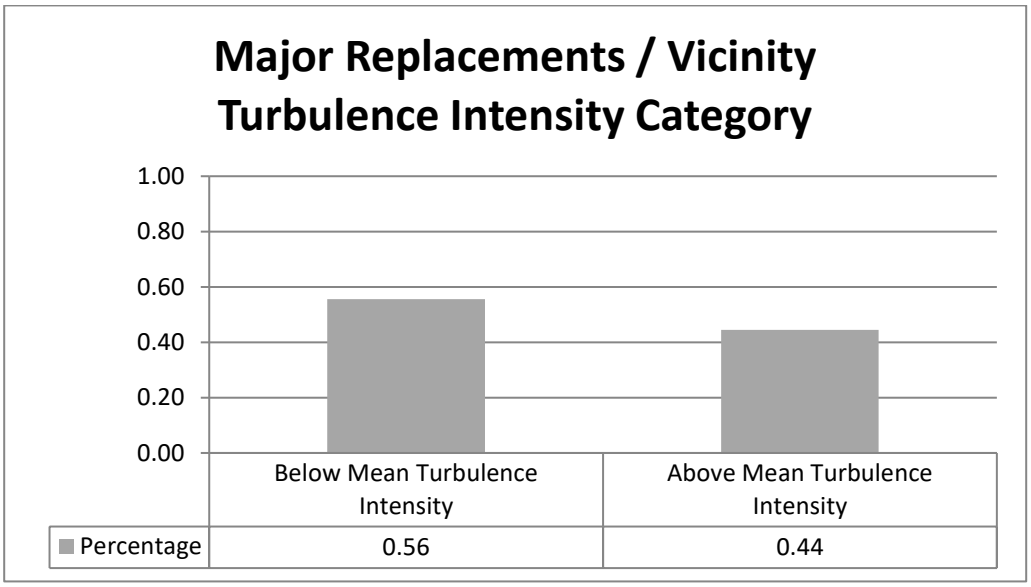

Figure 3-21: Effect of turbulence intensity of neighbouring turbines on major replacement failures

Figure 3-22 depicts the 95% confidence interval for wind farm 1, regarding the analysis of the effect of local turbulence intensity conditions on “major replacement” failures.

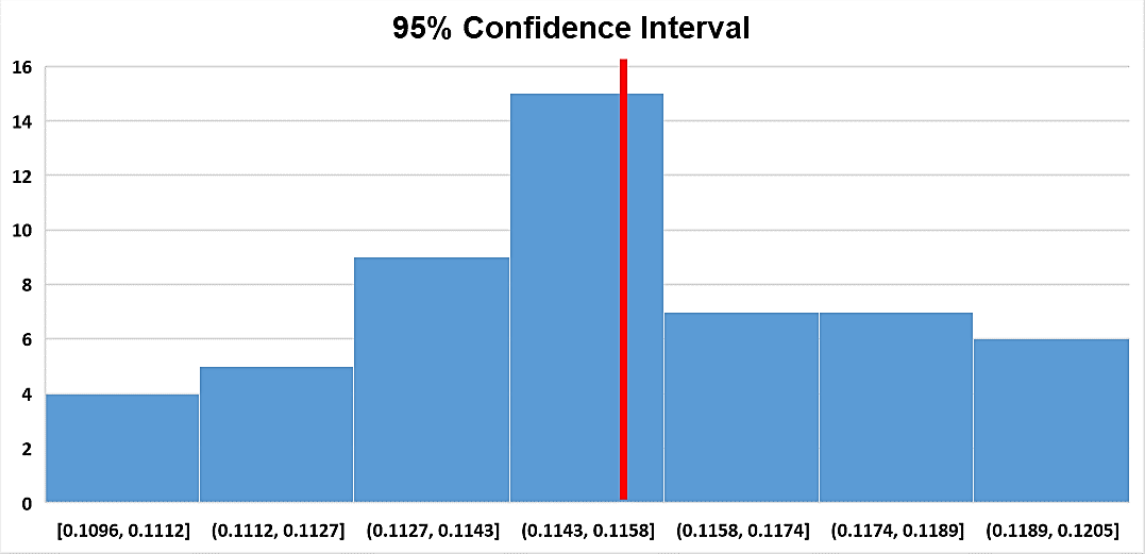

Figure 3-22: 95% confidence interval for neighbouring turbine turbulence intensity of wind farm 1

As can be seen in Figure 3-22, by using bootstrapping to a value of N equal to the number of major replacement failures for wind farm 1, the 95% confidence interval for the mean turbulence intensity of neighbouring turbines is $10.96\% < mean < 11.97\%$. The mean turbulence intensity for the turbines that experienced a “major replacement” failure for wind farm 1 is 11.53%, which is within the 95% confidence interval.

3.5.4.2 Site 2

The effect of turbulence intensity on “major replacement” type of failures for wind farm 2 is shown in Figure 3-23. As can be seen in Figure 3-23, the majority of turbines that experienced a “major replacement” type of failure were experiencing higher turbulence intensity than the mean turbulence intensity of wind farm 2.

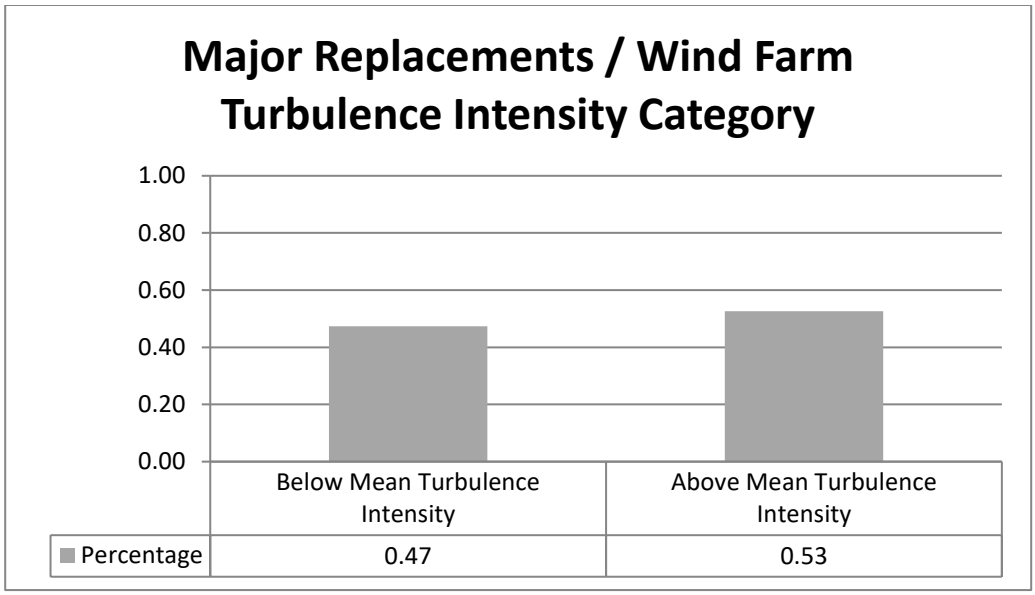

Figure 3-23: Effect of turbulence intensity of Wind Farm 2 on major replacement failures

The spread of the mean turbulence intensity for wind farm 2 is shown in Figure 3-24. As depicted in Figure 3-24, the turbulence intensity spread is approximately ±7%, which does not correspond to a significant variation relative to the turbulence intensity conditions experienced by the turbines that failed [34].

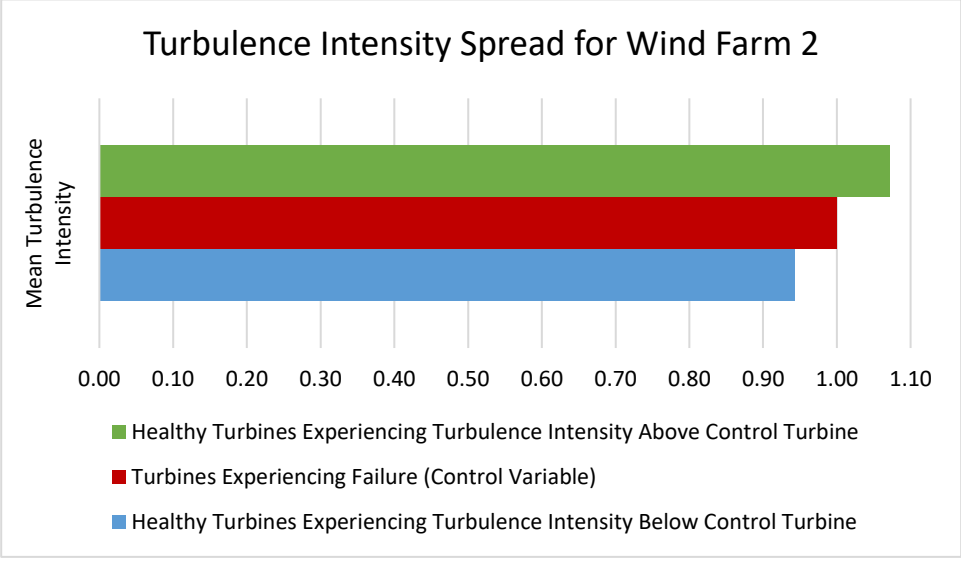

Figure 3-24: Mean turbulence intensity spread for wind farm 2

By using bootstrapping, Figure 3-25 depicts the 95% confidence interval for the average turbulence intensity of wind farm 2. The approach is identical to that used for wind farm 1.

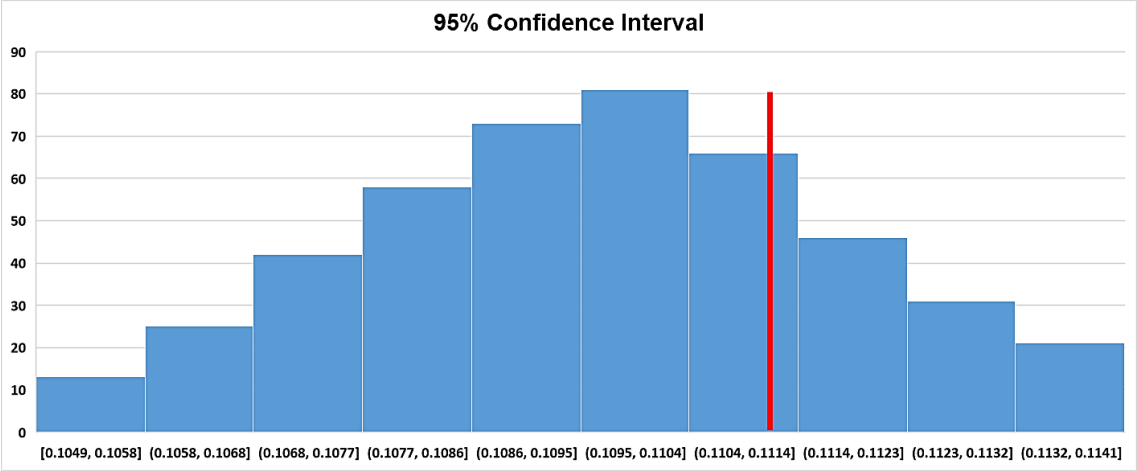

Figure 3-25: 95% confidence interval for mean turbulence intensity of wind farm 2

As can be seen in Figure 3-25, by using bootstrapping to a value of N equal to the number of major replacement failures for wind farm 2, the 95% confidence interval for the mean turbulence intensity is $10.49\% < mean < 11.41\%$. The mean turbulence intensity for the turbines that experienced a "major replacement" failure for wind farm 2 is 11.11%, which is within the 95% confidence interval.

The results of the effect of turbulence intensity with regards to neighbouring turbines are shown in Figure 3-26. As can be seen in Figure 3-26, most of the turbines that experienced a "major replacement" type of failure were experiencing higher turbulence intensity than the mean turbulence intensity of neighbouring wind turbines.

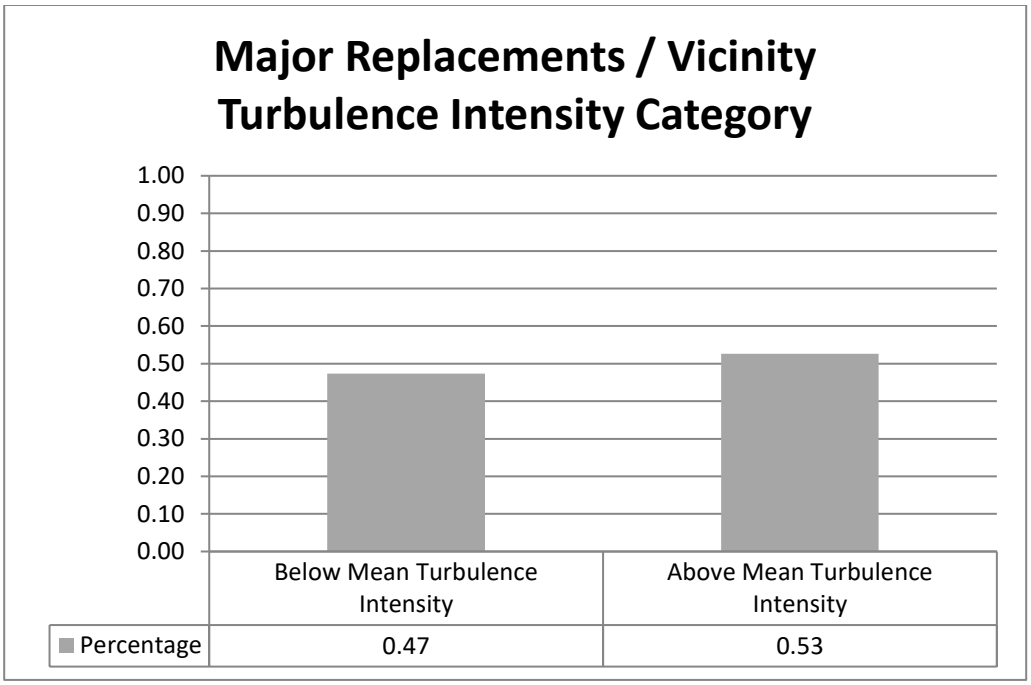

Figure 3-26: Effect of turbulence intensity of neighbouring turbines on major replacement failures

Figure 3-27 depicts the 95% confidence interval for wind farm 2, regarding the analysis of the effect of local turbulence intensity conditions on “major replacement” failures.

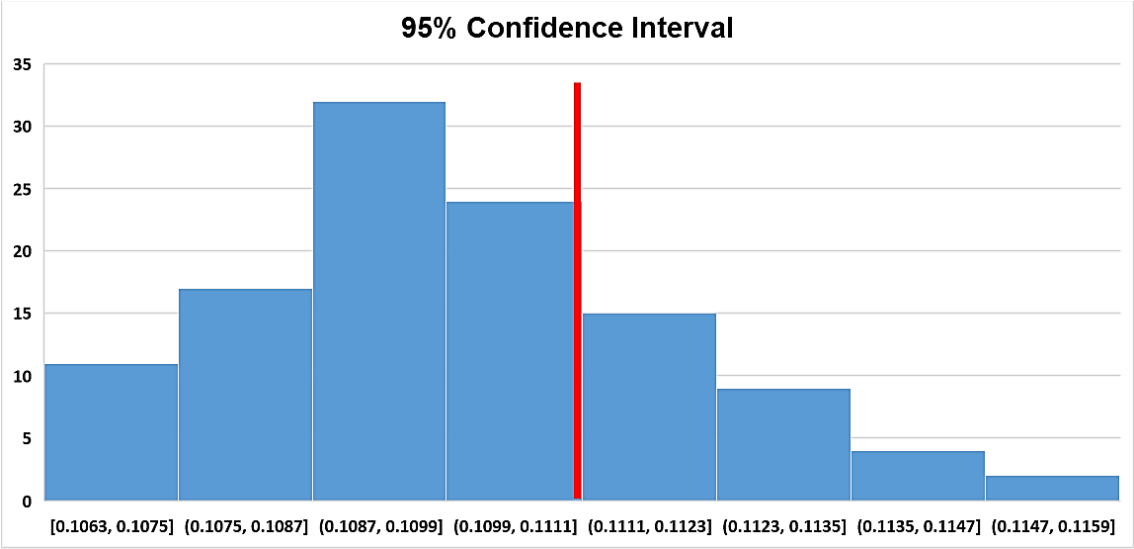

Figure 3-27: 95% confidence interval for neighbouring turbine turbulence intensity of wind farm 2

As can be seen in Figure 3-27, by using bootstrapping to a value of N equal to the number of major replacement failures for wind farm 2, the 95% confidence interval for the mean turbulence intensity of neighbouring turbines is $10.63\% < mean < 11.55\%$. The mean turbulence intensity for the turbines that experienced a "major replacement" failure for wind farm 2 is 11.11%, which is within the 95% confidence interval.

For both turbulence intensity conditions under investigation, namely wind farm average turbulence intensity and local average turbulence intensity, the mean turbulence intensity of the wind turbines having experienced "major replacement" failures was below the average "healthy" wind turbine turbulence intensity values, as was also shown in Figures 3-22 and 3-25.

3.5.5 Wind Direction Analysis

In this section, the results of the analysis of wind direction effect over unscheduled "major replacement" type of failures is presented. The turbine direction data for the entire lifetime of each wind farm has been analysed.

3.5.5.1 Site 1

The effect of wind direction on "major replacement" type of failures for wind farm 1 can be seen in Figure 3-28.

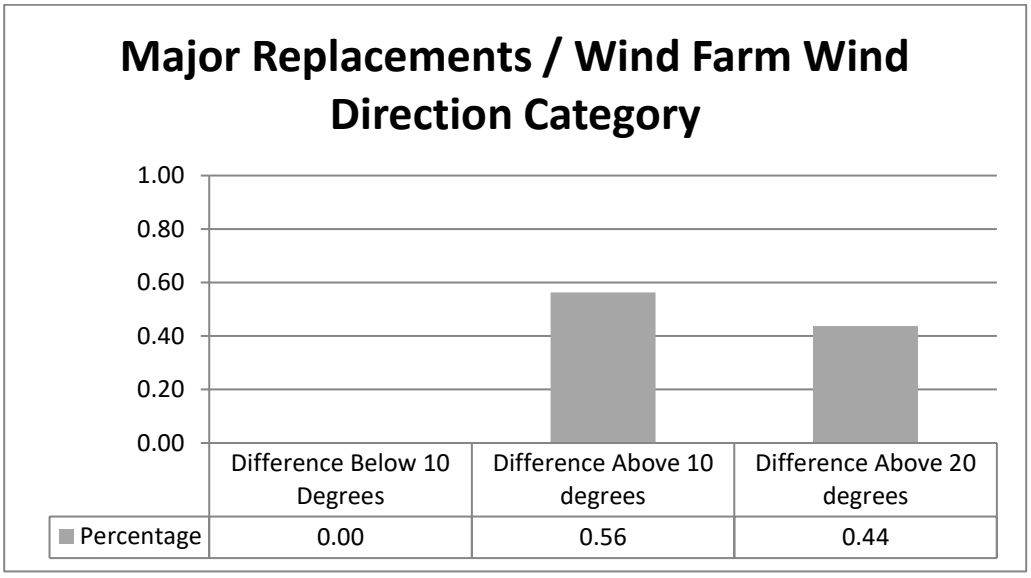

Figure 3-28: Effect of wind direction of Wind Farm 1 on major replacement failures

Figure 3-28 shows the difference between the mean wind direction of wind farm 1 and the mean wind direction experienced by the turbine that experienced a “major replacement” type of failure. It should be noted that all the turbines that experienced a major replacement failure had been facing at least a 10° difference with regards to the mean wind direction of wind farm 1. The percentage of turbines that experienced differences above 20° between the wind direction they were facing and the mean direction that wind farm 1 was facing is significant. This suggests that the turbines experiencing major replacements seem to be misaligned with respect to the mean wind direction of the wind farm.

Bootstrapping has been used to statistically estimate the confidence of our analysis [30]. In this case, N samples of the absolute value of the difference between the wind direction of a turbine and the mean of the population are taken, where N is the number of turbines with failure. The mean of each sample of N samples is calculated. The averaging of N number of samples is performed by resampling as many times as the observed dataset (i.e. size equal to the observed dataset). In this way a probability distribution for the mean of the absolute value of the difference between the wind direction of a turbine and the mean of the population can be estimated. Because of the averaging, it will be close to a normal distribution by the central limit theorem [31]. Figure 3-29 depicts the 95% confidence interval for wind farm 1.

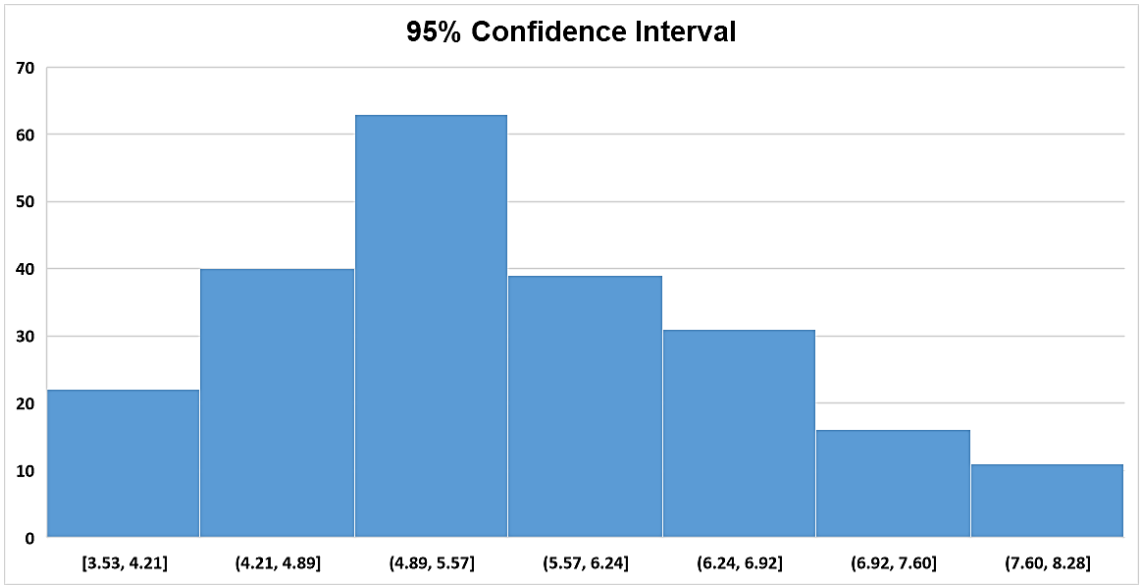

Figure 3-29: 95% confidence interval for difference between turbine wind direction and the mean of the all the turbines of wind farm 1

The difference between the wind direction of a turbine that experienced a "major replacement" failure and the mean of the all available wind turbines for wind farm 1 is 17.93^0, which is outside the 95% confidence interval, as depicted in Figure 3-29. This suggests that the turbines with a "major replacement" failure have experienced a significant deviation from the average wind farm direction.

The results of the effect of wind direction with regards to neighbouring turbines are shown in Figure 3-30:

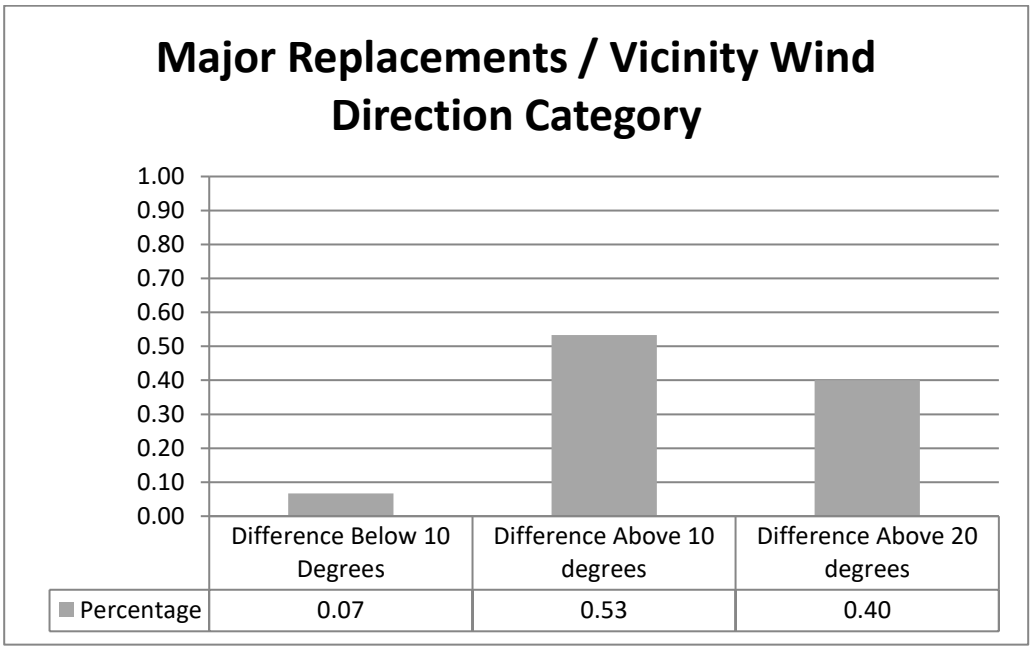

Figure 3-30: Effect of wind direction of neighbouring turbines on major replacement failures

As can be seen in Figure 3-30, the majority of the turbines that experienced a "major replacement" type of failure had been facing a 10° difference with regards to the mean wind direction of the neighbouring turbines. The number of turbines that experienced differences above 20° between the wind direction they were facing and the mean direction that neighbouring turbines were facing remains significant.

Figure 3-31 depicts the 95% confidence interval for wind farm 1, regarding the analysis of the effect of local wind direction conditions on “major replacement” failures.

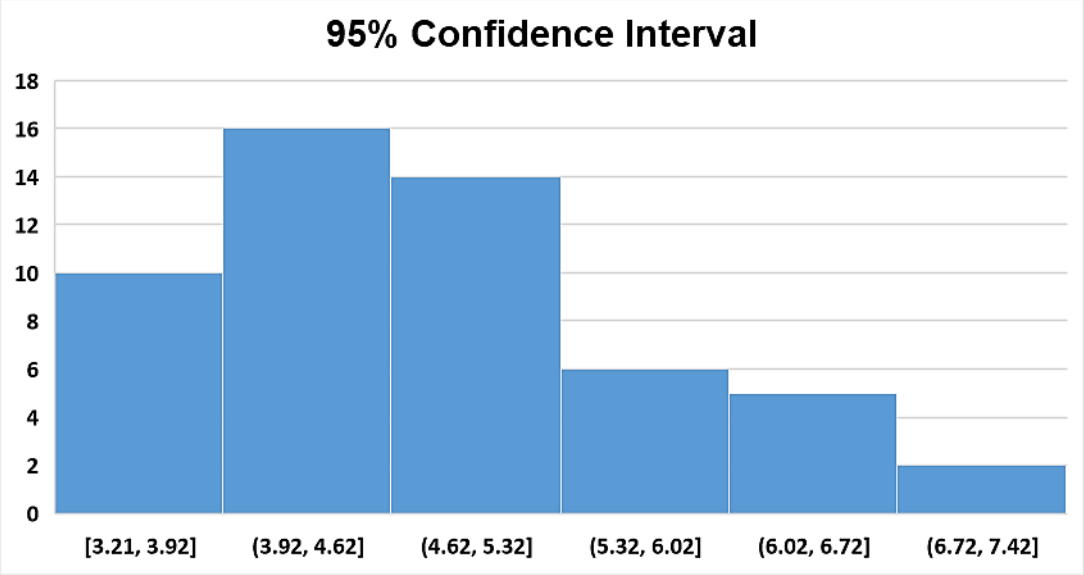

Figure 3-31: 95% confidence interval for difference between turbine wind direction and the mean of the all neighbouring turbines of wind farm 1

The difference between the wind direction of a turbine that experienced a “major replacement” failure and the mean of the all available neighbouring wind turbines for wind farm 1 is 14.87^0, which is outside the 95% confidence interval, as depicted in Figure 3-31. This suggests that the turbines with a “major replacement” failure have experienced a significant deviation from the average wind direction of the neighbouring turbines.

3.5.5.2 Site 2

The effect of wind direction on “major replacement” type of failures for wind farm 2 can be seen in Figure 3-32, where the difference between the mean wind direction of wind farm 2 and the mean wind direction experienced by the turbine that experienced a “major replacement” type of failure is depicted. It should be noted that approximately the vast majority of the turbines that experienced major replacement failures had been facing at least a 10^o difference with regards to the mean wind direction of wind farm 2.

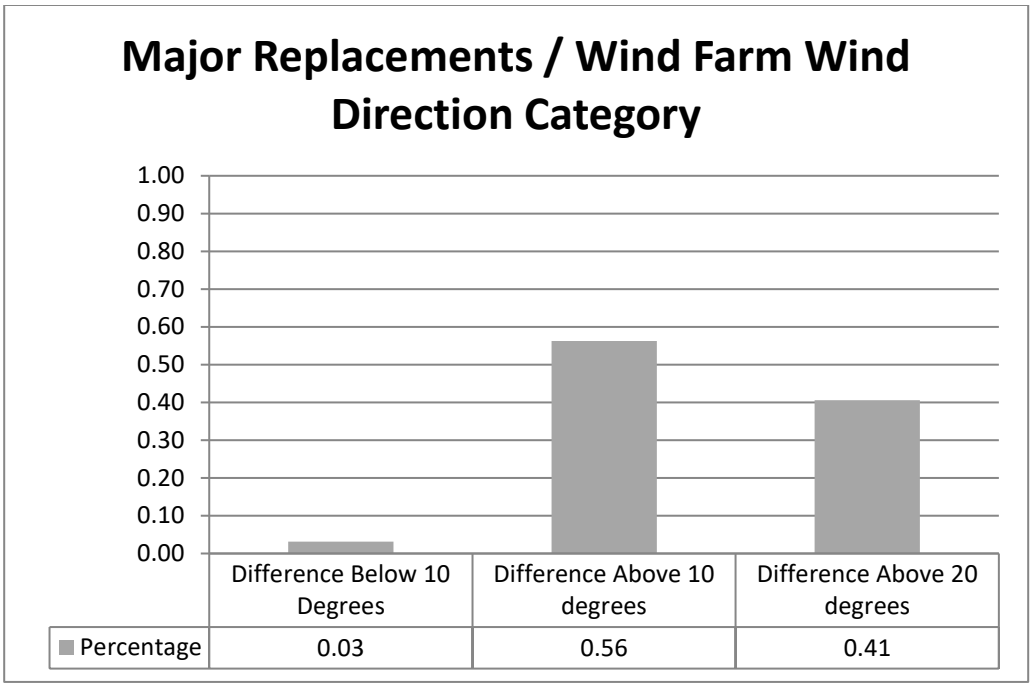

Figure 3-32: Effect of wind direction of Wind Farm 2 on major replacement failures

The percentage of turbines that experienced differences above 20° between the wind direction they were facing and the mean direction that wind farm 2 was facing is also significant. This suggests that the turbines experiencing major replacements seem to be misaligned with respect to the mean wind direction of the wind farm.

By using bootstrapping, Figure 3-33 depicts the 95% confidence interval for wind farm 2, regarding the analysis of the effect of wind direction conditions on "major replacement" failures. The approach is identical to that used for wind farm 1. The difference between the wind direction of a turbine that experienced a "major replacement" failure and the mean of the all available wind turbines for wind farm 2 is 19.71^{0}, which is outside the 95% confidence interval, as depicted in Figure 3-33. This suggests that the turbines with a "major replacement" failure have experienced a significant deviation from the average wind farm direction.

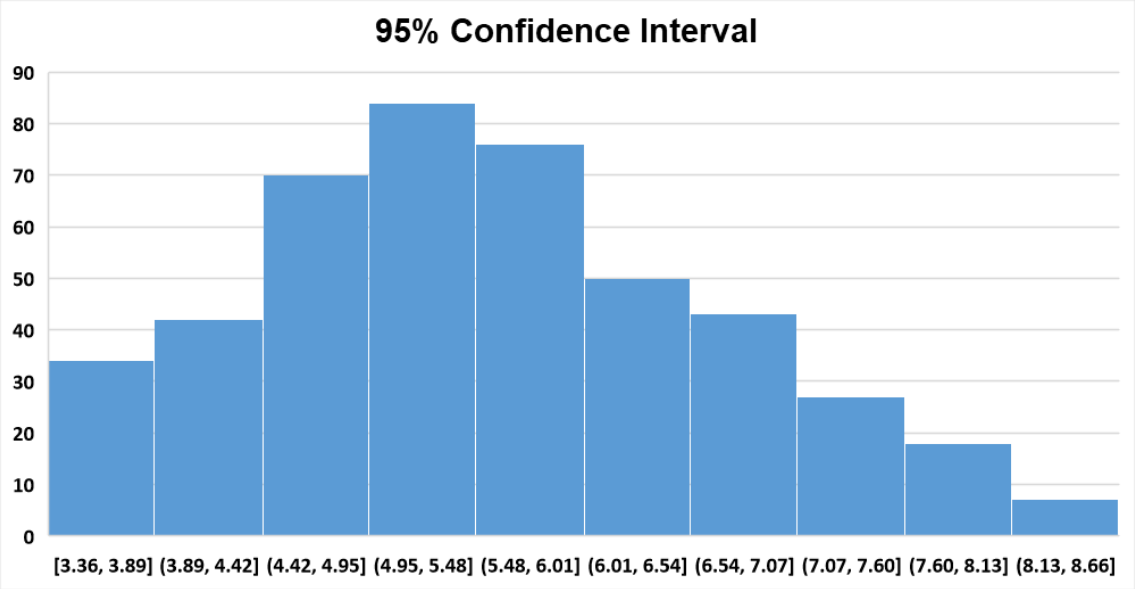

Figure 3-33: 95% confidence interval for difference between turbine wind direction and the mean of the all the turbines of wind farm 2

The results of the effect of wind direction with regards to neighbouring turbines are shown in Figure 3-34.

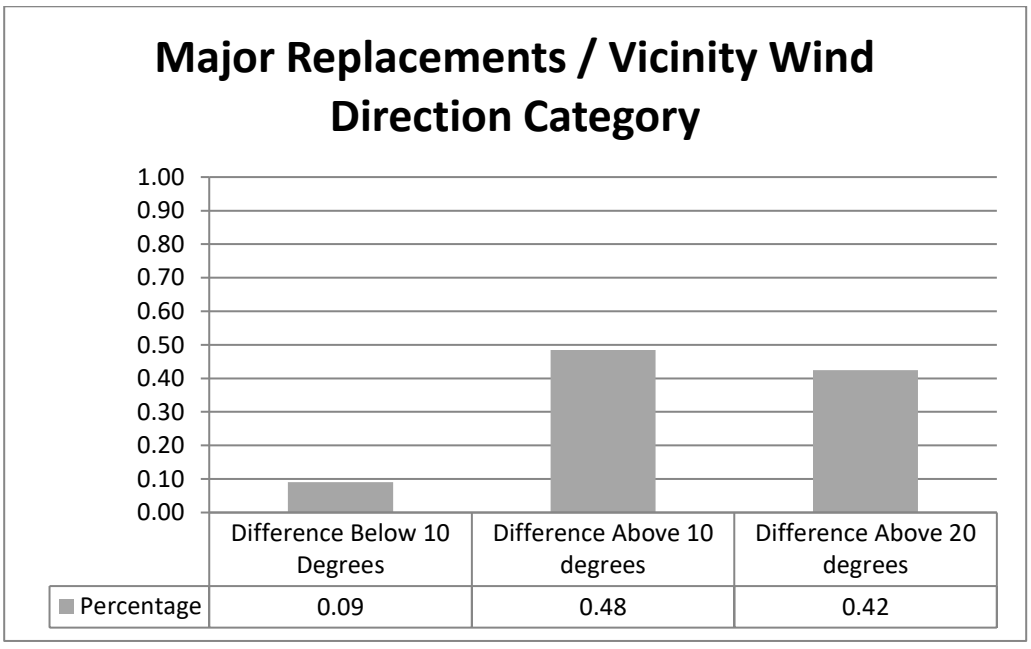

Figure 3-34: Effect of wind direction of neighbouring turbines on major replacement failures

As shown in Figure 3-31, the majority of the turbines that experienced a “major replacement” type of failure had been facing a 10° difference with regards to the mean wind direction of the neighbouring turbines. The percentage of turbines that experienced differences above 20° between the wind direction they were facing and the mean direction that neighbouring turbines were facing remains significant.

Figure 3-35 depicts the 95% confidence interval for wind farm 2, regarding the analysis of the effect of local wind direction conditions on “major replacement” failures.

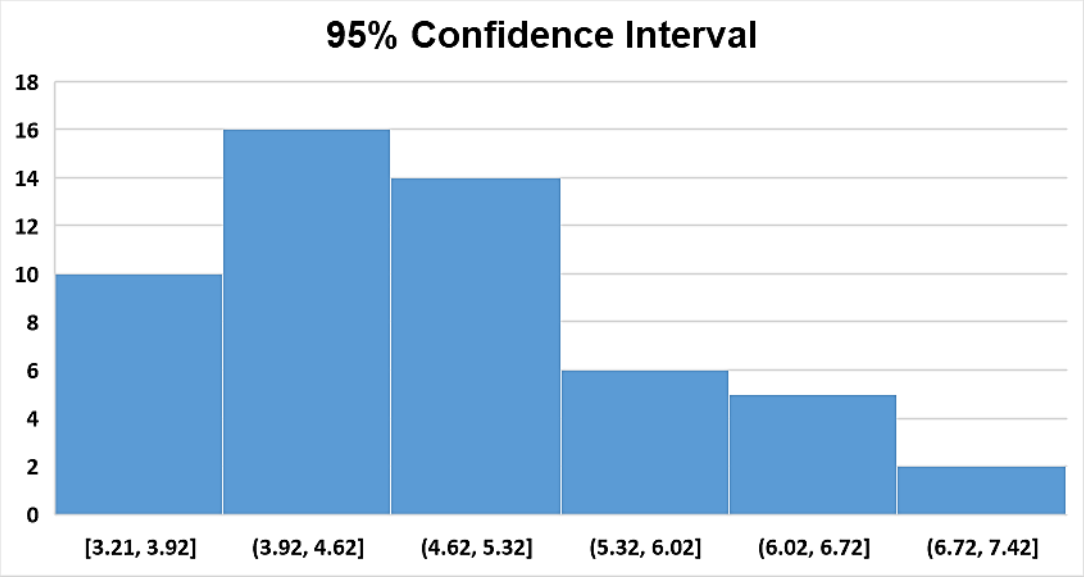

Figure 3-35: 95% confidence interval for difference between turbine wind direction and the mean of the all neighbouring turbines of wind farm 2

The difference between the wind direction of a turbine that experienced a “major replacement” failure and the mean of the all available neighbouring wind turbines for wind farm 2 is 16.48^{0}, which is outside the 95% confidence interval, as depicted in Figure 3-35. This suggests that the turbines with a “major replacement” failure have experienced a significant deviation from the average wind direction of the neighbouring turbines.

3.5.6 Capacity Factor Analysis

In this section, the results of the analysis of the capacity factor of the turbine which experienced a “major replacement” type of failure compared to the average capacity factor of the wind farm are presented. This analysis aims to provide proof that the wind turbines that experienced major replacements were fully operational until the failure occurred. It should be noted that all the turbines that were included in this analysis had a non-zero capacity factor during the period of interest.

3.5.6.1 Site 1

The comparison of the turbines, below mean capacity factor or above which experienced a “major replacement” type of failure compared to the average capacity factor of all available turbines in wind farm 1 is shown in Figure 3-36:

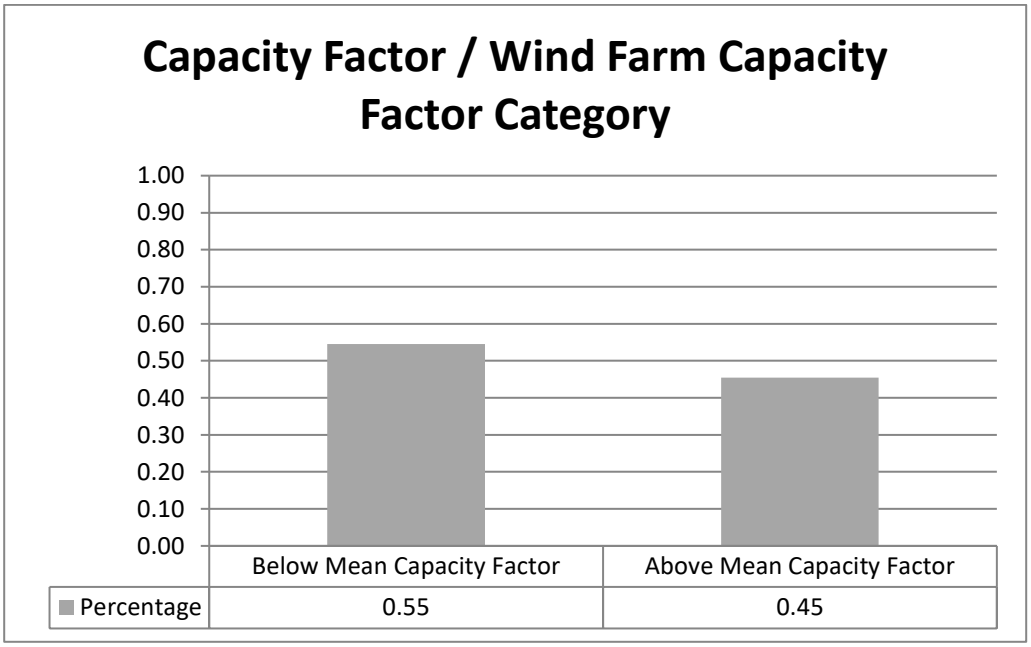

Figure 3-36: Comparison of the capacity factor of all turbines in wind farm 1 with regards to the capacity factor of the turbines which experienced major replacement failures

As can be seen in Figure 3-36, less than half of the turbines that experienced a “major replacement” type of failure displayed a higher capacity factor than the average capacity factor

of wind farm 1, and most displayed a lower capacity factor than the average capacity factor of wind farm 1. All the turbines that experienced a “major replacement” type of failure produced a non-zero value of their capacity factor prior to their failure which means that these turbines were performing properly before the failure occurred.

3.5.6.2 Site 2

The comparison of the capacity factor of the turbines which experienced a “major replacement” type of failure compared to the average capacity factor of all available turbines in wind farm 2 can be seen in Figure 3-37:

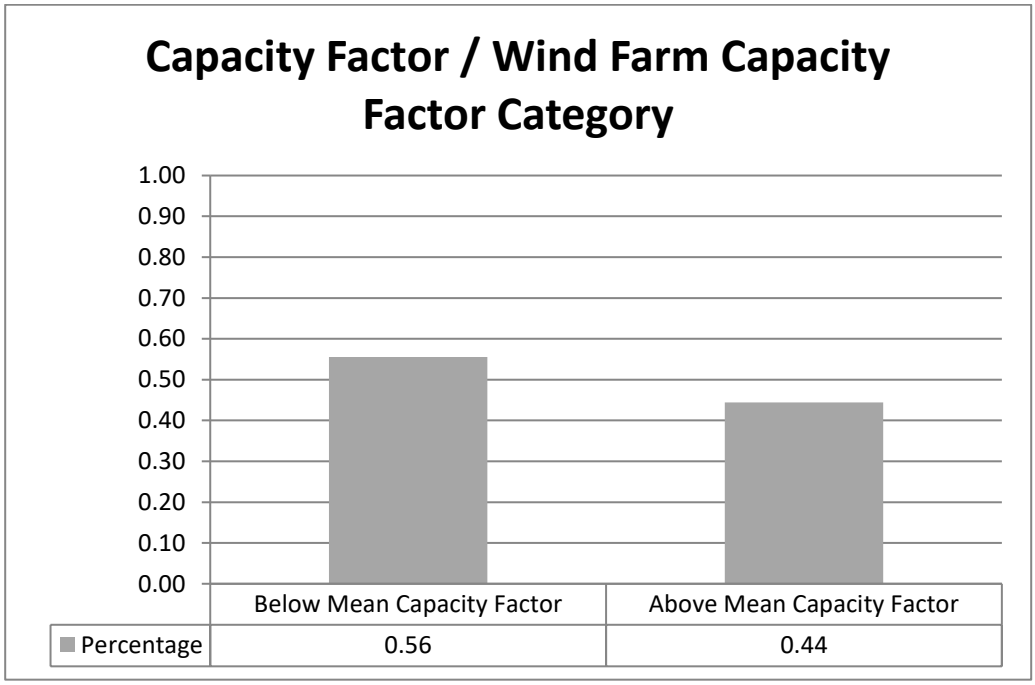

Figure 3-37: Comparison of the capacity factor of all turbines in wind farm 2 with regards to the capacity factor of the turbines which experienced major replacement failures

As can be seen in Figure 3-37, less than half of the turbines that experienced a “major replacement” type of failure displayed a higher capacity factor than the average capacity factor of wind farm 2, and most displayed a lower capacity factor than the average capacity factor of wind farm 2. All the turbines that experienced a “major replacement” type of failure produced

a non-zero value of their capacity factor prior to their failure which means that these turbines were performing properly before the failure occurred.

3.6 Discussion and Conclusion

This chapter has focused on the effect of wind speed, turbulence intensity and wind direction on “major replacement” type of failures for two offshore wind farms, both based in the UK.

Based on the offshore O&M data analysis this chapter answers the research question “how can we ensure reduced O&M costs?”. This chapter concludes that the analysis of offshore O&M data can provide some insights on the relationship between weather conditions and wind turbine failures. The findings of this analysis can be used for the prevention of failures and, consequently, allow for the reduction of O&M costs for offshore wind.

The analysis suggests that the mean wind speed and turbulence intensity are not significant factors which affect “major replacement” type of failures. It should be pointed that this does not mean that wind speed and turbulence intensity do not affect turbine failures. This analysis process has been based on certain assumptions but also on the availability of the SCADA data. This analysis is mainly interested in expensive failures such as drivetrain major replacements. This masks the correlation between all types of failures and the mean wind speed or turbulence intensity. Moreover, the SCADA data provided by the wind turbine manufacturer were three-day averaged data, which do not allow for further analysis of how sudden wind changes (i.e. gusts) affect turbines.

It should be noted that this does not mean that wind speed and turbulence intensity do not affect turbine failures. The number of failures that wind farm 1 has experienced over its lifetime is larger than the number of failures that wind farm 2 has experienced over its lifetime, and the mean wind speed that wind farm 1 has experienced over its lifetime is higher than the mean wind speed that wind farm 2 has experienced over its lifetime. As it is known that higher wind speeds suggest higher loads on turbines which mean higher possibility to experience failures, the average wind speed is one of the inputs that the wind farm controller will consider [19] [20].

The analysis shows that wind direction is an important factor which affects “major replacement” type of failures. It suggests that there is a correlation between wind direction and “major replacement” failures. For site 1, all the turbines with a “major replacement” type of failure have experienced at least a 10° wind direction difference with regards to the wind direction that the other turbines in the wind farm were facing. Moreover, most of the turbines with a “major replacement” type of failure had experienced a severe wind direction difference (i.e. wind direction difference above 20°). These numbers remain significantly high when compared with neighbouring turbines.

Similarly, for site 2, the vast majority of the turbines with a “major replacement” type of failure have experienced at least a 10° wind direction difference with regards to the wind direction that the other turbines in the wind farm were facing. Moreover, most of the turbines with a “major replacement” type of failure had experienced a severe wind direction difference (i.e. wind direction difference above 20°). Wind direction misalignment is another input that the wind farm controller will consider.

Further research is needed to gain more representative results. It should be noted that in this work a set of independent univariate analyses of the wind speed, turbulence intensity and wind direction has been conducted. Future work should include multivariate analysis and the cross-check between the correlation of the independent variables. Future analysis should also include more wind farms, different kind of turbines (i.e. machines from more than one manufacturer) and higher resolution SCADA data (i.e. 10-minute average values). This would allow for a more generalised analysis of how weather conditions affect offshore wind turbines.

Chapter 4 – Wind Farm Modelling

In this chapter, the development of a wind farm simulation model to investigate the effect of a wind farm controller is presented. The developed wind farm model has the following attributes:

1. Wake interactions are captured,
2. Turbulent wind fields are modelled, including the effects on the wake (i.e. dynamic inflow),
3. Permits the modelling of a wind farm comprising a large number of potentially unique wind turbines and
4. State-of-the art wind turbine controllers are included.

A wind farm controller is embedded, which permits investigation of the ability of a control system to improve O&M performance of a wind farm.

4.1 Introduction

At present, wind farms are utilised in a simple way: the constituent wind turbines are controlled as independent entities, with their objectives being simply to maximise energy capture while regulating structural loads. However, future scenarios for UK power generation envisage a substantial penetration of offshore wind energy. Hence, it will no longer be appropriate to operate wind farms in this simple manner.

That is, wind farms will have to provide ancillary services to the grid frequency support, spinning reserve and support to match supply and demand. The wind farms are also developed and designed to maximise the return on investment. To achieve that, ensuring that each wind

turbine is operated with the appropriate trade-off between loading and power production, is essential. For both cases, more flexible wind farm operation is required.

The development of a suitable wind farm model is prerequisite for the design of a wind farm controller. For controller development, the wind farm model should be able to run simulations close to real-time using a desktop PC, while being sufficiently detailed to include key wind turbine and wind field dynamics. The wind farm controller, which acts in response to network inputs, operator inputs and wind turbine inputs, utilises the Power Adjusting Controller (PAC) [1] capability to define the power output of individual turbines to manipulate the total power output of the wind farm.

4.2 Literature Review

The development of a wind farm model for wind farm controller design includes the accurate modelling of a wind farm. The wind farm model contains the wind turbine model, the wind field model, the wake interactions model and the wind farm controller model. In this section, a literature review of all available wind farm models is provided.

There are many published works of varying complexity detailing wind turbine and/or wind farm modelling. Studies focused on the electrical side tend to simplify the aerodynamic and drivetrain parts of a wind turbine model [35] [36] [37] [38] [39]. Similarly, wind energy researchers and mechanical engineers tend to simplify the generator and grid model.

For controller design and development applications, there is a need for the accurate representation of the following aspects:

- Wind field representation,
- Wake interaction,
- Rotor / aerodynamic modelling,
- Drivetrain model and
- Full envelope controller model.

Structural loads depend on the wind field / rotor interaction, so the modelling of the wind field and its interaction with rotor needs to be accurate. Wake modelling needs to be included in order to include the effect of upwind turbines on downstream turbines. Note - wind farm systems can be viewed as vortex systems; thus, upwind turbines are also influenced by the downstream dynamics. However, the computational cost associated with capturing this effect is not warranted by the relatively small improvement in predictive capability. The wake model should also include wake meandering, which affects the wind field downwind. Depending on the purpose of the wind farm model, models of various complexity have been developed.

4.2.1 Wind Field Modelling

To develop a wind farm model, an accurate representation of the ambient wind field is necessary. There are different models that can be used to simulate the wind field, and in this section the most important models will be presented and analysed.

The most widely used method to model three-dimensional ambient wind is the “Sandia method” [40]. This method is based on a method developed by Shinozuka *et al.* [41] and more clearly outlined by Smallwood [42]. Developed by P. S. Veers at the Sandia National Laboratories in the US in the late 1980’s, this model is widely used and is established as an industry standard for wind field modelling. The required inputs for the “Sandia method” are the single point Power Ppectral Density functions (PSDs) and the coherence function.

The basic approach of the Sandia method is to simulate point wind speed time series at different grid points in a plane perpendicular to the average wind flow, and then propagate this time series downstream using the mean wind speed. Veers assumes that Taylor’s frozen turbulence hypothesis is valid. The method’s main limitation is the storage requirements: in order to simulate a time series of length M for N number of points on the rotor plane requires at least as many storage locations. The coherence function is an important input as it describes how turbulence is correlated with spatial separation, mean wind speed and frequency.

An efficient algorithm for the simulation of turbulent atmospheric wind was developed by J. Mann [43]. This method is based on modelling the spectral tensor for atmospheric surface

layer turbulence at high wind speeds. It can be used to simulate two or three-dimensional fields of up to three components of the wind velocity.

The main advantage of this isotropic turbulence model is that it can describe the spectra and cross-spectra well for high frequencies that are relatively small compared to the length scale of the turbulence. The main disadvantages of this isotropic turbulence model are the equality of the variances of the velocity components is not supported by data, and that isotropy implies that the cross spectrum must be zero which is not the case for shear generated turbulence.

4.2.2 Wake Interactions Modelling

There are different models that can be used to simulate wake effects; in this section, the most important models will be presented and analysed. The development of an accurate wake model is very important for the wind industry. In the past 30 years, different approaches have been used to model the wind flow over wind farms. The wake modelling approaches can be divided into the following three main categories:

- Standard wake models,
- Hybrid and analytical wake models and
- Physics-based wake models.

Examples of the standard wake models are the Park model and the Eddy Viscosity model. These models are industry standard models for calculating wake losses. They are based on empirical equations and can be used for small or medium sized wind farms; however, their inability to capture the detailed characteristics affects their applicability to large wind farms.

The Park model was developed by Jensen and is an industry standard for calculating wake losses [44]. It is a simple model which uses an empirical equation based on a balance of momentum to model single wakes. This model neglects the near field behind the generator, where swirling vortices are contributing, and treats the wake behind the turbine as a negative jet. This model assumes an initial velocity deficit just behind the rotor plane which is equal to a third of the freestream velocity ($⅓U_0$), in accordance with classical theory. The wake expansion

depends on the wake decay constant, which is empirically determined. More sophisticated versions of the Park model allow the initial velocity deficit just behind the rotor to be calculated by the wind turbine's thrust coefficient, C_T.

The Eddy Viscosity (EV) model was developed by Ainslie and is an industry standard for calculating wake losses [45]. The EV model is based on a numerical solution of the differential equations governing the flow. The model solves the Reynolds Averaged Navier-Stokes (RANS) equations in axisymmetric (cylindrical) coordinates using several simplifications including a simple eddy viscosity turbulence closure.

The EV model neglects the complex near wake region (approximately 2-4 rotor diameters), where the relaxation of pressure gradients caused by the extraction of energy dominate. Hence, the model is only valid at downstream distances of at least two rotor diameters. The model assumes stationary conditions; furthermore, it assumes that for distances larger than 5 rotor diameters the wake profile is roughly Gaussian and the centreline deficit decays monotonically, with the rate of decay strongly dependent on the ambient turbulence intensity. The momentum deficit is a function of the turbine's thrust coefficient, C_T, and the downstream wake recovery strongly depends on the turbulence generated by the interaction of the wind turbine with the flow (wake shear layer) and the ambient turbulence.

The hybrid wake models are the Deep Array Wake Model (DAWM) model and the Large Wind Farm Model (LWFM) model. The analytical model of wind speed deficit in large wind farms is also a recently developed wake model. These models are all recently developed models for calculating wake losses and achieve acceptable levels of accuracy in close to real time simulations, which makes these models ideal for controller development.

The DAWM was developed by Brower and Robinson [46]. The main incentive for the development of the model is the inability of the standard wake models to consider the two-way interactions between the atmosphere and the turbines.

The DAWM approach is based on the theory developed by Frandsen [47], in which an array of wind turbines is represented as a region of high surface roughness. The roughness imposes drag on the atmosphere, introducing a change in the downstream profile of the planetary

boundary layer. Frandsen's theory assumes that the array of wind turbines is an infinite sea of undifferentiated surface; hence, it does not address the wake effects of individual wind turbines. To overcome this, the DAWM uses empirical equations to describe the growth of Internal Boundary Layers (IBLs) at roughness changes. The IBL growth approach relies on equations describing the downstream effect of roughness changes on the wind profile.

Each wind turbine is assumed to occupy a discrete area of increased roughness. As the wind reaches the wind turbine an IBL is created by the increased roughness. The wind profile of this IBL depends on the wind turbine roughness. As the wind passes the turbine, a second IBL is created, representing the transition back to ambient surface conditions. For the second IBL, the wind profile depends on the ambient roughness. Both IBLs grow with distance downstream.

The LWFM was developed by W. Schlez *et al.* for Garrad Hassan [48]. It is a conceptually similar approach to the DAWM, but the two methods differ in details. The LWFM can be described in the following three steps:

- Use the wind flow model that describes the ambient wind flow over the wind farm site,
- Place the wind turbines in the wind flow and calculate their effect on the ambient flow and
- Use a standard wake model which has as input the corrected ambient wind velocity to calculate the inter-turbine wind effects.

It should be noted that the wind turbine is treated as a disturbance to the ambient roughness, which influences the wind flow. Hence, an IBL grows due to the roughness change from ambient to increased (i.e. wind turbine roughness).

The analytical model of wind speed deficit in large wind farms was developed by S. Frandsen *et al.* [49]. This model handles "regular" array geometries, where the wind turbines are placed in straight rows with equidistant spacing between them. The model uses three different regimes to calculate the wind velocity over the wind farm. In the first regime, the wind turbines experience a multi-wake flow, which is caused from a single row of wind turbines. In the second regime, the wind turbines are exposed, not only to multiple wakes from a single row,

but also to wakes from neighbouring rows; it also corresponds to a change in wind flow caused by roughness change. The third regime is used for “infinitely” large wind farms, where the Planetary Boundary Layer (PBL) is affected from the Coriolis and friction forces.

The physics-based wake models are the Fuga model, the WindModeller and the Advanced Regional Prediction System (ARPS) model. These models are all recently developed models for calculating wake losses and achieve high levels of accuracy. The physics-based wake models can achieve high accuracy of the wind flow, as they consider a greater number of atmospheric parameters, but high accuracy leads to high computational time, which makes physics-based models inappropriate for controller development.

The Fuga model was developed by Ott *et al.* [50]. It is a linearized RANS (or CFD) model, which mimics the full CFD model’s behaviour very well in regions where the perturbations are relatively small (i.e. far field of wakes). Its key advantage is that a linearized model’s computational time can be 10^4 or 10^5 times faster than the corresponding CFD model, depending on the size of the modelled system. The linearization process is completely general, and could be applied to any set of flow governing equations. It should be noted that the Fuga model can only be applied to sites with homogenous terrain (e.g. offshore wind farms).

WindModeller is a RANS model which is based on the commercial ANSYS CFX software. It was further developed by Montavon *et al.* [51], with an addition of an actuator disk to model the wind turbine wakes. This model uses a k-ε turbulence closure, and has some key advantages compared to linearized models, such as accurate prediction of turbulence, better prediction of multiple wake effects and Separation and shade effects due to non-homogenous terrain [52].

The ARPS was developed by a non-hydrostatic mesoscale Numerical Weather Prediction (NWP) and Large Eddy Simulation (LES) model developed at Oklahoma University [53]. To include the effect of wind turbines, an actuator disk is used in the conservation of momentum equation by including a drag force. The PBL parameterization scheme is described by a 1.5-order Turbulent Kinetic Energy (TKE) equation.

4.2.3 Wind Turbine Modelling

The NREL 5MW wind turbine model is one of the most widely used turbine model for wind farm modelling and controller development applications [54]. There have been various publications of wind farm modelling and controller design where the wind turbine model is the NREL machine [55] [56] [57] [58] [59]. In this section, a brief overview of the NREL 5MW turbine model is provided.

The NREL 5MW wind turbine model comprises the following subsystems:

- An aerodynamics model,
- A drivetrain model,
- A generator model,
- A pitch actuator model,
- A turbine control model and
- A tower dynamics block.

The aerodynamics model is a simplified aeroelastic model based on lookup tables (C_P / C_T). Equations 4-1 and 4-2 are the governing static equations for the turbine aerodynamics [57]:

$$M_{shaft} = \frac{1}{2} v_{rot}^3 \rho A C_P(\lambda, \beta) \Omega^{-1} \quad [4\text{-}1]$$

$$F_{tow} = \frac{1}{2} v_{rot}^2 \rho A C_T(\lambda, \beta) \quad [4\text{-}2]$$

where M_{shaft} is the main shaft torque, V_{rot} is the average wind speed over the rotor, ρ is the air density, A is the rotor disk area, Ω is the rotor speed and C_P and C_T are the lookup tables derived from the geometry of the blades with inputs the tip speed ratio (λ) and the pitch angle (θ).

The drivetrain model is a third order model based on two rotating shafts connected through a gearbox. Equations 4-3, 4-4 and 4-5 are the governing equations for the turbine drivetrain dynamics [57]:

$$\dot{\Omega} = \frac{1}{I_{rot}}(M_{shaft} - \varphi K_{shaft} - \dot{\varphi} B_{shaft}) \quad [4\text{-}3]$$

$$\dot{\omega} = \frac{1}{I_{gen}}(-M_{gen} + \frac{1}{N}(\varphi K_{shaft} + \dot{\varphi} B_{shaft})) \quad [4\text{-}4]$$

$$\dot{\varphi} = \Omega - \frac{1}{N}\omega \quad [4\text{-}5]$$

where K_{shaft} is the torsion spring constant, B_{shaft} is the viscous friction, N is the gearbox ratio, ω is the generator speed, M_{gen} is the generator torque, φ is the shaft torsion angle and I_{gen} and I_{rot} are the inertias of the generator and rotor respectively. The generator model is a simple first order model, as shown in Equation 4-6 [57]:

$$\dot{M}_{gen} = \frac{1}{\tau_{gen}}(\frac{P_{ref}}{\omega} - M_{gen}) \quad [4\text{-}6]$$

where τ_{gen} is the time constant of the generator and P_{ref} is the power reference. The pitch actuator model is a second order model, described by Equations 4-7 and 4-8 [57]:

$$\ddot{\beta} = \frac{1}{\tau_{\beta}}\left(u_{\beta}^{\lambda} - \dot{\beta}\right) \quad [4\text{-}7]$$

$$u_{\beta} = K_{\beta}(\beta_{ref} - \beta_{meas}) \quad [4\text{-}8]$$

where β is the pitch angle, τ_{β} is the time constant, λ is the input delay from input u_{β}, is the pitch rate and K_{β} is the proportional regulator controlling the actuator.

The control strategy can be divided into two regions, the partial load operation and the full load operation. For the partial load case, the controller is a simple lookup table; the generator speed is the input and the generated power is the output. For the full load case, the generator speed remains constant and the rotor speed is controlled by blade pitching. Blade pitching is controlled by a non-linear PI controller. Finally, the tower dynamics are modelled as a second order model, as shown in Equation 4-9 [57].

$$\ddot{z} = \frac{1}{m_{tow}}(F_{tow} - K_{tow}z - B_{tow}\dot{z}) \quad [4\text{-}9]$$

where z is the tower deflection which is modelled as a spring-damper system with spring constant K_{tow} and damping B_{tow}.

4.2.4 Wind Farm Modelling

In the past decades, there has been increased interest in modelling of wind farms for power optimization purposes. A study by Heer *et al.* examined the maximization of the power output of wind farms by considering wake effects [55]. This approach was based on deriving one single parameter that captures the power coefficient of the wind farm. The total power coefficient is not wind speed dependent and depends only on the wind speed deficit. The wind farm modelling is based on the well-known wind farm simulators FAST [60] and the Aeolus SimWindFarm toolbox. The wind turbine model used is a simplified state space representation of the NREL 5MW, and the wake model is based on standard Park model. The optimization is based on the development of a Model Predictive Controller (MPC) controller which allows for decreased fatigue loads whilst tracking the optimal reference values. This research claims to achieve 1% increase in energy capture, but the energy gain depends greatly on the wake model and the Park model is not able to accurately capture wake deficits in large wind farms.

The SimWindFarm toolbox is a Simulink based, open source wind farm simulation model developed in the EU-FP7 project, Aeolus [57]. The main objective is to provide a publicly available simulation package for researchers developing wind farm level control solutions. The toolbox allows the user to define the wind turbine model, the number of wind turbines and the

position of each turbine in the wind farm. The wind turbine model used is the NREL 5MW model. The ambient wind field is created using the “Sandia method”. The wake deficit calculations depend on whether the user has chosen the Taylor’s frozen turbulence hypothesis to be valid or not [61]. If Taylor’s frozen turbulence hypothesis is assumed to be valid, the wake deficit model used is the Park model; otherwise, the analytical model of wind speed deficit in large wind farms is used.

Spudic *et al.* developed a wind farm model for power optimization purposes. A hierarchical [58] wind farm control approach was utilised to maintain the required wind farm power reference and reduce the structural loads of the wind turbines. The NREL 5MW model was used. The power output of the wind turbines was curtailed such that there was a reserve to provide enough droop for power adjustments. The wind farm controller strategy was, by design, only feasible for above rated operation.

Biegel [59] proposed a wind farm controller to minimise the structural loads on the wind turbines while tracking the reference power. The wind farm model consists of 6 turbines and was developed by using the SimWindFarm toolbox. The controller objectives were achieved for above rated wind speed operation only.

4.3 Research Opportunities

Most papers encountered in literature that investigated the development of wind farm controller applications have used simple models to represent the turbine, wind field and wake interactions. Depending on the type of the research, some studies used simplified models for the wind farm representation or the simplified models for the power system representation. A study by Poushpas [62] has created a high accuracy level wind farm model, but the maximum number of turbines used in this research is 50. Moreover, the aero-mechanical system was analysed in isolation; thus, a thorough investigation of the impact of the wind farm controller strategies to provide ancillary services to the power system operator was not possible.

This is identified as an area for further research. The novelty of this work is that compared to previous studies, the number of wind turbines in the wind farm model could be as high as 100, which allows for an accurate representation of modern onshore and offshore wind farms. The

wind farm model can represent the key complex dynamics of the wind turbines, wind field and wake interactions. The developed wind farm controller has a highly decentralised design, which has been shown to not introduce any significant additional feedback in the system, which makes the controller simpler to implement and tune. The wind farm controller acts in response to power system (i.e. network wind farm controller), operator and wind turbine inputs, whilst considering the Operation & Maintenance (O&M) data analysis. The investigation of the capability of the wind farm controller to provide ancillary services to the power system operator is investigated thoroughly in Chapter 7.

4.4 Wind Farm Simulation Model

The wind farm simulation model is based on the work of Poushpas [62]. The wind farm model consists of wind turbine models including the PAC, a wind field model, a wake interactions model and a wind farm controller model with various functionalities. In this section, an overview of the complete model is provided.

4.4.1 Wind Turbine Model Overview

The wind turbine model used in this study is the Simulink model of the Supergen 5MW Exemplar wind turbine [63]. Each turbine model includes a representation of dynamic inflow, key structural dynamics, a full envelope controller and a PAC.

4.4.1.1 Power Adjusting Controller Overview

The PAC is a generic type of controller, which allows the generated power of an individual wind turbine to be modified. This is achieved by regulating the difference between the generated power and the power available in the wind, to track an externally provided set point. By adjusting this set point (ΔP), the power output of each wind turbine can be manipulated as the operator requires [64]. The PAC is configured as a jacket around an existing full envelope controller without any modification to the wind turbine's full envelope controller, as shown in Figure 4-1 [64]. Hence, the PAC can be used on a large range of wind turbines.

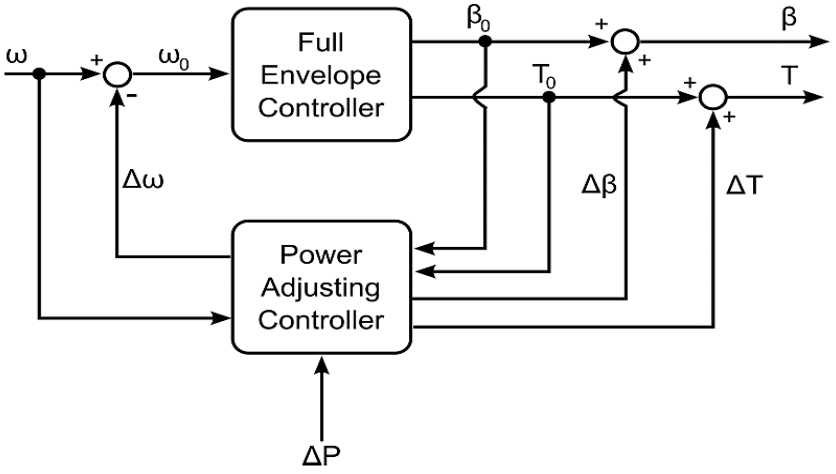

Figure 4-1: The power adjusting controller

The PAC alters the power output of a wind turbine by a set point ΔP. The input ΔP is provided externally, allowing the PAC to set the values of Δω, ΔT and Δβ independently from the current state of the wind turbine. This means that the controller does not contain any feedback. To achieve the change in power output, the wind turbine needs to move away from the normal operating curve. In above rated operation, this is achieved by adjusting the torque demand by an increment (ΔT). The full envelope controller regulates the rotor speed through pitch action, so the change ΔT is counteracted by a change in pitch angle. This allows for the power output to be altered whilst the rotor speed is controlled.

In below rated operation, the generator torque demand is used by the full envelope controller to regulate the rotor speed. Changes in wind speed which cause deviations in rotor speed are thus handled by changes in the torque demand. The implication of this is that an external request to reduce power by adjusting the torque demand must ensure that its effect on the rotor speed is hidden, so that the full envelope controller takes no action. To achieve this, the PAC produces a dummy signal, Δω. Δω is the change in generator speed caused by the use of the PAC. To decrease power output, pitching the blades results in a reduction in aerodynamic torque, which consequently reduces the generated power. Hence, a value for the change in pitch angle Δβ is requested. To increase power output, there is no pitch angle that allows the aerodynamic torque to match the generator torque. Hence, positive ΔP values can only be provided for a limited period of time, when operating in below rated conditions.

Assuming a constant wind speed, an example of the reduction of power in below rated operation is depicted in Figure 4-2 [64]. The generator torque is reduced by ΔT from point A to point B. This creates a difference between the aerodynamic torque of the rotor and the generator torque. Hence, the rotor speed increases towards point D while the generator speed increases towards point C. A change in the pitch angle, Δβ, changes the aerodynamic torque, and allows the aerodynamic operating point to return back to point B.

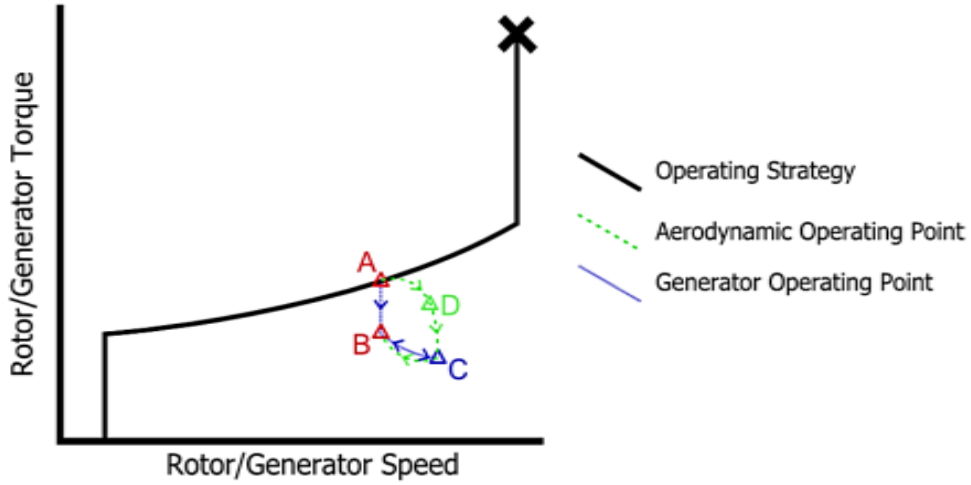

Figure 4-2: Movement of the operating point on the Torque-Speed plane

The PAC is operating under a set of supervisory rules [64]. These rules are a set of limits and flags designed to ensure that the turbine is safely operating within a predefined safe operating envelope on the torque – speed plane, as illustrated in Figure 4-3. These flags are utilised by the wind farm controller to ensure the safe operation of the wind turbines. As can be seen in Figure 4-3, the PAC operates under traffic light supervisory rules. When the turbine state is in the green / amber / red region, the corresponding GREEN / AMBER / RED flag is set by the PAC. The allowed operational region for the turbines is defined by the wind farm controller. The black boundary is the maximum limit that the turbine can be allowed to reach. Once the turbine's operational point reaches the black boundary, the PAC is turned off and the turbine is requested to recover to normal operating conditions. The PAC has also the ability to provide wind speed estimations, based on a reformulation of BEM theory [64]. It should also be noted

that the PAC is not specifically designed for the 5MW Supergen wind turbine; it has also been validated on the 2MW Supergen wind turbine [65].

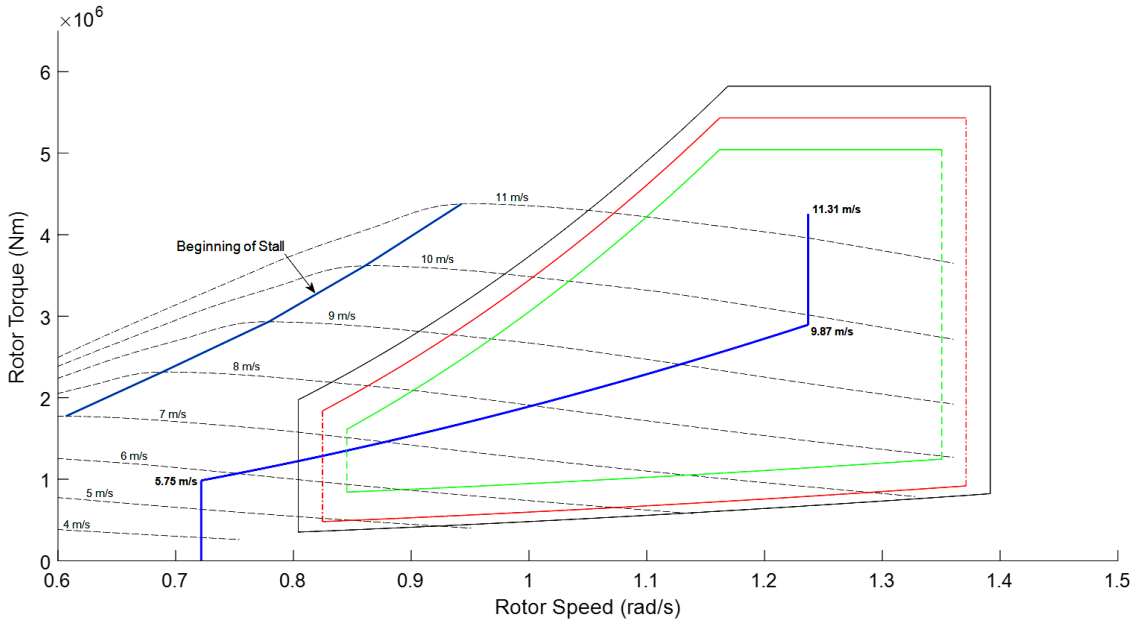

Figure 4-3: Operational strategy and PAC limits for the Supergen 5MW wind turbine

4.4.1.2 Supergen 5MW Wind Turbine Overview

The wind turbine model used in this study is the Simulink model of the Supergen 5MW Exemplar wind turbine [63]. The Supergen wind turbine is chosen as it is a with high fidelity model, suitable for fast simulation and controller design purposes [1] [62]. The Supergen 5MW turbine model has a similar structure to the NREL 5MW turbine model. The NREL 5MW turbine is a simplified turbine model to the Supergen 5MW model, and consequently its capability to simulate the complex turbine dynamics required to assess the performance of an offshore wind farm controller under various operational conditions is limited [62]. The Supergen 5MW wind turbine model is a non-linear Simulink model with parameters design to correspond to a 5MW Horizontal Axis Wind Turbine (HAWT). The turbine model includes a non-linear rotor/wind interaction dynamic model, a full envelope controller and a Power Adjusting

Controller. The turbine dynamic modes included are two blade modes, two tower modes, actuator dynamics and a simplified two mode drivetrain model [62]. The wind turbine is also equipped with a spatial filter used to generate the rotor effective wind speed [66] [67]. The operational strategy of the Supergen 5MW turbine is shown in Figure 4-3.

4.4.1.3 Dynamic Inflow Model Development

This section describes the design and development of an improved dynamic inflow model to be used for the Supergen 5MW wind turbine model. Dynamic inflow modelling is an important aspect of wind turbine modelling. There is a lag between the changes to the blade loading and the effect of the induced flow field. This lag can significantly impact the aerodynamic torque and thrust. The Supergen 5MW wind turbine model and the PAC have been equipped with a dynamic inflow model. For this model, the thrust coefficient local to the rotor is calculated using Equation 4-10 [64].

$$\hat{C}_T(\lambda_R, \beta) = \left(\frac{V_\infty}{V_R}\right)^2 C_T\left(\frac{\lambda_R V_R}{V_\infty}, \beta\right) = \frac{4\alpha_s(\lambda_R, \beta)}{1 - a_s(\lambda_R, \beta)} \quad [4\text{-}10]$$

where $\hat{C}_T$ is the reformulated thrust coefficient local to the rotor, λ_R is the tip speed ratio (relative to wind velocity at the rotor), β is the actual blade pitch angle, V_∞ is the wind speed far upstream from the rotor, V_R is the wind speed at the rotor, C_T is the thrust coefficient and α_s is the steady state induction factor.

The same approach can be used to calculate torque and power in terms of the local conditions at the rotor. An interpretation of standard BEM theory is that it is assumed that the rate of change of momentum in the upstream flow field is due to half the thrust applied by the rotor. In the context of the reformulation of BEM locally to the rotor, the standard BEM assumption regarding the rate of change in linear momentum is extended to the unsteady state situation [64],

$$\dot{V}_R = \frac{3\pi}{4R}(V_A - V_R)V_R - \frac{3\pi}{16R}V_R^2\hat{C}_T(\lambda_R, \beta) \quad [4\text{-}11]$$

where $\dot{V}_R$ is the rate of change of wind speed at the rotor, R is the rotor radius and V_A is the wind speed at the position of the rotor in its absence. Using Equation 4-10, Equation 4-11 may be expressed as follows [1]:

$$\dot{\alpha} = \frac{\dot{V}_A}{V_A} - \frac{\dot{V}_A \alpha}{V_A} + \frac{3\pi}{4R} V_A \left(\frac{(1-\alpha)}{(1-\alpha_s)}\right)(a_s - a) \quad [4\text{-}12]$$

where $\dot{\alpha}$ is the rate of change of the induction factor, α is the induction factor, $\dot{V}_A$ is the rate of change of the wind speed at the position of the rotor in its absence and V_A is the wind speed at the position of the rotor in its absence.

The section of fluid contributing to the change of linear momentum in this additional contribution extends upstream and downstream from the rotor. The section of stream tube involved cannot be made local to the rotor by choosing it to be short. Consequently, the wind speed in the absence of the rotor is not simply $V_{A,}$ but varies over the section of stream tube. Hence, the variation in V_A over this section of stream tube can be ignored; that is, the non-strictly locality to the rotor can be ignored. Hence, Equation 4-12 becomes,

$$\dot{a} = \frac{3\pi}{4R} V_A \left(\frac{(1-\alpha)}{(1-\alpha_s)}\right)(a_s - a) \quad [4\text{-}13]$$

Older versions of the Supergen 5MW wind turbine model [62] [64] use the simplified Equation 4-13. The turbine model used in this study is using the more accurate and realistic dynamic flow model, as described by Equation 4-12.

4.4.2 Wind and Wake Model Overview

The wind field and wake models have been developed by Poushpas [62]. In this section, a brief overview of the wind field model and wake interaction model is provided.

4.4.2.1 Wind Field Model Overview

The wind field is created using the "Sandia method" [40], as described in section 4.2.1, and is an industry standard method to model three-dimensional ambient wind. The method provides three-dimensional turbulence time series and is based on the work by Poushpas [62]. The wind field model creates low frequency correlated time series at the position in the longitudinal direction to represent a single point wind speed time for each turbine, and correlated time series of turbulence for the lateral direction. The high frequency turbulence components of the wind field are generated locally at the rotor using the Dryden spectrum. The high frequency components are randomly generated between two low frequency components, while keeping the correct spectrum.

All the wind field time series are generated offline and saved in files to be used later during the simulation, which significantly reduces computational time. The longitudinal turbulence component is the wind speed used by the wind turbine model. The lateral turbulence component is used to calculate wake meandering by iteratively estimating the centre position of an upwind turbine's wake.

4.4.2.2 Wake Model Overview

The wake model is based on the work by Poushpas [62] and includes the calculation of the wake centre, diameter and deficit. The wake deficit and diameter modelling are based on the analytical model of wind speed deficit in large wind farms, developed by S. Frandsen *et al.* [49], as described in subsection 4.2.2. The model calculates the effect that single or multiple upwind wakes have on the wind confronting a wind turbine, depending on the turbine's position in the wind farm. The single wake model assumes that the wake is produced from one upwind turbine. The multiple wake model includes the wake effect from multiple upwind turbines, after identifying the upwind turbine wakes that are affecting the turbine under consideration.

Wake meandering can be described as the large-scale movement of the entire wake downwind. The wake is assumed to be axisymmetric with a central point as its reference. The wake meandering is modelled as being solely the movement of the wake centre due to the effect of the lateral turbulence component of the wind field.

4.4.3 Wind Farm Controller Model Overview

The wind farm controller under development is a highly decentralised controller. This type of controller has many advantages, the most important of which is simplicity of implementation and design since the different tasks are separated. An illustration of the wind farm controller is shown in Figure 4-4:

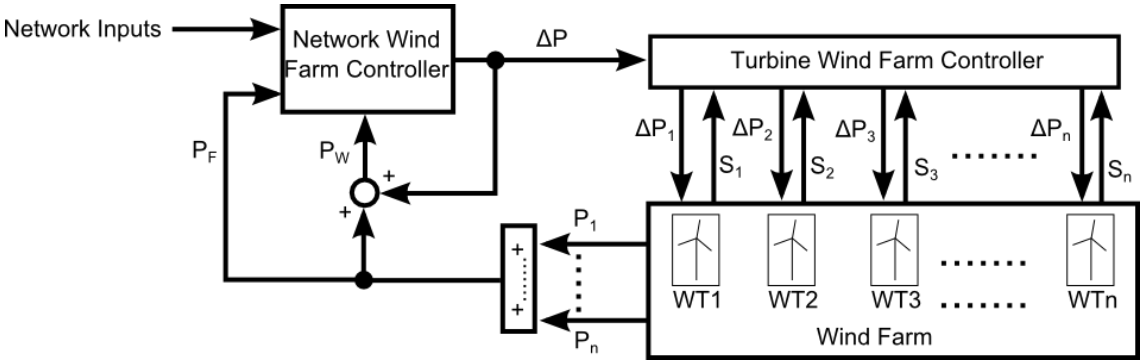

Figure 4-4: Wind farm controller overview

The wind farm controller inputs can be divided into two main categories, network wind farm controller inputs, and wind turbine inputs.

The wind farm controller outputs individual ΔP control signals to the turbines that are expected to provide the requested total power change required by the network wind farm controller.

4.4.3.1 Network Wind Farm Controller Inputs Overview

The wind farm controller can receive the requested total ΔP signal either from the wind farm operator or directly from the grid-side network wind farm controller. The grid-side network wind farm controller is designed to mimic the response of a synchronous generator to any frequency fluctuations of the grid, as explained in Chapter 6. The wind farm side of the network controller ensures the prioritization of the network controller signals over the wind farm operator signals.

The controller assumes the flexibility of the system operator to request a decrease in power output from the wind farm operator for droop control or due to network / line restrictions. The wind farm operator then receives the total output reduction and the wind farm controller ensures that the requested power reduction is achieved and maintained. The system operator can request an increase in power production, but such actions are not recommended as the turbines normally output the maximum power available and an increase could lead to excessive loading of the turbines. An increase in power output is only acceptable when the grid frequency reaches its marginal limits, as the grid stability takes priority.

The grid-side network wind farm controller follows the response of a synchronous generator and if the grid frequency at the point of common coupling reaches a pre-defined boundary the grid-side network wind farm controller signals the wind farm side network controller with a request in total ΔP. In this case, as the grid frequency has reached the accepted limits, all the available wind turbines are requested to provide the requested ΔP and improve grid stability.

4.4.3.2 Wind Turbine Inputs Overview

The wind farm controller accepts and considers inputs from the wind turbines. The PAC inputs to the wind farm are listed below:

- Wind speed estimation,
- Traffic light flags,
- Rejection flags and
- Recovery complete flags.

The wind speed estimator is used to prioritise the turbines to be used. As explained in subsection 3.6, higher wind speeds lead to increased failure rates; consequently, the turbines that are experiencing higher wind speeds are the ones to be asked to reduce their power output when necessary. This leads to load reduction on these machines, thereby improving reliability/availability.

The traffic light flags are used to ensure that the turbines are operating within acceptable boundaries. The rejection flags are used to check if the requested ΔP control signal is accepted

from the wind turbine. If the rejection flag is on, the turbine is unavailable to provide the requested ΔP. That could happen for two reasons: either the turbine has reached the maximum acceptable boundary set the PAC; or the turbine is operating at a low wind speed (i.e. operating at wind speeds lower than the PAC wind speed operating limit of 6.5ms^{-1}), in which case the turbine is already producing low levels and the energy capture is too low to achieve any level of sensible practical performance.

The recovery complete flags are provided from the PAC and allow the wind farm controller to check which turbines have completely recovered and can be used again to provide the requested ΔP. The wind farm controller also includes maintenance flags which are provided from the turbines. The maintenance flag allows the wind farm controller to check which turbines are unavailable to provide the ΔP, as they are not operating due to maintenance. After the prioritization of the wind turbines, the controller checks the type of priority and redistributes the total requested ΔP to the turbines.

4.4.4 Wind Farm Controller Design Strategy

The wind farm controller is designed to achieve the required ΔP change by dispatching control signals to the wind turbines. The controller functionality can be divided in three major categories: signal supervising; wind turbine availability and prioritization; and power dispatch.

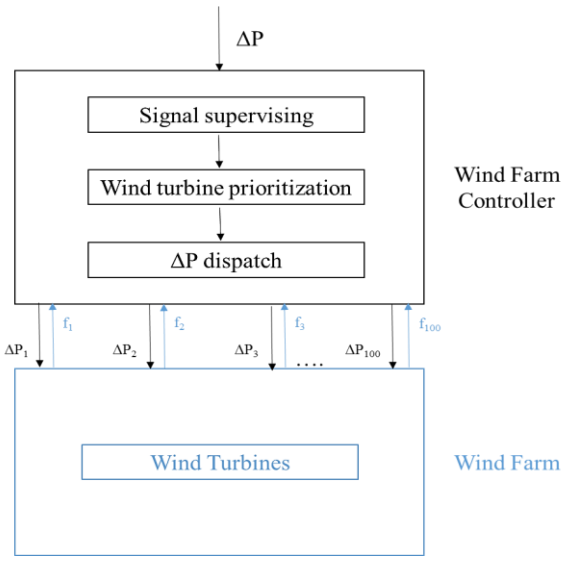

Figure 4-5: Wind farm controller functionalities overview

An illustration of the arrangement of the functionalities of the wind farm controller is provided in Figure 4-5. Since only flags produced from the PAC are used for dispatching the requested ΔP between the wind turbines, no feedback loop between the wind farm controller and the individual turbines is created.

4.4.4.1 Signal Supervising Strategy

The signal supervisor is used to define the type of the requested change in power, ΔP. There are two main types of response to a ΔP input. The first one is the low priority request, which is used for wind farm operator requests (i.e. droop control). In this case, the safe operation of the wind turbines is the highest priority. The wind farm operator is sometimes requested to decrease the power output of the wind farm due to power line restrictions, or the request of the system operator to provide spinning reserve (i.e. normal values 5% - 10% of the maximum available power) [68]. The second type of response is the high priority request, which is used for the network wind farm controller (e.g. synthetic inertia event). In this case, the power system stability takes priority to the wind farm assets. Figure 4-6 illustrates the flowchart of the control algorithm for the signal supervisor.

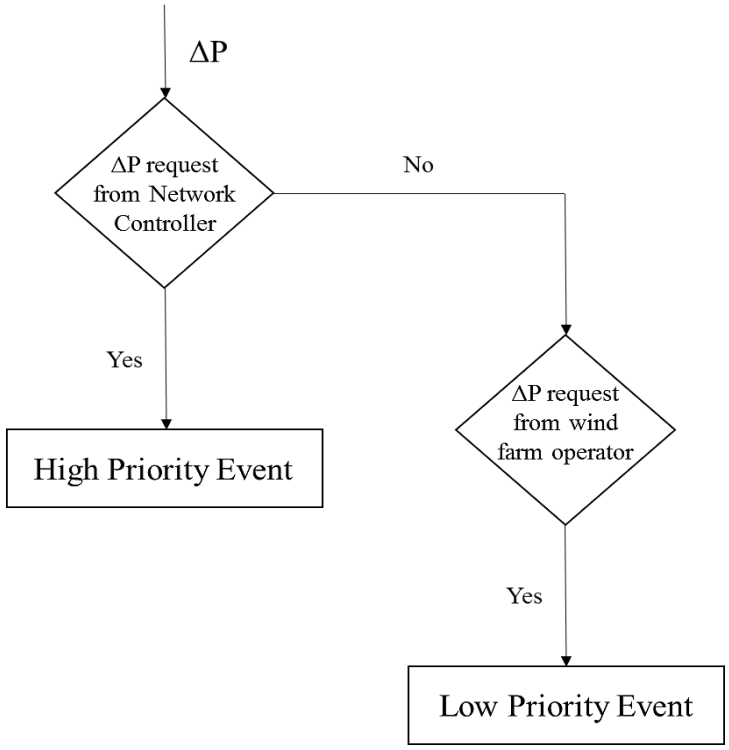

Figure 4-6: Flowchart of the control algorithm for the signal supervisor

It should be noted that the wind farm operator can request a high priority change in power, but such action is not recommended as it will increase loading on the turbines, which will eventually lead to increased failure rates and decreased turbine availability.

4.4.4.2 Wind Turbine Availability and Prioritization Strategy

The wind turbine availability and prioritization function of the wind farm controller is used to choose the turbines to be used to provide the requested ΔP. The determination of unavailable turbines is the first task. All the turbines that are not operating because they are under maintenance are defined as unavailable and cannot be used to provide the requested change in power. For high priority cases, only the unavailable and turbines with the rejection flag ON are excluded from providing ΔP. The flowchart of the control algorithm for the high priority availability and prioritization function of the wind farm controller is illustrated in Figure 4-7:

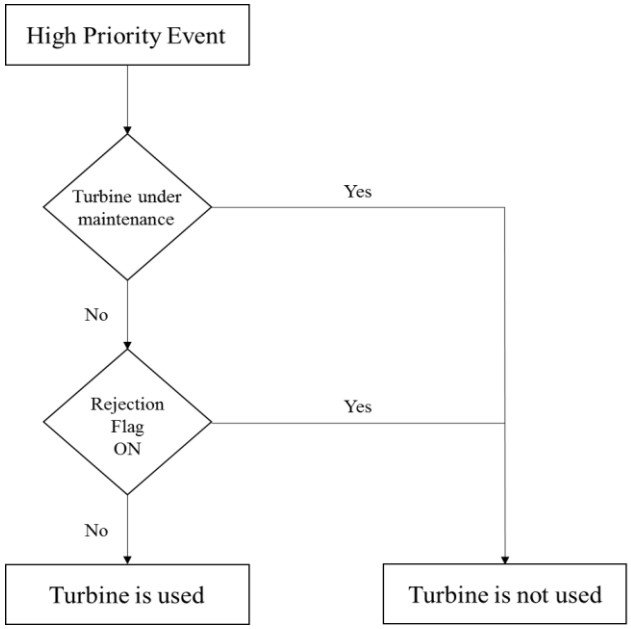

Figure 4-7: Flowchart of the control algorithm for the high priority availability and prioritization function of the wind farm controller

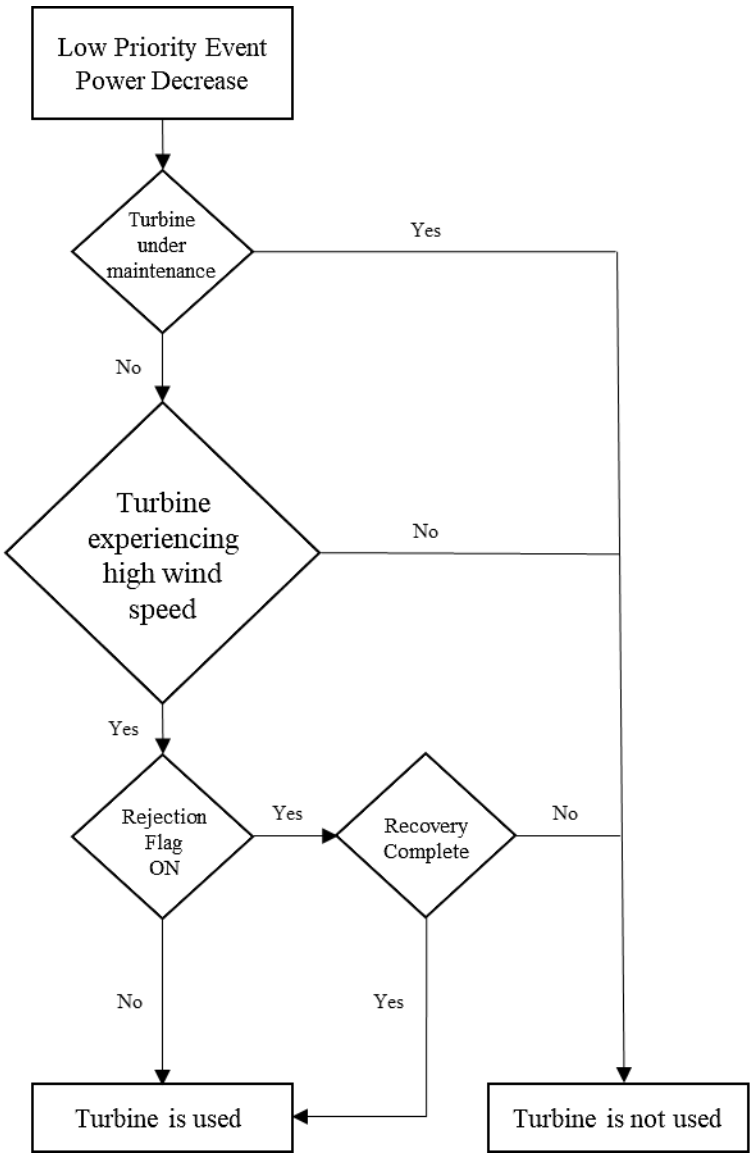

Figure 4-8: Flowchart of the control algorithm for the low priority and negative ΔP availability and prioritization function of the wind farm controller

For low priority cases, the controller prioritizes the turbines that will be used based on O&M and the status of the turbines. The controller also allows for flexible definition of the value of the percentage of turbine utilization, which are the turbines experiencing high wind speeds at the time of the power change request, to provide the required ΔP. In both cases, the reason is to decrease the loads these turbines are experiencing and, consequently, decrease the failure rates and protect the wind turbines. The controller checks the rejection flag to ensure that the

turbines can provide the requested ΔP; if the rejection flag is ON, the controller does not make use of the turbine until said turbine has fully recovered. Figure 4-8 illustrates the flowchart of the control algorithm for the low priority and negative ΔP availability and prioritization function of the wind farm controller.

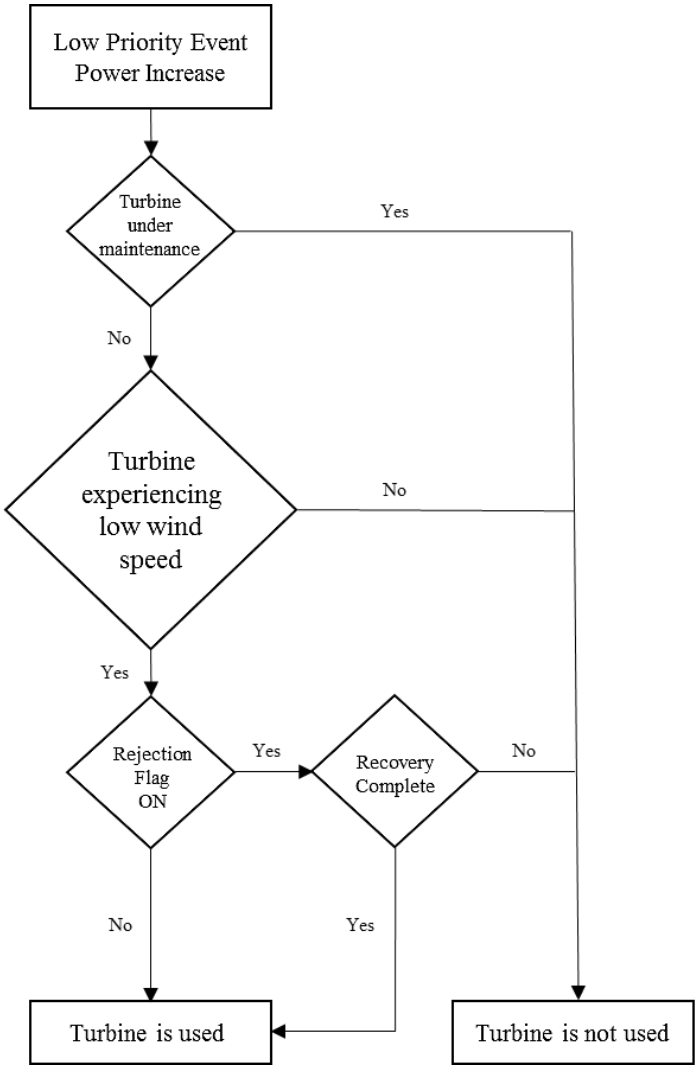

Figure 4-9: Flowchart of the control algorithm for the low priority and positive ΔP availability and prioritization function of the wind farm controller

Similarly, if an increase in power is requested, the controller prioritizes a percentage of the turbines that are experiencing low wind speeds. The controller also allows for flexible definition of the value of the percentage of turbine utilization, which are the turbines

experiencing lower wind speeds, to provide the requested ΔP. The controller checks the rejection flag to ensure that the turbines can provide the requested ΔP, and if the rejection flag is ON the controller does not make use of the turbine until the turbine has fully recovered. Figure 4-9 illustrates the flowchart of the control algorithm for the low priority and positive ΔP availability and prioritization function of the wind farm controller.

4.4.4.3 Power Dispatch Strategy

The power dispatch of the total requested ΔP to individual turbines is performed immediately after the prioritization of the wind turbines to be used is finished. Once the turbines to be used have been selected, the controller simply dispatches the total power change to the individual turbines. If the number of the available turbines decreases, i.e. a rejection flag changes to ON, then the controller increases the ΔP request for the remaining machines; furthermore, if a wind turbine recovers (i.e. selected turbine fully recovers) and is ready to provide a power change gain, then the controller decreases the ΔP request from the available wind turbines.

4.5 Wind Farm Model Simulation Results

In this section, the results of the simulation of the wind farm model are presented. The wind farm consists of 10 wind turbines which are positioned as shown in Figure 4-10.

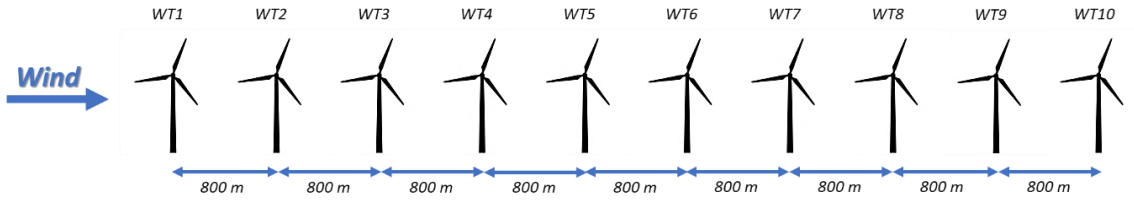

Figure 4-10: Wind farm layout

The simulations are used to assess the response of the wind farm controller to various power output request cases, whilst investigating the potential of the wind farm controller to provide ancillary services to the power system operator. The wind farm model is simulated for 3000s

for different mean wind speeds with 10% turbulence intensity. The model has been tested under three different mean wind speed scenarios: below rated, rated and above rated.

4.5.1 Testing of Updated Dynamic Inflow Model

The updated version of the dynamic inflow model, as described in 4.4.1.3, is created for the Supergen 5MW wind turbine model. The model has been tested against the previous version, in order to check whether the differences to the previous, simplified, dynamic inflow model version [64] [62]. The testing model is based on a single turbine, which is simulated for 800s at $8ms^{-1}$ mean wind speed. The wind farm operator requests for a total power reduction of 0.5MW to be provided for a total of 650s (i.e. between 150s – 800s). Figure 4-11 shows the effect of the two dynamic inflow models to the power output of the wind turbine model for constant wind speed of $8ms^{-1}$.

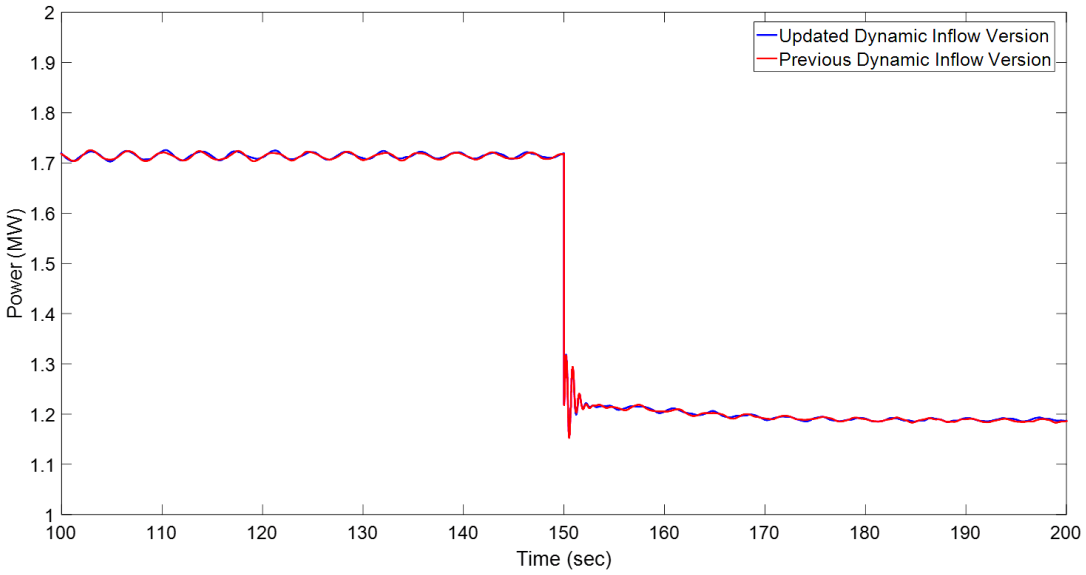

Figure 4-11: Comparison of dynamic inflow models for constant wind speed

As can be seen in Figure 4-11, both dynamic inflow models exhibit near-identical responses to the requested ΔP. This is expected as the wind speed is constant, so the terms regarding the rate of change of wind speed at the rotor of the updated version (i.e. Equation 4-12) are equal

to zero, which leads to the simplified older version (i.e. Equation 4-13) of the dynamic inflow model. Figure 4-12 shows the effect of the two dynamic inflow models to the power output of the wind turbine model for time-varying wind speed.

As can be seen in Figure 4-12, the two dynamic inflow models exhibit different responses. The updated version, which considers the rate of change of the wind speed at the position of the rotor in its absence, is illustrating a lag with respect to the older version. The updated version also appears to provide smoother results, which is expected, as the effects of the dynamic inflow model do not happen instantaneously, but occur over time.

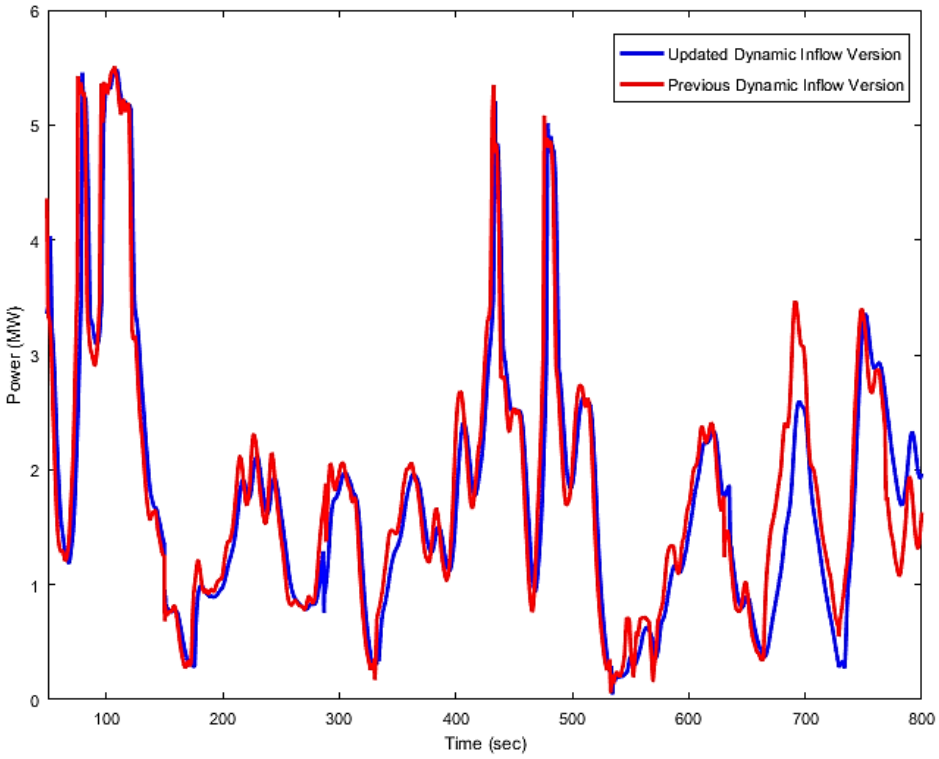

Figure 4-12: Comparison of dynamic inflow models for varying wind speed

4.5.2 Droop Control Simulation Results

For conventional power systems, with interconnected synchronous machines, frequency and active power are closely related. A load decrease implies the load torque decreases; if the mechanical torque acting to accelerate the prime mover does not change, naturally the rotational speed of the prime mover will increase. This leads to an increase in the AC frequency. The frequency fluctuations with a load change is what droop control is trying to remove. Synchronous generators are directly connected to the power system and use the governor to provide droop control.

Modern wind turbines are controlled in such a way that they do not provide droop control the same way a conventional power plant does; typically, only voltage support is provided. To provide primary response, wind farms are required to operate in curtailment, with 3% - 5% power reserve at any wind speed [69]. The wind farm controller is able to provide the required curtailment, whilst protecting the turbines that are more likely to experience a failure.

4.5.2.1 Below Rated Wind Speed Conditions

The wind farm model is simulated for 3000s at 8ms^{-1} mean wind speed with 10% turbulence intensity. The wind farm operator requests for a total power reduction of 5%, relative to normal operation, to be provided for a total of 1500s (i.e. between 1500s – 3000s). As this signal is not received by the network controller, it is assumed as a low priority request. Hence, the wind farm controller prioritizes the wind turbines and ensures that only some of the available machines, in this case 70%, are utilised to provide the requested power reduction. As explained in section 4.4.4.2, the turbines that are facing high wind speeds will be prioritised to reduce their power output, so as to reduce their mechanical loading. The comparison between the total power output of the wind farm under normal operation, the total power output of the wind farm under curtailed operation and the requested curtailment is shown in Figure 4-13. As can be seen in Figure 4-13, at 1500s the operator requests a curtailment of power production equal to 5% of normal production. To provide the required power reduction, the controller gradually decreases the total power; limitation to the rate of change of power is utilised to minimise shocks on the wind turbines.

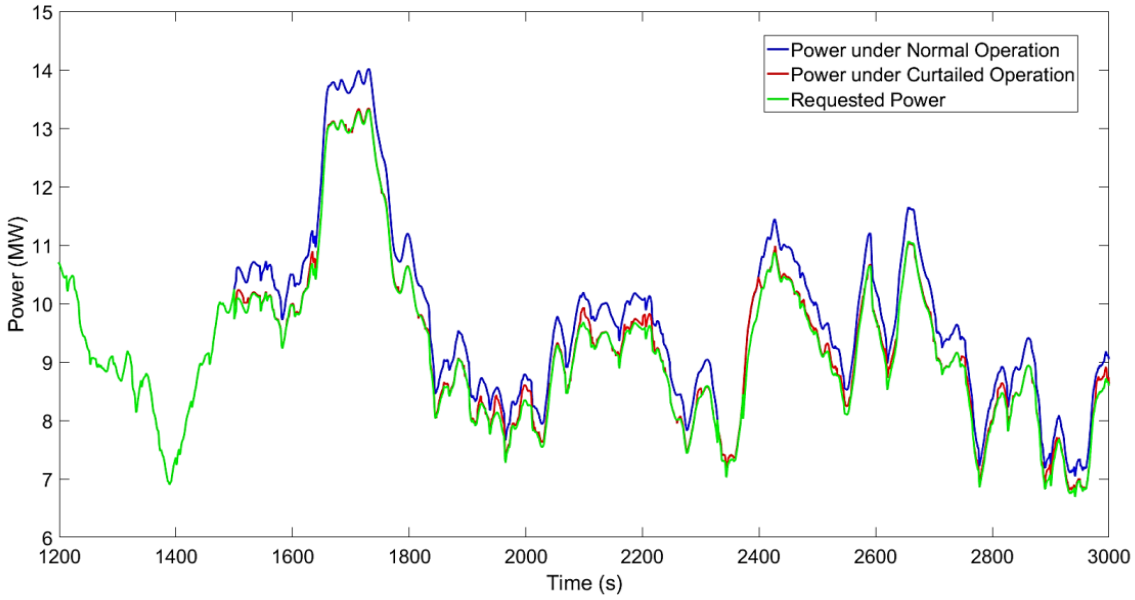

Figure 4-13: Comparison of total power output for normal operation and 5% power curtailment for below rated conditions when some turbines are utilised

The comparison also shows the variation between the power requested by the operator, the power provided by the wind farm and the power production under normal operation. In this case, the controller considers the request as a low priority event and ensures that the turbines utilised to provide the power reach the new set point gradually. The wind turbine controller prioritises the 7 wind turbines (i.e. 70%) that at 1500s experience the highest wind speeds to reduce the loads on these turbines.

As can be seen, the requested power cannot be achieved at all times; this is because the mean wind speed is below rated, but also, due to wake effects, some wind turbines will be experiencing wind speeds that are lower still. Figure 4-14 shows the number of wind turbines that are used by the wind farm controller to provide the requested ΔP:

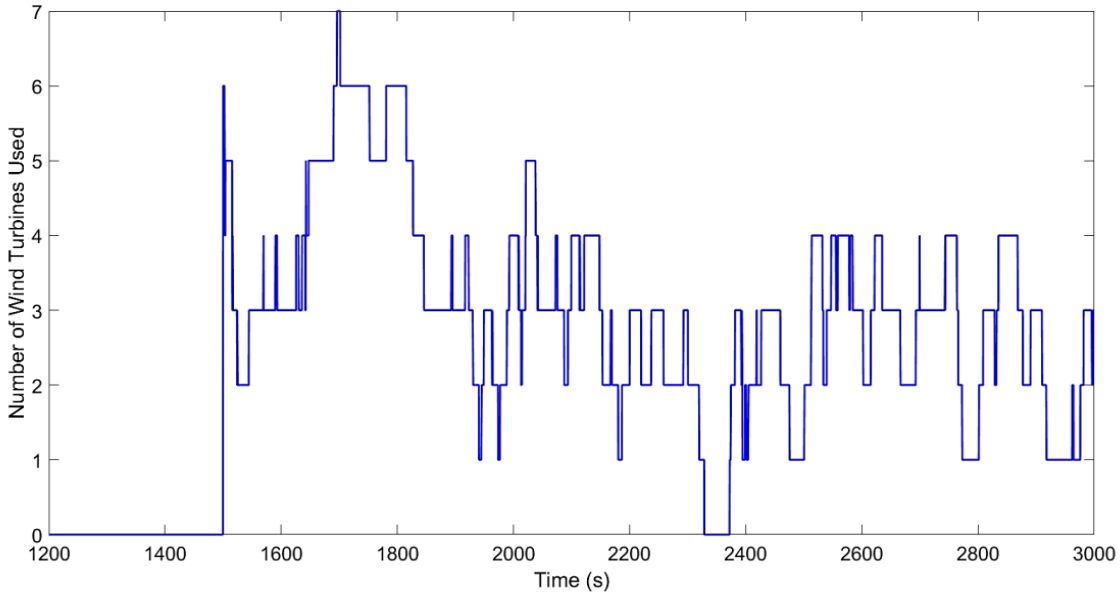

Figure 4-14: Number of turbines used to provide the requested power curtailment

As can be seen in Figure 4-14, the number of wind turbines used is changing based on the operational point that each of the prioritised wind turbine is experiencing. The number fluctuates between zero, minimum, and seven, maximum. Figure 4-15 depicts the requested ΔP for all the turbines in the wind farm. Wind turbines 6, 7 and 9 have not been used to provide any ΔP, as they are the turbines experiencing the lowest wind speed at the time of the request, as can be seen in Figure 4-16. The wind turbines utilised to provide the additional power are the ones experiencing the highest wind speeds at the time of the request to reduce their loads.

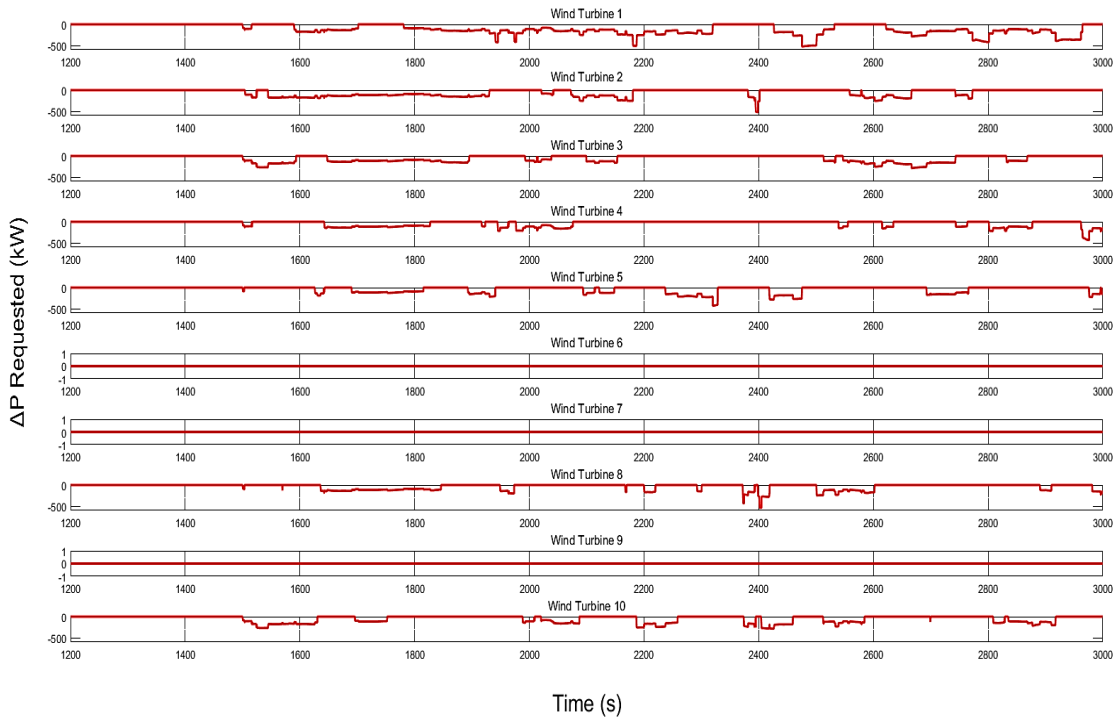

Figure 4-15: Requested ΔP per turbine

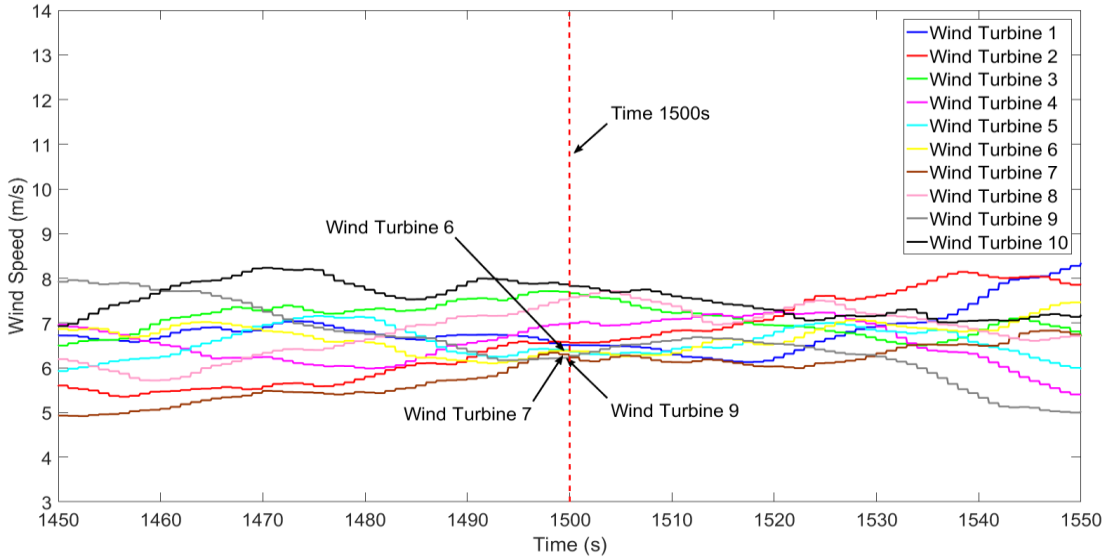

Figure 4-16: Wind speed for all turbines at time of request

For the utilised turbines, the investigation of the availability of the wind turbines shows the reason the turbines reject to provide the power reduction. To investigate the reason behind the rejection, wind turbine 2 has been chosen for further analysis. Figure 4-17 shows the ΔP allocation in conjunction with the PAC rejection and recovery complete flags for wind turbine 2. As can be seen, the turbine is not providing the power curtailment until the rejection flag changes from ON (i.e. rejection flag equal to 1) to OFF (i.e. rejection flag equal to 0). The turbine is then asked to provide the required ΔP until the rejection flag returns to ON. The wind farm controller does not request a ΔP until the rejection flag is OFF and the recovery compete flag is ON (i.e. recovery complete flag equal to 1). It should be noted that the wind farm controller ensures that the turbine is completely recovered (i.e. recovery complete flag equal to 1) and available (i.e. rejection flag equal to 0) before requesting a new ΔP.

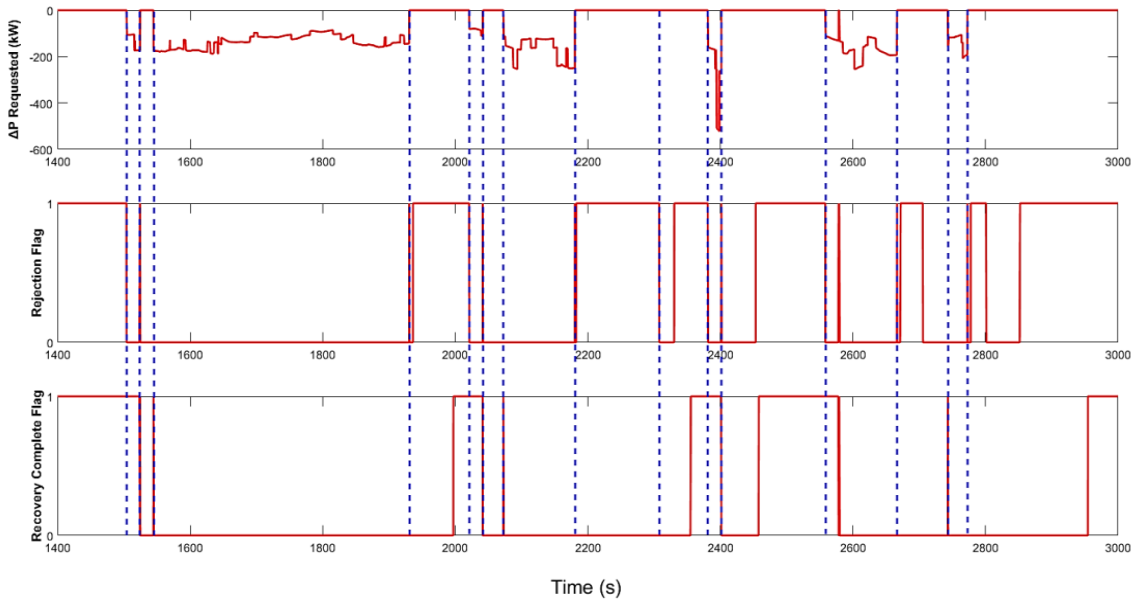

Figure 4-17: Investigation of ΔP request signals based on rejection and recovery complete flags for wind turbine 2

Figure 4-18 depicts the relationship between wind speed and rejection flag for wind turbine 2. As can be seen, when the wind speed moves below 6.5ms^{-1} the rejection flag is set to ON, which, as seen in Figure 4-17, does not allow the wind turbine to provide the ΔP. The low wind speed procedure takes place when the turbines are experiencing wind speeds below 6.5ms^{-1}

threshold, and once the wind speed above the threshold then the rejection flag is revoked, and the turbine can be used again to provide the requested ΔP.

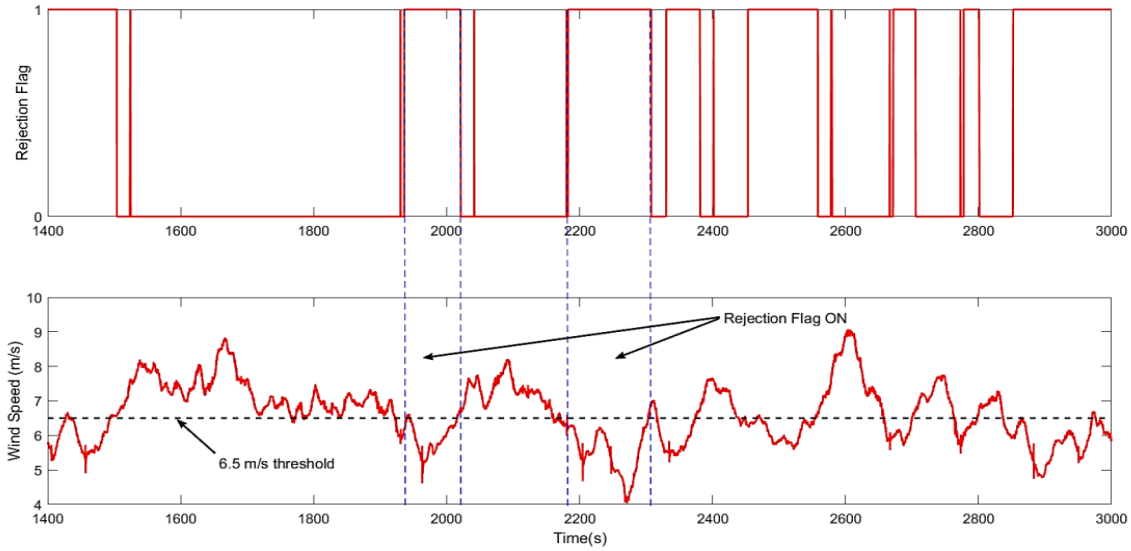

Figure 4-18: Wind speed with regards to the rejection flag for wind turbine 2

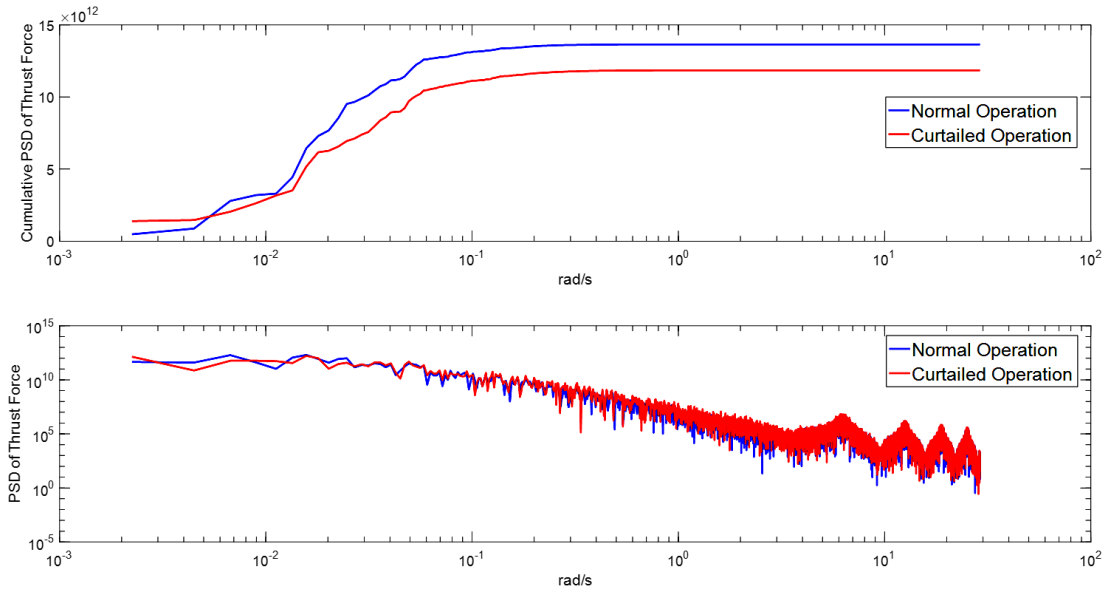

Figure 4-19: PSD and cumulative PSD plots for rotor aerodynamic thrust force of wind turbine 2

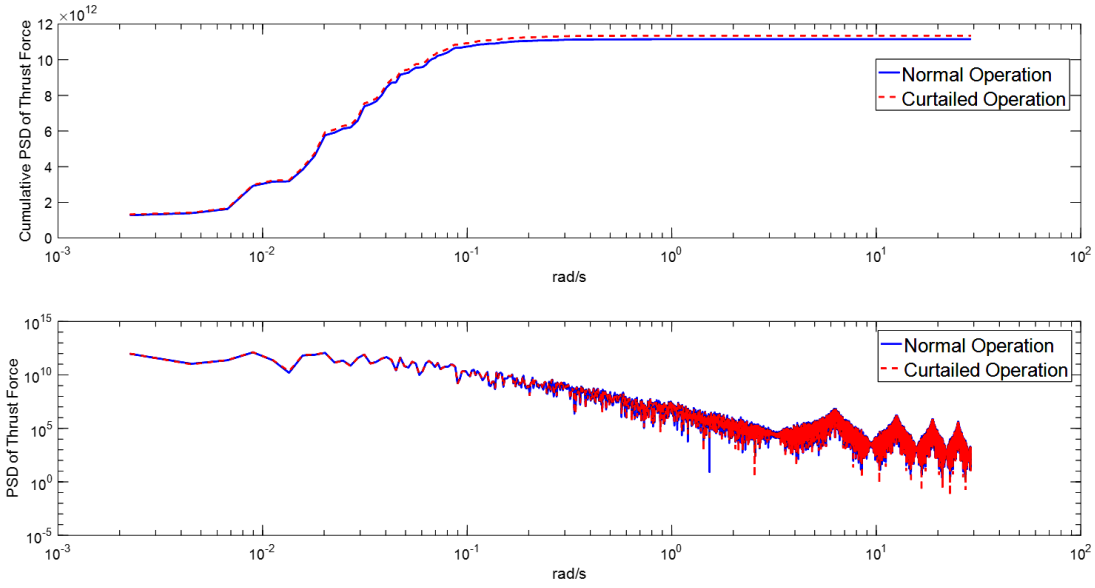

Figure 4-20: PSD and cumulative PSD plots for rotor aerodynamic thrust force of wind turbine 9

Figures 4-19 and 4-20 show the PSD and cumulative PSD of wind turbines 2 and 9 respectively. Wind turbine 2 has been used to provide ΔP, while wind turbine 9 is not used.

As can be seen in Figure 4-19, for wind turbine 2 the level of the thrust force is significantly reduced, resulting in decreased loads on the turbine while, as shown in Figure 4-20, the loads remain relatively constant for wind turbine 9, simply because wind turbine 9 was never asked to operate off its conventional strategy. It should be noted though, that due to the power reduction on upstream turbines, wind turbine 9 is now experiencing slightly higher thrust forces.

The wind farm model is simulated for 3000s at 8ms^{-1} mean wind speed with 10% turbulence intensity. The wind farm operator requests for a total power reduction of 5% to be provided for a total of 1500s (i.e. between 1500s – 3000s). As this signal is not received by the network controller, it is treated as a low priority request. Hence, the wind farm controller ensures that all the available machines are utilised to provide the requested power reduction. The comparison between the total power output of the wind farm under normal operation, the

total power output of the wind farm under curtailed operation and the requested curtailment is shown in Figure 4-21.

As can be seen in Figure 4-21, at 1500s the operator requests a curtailment of power production equal to 5% of normal production. In this case the controller considers the request as a low priority effect and ensures that the turbines utilised to provide the power reach the new set point gradually. The wind turbine controller utilises all the wind turbines (i.e. 100%).

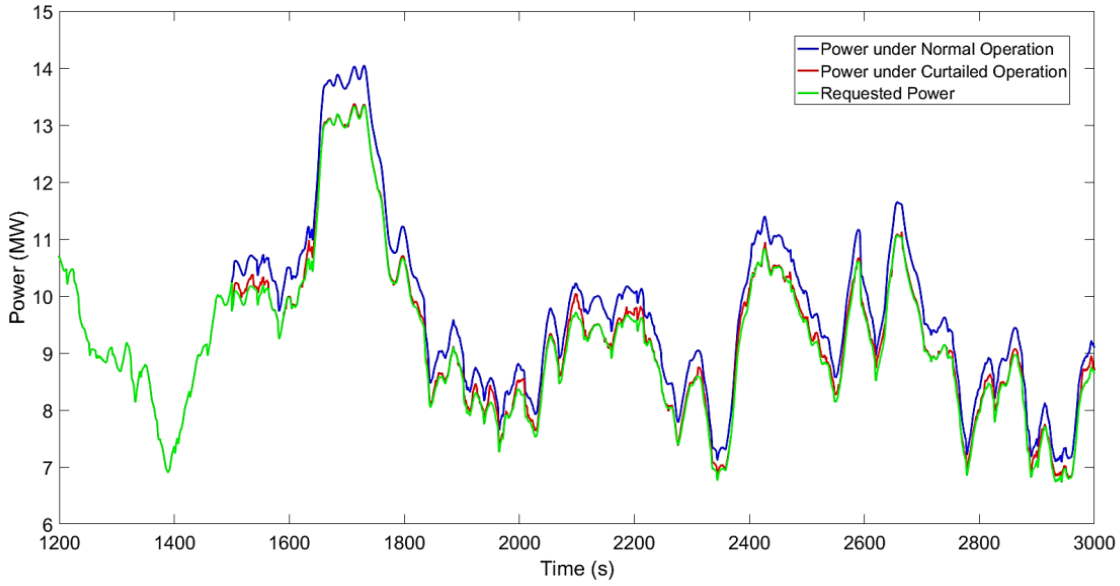

Figure 4-21: Comparison of total power output for normal operation and 5% power curtailment for below rated conditions when all turbines are utilised

As can be seen in Figure 4-21, the requested power cannot be achieved at all times as the turbines might have been unable to provide the ΔP requested from the controller, but the response is better that when 7 wind turbines were utilised. For example, at approximately 2300 seconds the response of the wind farm using only 7 turbines is almost zero as there is no turbine available to provide the ΔP, while at the same time some ΔP is produced for the wind farm utilising all the wind turbines.

Figure 4-22 shows the number of wind turbines that are used by the wind farm controller to provide the requested ΔP. As can be seen, the number of wind turbines used is changing based on the operational point that each of the prioritised wind turbine is experiencing. The number fluctuates between one, minimum, and nine, maximum. In contrast to the case where the controller used a certain number of turbines to provide the ΔP, in the unconstrainted case the wind farm controller ensures that there is always at least one wind turbine trying to provide the ΔP.

Figure 4-23 depicts the wind speeds for all the turbines in the wind farm. Since all the turbines are used to provide the required ΔP, the controller has no need for prioritisation based on the wind speed the wind turbines are experiencing.

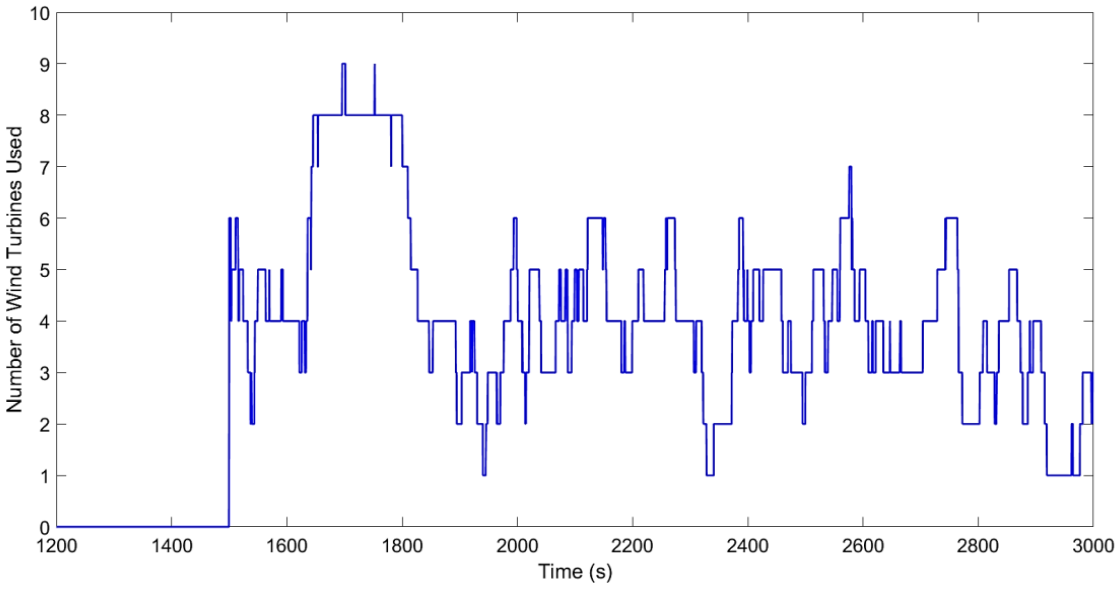

Figure 4-22: Number of turbines used to provide the requested power curtailment

Figure 4-24 shows the wake deficit for all the turbines in the wind farm. As can be seen, wind turbine 1 experiences no wake deficit as it does not have a turbine upstream. Wind turbine 2 experiences the effect of the wake of wind turbine 1, while turbine 3 experiences the wake

deficit from, initially, turbine 2 and then turbine 1. The same effect is experienced by all the downstream wind turbines.

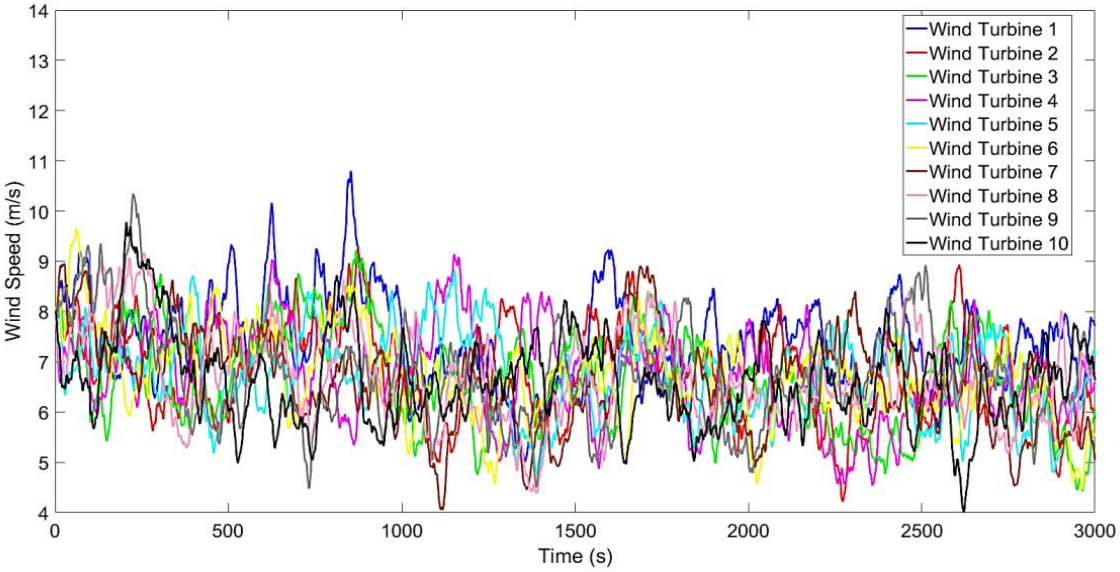

Figure 4-23: Wind speed for all turbines over simulation period

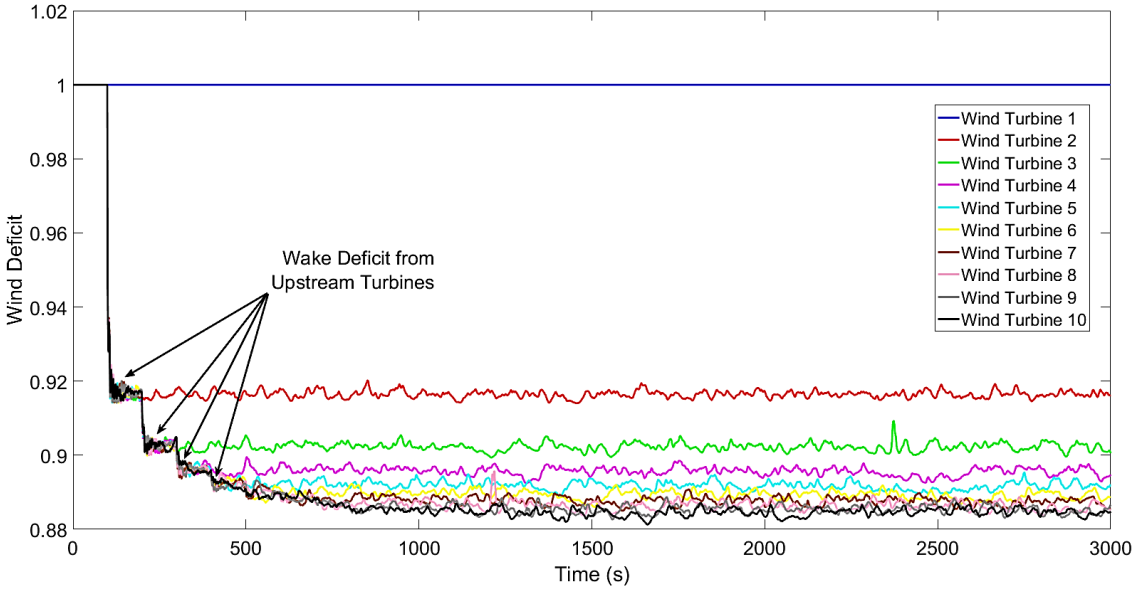

Figure 4-24: Wake deficit for all turbines over simulation period

4.5.2.2 Rated Wind Speed Conditions

The wind farm model is simulated for 3000s at 11ms^{-1} mean wind speed with 10% turbulence intensity. The wind farm operator requests for a total power reduction of 5% to be provided for a total of 1500s (i.e. between 1500s – 3000s). As this signal is not received by the network controller, it is treated as a low priority request. Hence, the wind farm controller prioritizes the wind turbines and ensures that only some of the available machines, in this case 70%, are utilised to provide the requested power reduction. As explained in section 4.4.4.2, the turbines that are facing high wind speeds will be prioritised to reduce their power output, resulting in a load reduction on these machines. The comparison between the total power output of the wind farm under normal operation, the total power output of the wind farm under curtailed operation and the requested curtailment is shown in Figure 4-25.

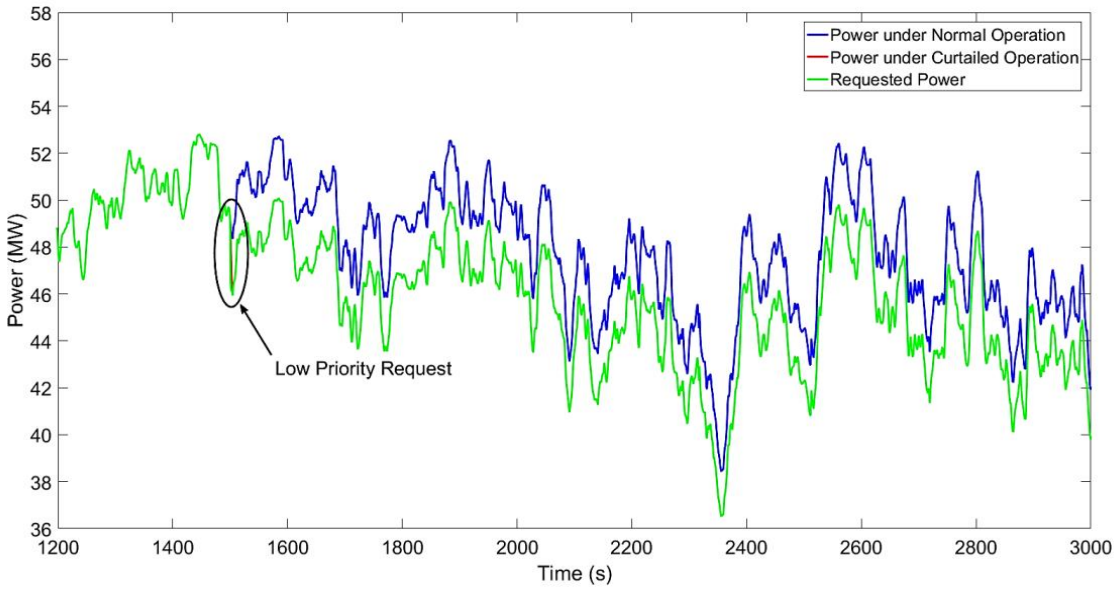

Figure 4-25: Comparison of total power output for normal operation and 5% power curtailment for rated conditions when some turbines are utilised

As can be seen in Figure 4-25, at 1500s the operator requests a curtailment of power production equal to 5% of normal production. To provide the required power reduction, the controller gradually decreases the total power to minimise the shocks on the wind turbines. The comparison also shows the variation between the power requested by the operator, the

power provided by the wind farm and the power production under normal operation. In this case, the controller treats the request as a low priority effect and ensures that the turbines utilised to provide the power reach the new set point gradually. The wind turbine controller prioritises the 7 wind turbines (i.e. 70%) that at 1500s experience the highest wind speeds to reduce the loads on these turbines. As can be seen, the requested power is achieved at all times, as the turbines are able to provide the ΔP requested from the controller, even during periods when wind speeds the turbines are experiencing are below the rated wind speed. Figure 4-26 shows the number of wind turbines that are used by the wind farm controller to provide the requested ΔP.

As can be seen in Figure 4-26, the number of wind turbines used remains constant, which means that the prioritised wind turbines are able to provide the requested ΔP for the requested period of time. Figure 4-27 depicts the requested ΔP for all the turbines in the wind farm.

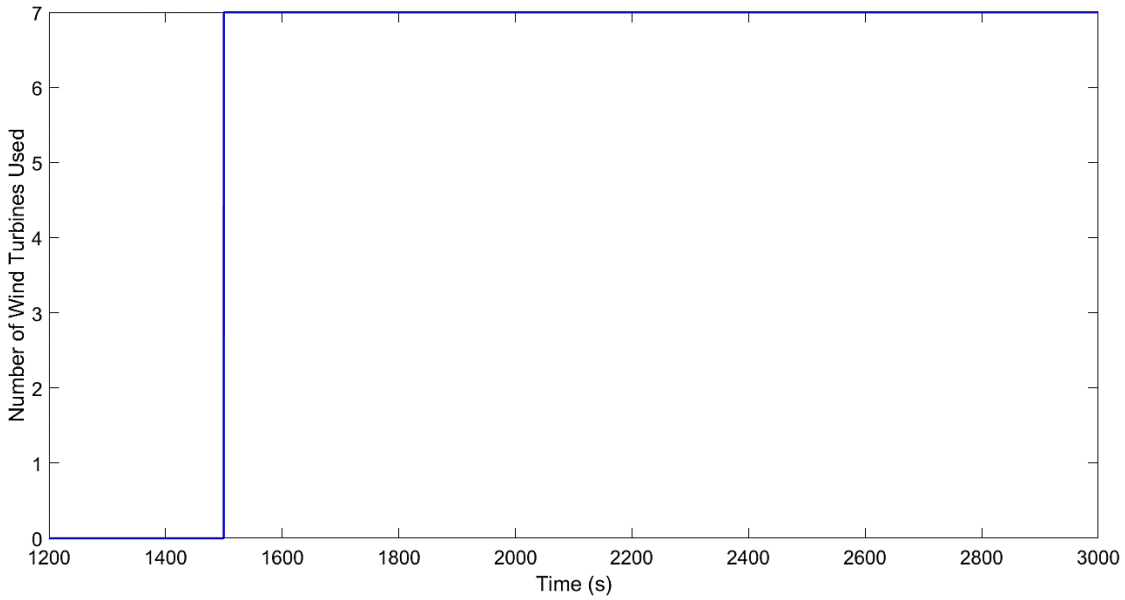

Figure 4-26: Number of turbines used to provide the requested power curtailment

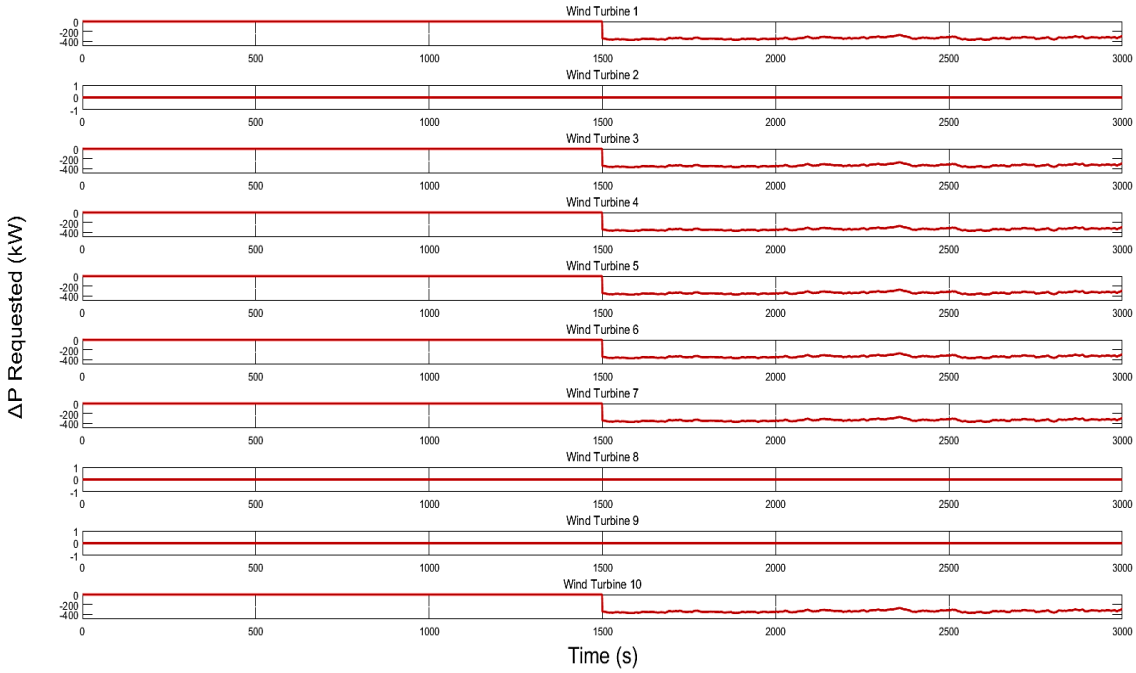

Figure 4-27: Requested ΔP per turbine

As shown in Figure 4-27, wind turbines 2, 8 and 9 have not been used to provide any ΔP, as they are the turbines experiencing the lowest wind speed at the time of the request, as can be seen in Figure 4-28. The wind turbines utilised are the ones experiencing the highest wind speeds at the time of the request to reduce their loads.

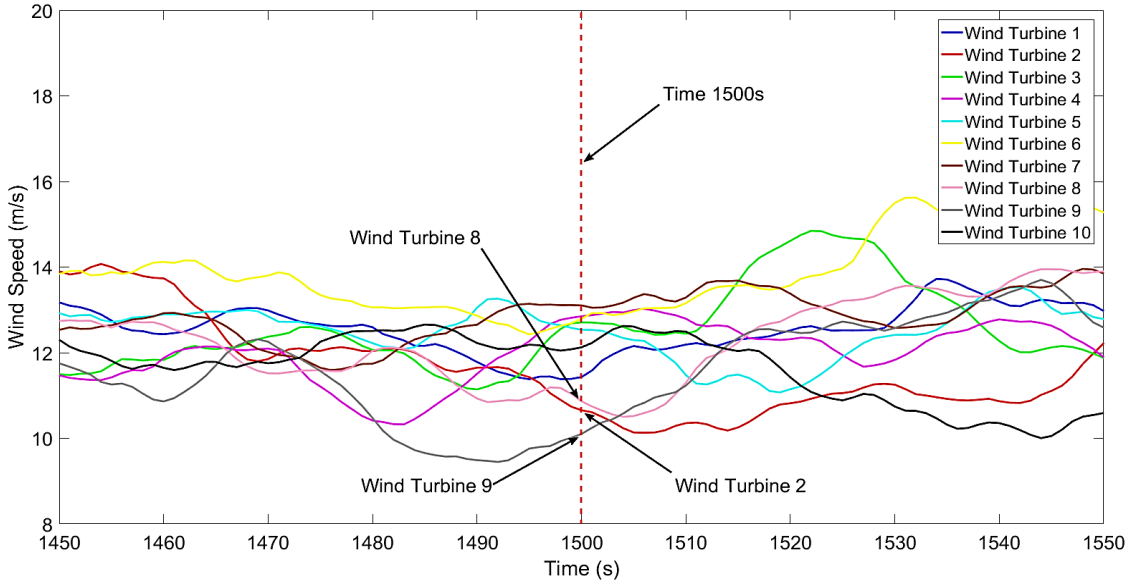

Figure 4-28: Wind speed for all turbines at time of request

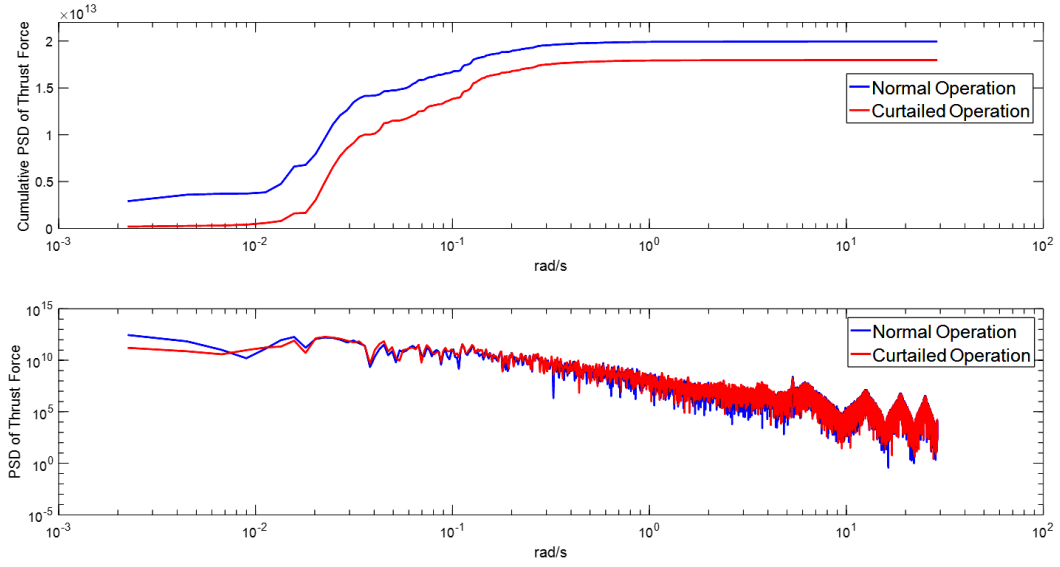

Figure 4-29: PSD and cumulative PSD plots for rotor aerodynamic thrust force of wind turbine 3

For the investigation of the load reduction on the utilised turbines, wind turbine 3 has been chosen for analysis. Figure 4-29 depicts the PSD and cumulative PSD of wind turbine 3. As can be seen in Figure 4-29, for wind turbine 3 the level of the thrust force is significantly reduced, resulting in decreased loads on the turbine.

Figure and 4-30 depicts the wake deficits for all the turbines in the wind farm. As can be seen in Figure 4-30, wind turbine 1 experiences no wake deficit as it does not have a turbine upstream. Wind turbine 2 experiences the effect of the wake of wind turbine 1, while turbine 3 experiences the wake deficit from, initially, turbine 2 and then turbine 1. The same effect is experienced by all the downstream wind turbines.

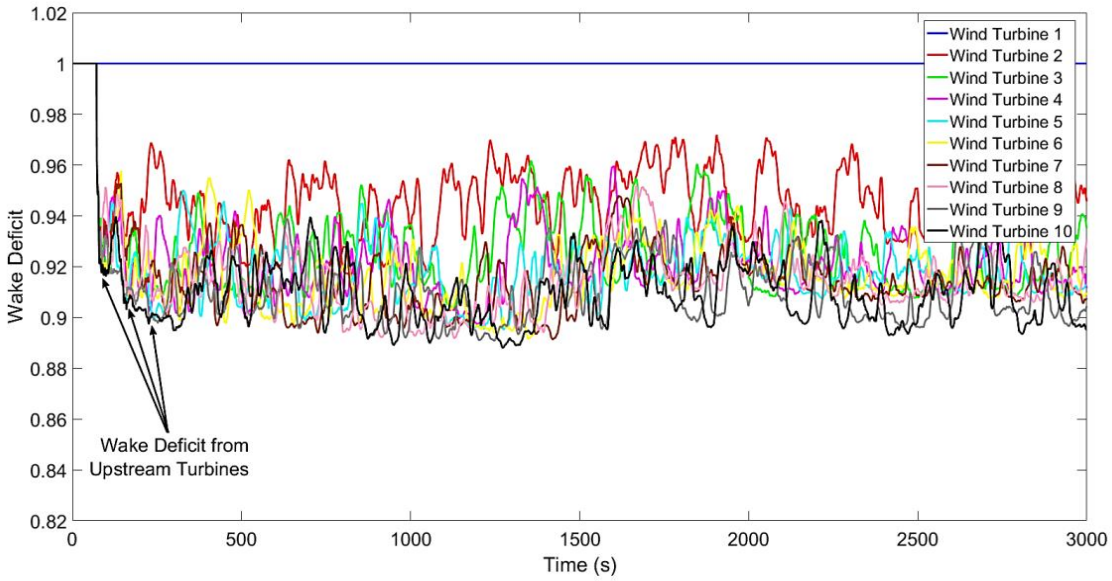

Figure 4-30: Wake deficit for all turbines over simulation period

4.5.2.3 Above Rated Wind Speed Conditions

The wind farm model is simulated for 3000s at 15ms^{-1} mean wind speed with 10% turbulence intensity. The wind farm operator requests for a total power reduction of 5% to be provided for a total of 1500s (i.e. between 1500s – 3000s). As this signal is not received by the network controller, it is treated as a low priority request. Hence, the wind farm controller prioritizes the

wind turbines and ensures that only some of the available machines, in this case 70%, are utilised to provide the requested power reduction. As explained in section 4.4.4.2, the turbines that are facing high wind speeds will be prioritised to reduce their power output, resulting to a load reduction on these machines. The comparison between the total power output of the wind farm under normal operation, the total power output of the wind farm under curtailed operation and the requested curtailment is shown in Figure 4-31:

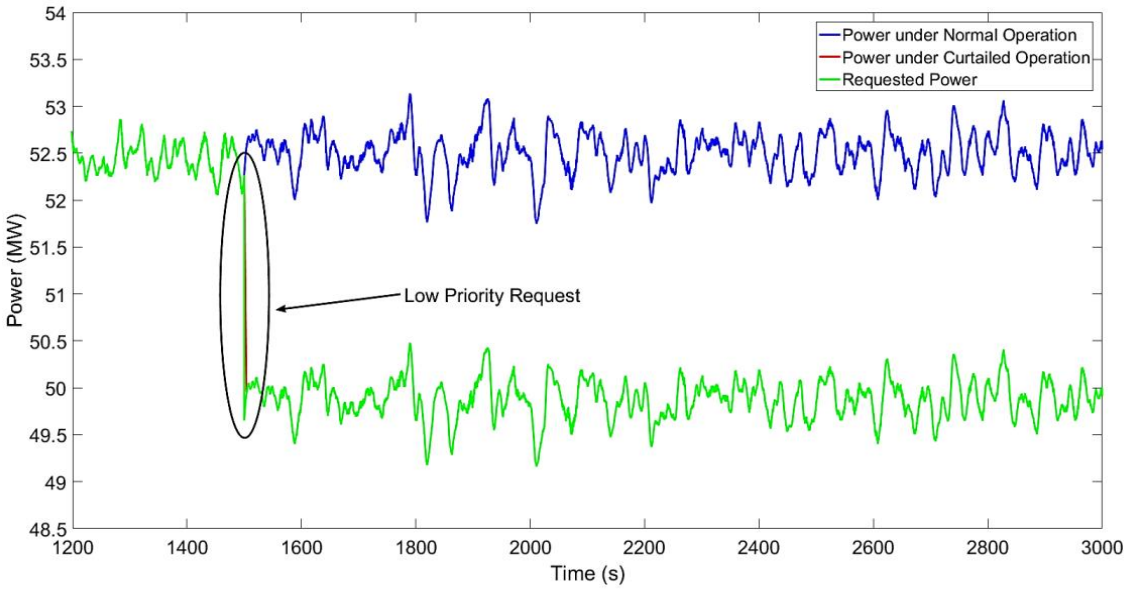

Figure 4-31: Comparison of total power output for normal operation and 5% power curtailment for above rated conditions when some turbines are utilised

As can be seen in Figure 4-31, at 1500s the operator requests a curtailment of power production equal to 5% of normal production. The comparison also shows the difference between the power requested by the operator, the power provided by the wind farm and the power production under normal operation. In this case, the controller considers the request as a low priority effect and ensures that the turbines utilised to provide the power reach the new set point gradually. The wind turbine controller prioritises the 7 wind turbines (i.e. 70%) that at 1500s experience the highest wind speeds to reduce the loads on these turbines. As can be seen, the requested power is achieved at all times, as the turbines are able to provide the ΔP

requested from the controller. Figure 4-32 shows the number of wind turbines that are used by the wind farm controller to provide the requested ΔP.

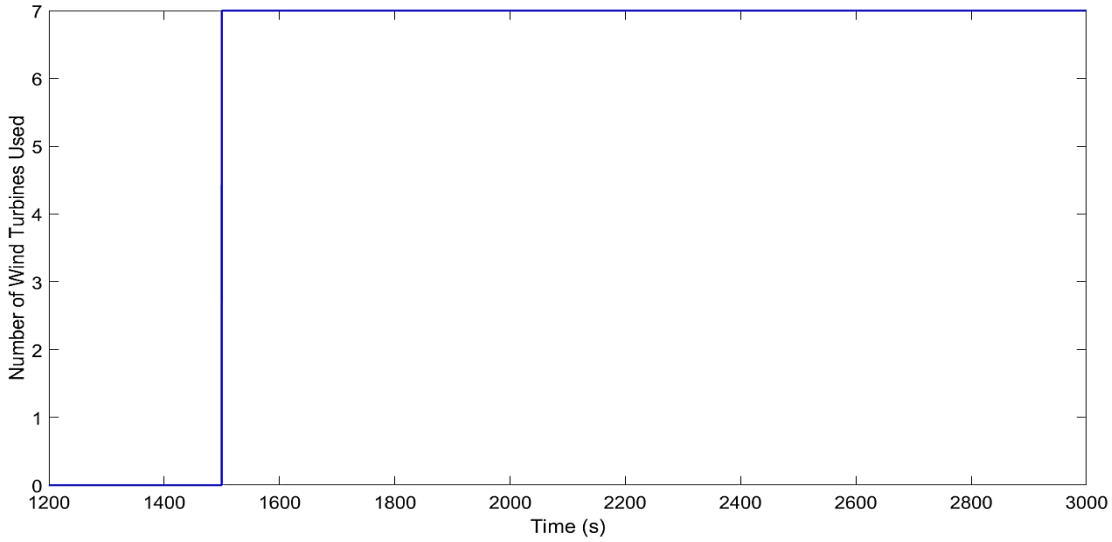

Figure 4-32: Number of turbines used to provide the requested power curtailment

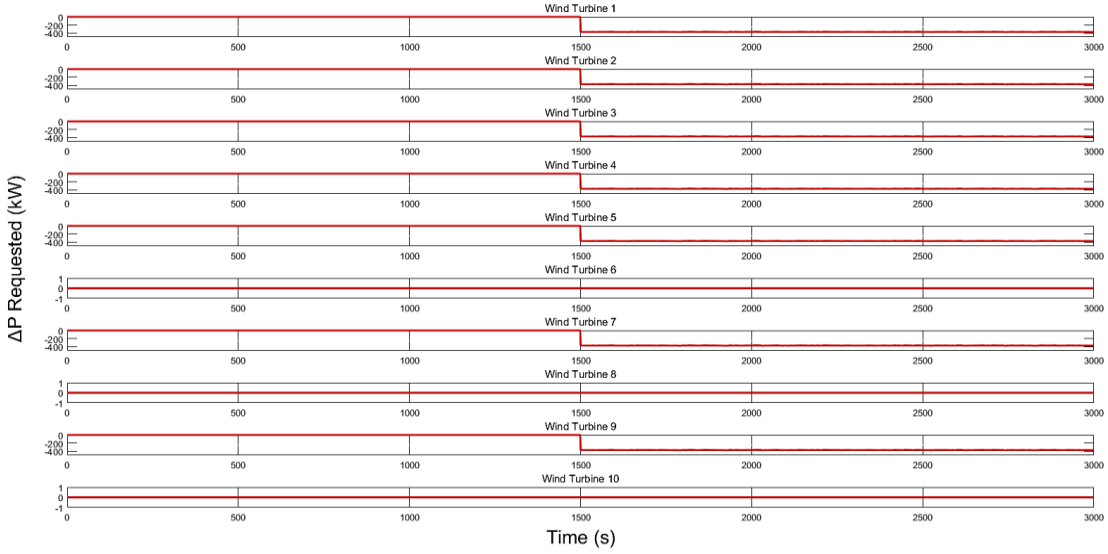

Figure 4-33: Requested ΔP per turbine

As can be seen in Figure 4-32, the number of wind turbines used remains constant which means that the prioritised wind turbines are able to provide the requested ΔP for the requested period of time. Figure 4-33 depicts the requested ΔP for all the turbines in the wind farm.

As shown in Figure 4-33, wind turbines 6, 8 and 10 have not been used to provide any ΔP, as they are the turbines experiencing the lowest wind speed at the time of the request, as can be seen in Figure 4-34. The wind turbines utilised are the ones experiencing the highest wind speeds at the time of the request to reduce their loads.

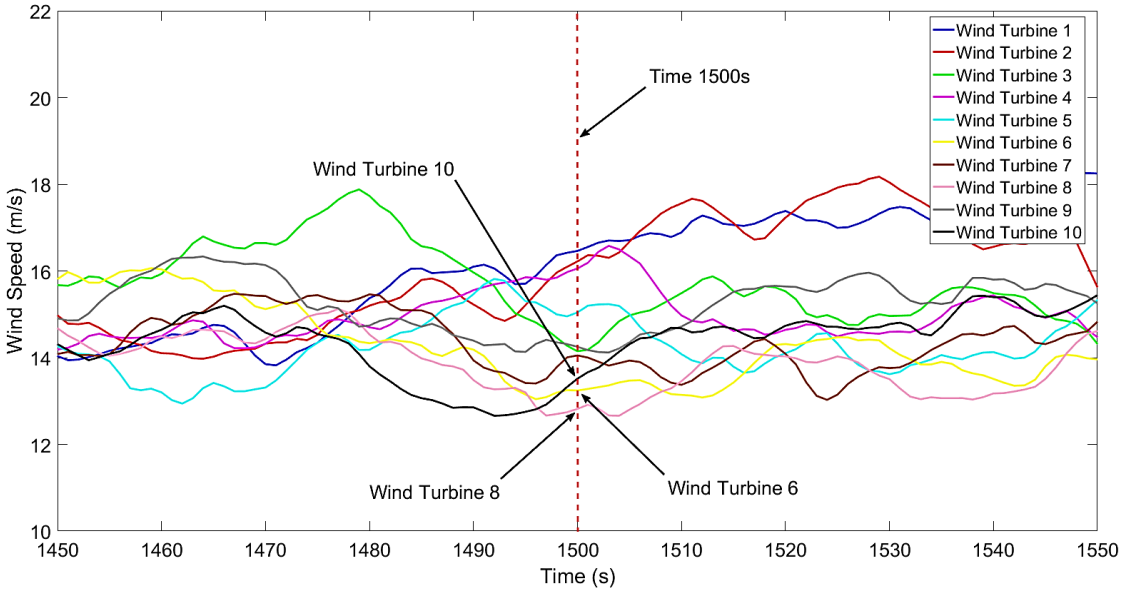

Figure 4-34: Wind speed for all turbines at time of request

For the investigation of the load reduction on utilised turbines, wind turbine 9 has been chosen for analysis. Figure 4-35 depicts the PSD and cumulative PSD of wind turbine 9. As can be seen in Figure 4-35, for wind turbine 9 the level of the thrust force is significantly reduced, resulting to decreased loads on the turbine.

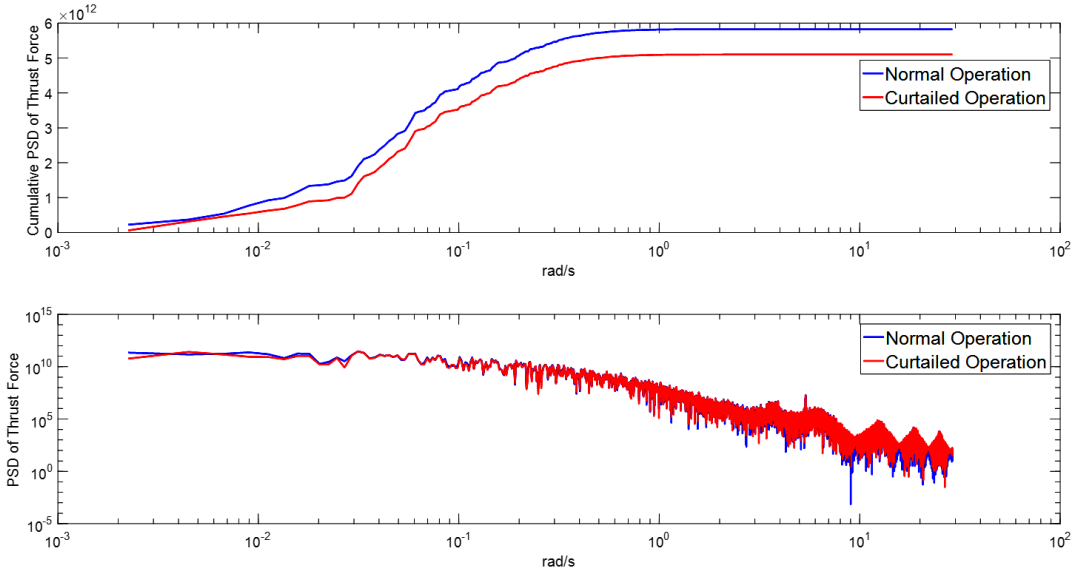

Figure 4-35: PSD and cumulative PSD plots for rotor aerodynamic thrust force of wind turbine 9

4.5.3 Network Controller Primary Response Simulation Results

Inertia in power systems can be described as the resistance to change. For conventional power systems with interconnected synchronous machines, inertia is provided by the large synchronous rotating masses, which react immediately to any imbalance between the power supply and the demand. High inertia in a power system provides high levels of frequency stability. Modern wind turbines are decoupled from the grid and thus do not contribute to grid inertia. The contribution of turbines to short term frequency stability can be defined as synthetic inertia.

Inertial response is the release/absorption of rotational kinetic energy of the rotor in response to a torque imbalance (between the mechanical torque accelerating the rotor and the electrical torque decelerating the rotor). For wind farms, synthetic inertia can be produced by instantaneously increasing the power output during a frequency fluctuation. For primary response, the required response time is required to be less than 10s [70], and should be able to be sustained for a minimum of 20 seconds after an event has occurred [70]. Ideally for

synthetic inertia purposes, the response should occur within 200ms [71]. An investigation of synthetic inertia by National Grid concluded that a power increase of 5% - 10% during a grid frequency drop to 49.2Hz for approximately 8 seconds would be sufficient to ensure frequency stability [71].

Increasing the power output of a wind farm for synthetic inertia events is demonstrated in this section. Most wind farm controllers in literature can only provide primary response in above rated operation [56] [58] [59]. The wind farm controller can provide increased power, without the use of droop control, in below rated operation by utilizing the functionality of the PAC.

The PAC can provide positive ΔP in below rated operation for a small period by requesting an increase in generator torque demand. The turbine's strategy in below rated wind speeds is to provide the maximum available power so as to maximise financial profits. This means that there is no more available energy in the wind to counteract the increase in generator torque; consequently, the rotor will start to slow down until it reaches the PAC's pre-defined black limit. At that point, the turbine is not allowed to provide the requested ΔP and is set to recover to its normal strategy.

4.5.3.1 Below Rated Wind Speed Conditions

The wind farm model is simulated for 3000s at 8ms^{-1} mean wind speed with 10% turbulence intensity. The wind farm operator requests for a total power increase of 5% to be provided for a total of 20s (i.e. between 1500s – 1520s). As this signal is received by the network controller, it is assumed as a high priority request. Hence, the wind farm controller utilises all the available wind turbines to provide the requested power increase. The comparison between the total power output of the wind farm under normal operation, the total power output of the wind farm under curtailed operation and the requested curtailment is shown in Figure 4-36:

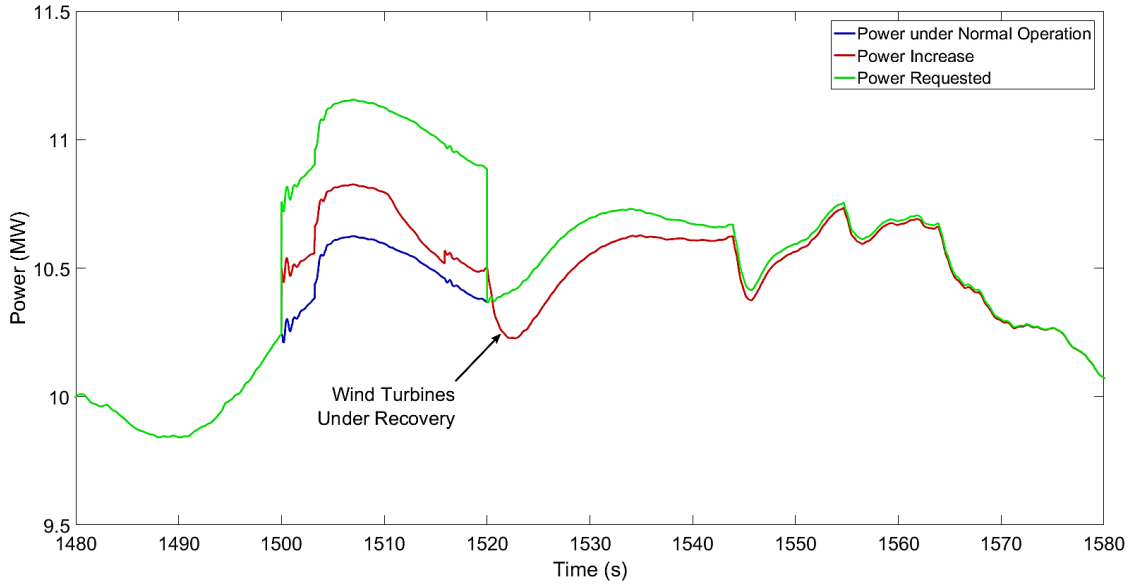

Figure 4-36: Comparison of total power output for normal operation and 5% synthetic inertia power increase for below rated conditions

As can be seen in Figure 4-36, at 1500s the operator requests an increase of power production equal to 5% of normal production. The comparison also shows the variation between the power requested by the network controller, the power provided by the wind farm and the power production under normal operation. In this case, the controller treats the request as a high priority effect and ensures that all the available turbines are utilised to provide the power reach the new set point instantaneously. As can be seen, the requested power cannot be reached at any point, as the turbines are unable to provide the total ΔP requested from the controller. The change in power happens instantaneously, which gives the wind farm controller the ability to provide synthetic inertia services to the system operator. It should be noted that even though the wind farm response does not match the request, there is still some additional power injected to the grid, which, for below rated conditions, is quite significant. Once the ΔP request is not required, the turbines are set to recover to their normal operational points. Figure 4-37 illustrates the response of the first three wind turbines (i.e. 1, 2 and 3) to the positive ΔP requested from the wind farm controller.

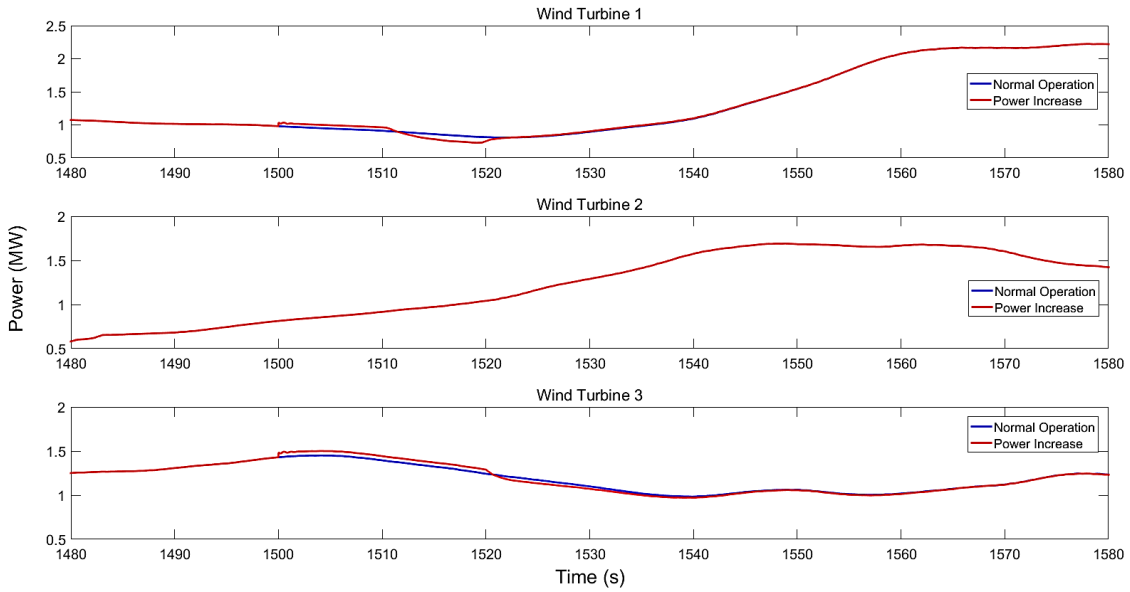

Figure 4-37: Power production comparison for wind turbines 1, 2 and 3

As can be seen in Figure 4-37, turbine 1 can only provide the requested ΔP for approximately 10 seconds, turbine 2 cannot provide any ΔP while turbine 3 is able to provide the requested ΔP for the full 20 second period.

Figure 4-38 depicts the generator speed / torque diagram for wind turbine 1. As can be seen the wind turbine is operating normally until an increase in generator torque is requested from the wind farm controller. The turbine provides the requested increased power until it reaches the PAC's black limit. At that point, the turbine cannot provide the ΔP anymore, and the turbine recovers to its normal operation.

Figure 4-39 shows the requested ΔP for all the turbines in the wind farm. As this request has high importance, the controller requests from all the turbines to provide a ΔP, without considering their operating conditions.

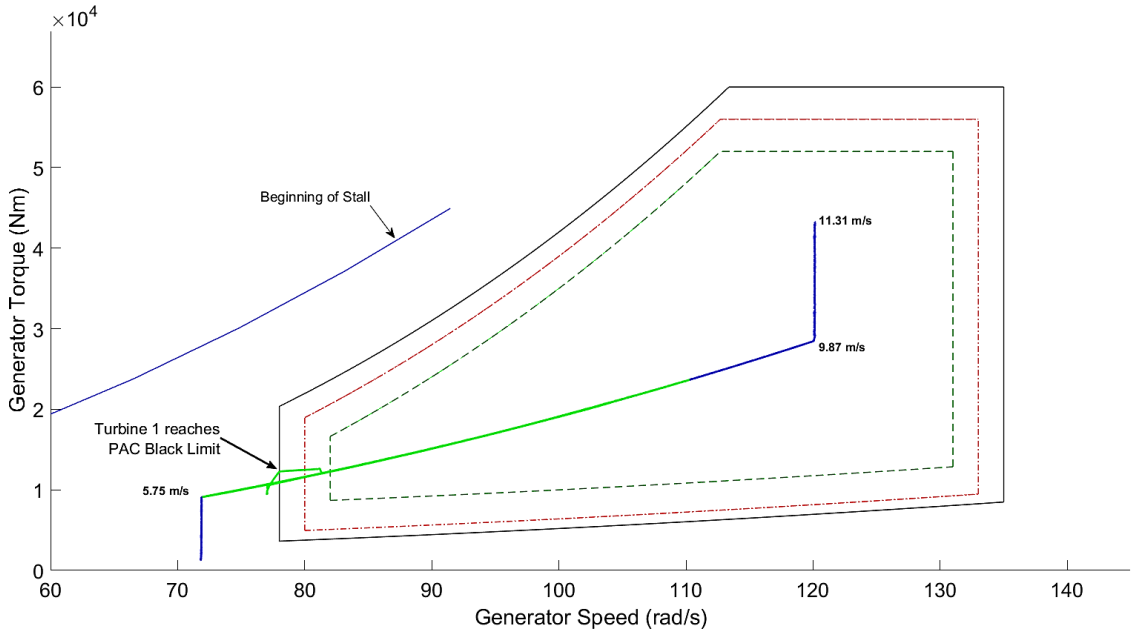

Figure 4-38: Wind turbine generator speed / torque diagram including PAC limits and operational strategy for wind turbine 1

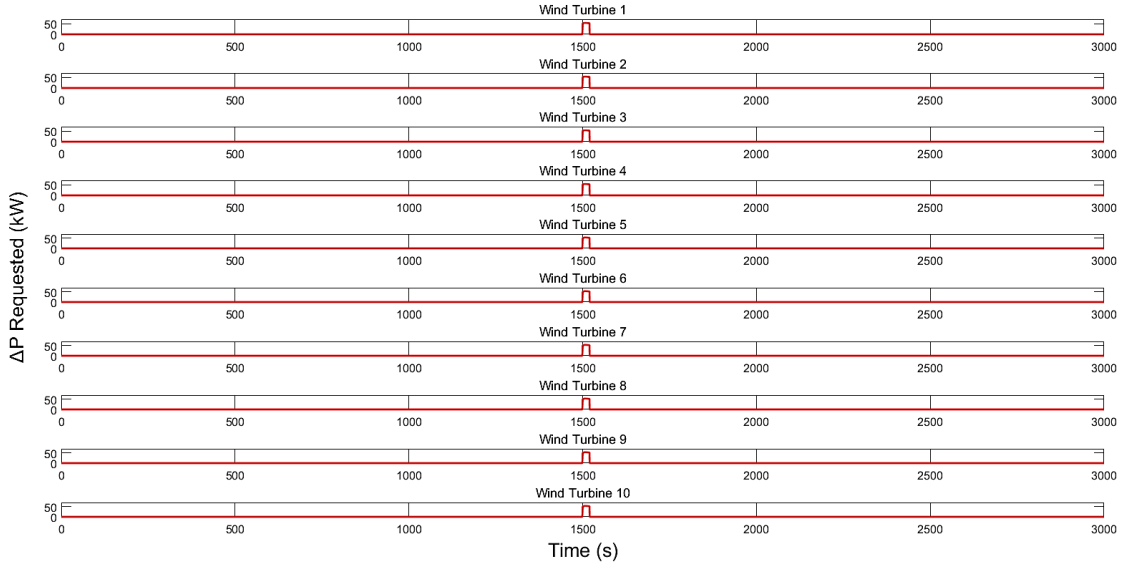

Figure 4-39: Requested ΔP per turbine

To investigate the changes in mechanical loading on utilised turbines, wind turbine 3 has been chosen for analysis. Figure 4-40 depicts the PSD and cumulative PSD of wind turbine 3. As can be seen, for wind turbine 3 the level of the thrust force is slightly increased, resulting in increased loads on the turbine. The load increase is barely noticeable, as the increased loading period is only 20 seconds, which is a small portion of the simulation time.

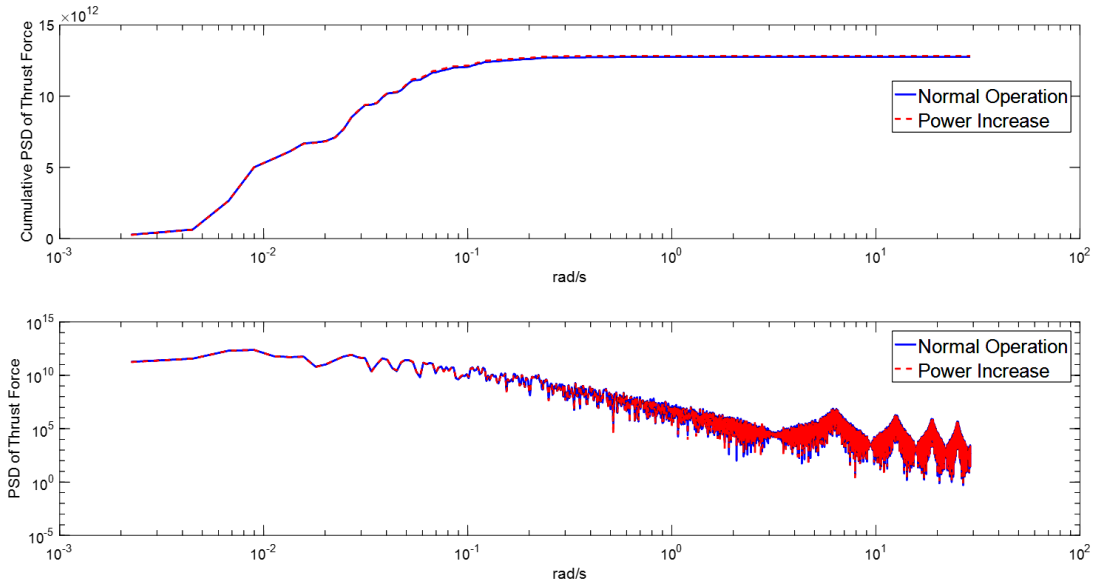

Figure 4-40: PSD and cumulative PSD plots for rotor aerodynamic thrust force of wind turbine 3

4.5.3.2 Rated Wind Speed Conditions

The wind farm model is simulated for 3000s with a mean wind speed of 11ms^{-1} and a turbulence intensity of 10%. The wind farm operator requests for a total power increase of 5% to be provided for a total of 20s (i.e. between 1500s – 1520s). As this signal is received by the network controller, it is treated as a high priority request. Hence, the wind farm controller utilises all the available wind turbines to provide the requested power increase. The comparison between the total power output of the wind farm under normal operation, the total power output of the wind farm under curtailed operation and the requested curtailment is shown in Figure 4-41.

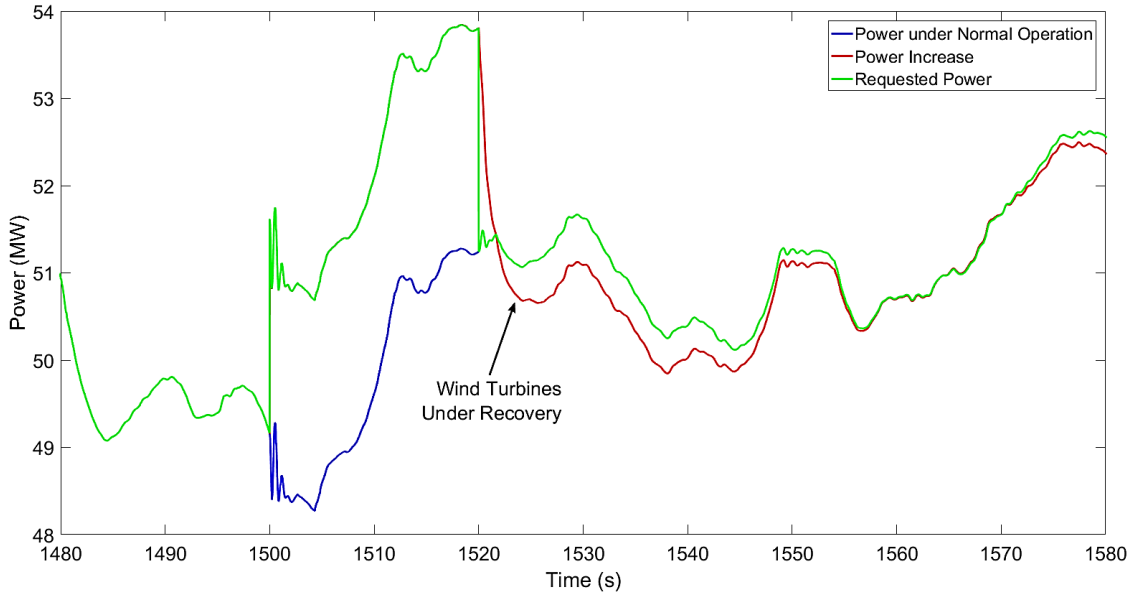

Figure 4-41: Comparison of total power output for normal operation and 5% synthetic inertia power increase for rated conditions

As can be seen in Figure 4-41, at 1500s the operator requests an increase of power production equal to 5% of normal production. The comparison also shows the variation between the power requested by the network controller, the power provided by the wind farm and the power production under normal operation. In this case, the controller considers the request a high priority effect, and ensures that all the available turbines are utilised to provide the power reach the new set point instantly. As can be seen, the requested power is reached instantaneously as the turbines provide the ΔP requested from the controller, which gives the wind farm controller the ability to provide synthetic inertia services to the system operator. It should be noted that the power increases instantly and the increase is maintained for the duration of 20 seconds. Hence, the wind farm controller can provide primary response services to the system operator, without the need of droop control, when operating at rated wind speeds.

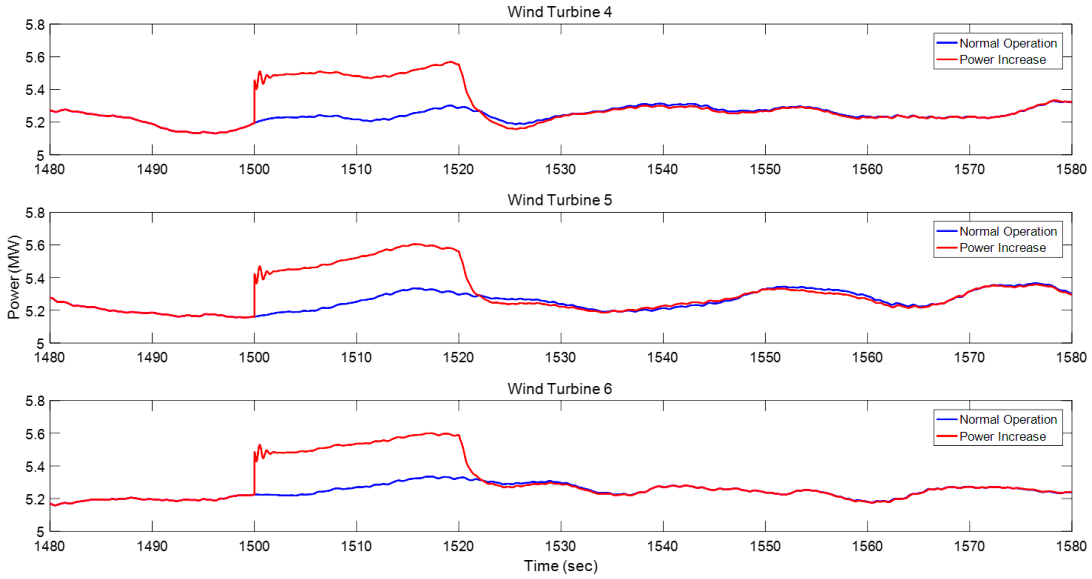

Figure 4-42: Power production comparison for wind turbines 4, 5 and 6

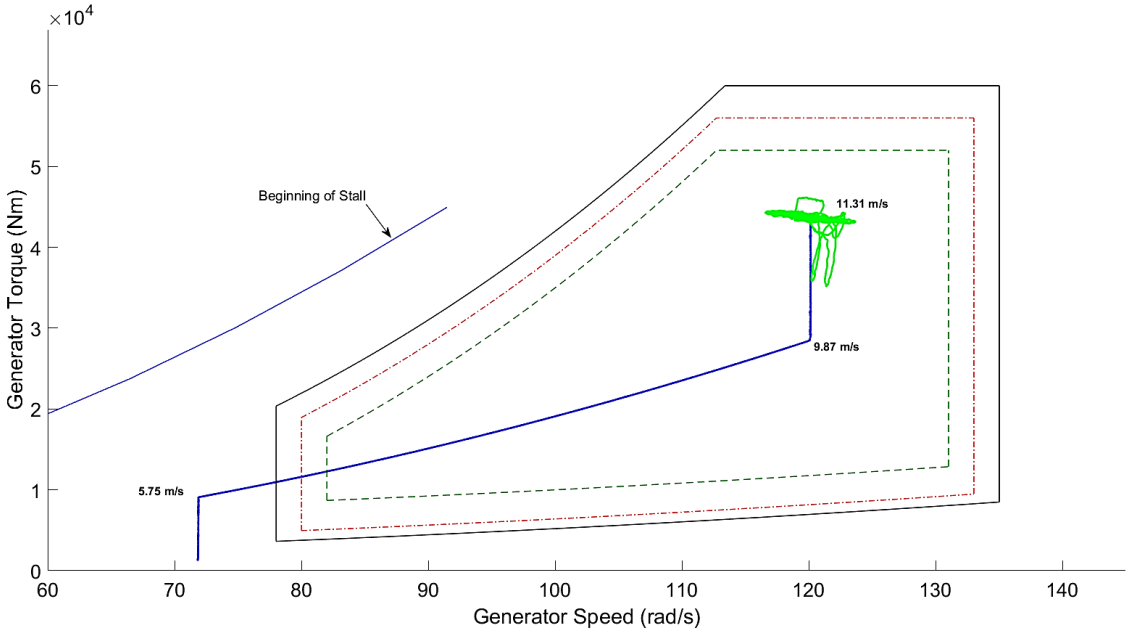

Figure 4-43: Wind turbine generator speed / torque diagram including PAC limits and operational strategy for wind turbine 4

Figure 4-42 illustrates the response of three wind turbines (i.e. 4, 5 and 6) to the positive ΔP requested from the wind farm controller. As can be seen in Figure 4-42, all the turbines are able to provide the requested ΔP for the full 20 second period.

Figure 4-43 depicts the generator speed / torque diagram for wind turbine 4. As can be seen the wind turbine is operating normally until an increase in generator torque is requested from the wind farm controller. The turbine provides the requested increased power, while remaining within the PAC green limit boundary. Hence, the turbine is capable of providing the power increase for the requested period. When the ΔP from the wind farm controller is not requested from the turbine, the turbine recovers to its normal operation.

Figure 4-44 shows the requested ΔP for all the turbines in the wind farm. As this is a high importance request, the controller requests from all the turbines to provide a ΔP, without considering their operating conditions.

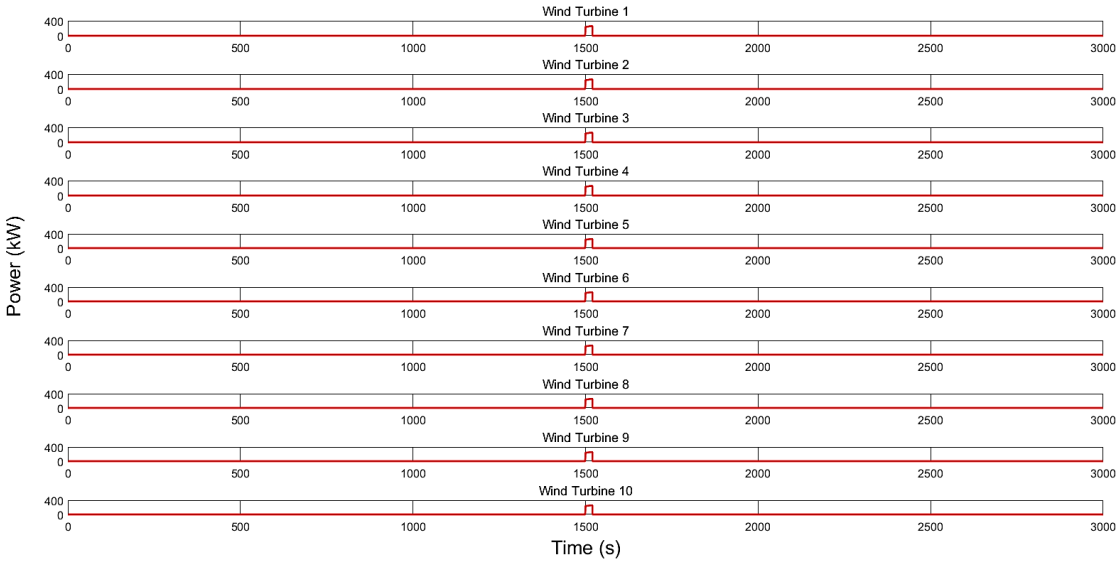

Figure 4-44: Requested ΔP per turbine

For the investigation of the load reduction on utilised turbines, wind turbine 4 has been chosen for analysis. Figure 4-45 depicts the PSD and cumulative PSD of wind turbine 4. As can be seen,

for wind turbine 4 the level of the thrust force is slightly increased, resulting to increased loads on the turbine. The load increase is barely noticeable, as the increased loading period is only 20 seconds, which is a small portion of the simulation time.

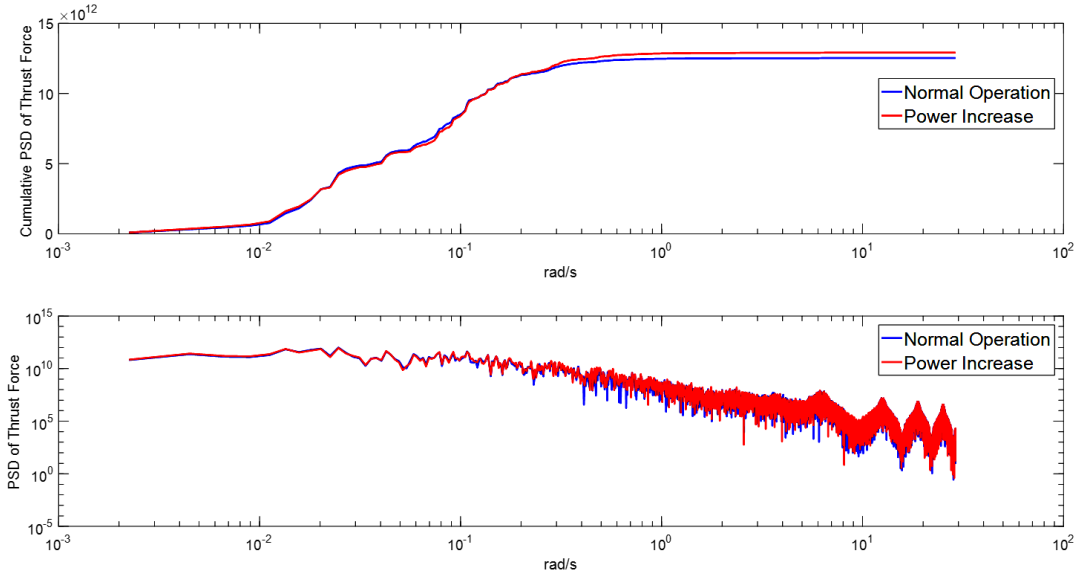

Figure 4-45: PSD and cumulative PSD plots for rotor aerodynamic thrust force of wind turbine 4

4.5.3.3 Above Rated Wind Speed Conditions

The wind farm model is simulated for 3000s at 15ms^{-1} mean wind speed with 10% turbulence intensity. The wind farm operator requests for a total power increase of 5% to be provided for a total of 20s (i.e. between 1500s – 1520s). As this signal is received by the network controller, it is assumed as a high priority request. Hence, the wind farm controller utilises all the available wind turbines to provide the requested power increase. The comparison between the total power output of the wind farm under normal operation, the total power output of the wind farm under curtailed operation and the requested curtailment is shown in Figure 4-46.

As can be seen in Figure 4-46, at 1500s the operator requests an increase of power production equal to 5% of normal production. The comparison also shows the difference between the power requested by the network controller, the power provided by the wind farm and the power production under normal operation. In this case, the controller considers the request as

a high priority effect and ensures that all the available turbines are utilised to provide the power reach the new set point instantly. As can be seen, the requested power is reached instantaneously as the turbines provide the ΔP requested from the controller, which gives the wind farm controller the ability to provide synthetic inertia services to the system operator. It should be noted that the power increases instantly and the increase is maintained for the duration of 20 seconds. This demonstrates that the wind farm controller can provide primary response services to the system operator, without the need of droop control, when operating at above rated wind speeds.

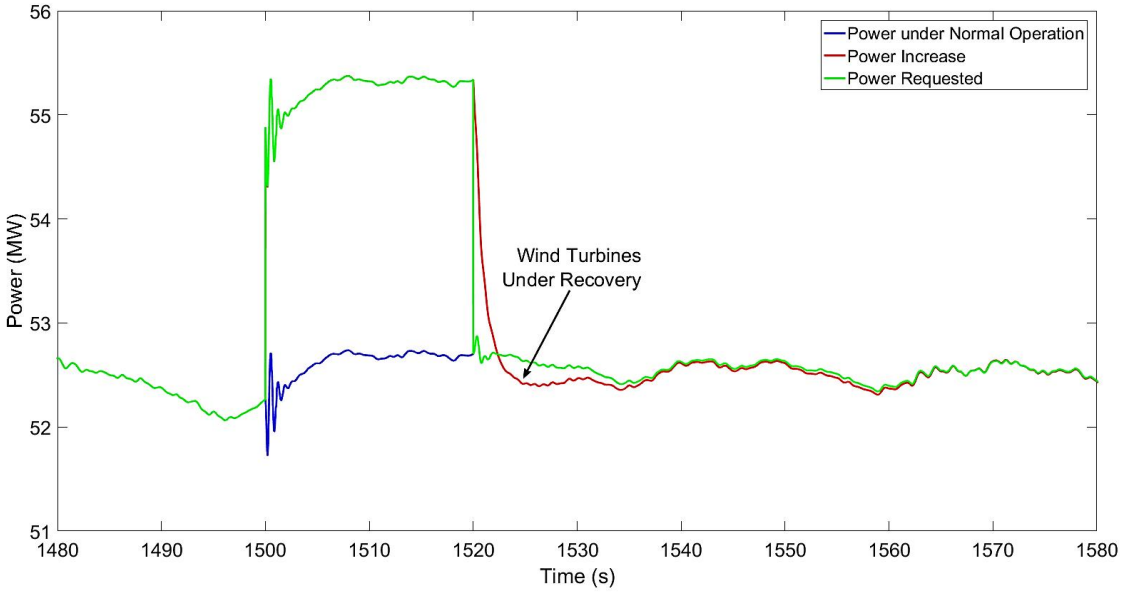

Figure 4-46: Comparison of total power output for normal operation and 5% synthetic inertia power increase for above rated conditions

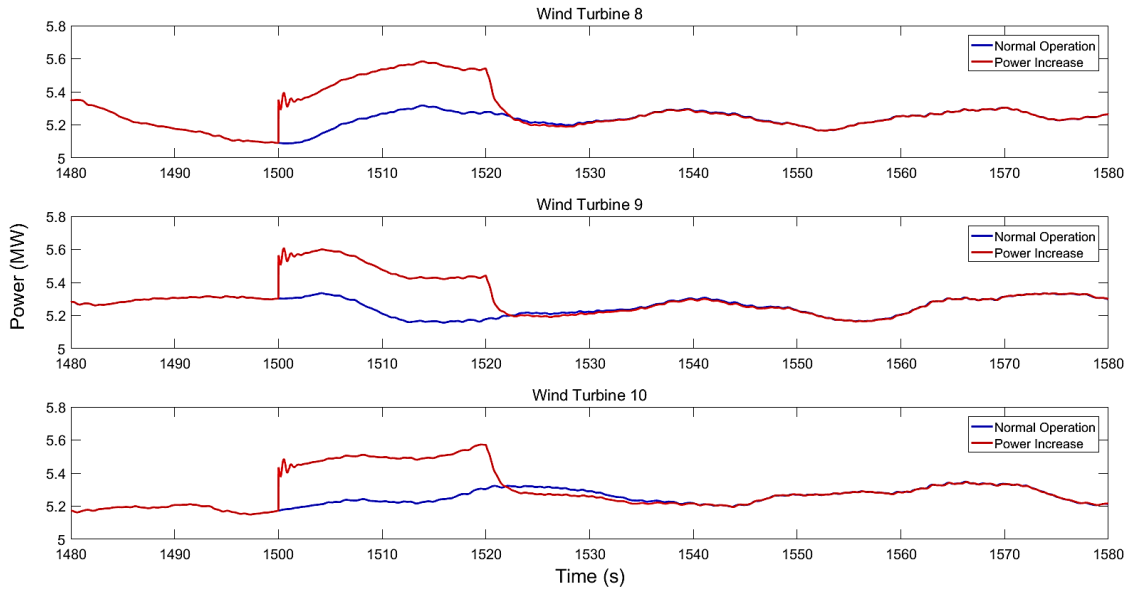

Figure 4-47: Power production comparison for wind turbines 8, 9 and 10

Figure 4-47 illustrates the response of three wind turbines (i.e. 8, 9 and 10) to the positive ΔP requested from the wind farm controller. As can be seen in Figure 4-47, all the turbines are able to provide the requested ΔP for the full 20 second period.

Figure 4-48 depicts the generator speed / torque diagram for wind turbine 8. As can be seen, the wind turbine is operating normally until an increase in generator torque is requested from the wind farm controller. The turbine provides the requested increased power, while remaining within the PAC green limit boundary. Hence, the turbine is capable of providing the power increase for the requested period. When the ΔP from the wind farm controller is not requested from the turbine, the turbine recovers to its normal operation.

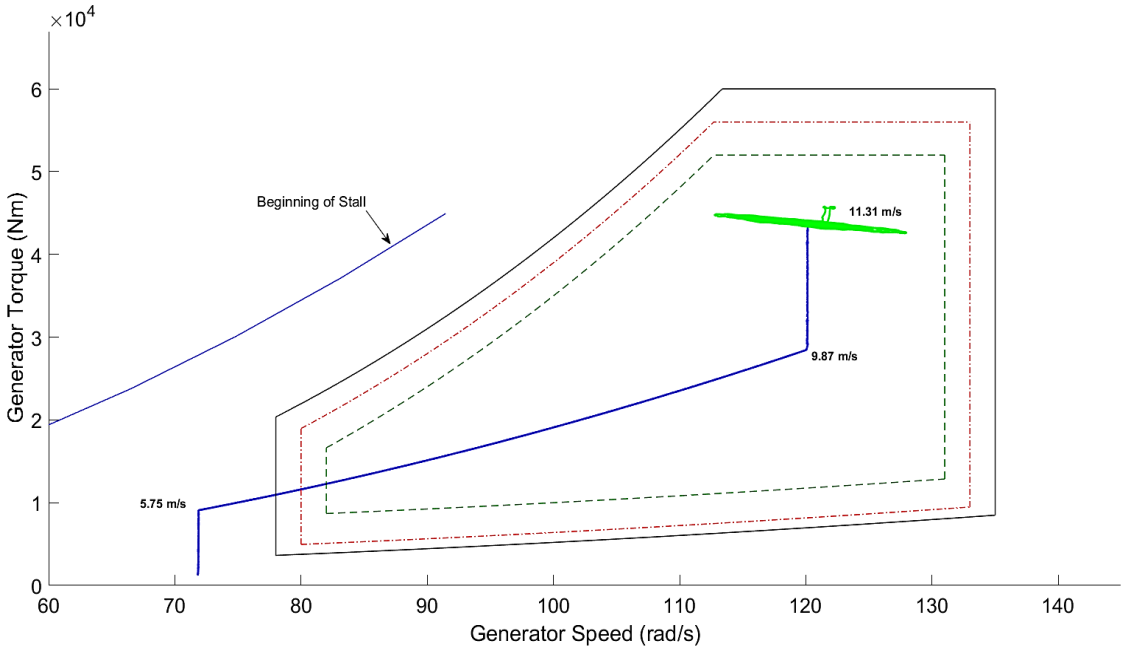

Figure 4-48: Wind turbine generator speed / torque diagram including PAC limits and operational strategy for wind turbine 8

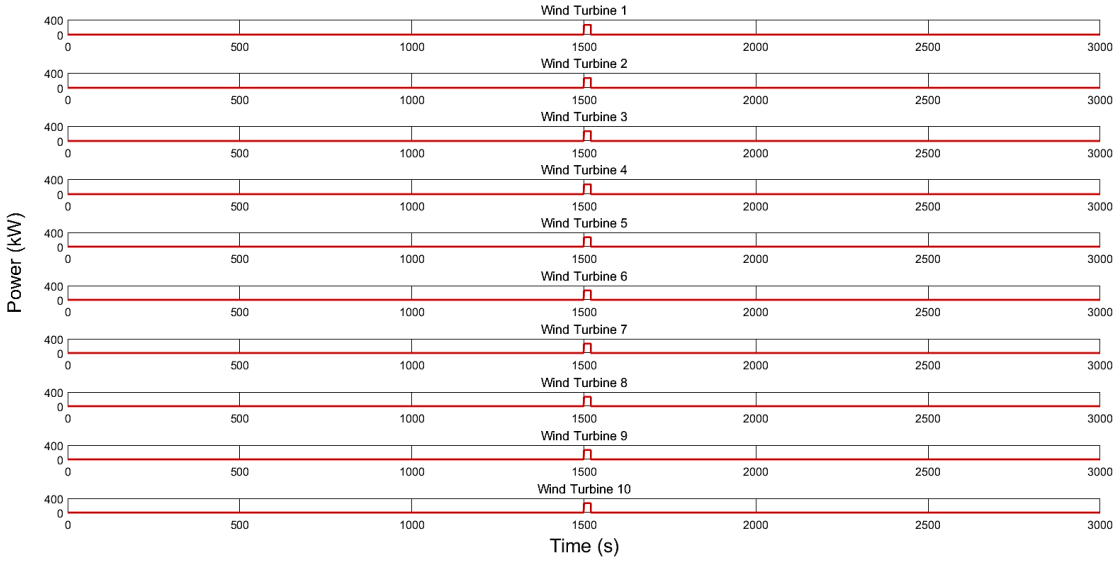

Figure 4-49: Requested ΔP per turbine

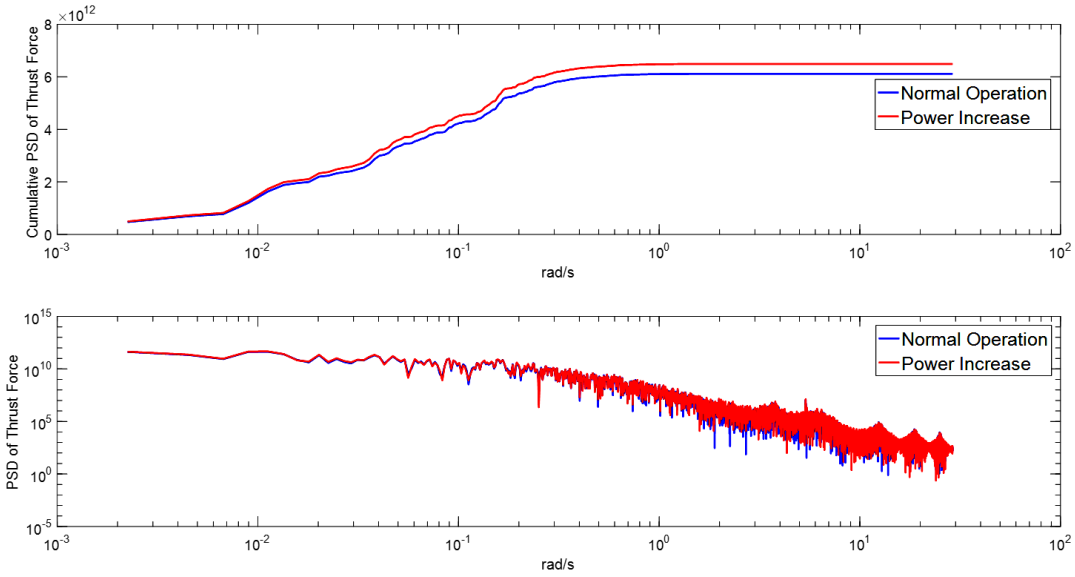

Figure 4-50: PSD and cumulative PSD plots for rotor aerodynamic thrust force of wind turbine 8

Figure 4-49 shows the requested ΔP for all the turbines in the wind farm. As this is a high importance request, the controller requests from all the turbines to provide a ΔP, without considering their operating conditions.

To investigate the impact of mechanical loading due to the control systems acting on utilised turbines, wind turbine 8 has been chosen for analysis. Figure 4-50 depicts the PSD and cumulative PSD of wind turbine 8. As can be seen, for wind turbine 8 the level of the thrust force is slightly increased, resulting to increased loads on the turbine.

4.6 Discussion and Conclusion

This chapter has focused on the development of a wind farm model and a wind farm controller capable of providing ancillary services to the power network operator. Based on the wind farm simulation results, this chapter answers the research question “can we operate wind farms flexibly under all operational conditions?”. This chapter concludes that the wind farm controller can be utilised to provide flexible operation of the wind farm under various

environmental conditions, as the simulation results suggest that the wind farm controller can successfully accomplish the requested power adjustments.

The wind farm controller has a highly decentralised structure. It can respond to inputs from the network controller and the wind farm operator, and considers the turbine conditions and the PAC information flags before allocating ΔP to turbines. It allows for a flexible operation of the wind farm, similar to the operation of a conventional power plant. The controller can provide ancillary services to the grid, such as droop control and synthetic inertia response, increasing the grid stability.

The wind farm controller can provide spinning reserve when necessary. The droop control algorithm can be used for all wind conditions. For below rated operating conditions, the prioritization of the wind turbines to be used is achieved by following the O&M analysis findings presented in chapter 3, thereby increasing turbine reliability/availability. The prioritization of wind turbines to be used for droop control can have a negative effect on the ability of the wind farm to provide droop control services for below rated wind speed conditions. The operator has the ability to change the number of wind turbines utilised from a certain percentage (e.g. 70%) to all available. This could be a way to mitigate the effect of the unavailability of some turbines to provide the requested ΔP due to operating constraints.

For rated or above rated operating conditions, the wind farm controller facilitates the provision of droop control whilst regulating wind turbine fatigue. In these operating conditions, there is no need for the operator to request ΔPs from all the turbines in the wind farm, as the simulation results show that the required power can always be achieved by using only a proportion of available turbines.

The wind farm controller responds to signals from the network wind farm controller and can provide ancillary services to the system operator. These signals are prioritised, as grid stability is always of paramount importance. For below rated operating conditions, the wind farm controller cannot always provide the additional power required to provide droop control for a prolonged period of time; however, it reacts instantaneously, which helps the wind farm provide synthetic inertia, thereby enhancing grid stability. For rated or above rated operating conditions, the wind farm controller is capable of providing both primary response and

synthetic inertia services to the system operator. Further investigation on this scenario is needed.

The wind farm model developed for this Chapter consists of 10 wind turbines, but a larger wind farm model consisting of 100 turbines and allowing for a realistic representation of modern offshore wind farms is presented in Chapter 5. The wind farm model is designed for fast simulation and controller development. The wind field model is based on industry standards, while the wake model allows not only for wake interaction calculations, but also includes the effect of wake meandering due to the lateral wind component. The assessment of the effect of the developed wind farm controller on power system stability is presented and discussed in chapter 7.

Chapter 5 - Large Scale Wind Farm Simulation Modelling

In this chapter, the wind farm simulation model is expanded to include 100 wind turbines. The large-scale wind farm model is representative of modern offshore wind farms, which consist of tens of multi-megawatt machines. The wind farm model has the following attributes: the representation of wind field and wake interactions; sufficiently fast to allow a large number of turbines to be simulated simultaneously; permits the inclusion of a wind farm controller, which, in this work, considers the findings of the Operation & Maintenance (O&M) data analysis to safeguard the turbines that are more likely to fail; and, finally, allow the wind farm controller to alter the power output based on signals received from the network or the wind farm operator.

5.1 Introduction

Onshore wind farms are already producing power at very low prices which allows for direct competition with conventional power plants. Offshore wind is different to onshore, mainly due to the harsh environmental conditions the offshore turbines would have to experience. Hence, turbines with higher rated power are used for offshore wind farms. Currently, onshore wind turbines with 1.5 - 3MW rated power are used [72] with an average rating of 2.7MW [73], while modern offshore machines have an average rated power of approximately 6MW [74]; moreover, the trend suggests that this value will only grow.

The size of the wind farms also differs between onshore and offshore. For the EU, in 2017 the average size of the grid-connected offshore wind farms was 493MW [74] and is expected to continue increasing, while for onshore wind the average grid-connected size was approximately 45 MW [75], mainly due to the need for small-scale distributed generation by wind farms. To be able to simulate the effect of the integration of modern offshore wind farms to the power network, the development of a large-scale wind farm model is required. Hence, the development

of the large-scale, 100 wind turbines, wind farm model is used to assess the capabilities of the wind farm controller to provide ancillary services to the system operator and improve power network stability.

5.2 Research Opportunities

The ability of accurately representing modern wind farms is crucial for the accurate study and representation of the future power system and the assessment of the increasing integration of wind farms. It was decided that this is an interesting area for further research. The novelty of this work is that the maximum number of wind turbines in the wind farm model is 100, which is representative of a modern offshore wind farm and enables full evaluation of wind farm control strategies [74]. The assessment of the wind farm controller capabilities to provide services to the network operator is presented in this Chapter. The integration of the large-scale wind farm and the analysis of the effect of the wind farm controller on the power system will be investigated thoroughly in Chapter 7.

5.3 Large Wind Farm Model Simulation Results

The wind farm simulation model has been based on the work presented in Chapter 4. The wind farm consists of 100 wind turbines which are positioned in ten rows, with ten turbines per row, parallel to the wind direction with 800m longitudinal distance (i.e. between each row) and 400m lateral distance (i.e. between each column), as can be seen in Figure 5-1. The model is used to assess the response of the wind farm controller to various power output request scenarios, whilst investigating the potential of the wind farm controller to provide ancillary services to the power system operator. The wind farm model is simulated for 600s for different mean wind speeds, all with 10% turbulence intensity. The model has been tested under three different mean wind speed scenarios: 8m/s i.e. below rated; rated, which occurs at 11m/s; and a wind speed of 15m/s i.e. above rated.

For all wind speeds, droop control simulations involve the wind farm operator requesting a total power reduction of 5% to be provided for a total of 300s, starting at t = 300s. As this signal is not received by the network controller, it is treated as a low priority request. Hence,

the wind farm controller prioritizes the wind turbines and ensures that only some of the available machines, in this case 70%, are utilised to provide the requested power reduction.

For the same set of wind speeds, additional simulations are conducted to investigate the wind farms ability to provide grid support. In this case, the wind farm operator requests for a total power increase of 5% to be provided for a total of 20s, starting from t = 300s. As this signal is received by the network controller, it is treated as a high priority request. Hence, for these simulations, the wind farm controller utilises all the available wind turbines to provide the requested power increase.

The simulation results for the average wind speed and power production for all the wind speed scenarios are depicted in Appendix A. The effect of the wake interactions between the wind turbines is apparent, as the downstream wind turbines experience lower wind speed and, consequently, produce less power.

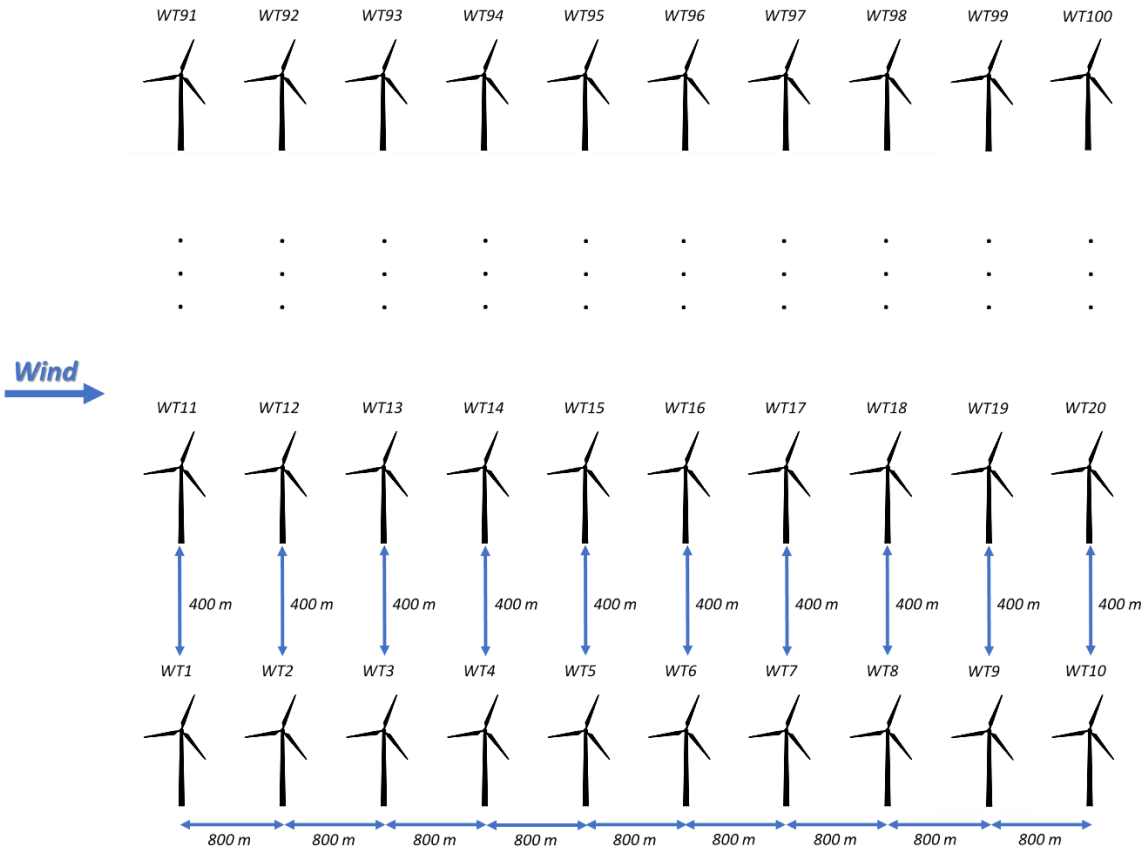

Figure 5-1: Wind farm layout

For the wind farm model creation within the Simulink environment, an initialisation script has been developed, which allows for the automated creation of the wind farm model based on the user defined parameters. The total number of turbines in the wind farm, simulation time, mean wind speed and turbulence intensity are all specified in this script. This simplifies the creation of wind farm models and ensures that the Simulink model is correctly constructed.

5.3.1 Droop Control Simulation Results

The use of fully rated converters does not allow modern wind turbines to be directly connected to the grid, and the turbine generator cannot provide droop control the same way a conventional power plant can. To provide primary response, wind farms are required to operate in curtailment, with 3% - 5% power reserve at any wind speed [69]. The ability of a large wind farm to provide the required curtailment, for different wind conditions, is assessed in this section, while the wind farm controller protects the turbines that are more likely to experience a failure.

5.3.1.1 Below Rated Wind Speed Conditions

As explained in Chapter 4, the turbines that are facing high wind speeds will be prioritised to reduce their power output, resulting in a load reduction on these machines. The comparison between the total power output of the wind farm under normal operation, the total power output of the wind farm under curtailed operation and the requested curtailment is shown in Figure 5-2.

As can be seen in Figure 5-2, at 300s the operator requests a curtailment of power production equal to 5% of normal production. To avoid unnecessary mechanical loading being imparted on the machines, the controller gradually decreases the total power. The controller considers the request as a low priority effect and ensures that the turbines utilised to provide the power reach the new set point gradually. The wind turbine controller prioritises the 70 wind turbines (i.e. 70%) that at 300s experience the highest wind speeds, thereby reducing the mechanical loading on said turbines. As can be seen, the requested power cannot be achieved at all times, as some of the prioritised turbines are unable to provide the ΔP requested from the controller. Figure 5-3 shows the number of wind turbines used by the wind farm controller to provide the requested ΔP.

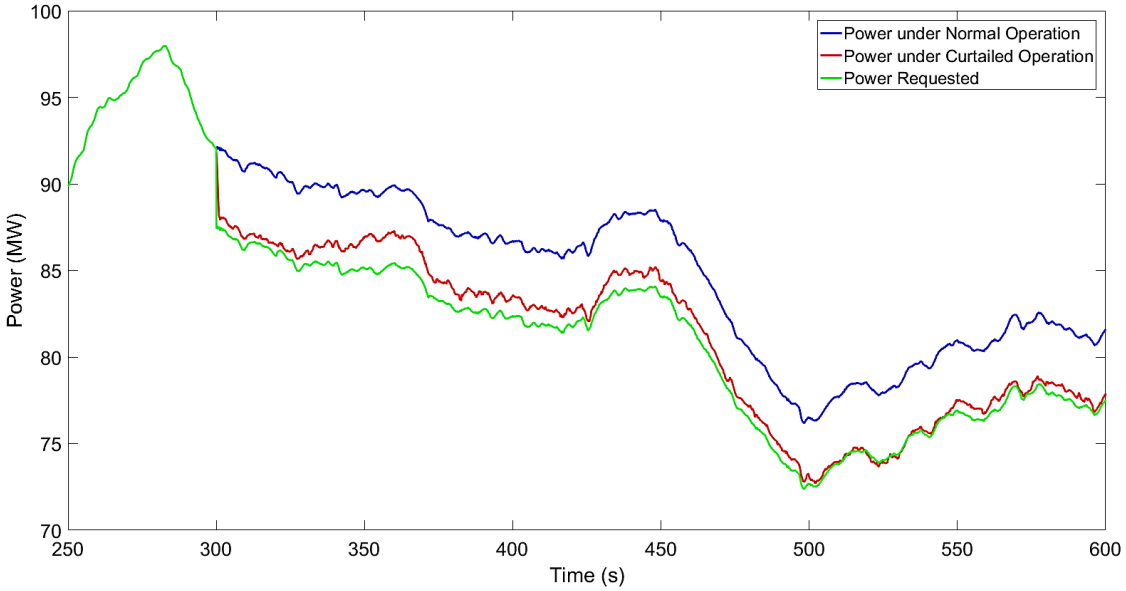

Figure 5-2: Comparison of total power output for normal operation and 5% power curtailment for below rated conditions when prioritised turbines are utilised

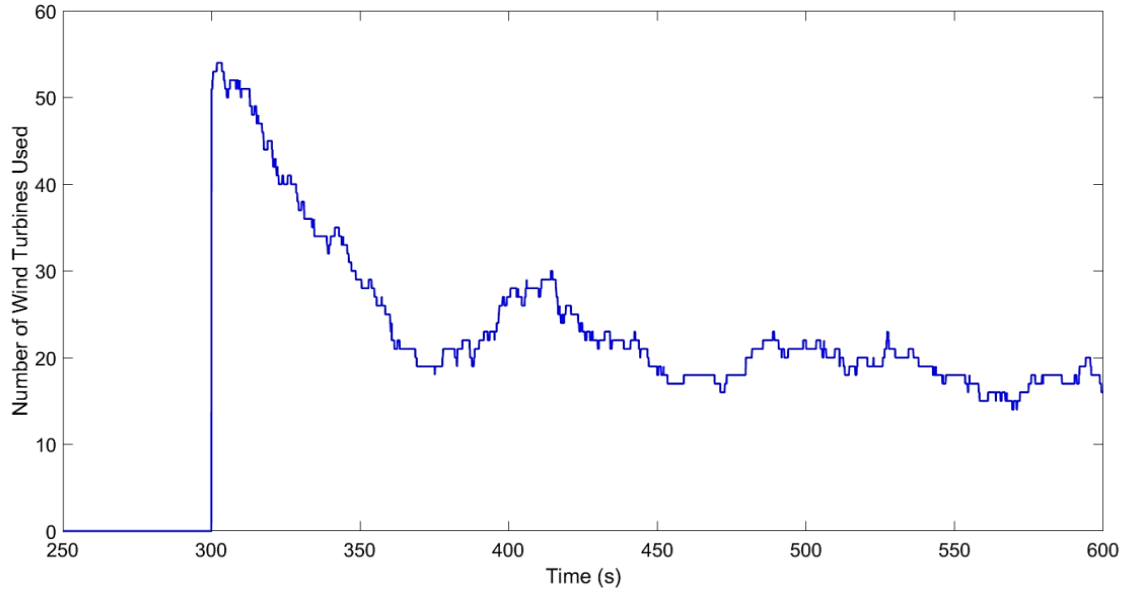

Figure 5-3: Number of turbines used to provide the requested power curtailment

As can be seen in Figure 5-3, the number of wind turbines used is changing based on the operational point that each of the prioritised wind turbine is experiencing. The number fluctuates between 14 and 54. It should be noted that even though the wind farm controller requests a ΔP from 70 turbines, that number is never reached due to constraints set by the wind field. Figure 5-4 depicts the requested ΔP for 5 turbines in the wind farm, namely wind turbines 4, 32, 48, 63 and 96.

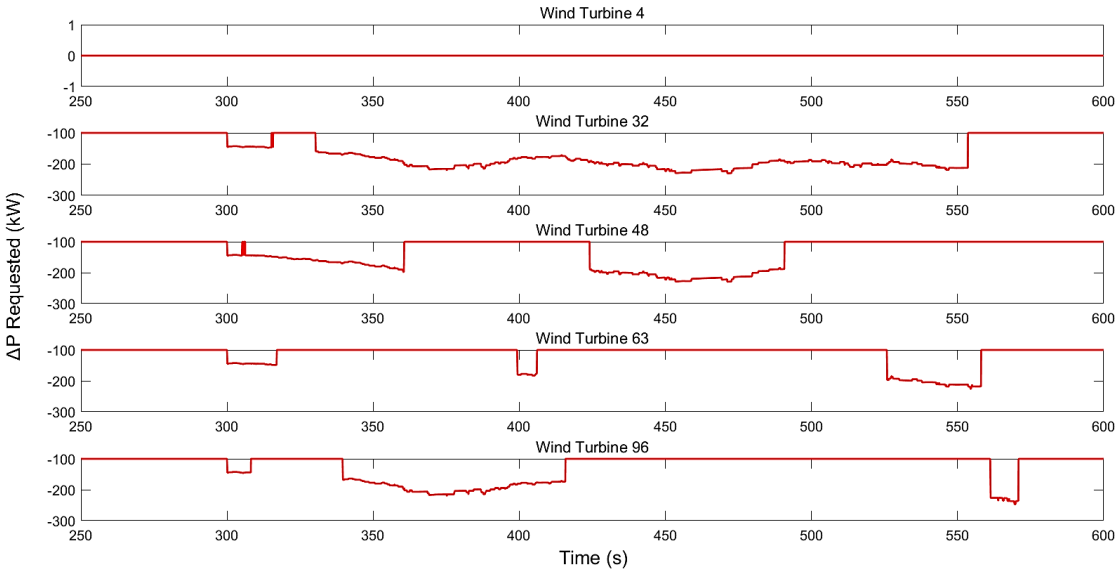

Figure 5-4: Requested ΔP per wind turbine, for turbines 4, 32, 48, 63 and 96

As illustrated in Figure 5-4, wind turbine 4 has not been requested to provide any ΔP. Wind turbines 32, 48, 63 and 96 have all been utilised to provide a ΔP, but none of these turbines could provide the ΔP for the whole required period.

For the utilised turbines, the investigation of the availability of the wind turbines shows the reason the turbines are rejected for providing power reduction. To investigate the reason behind the ΔP rejection, wind turbine 32 has been chosen for further analysis. Figure 5-5 shows the ΔP allocation with regards to the PAC rejection and recovery complete flags for wind turbine 32. As can be seen, at 300s turbine 32 starts providing the power curtailment until the

rejection flag changes from OFF (i.e. rejection flag equal to 0) to ON (i.e. rejection flag equal to 1). The turbine is then asked to stop providing the required ΔP and recover; hence, the recovery complete flag changes from recovery completed (i.e. recovery complete flag equal to 1) to wind turbine under recovery (i.e. recovery complete flag equal to 0). The wind farm controller does not request a ΔP until the rejection flag is OFF (i.e. rejection flag equal to 0) and the turbine has completed its recovery (i.e. recovery complete flag equal to 1). It should be noted that the wind farm controller ensures that the turbine is completely recovered before requesting a ΔP.

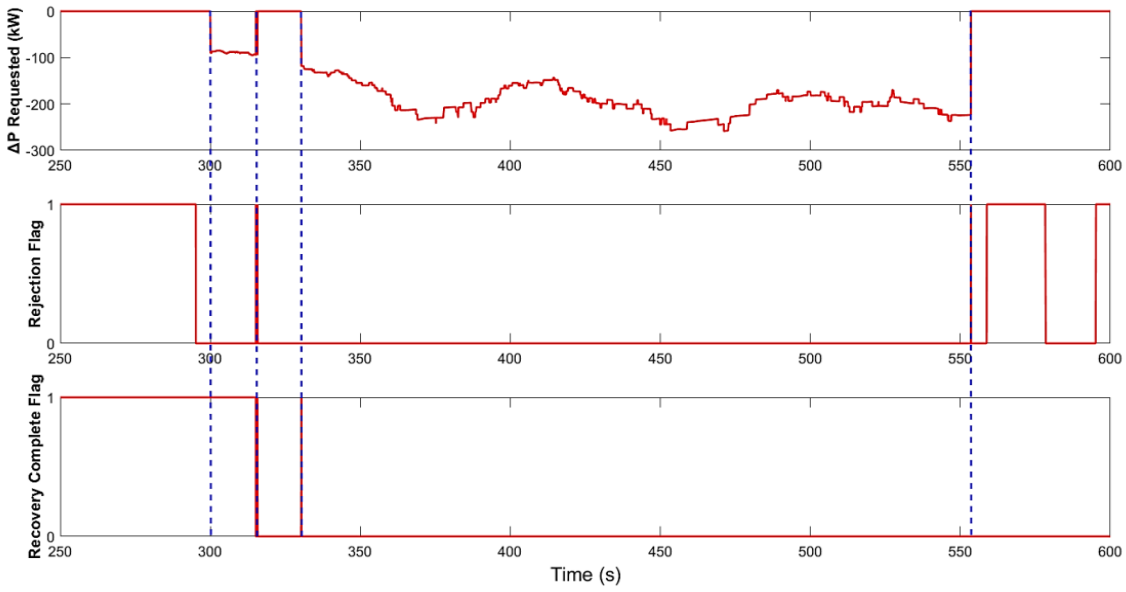

Figure 5-5: Investigation of ΔP request signals based on rejection and recovery complete flags for wind turbine 32

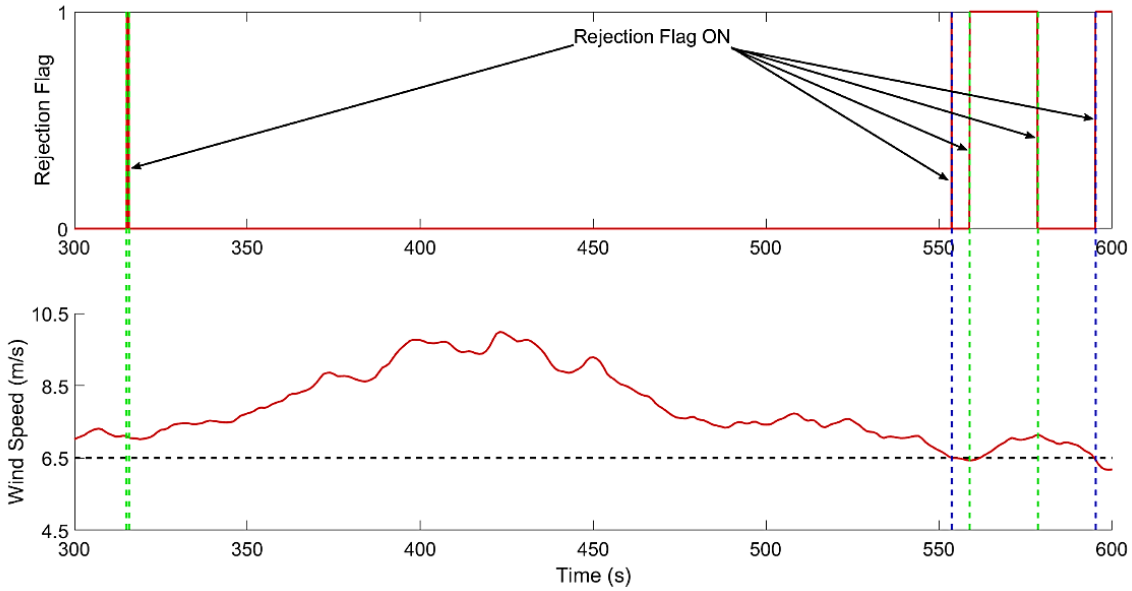

Figure 5-6: Wind speed with regards to the rejection flag for wind turbine 32

Figure 5-6 depicts the relationship between wind speed and rejection flag for wind turbine 32. As can be seen, the blue dashed line is used to illustrate the cases when the rejection flag is set to ON because the wind speed moves below 6.5ms^{-1}. The low wind speed procedure takes place when the turbine is experiencing wind speeds below 6.5ms^{-1} threshold [1] [62], and once the wind speed gets above the threshold then the rejection flag is revoked. The green dashed lines are used to illustrate the cases when the rejection flag is set to ON, but the wind speed is above 6.5ms^{-1}. For these cases, further investigation to understand the reason behind the rejection of the requested ΔP is required.

Figure 5-7 depicts the generator speed / torque diagram for wind turbine 32. As can be seen, the wind turbine reaches the PAC black limit twice, which would automatically set the rejection flag to ON and require the turbine to recover to normal operation. This explains why, as seen in Figure 5-6, the rejection flag is set to ON two times (i.e. green dashed line), when the wind speed is above the minimum threshold (i.e. 6.5ms^{-1}).

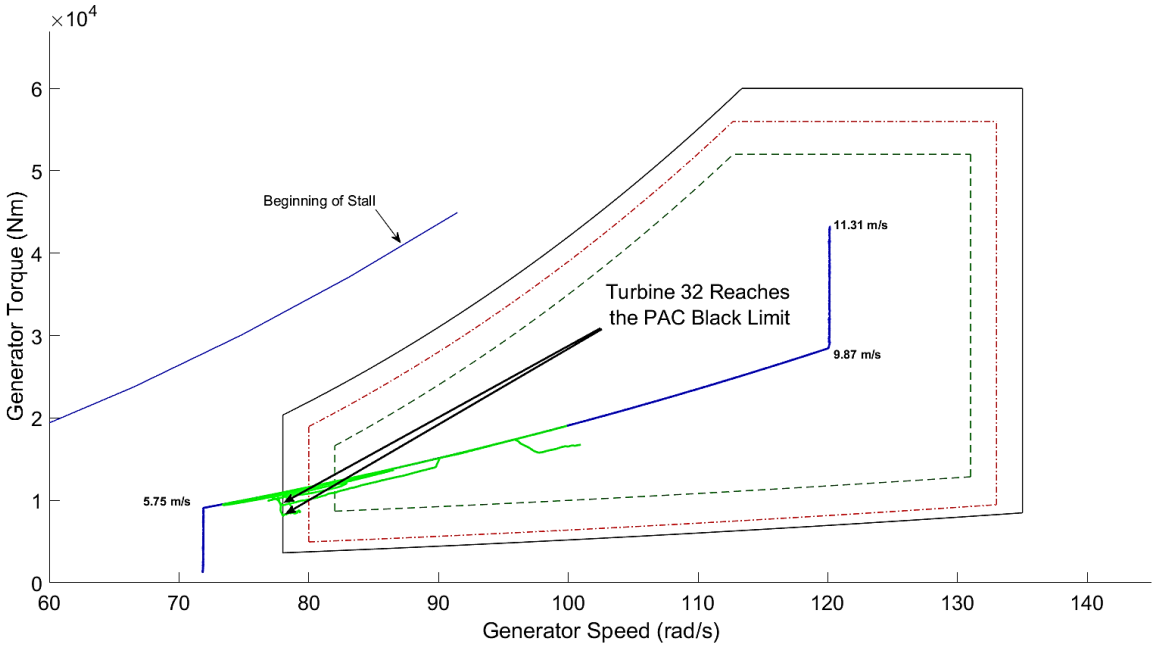

Figure 5-7: Wind turbine generator speed / torque diagram including PAC limits and operational strategy for wind turbine 32

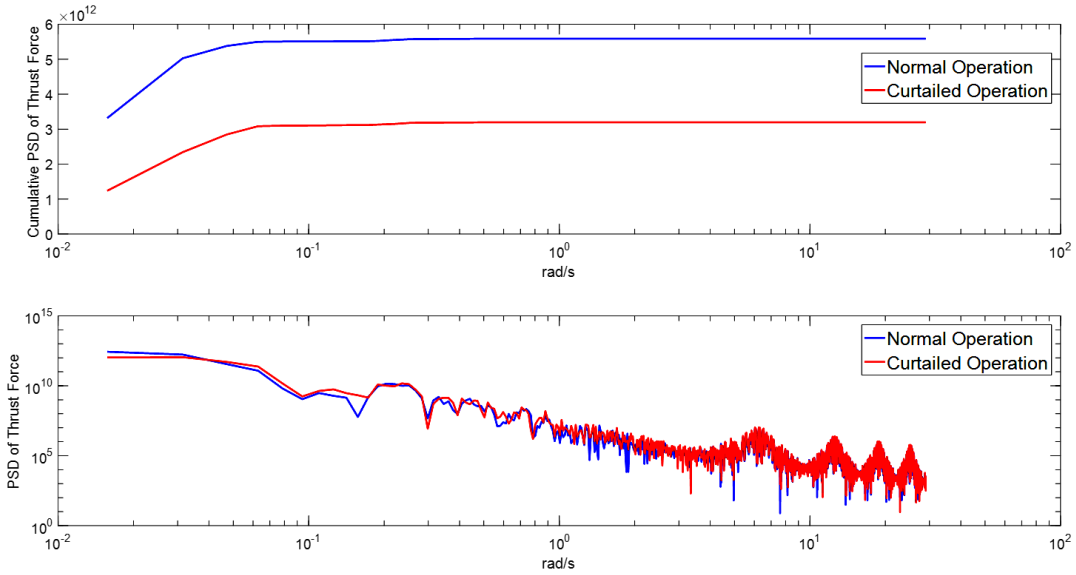

Figure 5-8: PSD and cumulative PSD plots of rotor aerodynamic thrust for wind turbine 32

Figure 5-8 shows the Power Spectral Density (PSD) and cumulative PSD of the aerodynamic thrust for wind turbine 32. As can be seen in Figure 5-8, for wind turbine 32 the level of the thrust force is significantly reduced during curtailed operation, resulting in decreased loads on the turbine.

The comparison between the total power output of the wind farm under normal operation, the total power output of the wind farm under curtailed operation and the requested curtailment is shown in Figure 5-9. The requested power cannot be achieved at all times, ultimately due to the constraints imposed by the wind field; however, the response is better than when 70% wind turbines were utilised. Figure 5-10 shows the number of wind turbines used by the wind farm controller to provide the requested ΔP.

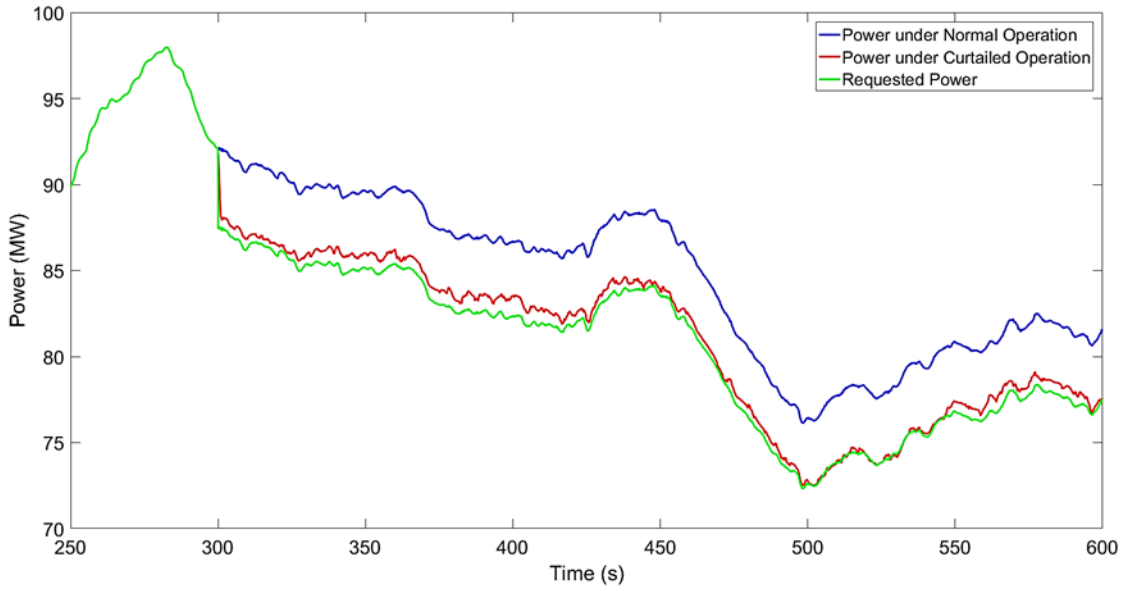

Figure 5-9: Comparison of total power output for normal operation and 5% power curtailment for below rated conditions when all turbines are utilised

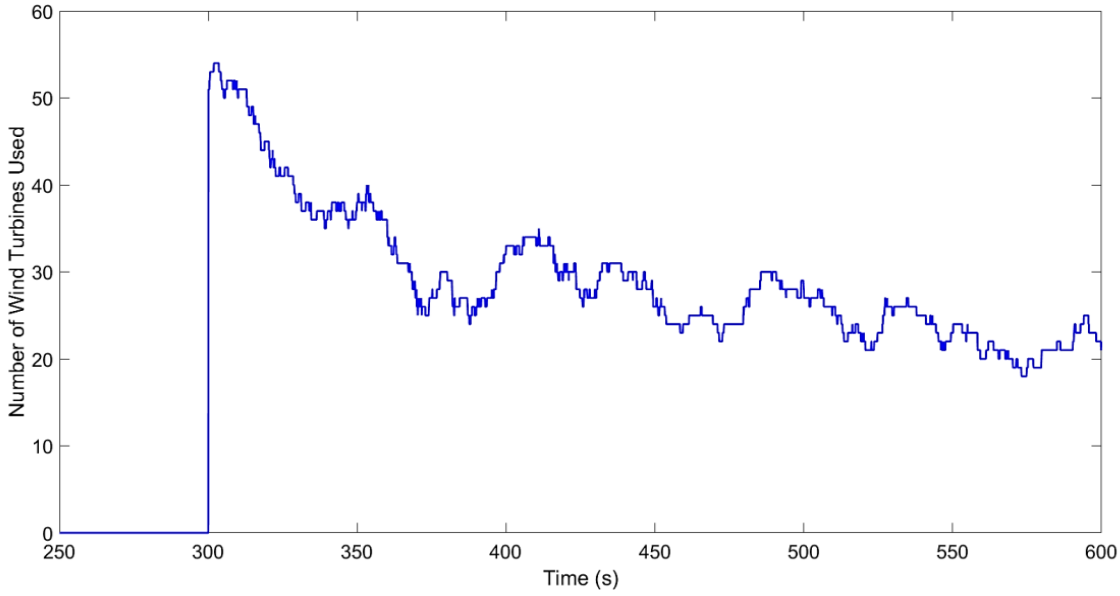

Figure 5-10: Number of turbines used to provide the requested power curtailment

As can be seen in Figure 5-10, the number of wind turbines used is changing based on the operational point that each of the prioritised wind turbine is experiencing. The number fluctuates between 18 and 54. It should be noted that even though the wind farm controller requests a ΔP from 100 turbines, that number is never reached ultimately due to constraints imposed by the wind field.

5.3.1.2 Rated Wind Speed Conditions

As explained in Chapter 4, the turbines that are facing high wind speeds will be prioritised to reduce their power output, resulting in a load reduction on these machines. The comparison between the total power output of the wind farm under normal operation, the total power output of the wind farm under curtailed operation and the requested curtailment is shown in Figure 5-11.

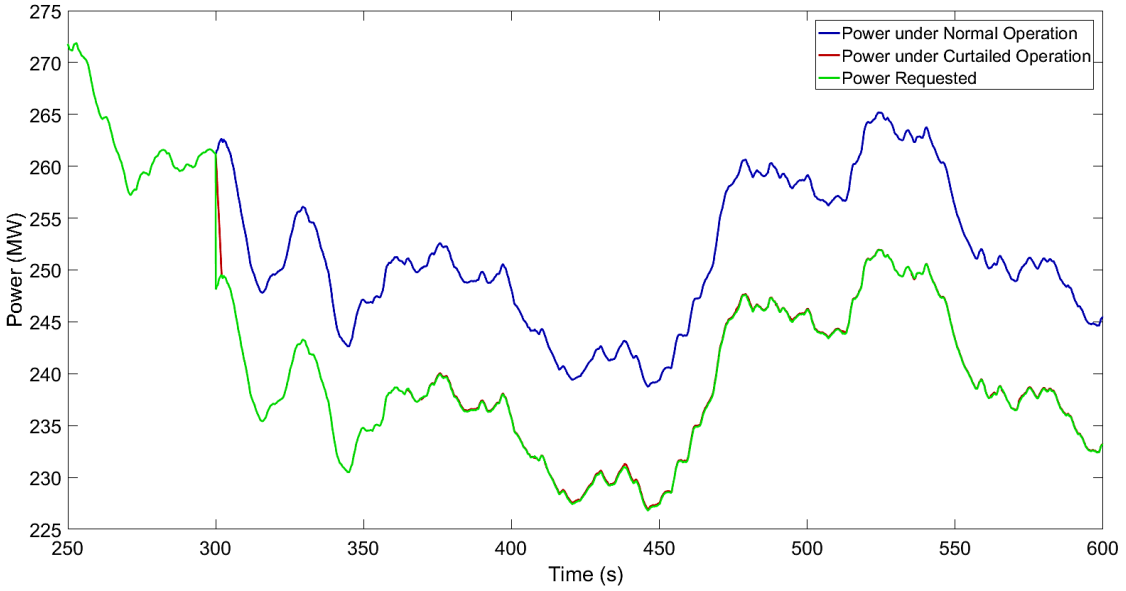

Figure 5-11: Comparison of total power output for normal operation and 5% power curtailment for rated conditions when some turbines are utilised

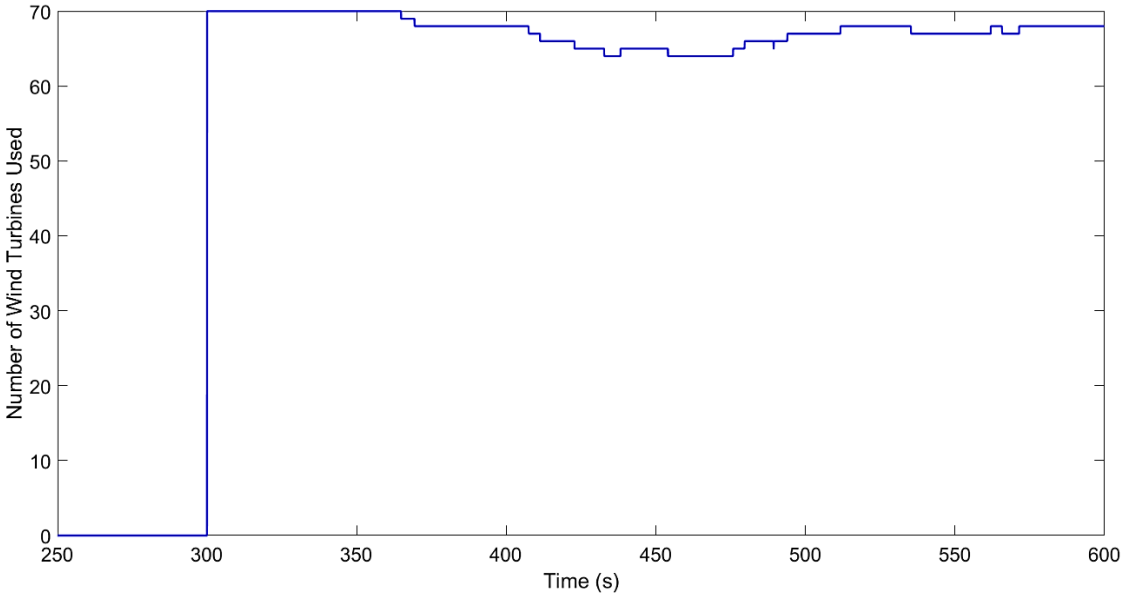

Figure 5-12: Number of turbines used to provide the requested power curtailment

As can be seen in Figure 5-11, at 300s the operator requests a curtailment of power production equal to 5% of normal production. The wind turbine controller prioritises the 70 wind turbines (i.e. 70%) that at 300s experience the highest wind speeds to reduce the loads on these turbines. As can be seen, the requested power is achieved at all times, ultimately due there being far fewer constraints imposed by the wind field. Those that remain are associated with wake deficits. Figure 5-12 shows the number of wind turbines that are used by the wind farm controller to provide the requested ΔP.

As can be seen in Figure 5-12, the number of wind turbines used is changing based on the operational point that each of the prioritised wind turbine is experiencing. The number fluctuates between 64 and 70. Figure 5-13 depicts the requested ΔP for 5 turbines in the wind farm, namely wind turbines 18, 30, 51, 74 and 86.

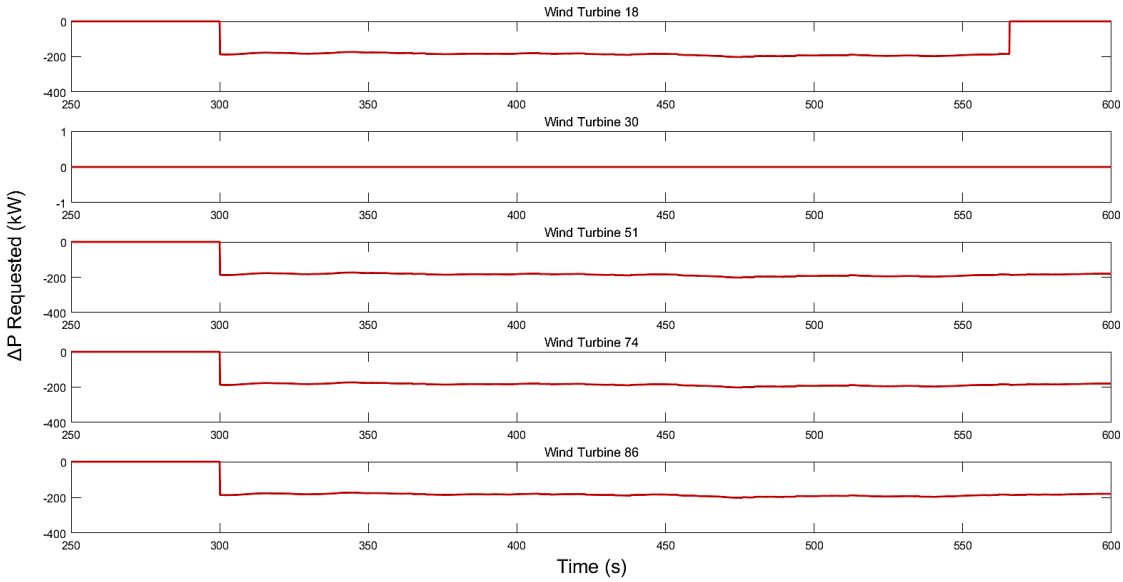

Figure 5-13: Requested ΔP per wind turbine, for turbines 18, 30, 51, 74 and 86

As illustrated in Figure 5-13, wind turbine 30 has not been requested to provide any ΔP. Wind turbines 18, 51, 74 and 86 have all been utilised to provide a ΔP. Turbine 18 has not been able

to provide the requested ΔP for the total required period, but all the other utilised turbines (i.e. 51, 74 and 86) have provided the requested ΔP for the total required period.

To investigate the reason behind the ΔP rejection, wind turbine 18 has been chosen for further analysis. Figure 5-14 shows the ΔP allocation with regards to the PAC rejection and recovery complete flags for wind turbine 18. As can be seen, at 300s turbine 18 starts providing the power curtailment until the rejection flag changes from OFF (i.e. rejection flag equal to 0) to ON (i.e. rejection flag equal to 1). The turbine is then asked to stop providing the required ΔP and recover. The wind farm controller does not request a ΔP until the rejection flag is OFF (i.e. rejection flag equal to 0) and the turbine has completed its recovery (i.e. recovery complete flag equal to 1). It should be noted that the wind farm controller ensures that the turbine is completely recovered before requesting a ΔP.

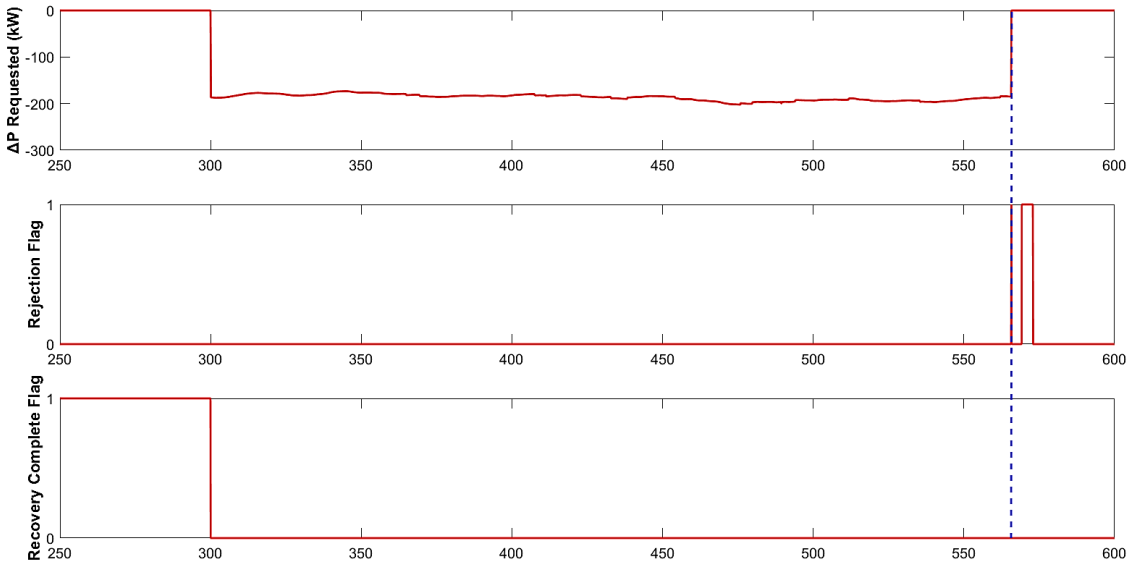

Figure 5-14: Investigation of ΔP request signals based on rejection and recovery complete flags for wind turbine 18

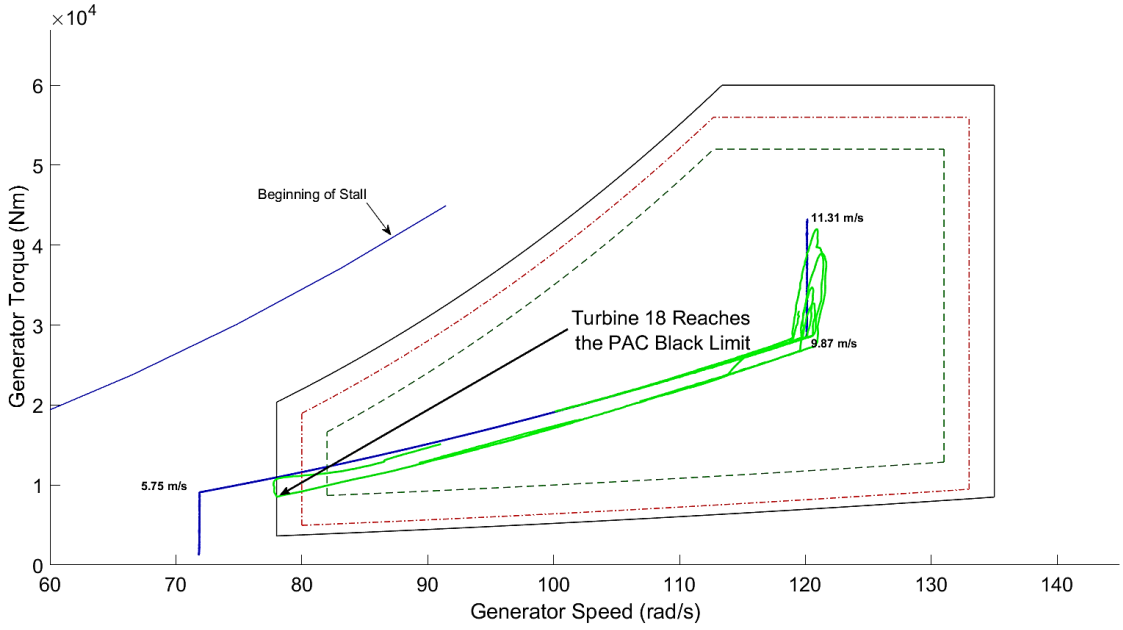

Figure 5-15: Wind turbine generator speed / torque diagram including PAC limits and operational strategy for wind turbine 18

Figure 5-15 depicts the generator speed / torque diagram for wind turbine 18. As can be seen the wind turbine reaches the PAC black limit, which would automatically set the rejection flag to ON and require the turbine to recover. This explains why, in Figure 5-14, the rejection flag is set to ON.

Figure 5-16 shows the PSD and cumulative PSD of the aerodynamic thrust for wind turbine 18. As can be seen in Figure 5-16, for wind turbine 18 the level of the thrust force is significantly reduced during curtailed operation, resulting to decreased loads on the turbine.

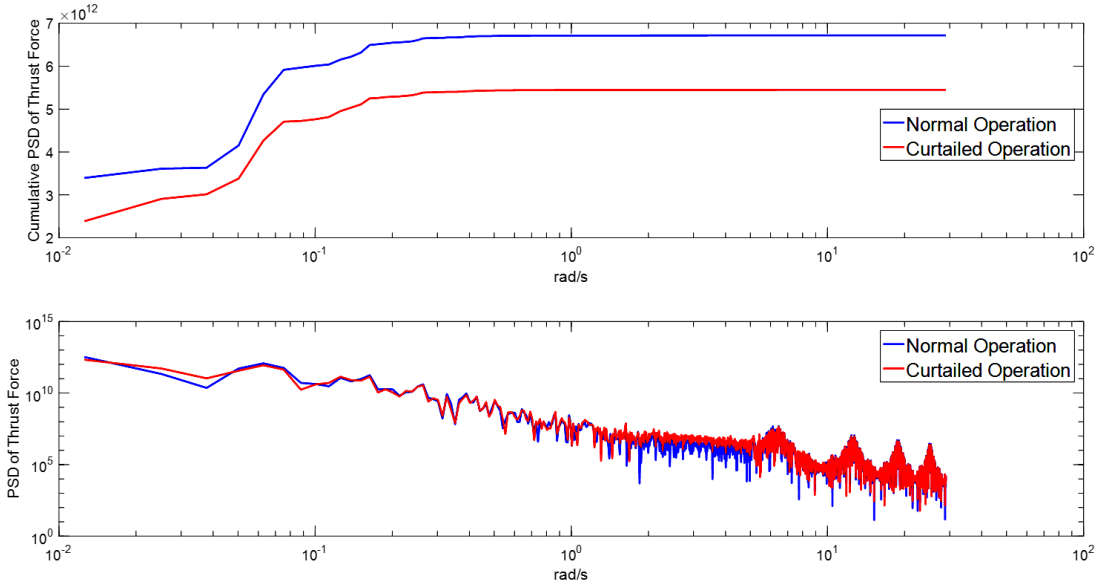

Figure 5-16: PSD and cumulative PSD plots of rotor aerodynamic thrust for wind turbine 18

5.3.1.3 Above Rated Wind Speed Conditions

As explained in Chapter 4, the turbines that are facing high wind speeds will be prioritised to reduce their power output, resulting to a load reduction on these machines. The comparison between the total power output of the wind farm under normal operation, the total power output of the wind farm under curtailed operation and the requested curtailment is shown in Figure 5-17.

As can be seen, the requested power is achieved at all times, due to the lack of constraints being imposed by the wind field. Figure 5-18 shows the number of wind turbines that are used by the wind farm controller to provide the requested ΔP.

As can be seen in Figure 5-18, the number of wind turbines used remains constant, which means that all the prioritised wind turbines are able to provide the requested ΔP for the requested period of time. Figure 5-19 depicts the requested ΔP for 5 turbines in the wind farm, namely wind turbines 7, 36, 55, 80 and 93.

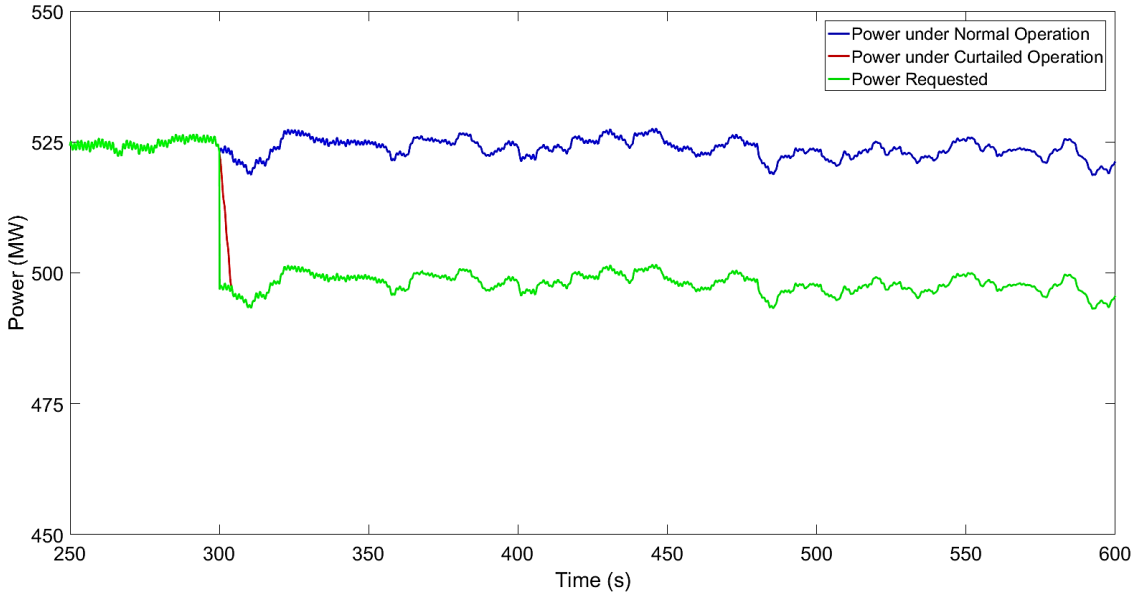

Figure 5-17: Comparison of total power output for normal operation and 5% power curtailment for above rated conditions when some turbines are utilised

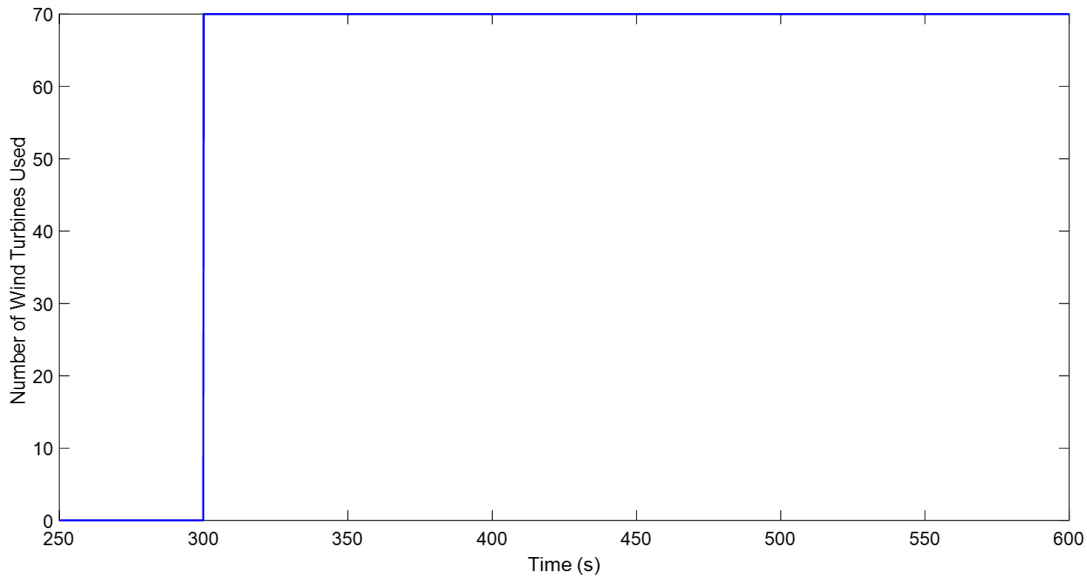

Figure 5-18: Number of turbines used to provide the requested power curtailment

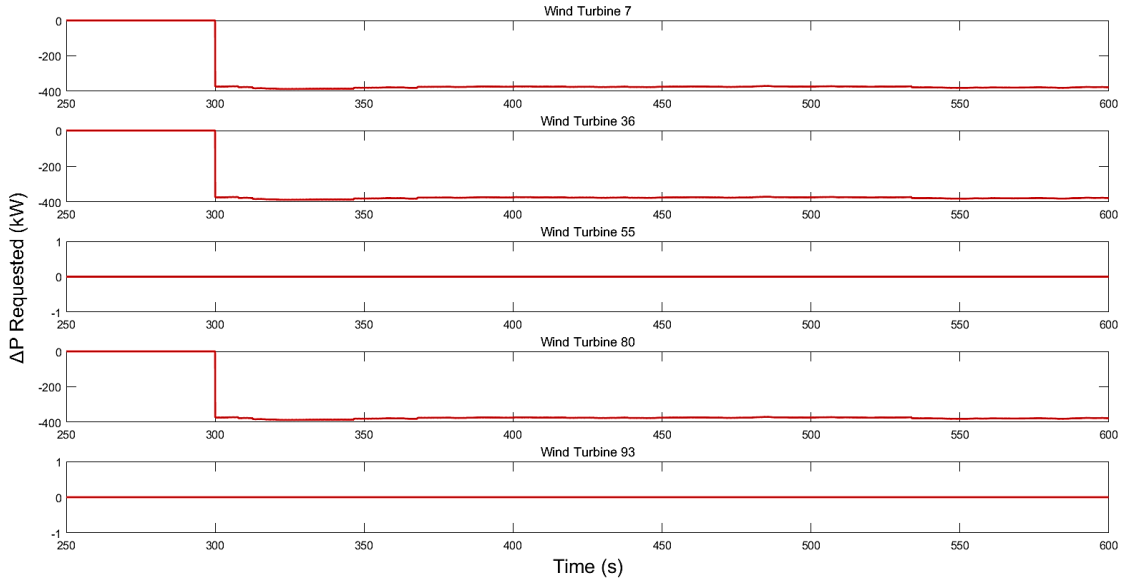

Figure 5-19: Requested ΔP per wind turbine, for turbines 7, 36, 55, 80 and 93

As illustrated in Figure 5-19, wind turbines 55 and 93 have not been requested to provide any ΔP. Wind turbines 7, 36 and 80 have all been utilised to provide a ΔP, and all have provided the requested ΔP for the total required period.

For the investigation of the load reduction on the utilised turbines, wind turbine 80 has been chosen for further analysis. Figure 5-20 shows the PSD and cumulative PSD of the aerodynamic thrust for wind turbine 80. As can be seen, for wind turbine 80 the level of the thrust force is significantly reduced during curtailed operation, resulting in decreased loads on the turbine.

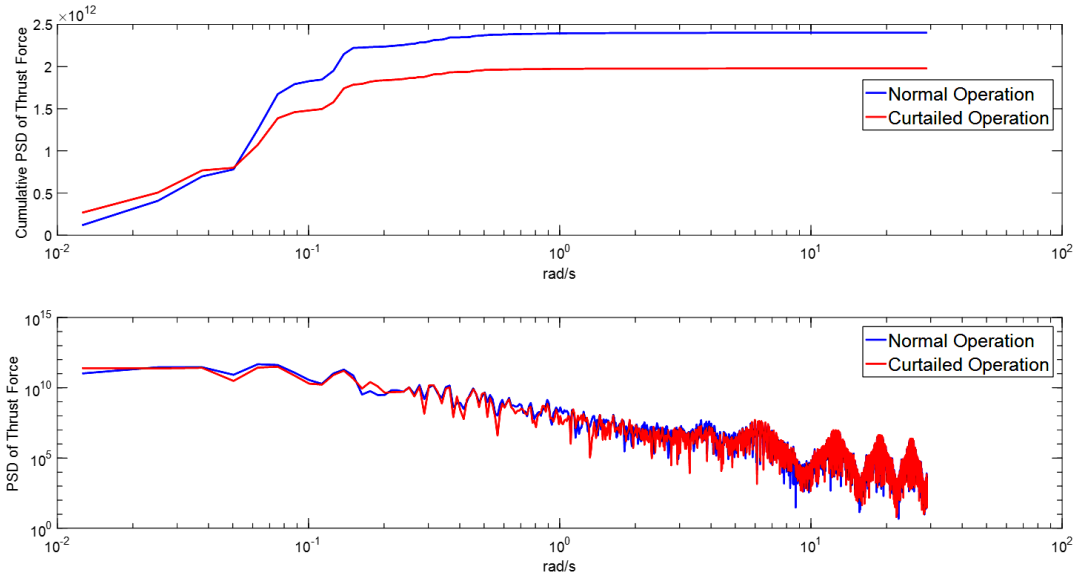

Figure 5-20: PSD and cumulative PSD plots of rotor aerodynamic thrust for wind turbine 80

5.3.2 Network Controller Primary Response Simulation Results

Providing frequency stability services to the system operator is essential. Owing to their large size, both in terms of power rating and inertia, it is expected that large offshore wind farms will be required to provide such services in the future. The wind farm controller allows flexible wind farm operation at all operating conditions, below or above rated. This section assesses the capability of the wind farm controller to provide synthetic inertia and primary response services to the system operator. For primary response, the response time is required to be less than 10s [70], and should be able to be sustained for a minimum of 20 seconds after an event has occurred [70]. For synthetic inertia purposes, the response should occur within 200ms [76].

5.3.2.1 Below Rated Wind Speed Conditions

The comparison between the total power output of the wind farm under normal operation, the total power output of the wind farm under curtailed operation and the requested curtailment is shown in Figure 5-21.

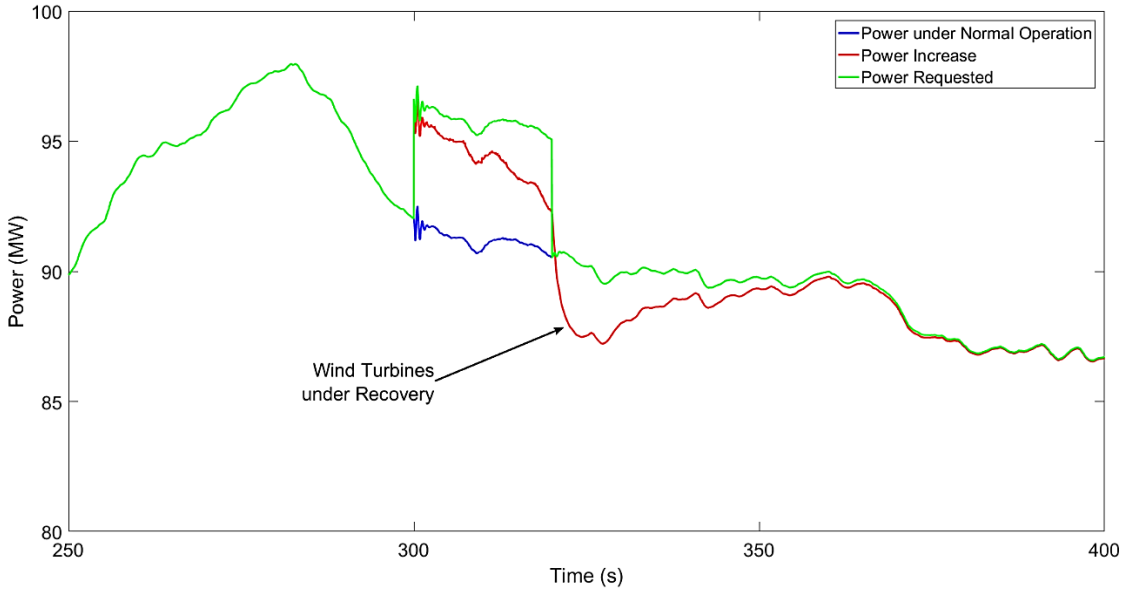

Figure 5-21: Comparison of total power output for normal operation and 5% synthetic inertia power increase for below rated conditions

As can be seen in Figure 5-21, the requested power cannot be reached at any point, ultimately due to the constraints imposed by the wind field. The change in power happens instantaneously, which gives the wind farm controller the ability to provide synthetic inertia services to the system operator. It should be noted that even though the wind farm response does not match the request, there is still some additional power injected to the grid, which, for below rated conditions, is quite significant. Figure 5-22 illustrates the response of 5 wind turbines, namely wind turbines 19, 25, 44, 65 and 82 to the positive ΔP requested from the wind farm controller.

As can be seen in Figure 5-22, turbine 44 can only provide the requested ΔP for a small period of time, turbines 19 and 25 cannot provide any ΔP while turbines 65 and 82 are able to provide the requested ΔP for the full 20 second period.

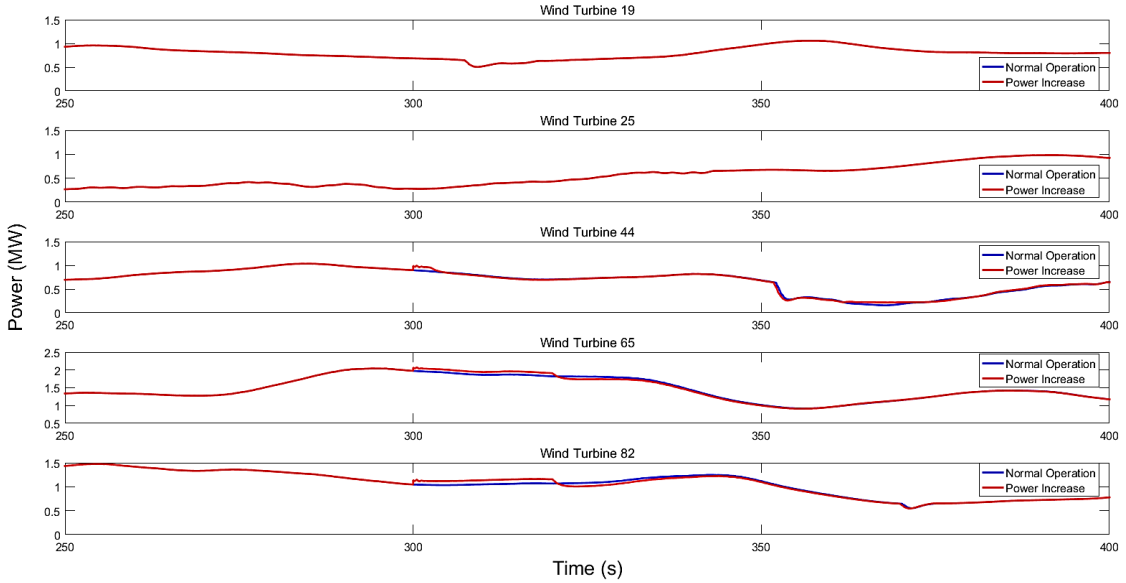

Figure 5-22: Power production comparison for wind turbines 19, 25, 44, 65 and 82

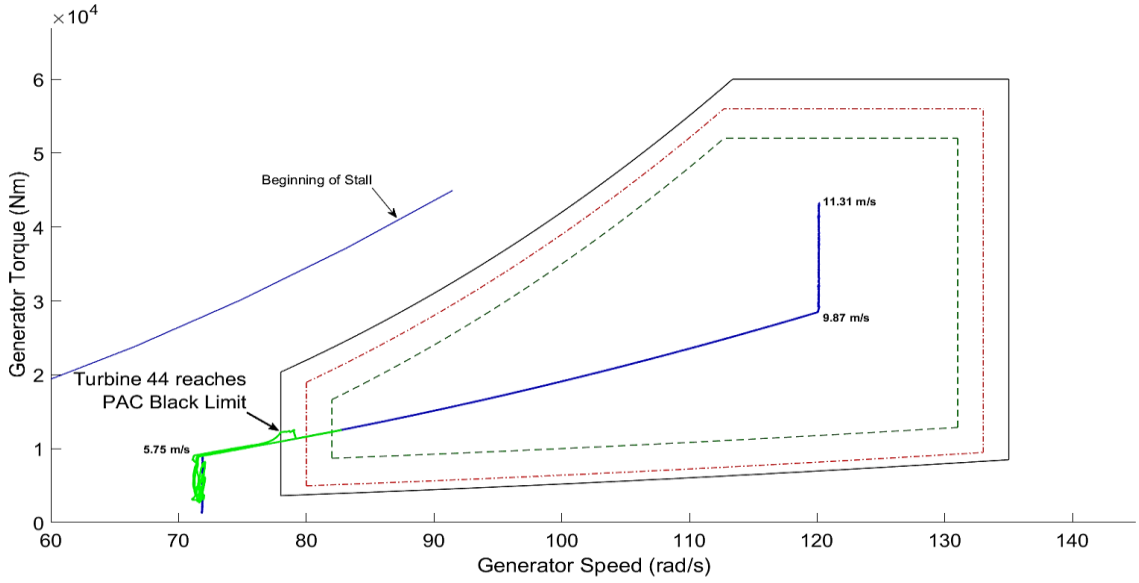

Figure 5-23: Wind turbine generator speed / torque diagram including PAC limits and operational strategy for wind turbine 44

Figure 5-23 depicts the generator speed / torque diagram for wind turbine 44. As can be seen, the wind turbine is operating normally until an increase in generator torque is requested from the wind farm controller. The turbine provides the requested increased power until it reaches the PAC's black limit. At that point, the turbine cannot provide the ΔP anymore, and the turbine recovers to its normal operation point. Figure 5-24 depicts the requested ΔP from the wind farm controller for wind turbines 19, 25, 44, 65 and 82. As can be seen a positive ΔP has been requested from all the available turbines in the wind farm.

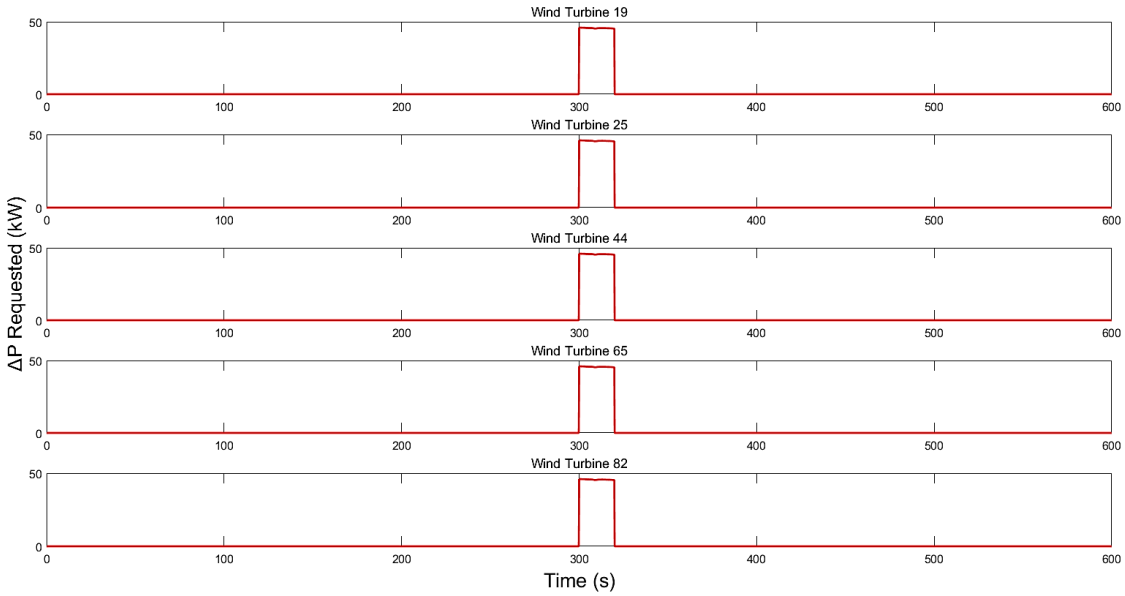

Figure 5-24: Requested ΔP per turbine for wind turbines 19, 25, 44, 65 and 82

For the investigation of the load reduction on utilised turbines, wind turbine 44 has been chosen for analysis. Figure 5-25 depicts the PSD and cumulative PSD of the aerodynamic thrust force for wind turbine 44. As can be seen, the level of the thrust force is slightly increased, resulting to increased loads on the turbine. The load increase is barely noticeable, as the increased loading period is only 20 seconds, which is a small portion of the simulation time and the requested power increase was approximately 50kW per wind turbine, which corresponds to relatively small thrust force increase.

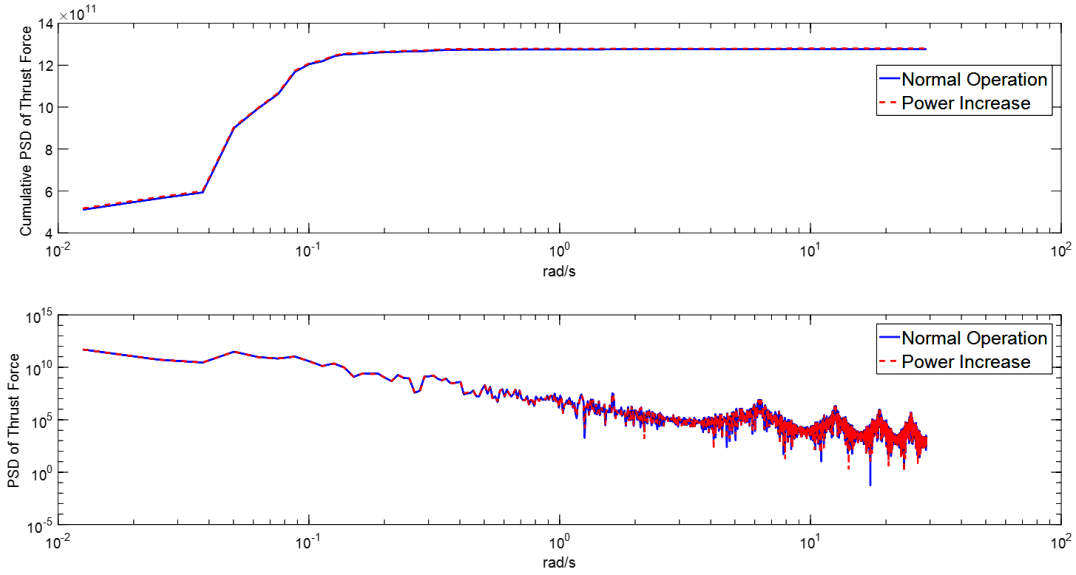

Figure 5-25: PSD and cumulative PSD plots of the rotor aerodynamic thrust force for wind turbine 44

5.3.2.2 Rated Wind Speed Conditions

The comparison between the total power output of the wind farm under normal operation, the total power output of the wind farm under curtailed operation and the requested curtailment is shown in Figure 5-26.

As can be seen in Figure 5-26, the requested power is reached instantaneously as the turbines provide the ΔP requested from the controller; that is, the wind farm is completely capable of providing short term frequency support to the system operator. It should be noted that the power increases instantly and the increase is maintained for the duration of 20 seconds. Figure 5-27 illustrates the response of 5 wind turbines, namely wind turbines 13, 34, 60, 71 and 100 to the positive ΔP requested from the wind farm controller.

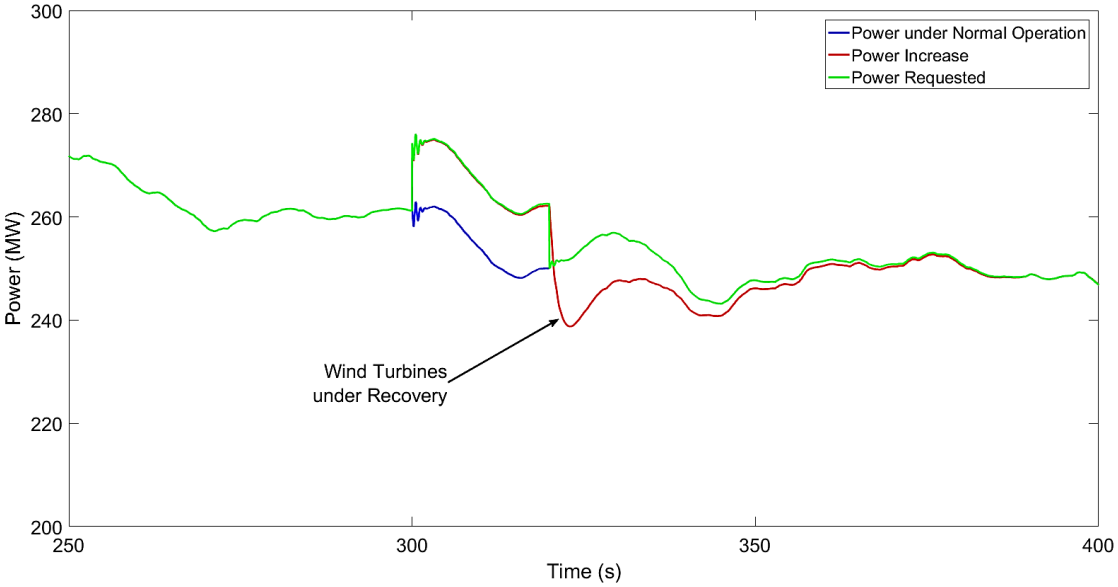

Figure 5-26: Comparison of total power output for normal operation and 5% synthetic inertia power increase for rated conditions

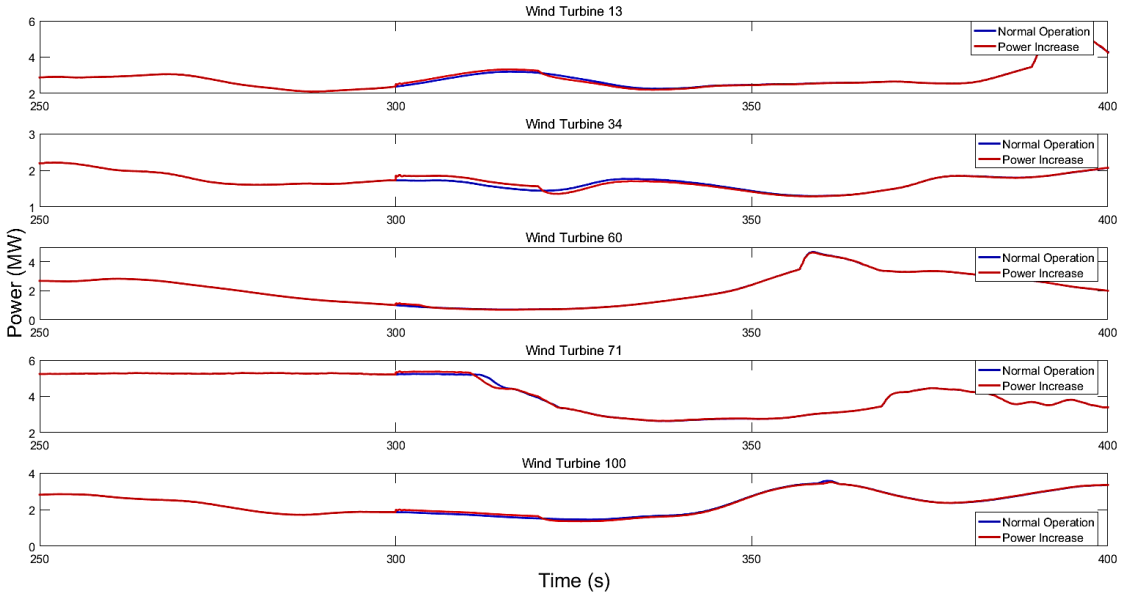

Figure 5-27: Power production comparison for wind turbines 13, 34, 60, 71 and 100

As can be seen in Figure 5-27, turbines 60 and 71 can only provide the requested ΔP for a small period of time, while turbines 13, 34 and 100 are able to provide the requested ΔP for the full 20 second period.

Figure 5-28 depicts the generator speed / torque diagram for wind turbine 60. As can be seen, the wind turbine is operating normally until an increase in generator torque is requested from the wind farm controller. The turbine provides the requested increased power until it reaches the PAC's black limit. At that point the turbine cannot provide the ΔP anymore, and the turbine recovers to its normal operation point.

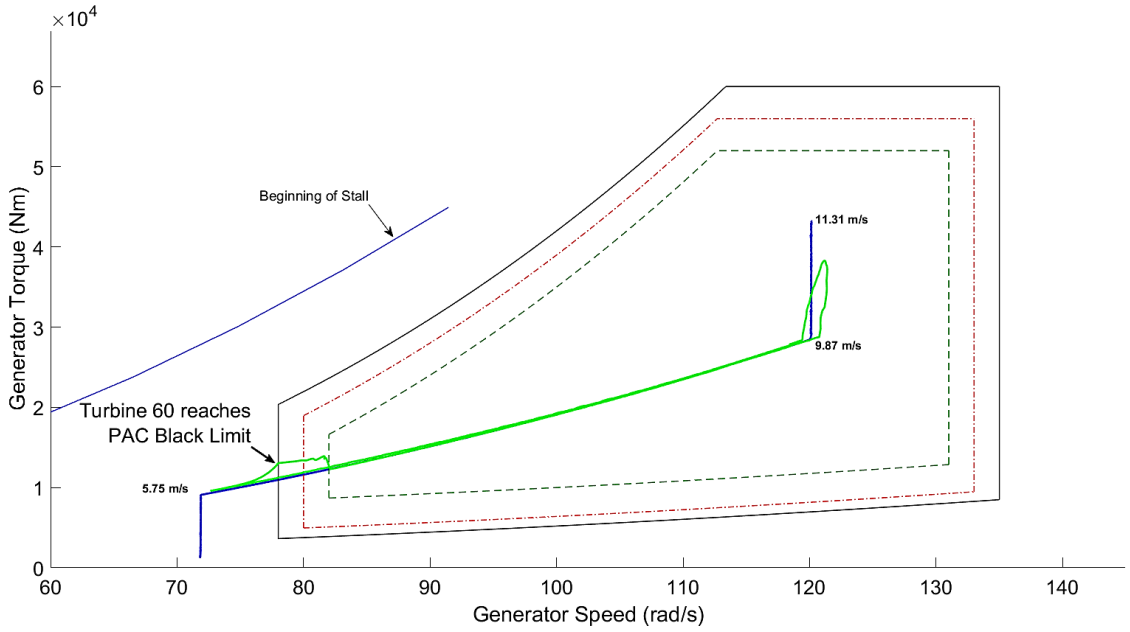

Figure 5-28: Wind turbine generator speed / torque diagram including PAC limits and operational strategy for wind turbine 60

Figure 5-29 shows the requested ΔP from the wind farm controller for wind turbines 13, 34, 60, 71 and 100. As can be seen, a positive ΔP has been requested from all the available turbines in the wind farm.

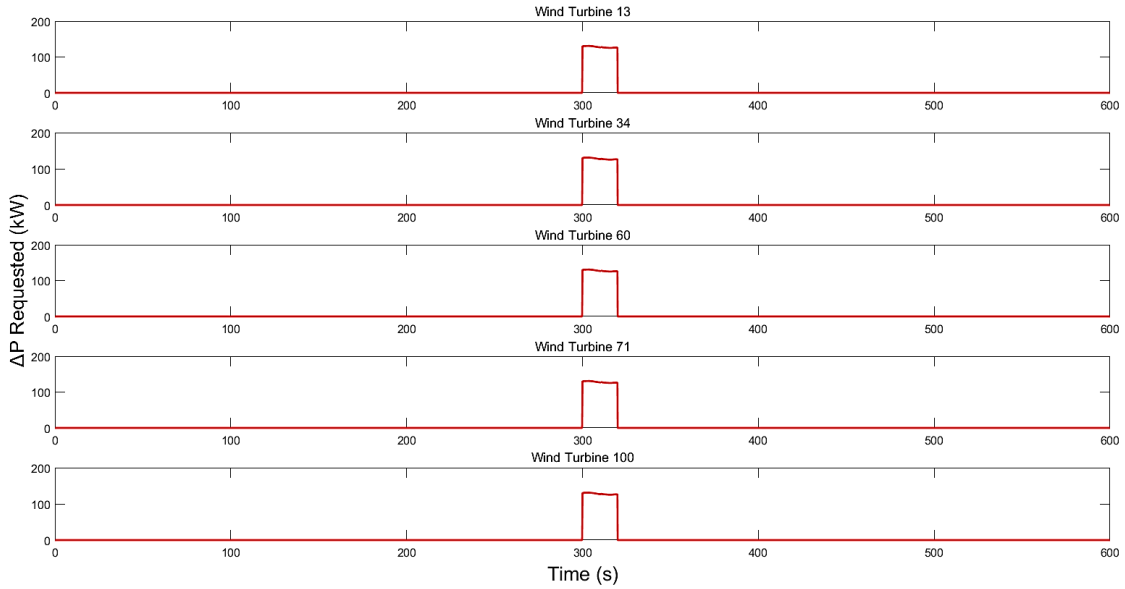

Figure 5-29: Requested ΔP per turbine for wind turbines 13, 34, 60, 71 and 100

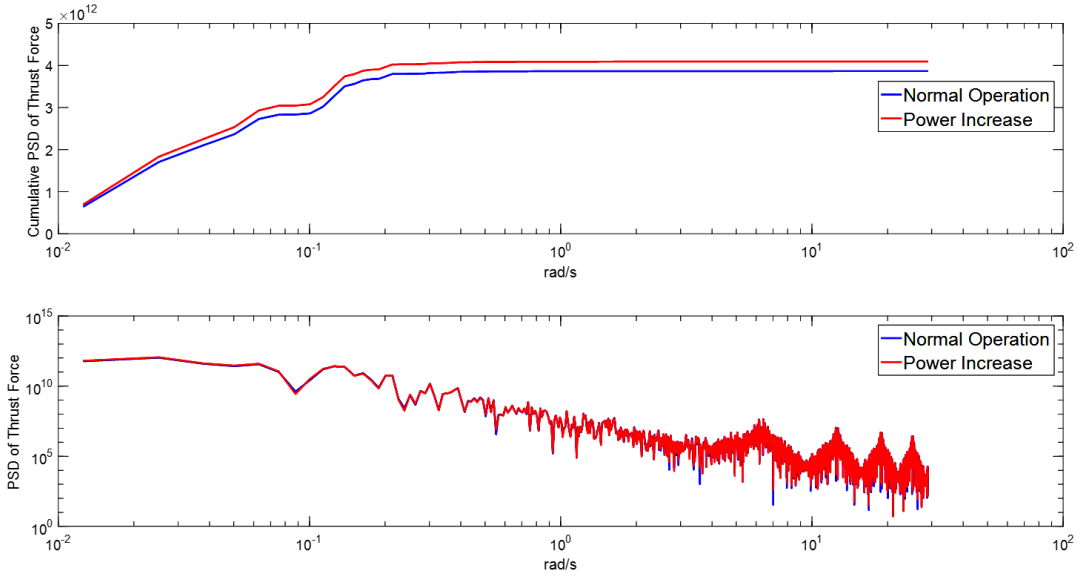

Figure 5-30: PSD and cumulative PSD plots of the rotor aerodynamic thrust force for wind turbine 100

For the investigation of the load reduction on utilised turbines, wind turbine 100 has been chosen for analysis. Figure 5-30 depicts the PSD and cumulative PSD of the aerodynamic thrust force for wind turbine 100. As can be seen, the level of the thrust force is slightly increased, resulting to increased loads on the turbine. The load increase is barely noticeable, as the increased loading period is only 20 seconds, which is a small portion of the simulation time and the requested power increase was approximately 100kW per wind turbine, which corresponds to relatively small thrust force increase.

5.3.2.3 Above Rated Wind Speed Conditions

The comparison between the total power output of the wind farm under normal operation, the total power output of the wind farm under curtailed operation and the requested curtailment is shown in Figure 5-31.

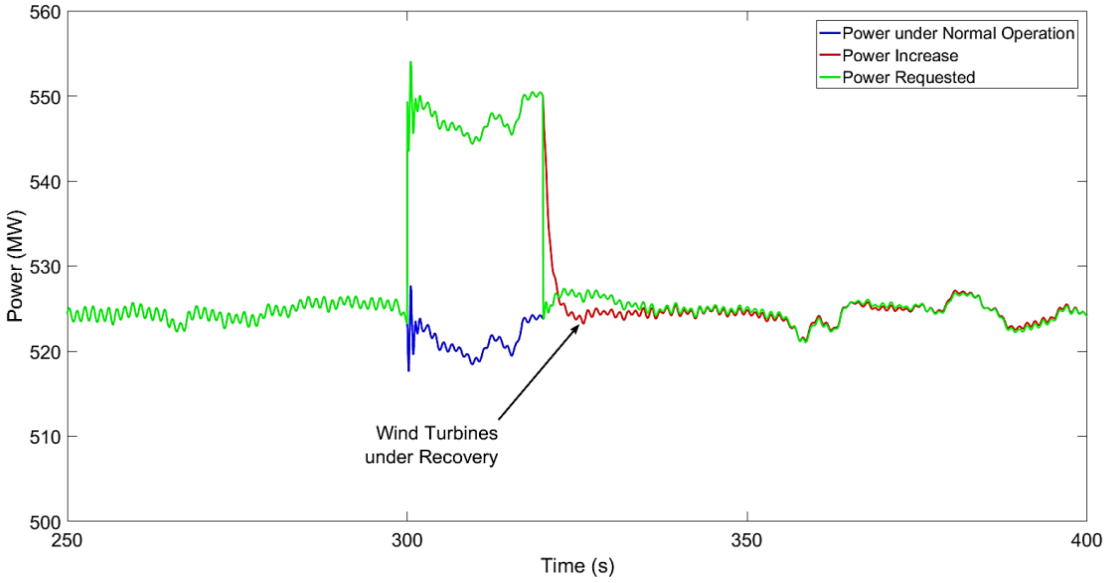

Figure 5-31: Comparison of total power output for normal operation and 5% synthetic inertia power increase for above rated conditions

As can be seen in Figure 5-31, the requested power is reached instantaneously as the turbines provide the ΔP requested from the controller, which gives the wind farm controller the ability to provide synthetic inertia services to the system operator. It should be noted that the power

increases instantly and the increase is maintained for the duration of 20 seconds. This results to the fact that the wind farm controller can provide primary response services to the system operator, without the need of droop control, when operating at above rated conditions. Figure 5-32 illustrates the response of 5 wind turbines, namely wind turbines 1, 22, 47, 67 and 85 to the positive ΔP requested from the wind farm controller.

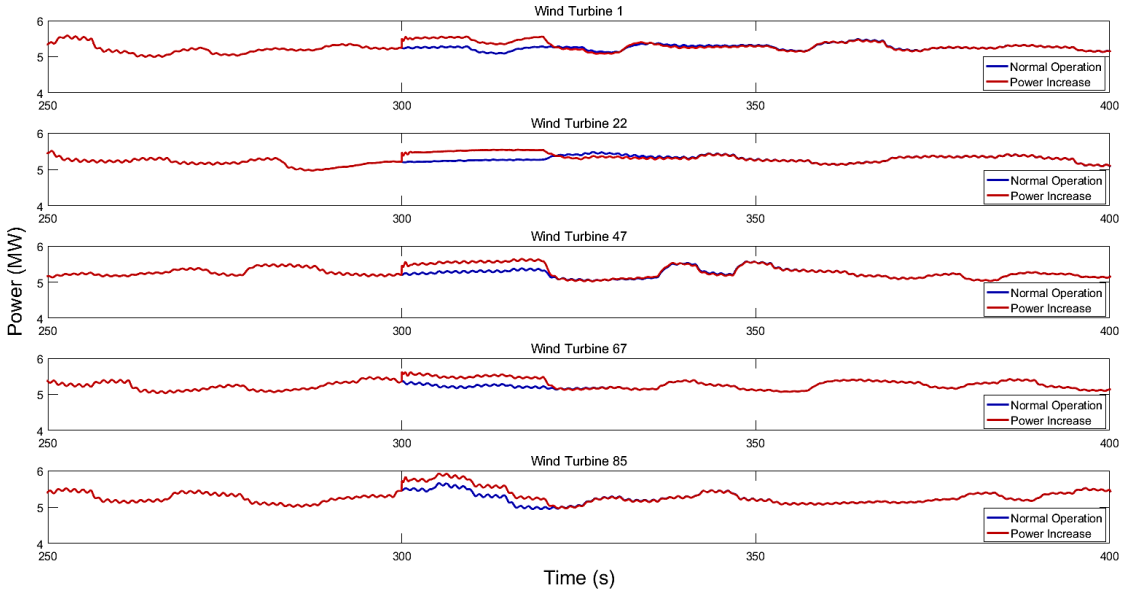

Figure 5-32: Power production comparison for wind turbines 1, 22, 47, 67 and 85

As can be seen in Figure 5-32, all the turbines are able to provide the requested positive ΔP for the full 20 second period.

Figure 5-33 depicts the generator speed / torque diagram for wind turbine 22. As can be seen, the wind turbine is operating normally until an increase in generator torque is requested from the wind farm controller. The turbine provides the requested increased power until the wind farm controller ceases the ΔP, and then recovers to its normal operation point. It should be noted that turbine 22 operates within the green PAC limit.

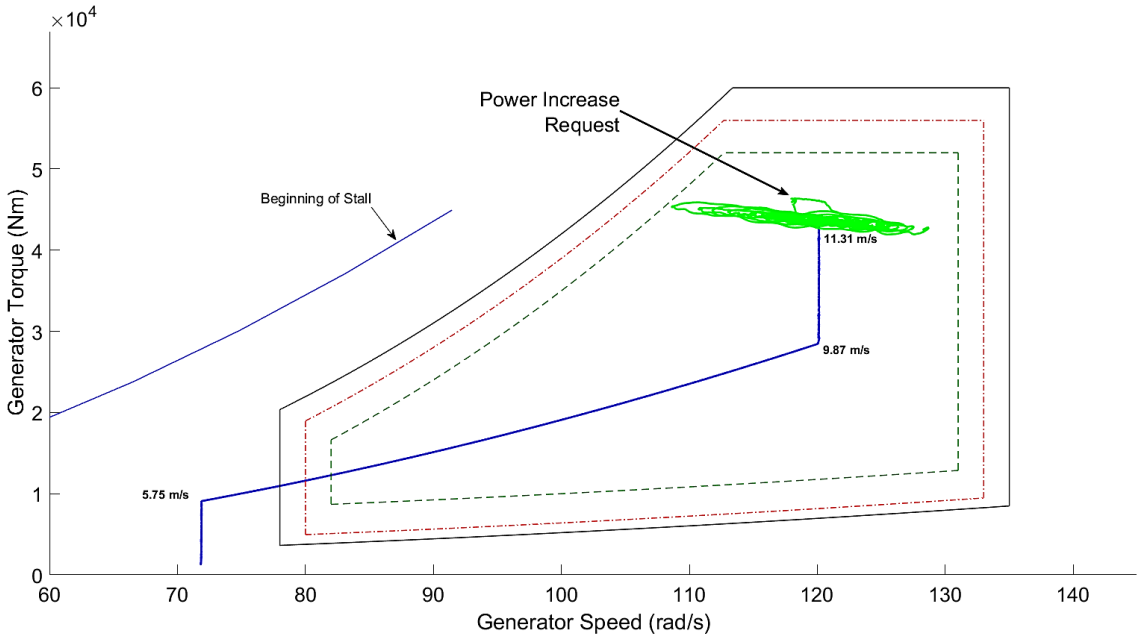

Figure 5-33: Wind turbine generator speed / torque diagram including PAC limits and operational strategy for wind turbine 22

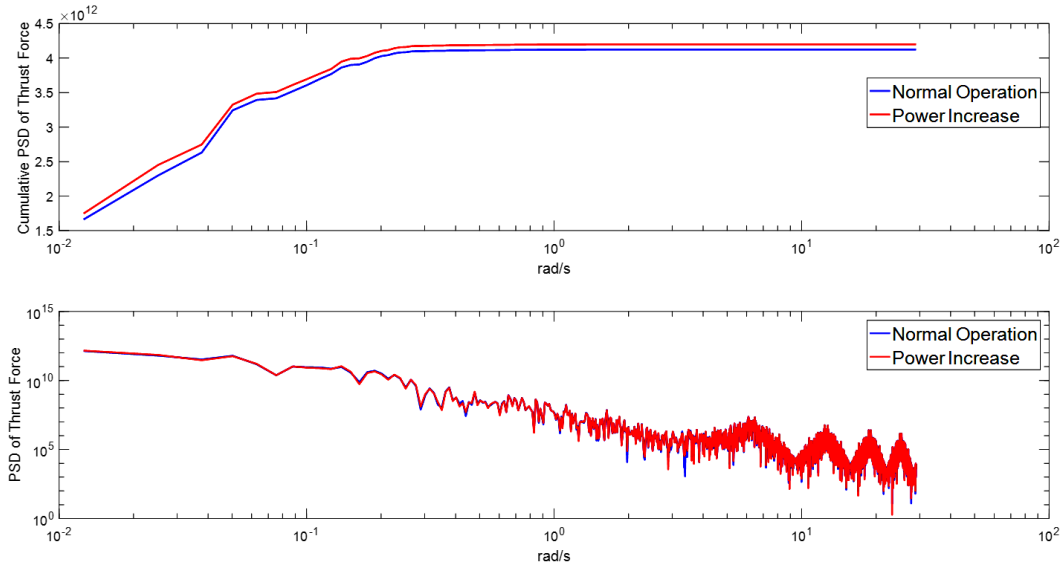

Figure 5-34: PSD and cumulative PSD plots of the rotor aerodynamic thrust force for wind turbine 22

For the investigation of the load reduction on utilised turbines, wind turbine 44 has been chosen for analysis. Figure 5-34 depicts the PSD and cumulative PSD of the aerodynamic thrust force for wind turbine 22. As can be seen, the level of the thrust force is increased, resulting to increased loads on the turbine.

5.4 Discussion and Conclusion

This chapter has focused on the development of a large wind farm model and a wind farm controller capable of providing ancillary services to the power network by utilising the wind farm controller. The wind farm model consists of 100 wind turbines, allowing for a realistic representation of modern offshore wind farms. Based on the wind farm simulation results, this chapter answers the research question “can we operate large (offshore) wind farms flexibly under all operational conditions?”. This chapter concludes that the wind farm controller can be utilised to provide flexible operation of offshore wind farm under various environmental conditions. The simulation results, under different operating conditions, suggest that the wind farm controller can successfully accomplish the requested power adjustments and provide ancillary services to the system operator.

The wind farm controller can provide power reserve services under all operational conditions when required, whilst protecting the wind turbines and, by following the O&M analysis presented in chapter 3, ensuring increased turbine availability. The droop controller mode is able of delivering the requested power decrease, while improving turbine availability by load reduction on the turbines that are more likely to experience a failure.

Moreover, the controller can provide synthetic inertia response under any operational conditions, thus, increasing power system frequency stability. The capability of the controller to provide primary response services to the system operator depends on the operational conditions the wind farm is experiencing. For below rated conditions, this functionality is restricted to the operational point of each individual turbine, as turbines may not be able to provide the requested ΔP for the required time span. For rated and above rated conditions, the wind farm is able to provide synthetic inertia response and primary response services to the system operator. The effect of the wind farm controller on the power system will be presented and discussed in chapter 7.

The utilisation of the droop controller capability can also allow for the improved capability to provide primary response services even when experiencing below rated wind conditions. Furthermore, the droop controller may allow for expanded functionality of the wind farm controller to provide not only primary but also secondary response services to the system operator. For the assessment of the ability of the wind farm controller to provide secondary response services when droop controller mode is utilised, further research is required.

Chapter 6 - Power System, VSC-HVDC and Network Wind Farm Controller Modelling

In this chapter, the development of a power system simulation model, which will be utilised to investigate the effectiveness of the wind farm controller in providing ancillary services to the system operator, is presented. The developed power system model is capable of representing a typical power system including a large wind farm. The model is also used for the development of a network wind farm controller, which checks for frequency deviations, providing ΔP signals to the wind farm controller to alter the power output of the wind farm based on network events, thus improving frequency stability.

The development of a VSC-HVDC simulation model and a network wind farm controller, which is used to connect the wind farm to the grid, is presented. The developed HVDC model is used to represent the transfer of power from the offshore wind farm to the power network. The network wind farm controller developed provides signals to the HVDC converters and the wind farm controller, requesting for ΔP in power output to provide synthetic inertia and primary frequency response services to the grid operator. The model permits investigation of the potential of the developed wind farm controller to provide ancillary services to the system operator.

6.1 Introduction

Future power production in the UK is expected to be heavily dependent on renewable technologies, primarily wind energy. The UK primary target is to achieve 15% of its total energy consumption to be provided by renewables by 2020 [77]. The Large Combustion Plant Directive (LCPD) has already opted-out 11.37GW of coal and gas power plants by the end of 2015 [78]. Since 1st January 2016, the Industrial Emission Directive (IED) has set new minimum standards

for Emission Limit Values (ELVs), which have imposed further constraints on coal power plants [79]. Due to the above directives, conventional synchronous machine power plants are expected to be replaced mainly by renewable technologies, the vast majority of which are decoupled from the grid. This situation will reduce system inertia and hence frequency stability.

The GB power system is not highly connected to the European power network and cannot utilise the high levels of frequency stability the highly-interconnected EU network can provide. The British network consists of an onshore transmission network connecting England, Scotland and Wales and an offshore transmission network connecting Ireland and Europe to the Great Britain. The British installed generation capacity is approximately 85GW [77] and renewable technologies increase their share annually, as illustrated in Figure 6-1 [80]. To provide synthetic inertia and ensure high levels of frequency stability, it is evident that new control strategies for renewable technologies must be developed.

The development of a power system model capable of investigating the effect of a wind farm controller and the integration of offshore wind farms is presented. The power system modelling starts with a simple model, initially comprising a few synchronous generators. It is later upscaled to include more synchronous generators and more accurate transmission network topologies. The next step of the development included the development of the northern Scottish transmission network in isolation, followed by the connection of the northern Scottish transmission network to a simplified version of the GB transmission system.

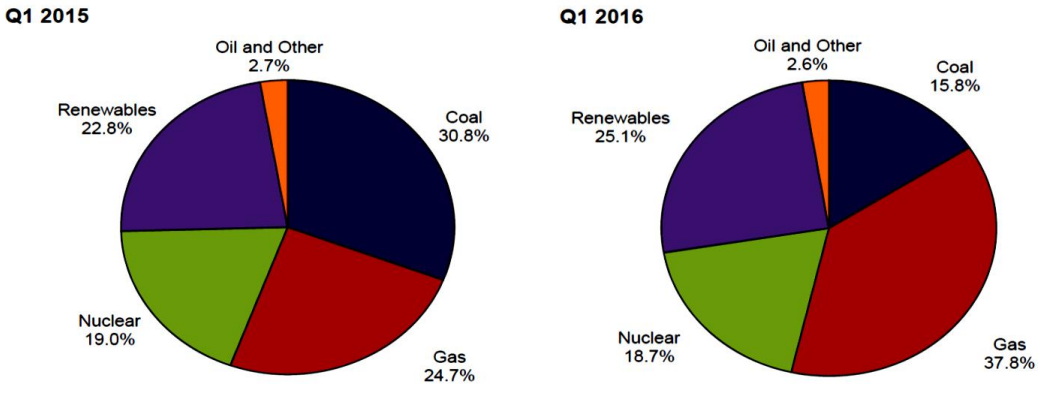

Figure 6-1: Comparison of British generation per sector for Q1 of 2015 and 2016 [80]

As more offshore wind farms are being developed, the need to move further away from the mainland to achieve higher wind speeds, thus higher power production, is imminent. As the distances increase, the use of High Voltage Direct Current (HVDC) links to connect offshore wind farms to the main power network has gained more interest.

HVDC configurations are equipped with power converters, which provide a way of controlling the power flow, increasing the flexibility of operators. The network wind farm controller takes advantage of the HVDC link controllability, along with the flexibility of the wind farm controller developed in Chapter 4, to allow the wind farms to be operated in a more flexible manner, thereby making it possible for wind farm operators to provide ancillary services, in so doing improving the stability of the power system.

6.2 Literature Review

The development of a power system model used for the assessment of the wind farm controller effect on the grid includes the detailed representation of conventional large synchronous generators equipped with detailed governor and excitation controls, buses with step-up and step-down transformers, loads, accurate transmission line representation and modelling of the connection between the offshore wind farm and the power system.

The development of the Voltage Source Converter (VSC) HVDC link connecting the wind farm to the power system is used for the assessment of the wind farm controller capability. The network wind farm controller will use the frequency measurements at the point of common coupling to request power adjustments (i.e. ΔP signals) from the wind farm controller in order to provide ancillary services to the grid. The network wind farm controller utilises the HVDC link capabilities by requesting power adjustments (i.e. ΔP signals) from the onshore and offshore substations, whilst ensuring DC link stability.

6.2.1 Power System Modelling

There are different models with various complexity that can be used for power system simulation. This research aims to evaluate the effect of wind farm controllers on the GB power network, thus a realistic representation of the GB transmission system is very important. The

construction of dynamic representative model of the British transmission network has been proposed and developed by various researchers. The main advantage of such representative network is that it is developed by modifying a reference network instead of assuming a fictitious network representation. All the representative models have been developed by assuming a reduced number of nodes to represent the GB electricity transmission power system.

Studies by Kunjumuhammed *et al.* [81] and Shen [82] consider a 29-node model based on the Reduced Great British Network (RGBN) model, which is a reduced British network power flow model, as illustrated in Figure 6-2 [82]. This model consists of 29 nodes interconnected via 98 transmission lines, and contains 65 various types of generators. The RGBN model is based on the work of Bell *et al.* [83] and Belivanis *et al.* [84]. The network represents the main routes of the British transmission network and has been used to investigate how different levels of renewable energy penetration would affect system stability. The RGBN model has been validated against load flow reference scenarios provided by the National Grid Electricity Transmission (NGET) [85], where the penetration levels have been based on the National Grid future network scenarios, Slow Progression Scenario (SPS), Gone Green Scenario (GGS) and Accelerated Growth Scenario (AGS).

There is significant variation between the National Grid future network scenarios. The SPS assumes a more traditional future forecast, with slower progress to achieving environmental goals. The GGS assumes that all energy targets are met, namely, 15% of all energy from renewable sources by 2020, GHG emissions reduction meeting their targets (i.e. 80% reduction in GHG emissions by 2050). In the AGS study, the demand is assumed the same as in the GGS, but there is increased development of offshore generation. For the SPS study, the total capacity of wind is assumed to be 16 GW (10 GW offshore) by 2020 and 31 GW (19 GW offshore) by 2030, while the GGS assumes a total wind installed capacity of 30 GW (17 GW offshore) by 2020 and 55 GW (37 GW offshore) by 2030, and AGS assumes a total wind installed capacity of 39 GW (24 GW offshore) by 2020 and 73 GW (49 GW offshore) by 2030 [86].

A simulation approach has been developed by Wong *et al.* [87], as a single “unified model” which has the capability to unify the generation, transmission and distribution layers and allow

for various novel technologies to be tested. An overview of the simplified power system structure of the "unified model" can be seen in Figure 6-3. Based on the work of Graham [88] and Jacobson *et al.* [89], the "unified model" was constructed around the object-oriented system modelling technique, where the model is highly modular and closely resembles the real network.

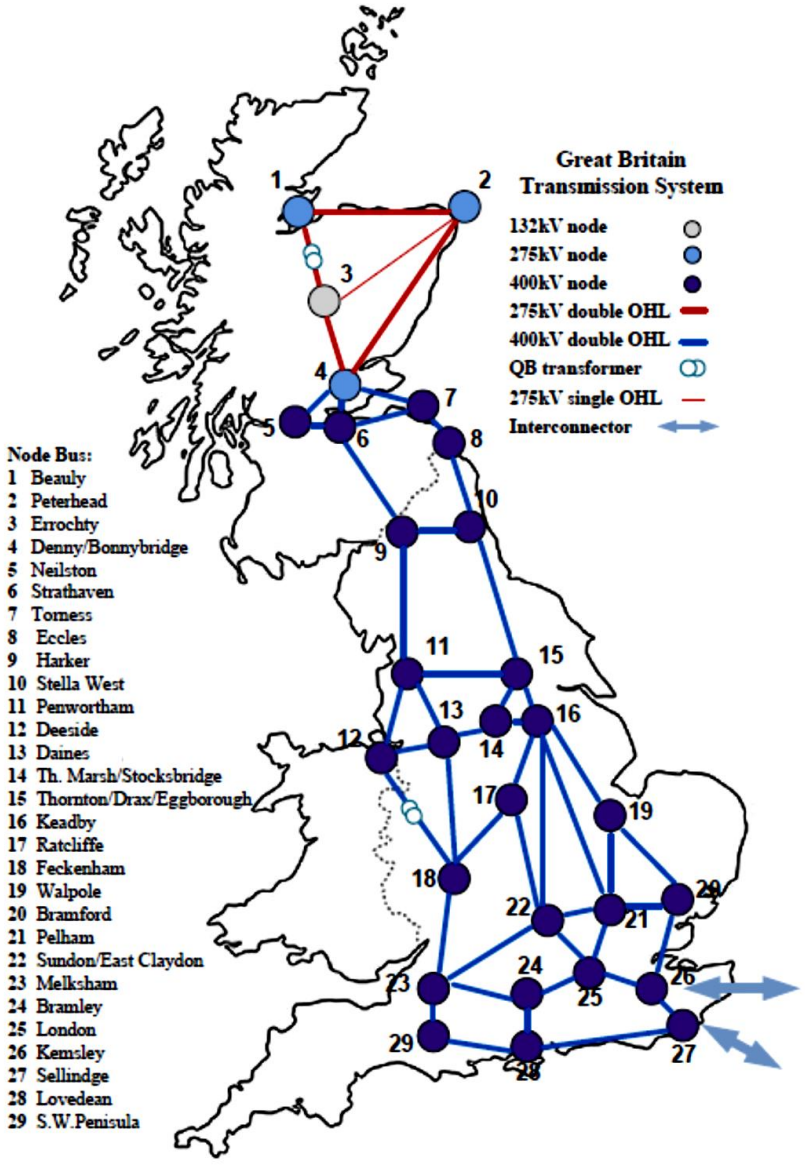

Figure 6-2: RGBN model overview [82]

Another network modelling approach has been developed by Xia *et al.* [90], where the British transmission network is modelled by an equivalent 21-bus model. The 21-bus model has been previously developed by Jun *et al.* [91], and has been calibrated to cater for different system profiles to ensure that the model can be used for various operating conditions. The static data has been taken from historical generation and demand data, and the dynamic data has been acquired from the PSS/E software [92], in which all the generators are assumed to be round-rotor with typical parameters based on published work [93] [94]. The scenarios tested by this model were the National Grid future networks scenarios (i.e. SPS, GGS and AGS).

Murrell *et al.* [95] also created a model of the British transmission power system to investigate the effect of high penetration levels of wind energy. This model was a simplified approach to simulate the power system, as the generation was assumed as one representative generator, along with the loss of load and the primary, secondary and operating reserve. The model was validated based on a major National Grid incident report, which occurred on May 2008; however, due to the model simplifications, the validation results seem to be less accurate than expected for the investigation of new types of technologies.

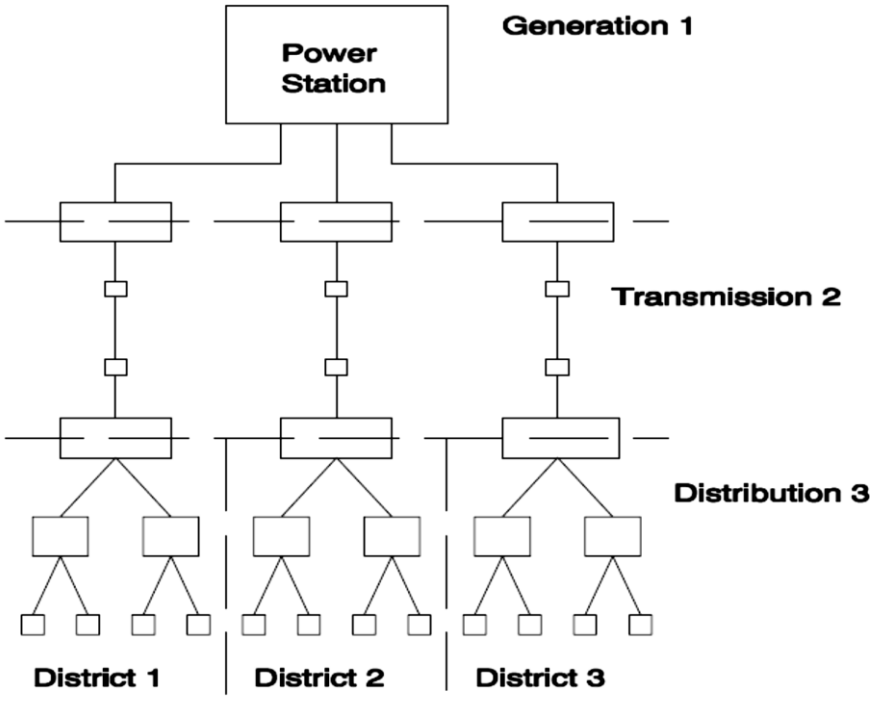

Figure 6-3: "Unified model" structure overview [87]

Research by Rakibuzzaman *et al.* [96] proposed a reduced dynamic equivalent model of the northern Scottish transmission power system. This model was based on the work of Kunjumuhammad [81] and Shen [82], but it allowed for a simplified representation of the RGBN system, as the network elements south to node 4 had not been accurately modelled and they were represented by an external grid behind a transformer. This is a useful representation of the northern Scottish power system, as it allows for better analysis of a certain topology and provides an insight on the assessment of the effect of new technologies, such as the proposed wind farm controller, on the power system. In this work the evaluation of the effect of wind farm controller strategies on the GB power system network will be assessed by using the RGBN and the northern Scottish transmission power system model.

6.2.2 Grid Frequency Measurement Techniques

Maintaining grid frequency stability is essential for every system operator. Estimating the system's frequency and its rate of change allows system operators to ensure power system protection and control. In the past, there have been various studies investigating different methods of achieving accurate frequency measurements. The most widely used method of estimating the electricity system frequency is the Phase-Locked Loop (PLL) [97] [98] [99]. The PLL is a feedback control system that constantly adjusts the phase of a locally generated signal to match the frequency of the input signal, and for power systems the PLL is adjusted to match the system's voltage frequency [100].

To date, the most widely used PLL controller for power systems is the Synchronous Reference Frame-PLL (SRF-PLL). The topology of the SRF-PLL is illustrated in Figure 6-4 [101]. The algorithm of this controller is based on the transformation of the voltage input from an $\alpha - \beta$ stationary reference frame to a $d - q$ rotating synchronous reference frame, by using the park transformation technique [94]. The q component is then fed through a PI controller. The reference value of the q component is zero if the objective is to synchronise with the voltage. The predicted q-component is all that goes into the PI controller. The output is frequency, which is then integrated up to get the phase estimation. The phase estimation is then fed into the Park transformation and so the loop is closed. Some variants of the SRF-PLL control system include filters, which normally split the positive and negative sequence components for acceptable performance during faults.

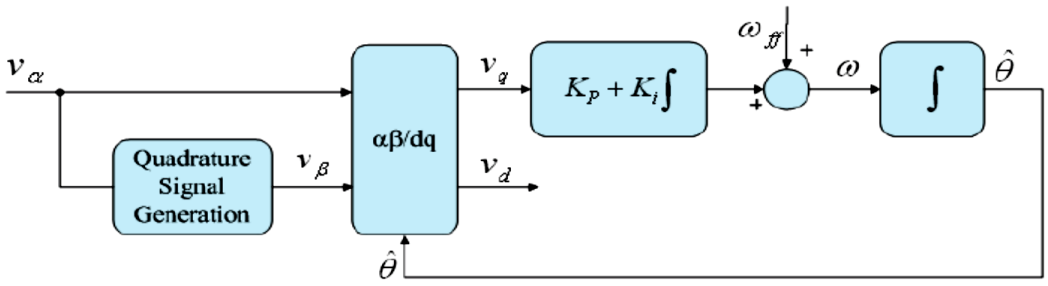

Figure 6-4: Block diagram of the SRF-PLL [101]

The SRF-PLL yields good results for balanced operation and low harmonic distortions in the system. However, in the presence of voltage imbalances and high-order harmonics the overall dynamic performance of the SRF-PLL becomes deficient [97]. The Dual Second Order Generalized Integrator-PLL (DSOGI-PLL) has the potential to overcome these limitations and allow for voltage synchronization under grid faults. The DSOGI-PLL controller was developed by Rodríguez *et al.* [102] and has a PLL design approach to that found in the SRF-PLL. The difference is that the SOGI applies filtering to remove harmonic content and split the positive and negative sequences as can be seen in Figure 6-5 [102]. The outputs of the DSOGI section of the algorithm are the positive α – β components. These are then transformed into the d - q frame using a modified Park transformation, designed for converting from the α – β frame to the d - q frame. Then the process is similar to the SRF-PLL, with selection of the q-component and passing it through a PI controller.

The filtering capability is a crucial aspect for PLL applications. Another widely used frequency estimation method is the zero-crossing technique. These techniques are simple, fast, and measure the time interval between crossings [103] [104]. The limitations of these techniques are that they are not capable to quickly respond to signals with harmonics [105] and perform poorly under faults [104].

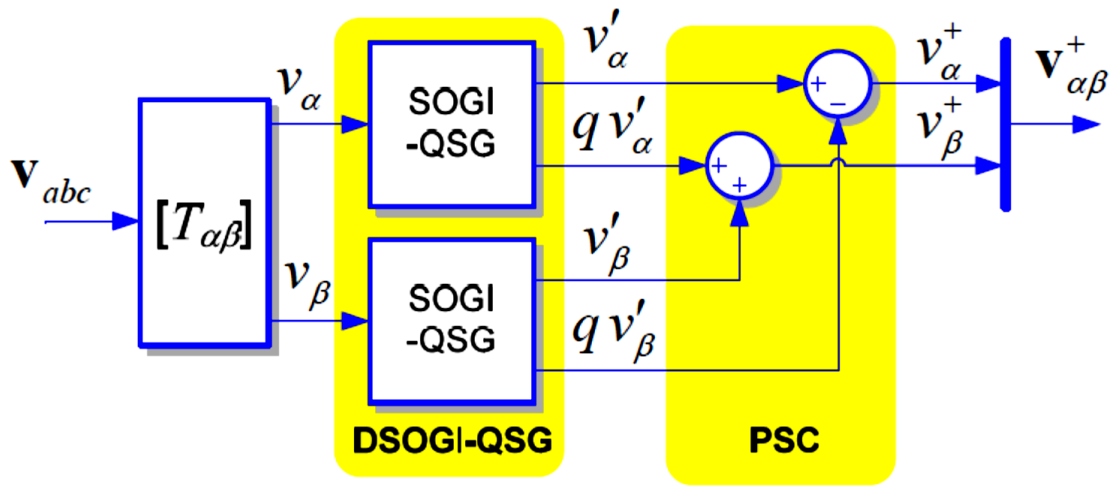

Figure 6-5: Block diagram of the DSOGI -PLL [102]

Phasor Measurement Units (PMUs) are another option to estimate system frequency. Various studies have explored the potential of PMU in system stability studies [106], islanded sections detection studies [107] and power system restoration studies [108]. The PMU is an algorithm which uses discrete fast Fourier transforms (FFTs) applied to samples of the voltage, as illustrated in Figure 6-6 [109]. The PMU architecture assumes that the input signals are correlated to quadrature waveform at the nominal system frequency (i.e. 50 Hz). The output is a single phasor with magnitude proportional to the system voltage on each phase, and a phase rotating at a rate of $2\pi(f - f_0)$ [109].

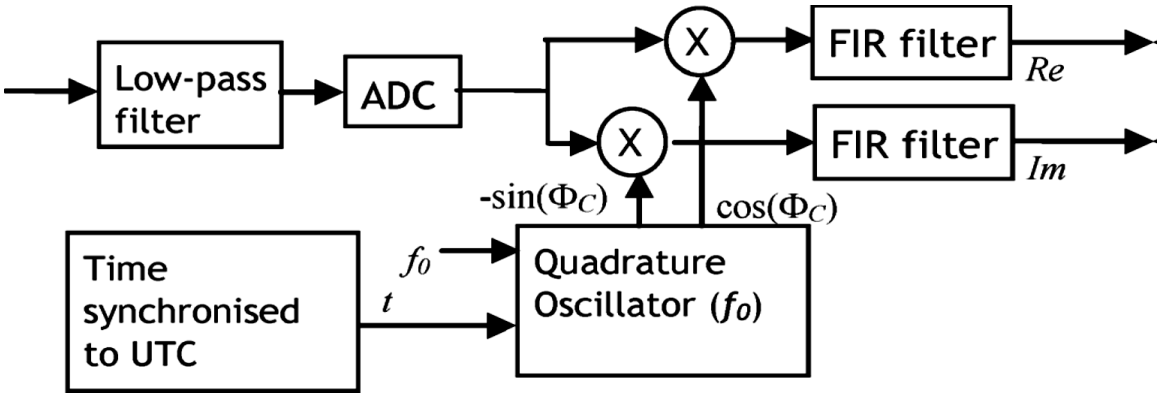

Figure 6-6: Single-phase section of conventional PMU [109]

The possibility of using the synchronous machine as a system measurement device is also considered in this work. The rotor speed measurement is used to assess the system frequency.

6.2.3 HVDC systems

HVDC transmission technology uses power electronics to control power flow, transport power over long distances and solve network line constraints. Additionally, HVDC systems can be used to connect two separate power networks, which are not synchronised or even have the same system frequency (i.e. 50Hz-60Hz) [110].The power electronics used for HVDC systems are designed for high power and voltage ratings [111].

The main advantages of the HVDC configurations compared to conventional AC systems are listed below [112]:

- HVDC is the only solution to interconnecting asynchronous systems,
- DC losses are less compared to AC (for the same conductor),
- DC systems are modular (i.e. can be built in stages if generation is being added over a longer period),
- HVDC systems are more reliable as they cannot be overloaded by outage of parallel AC lines,
- HVDC represents the most economical solution for onshore transmission for distances greater than approximately 600km, and
- HVDC is an economical alternative for submarine transmission for distances greater than approximately 90km [113].

Figure 6-7 illustrates the two main types of HVDC converters, the line-commutated converters and the self-commutated converters. The line-commutated Current Source Converters (CSCs)

represent the traditional HVDC system. A typical configuration of line-commutated CSC-HVDC system is illustrated in Figure 6-8 [111].

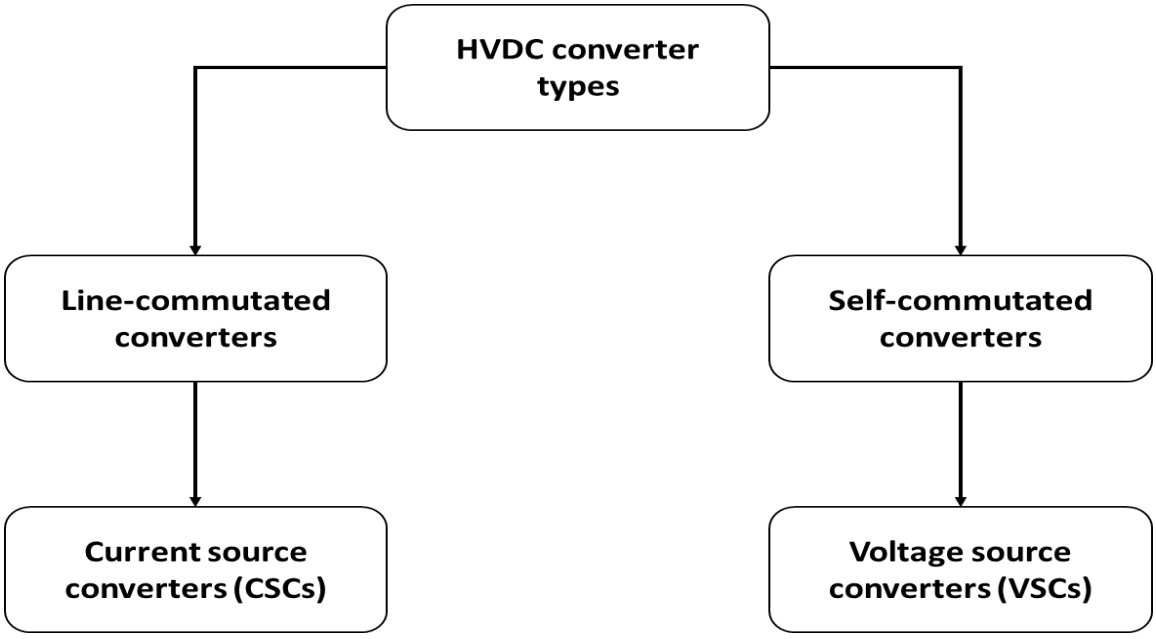

Figure 6-7: Types of HVDC converters

The line-commutated CSCs use thyristors as switching devices. The converters are utilised to convert the power from AC to DC (i.e. rectifier) at the sending substation and from DC to AC (i.e. inverter) at the receiving substation. As shown in Figure 6-8, the traditional HVDC configuration consists of the following elements:

- AC filters which are used to suppress the converter generated harmonics,
- Shunt capacitor banks which are compensating the converter's reactive power consumption during the conversion process,
- DC filters which reduce or smoothen the ripples produced in the DC transmission line current,

- The converter bridges which are used to convert power from AC to DC and DC to AC, and

- The DC cables to transport the power.

The line-commutated CSC-HVDC link operates with one converter controlling the direct voltage and the other converter controlling the current through the DC link. The two substation control systems communicate using a telecommunication link. The power reversal is obtained by reversing the polarity of the DC in both converters. Dynamic reactive power control is not possible with this type of HVDC type [114].

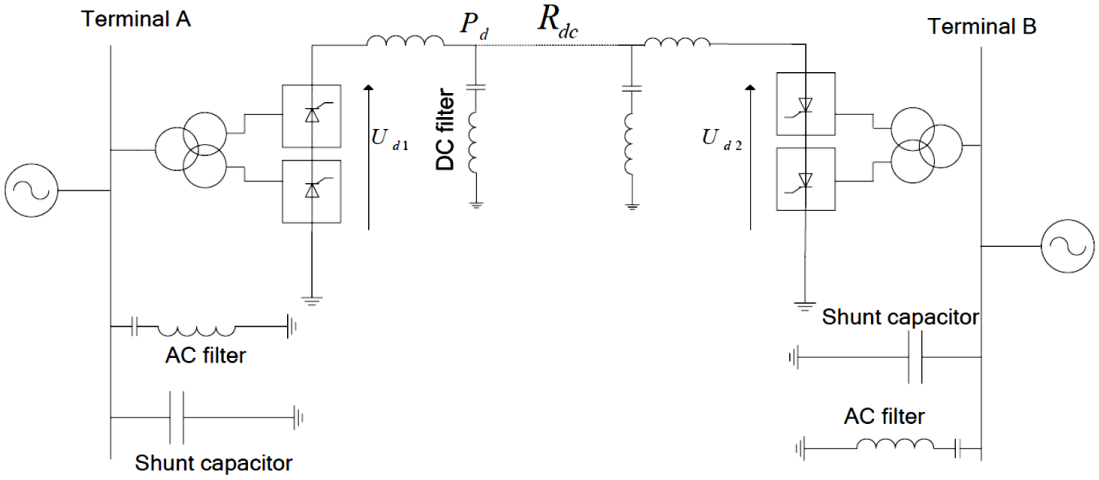

Figure 6-8: Typical configuration of line-commutated CSC-HVDC system [111]

Self-commutated converters use IGBTs or GTOs as switching devices. Both types of switching devices have controllable turn-off capabilities. The VSC-HVDC system can be considered as a controllable voltage source [111]. The VSC-HVDC link allows has the additional following capabilities compared to the line-commutated CSC-HVDC link [115]:

- Allows independent control of active and reactive power,

- Allows for black start capability,
- Has increased dynamic performance (i.e. improved power inertia and less harmonics), and
- Has low space requirements.

This type of HVDC link, due to its operational advantages, is expected to be used more often in transmission and distribution systems in the future. A typical configuration of self-commutated VSC-HVDC system is illustrated in Figure 6-9 [111].

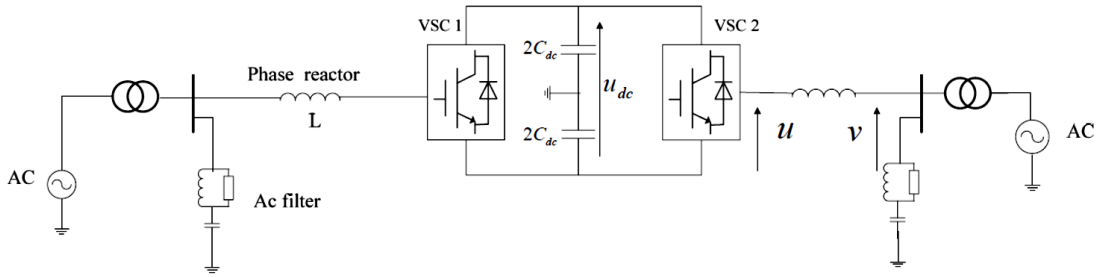

Figure 6-9: Typical configuration of self-commutated VSC-HVDC system [111]

For the self-commutated VSC-HVDC system the converters are utilised to convert the power from AC to DC (i.e. rectifier) at the sending substation and from DC to AC (i.e. inverter) at the receiving substation. As shown in Figure 6-9, the VSC- HVDC configuration consists of:

- AC filters which are used to suppress the converter generated harmonics,
- The converter bridges which are used to convert power from AC to DC and DC to AC, and

- DC capacitors which reduce or smoothen the ripples produced in the DC transmission line current.

Due to its higher controllability compared to the line-commutated CSC-HVDC, for this research the development of a VSC-HVDC link connecting the offshore wind farm to the AC GB transmission network has been chosen.

6.2.4 Network Wind Farm Controller

For the decentralised wind farm controller under development, it is essential to capture system instabilities to send the appropriate signals to the wind turbines and provide ancillary services to the system operator. Previous studies have had different views on how offshore wind can have increased flexibility and provide ancillary services to the grid.

A study by Asadollah *et al.* [116] suggests a centralized wind farm power controller, where the centralized controller sends power reference signals to individual wind turbines. The wind farm controller measures the voltage and current at the Point of Common Coupling (PCC) and send individual signals to the converters of each wind turbine to request active and reactive power. This approach looks similar to the wind farm controller under development but has some disadvantages. One drawback is that it is not considering the health of each wind turbine and the effect of the power reference to it. Another disadvantage is that the reference values can go up to the maximum available, which means that if the turbine is already at maximum power it cannot provide power increments, but only power decrements. Additionally, for this controller to function the turbines need to be equipped with back-to-back converters, and finally, the wind farm controller only focusses on reactive power control to provide voltage control at the PCC.

A research carried out by Yan *et al.* [117] developed a wind farm control strategy to provide reactive compensation and provide voltage control services to the grid. The connection is assumed to be an HVAC link, and the controller based on the power factor of each turbine and the voltage at the PCC configures the dynamic reactive compensation of the wind turbines. The

main disadvantage of this approach is its limitations to provide any other ancillary services to the system operator other than voltage control. Furthermore, the controller does not consider the state of each wind turbine and cannot request the turbine to provide anything other than the maximum available power.

A study by Pierik *et al.* [118] examines the controllability of nine different types of wind farms. This study was focused on controller development for individual wind turbines in order to manipulate the wind farm power output. The study has developed various wind turbine model able to accommodate different controller strategies if requested. This approach does not utilise the full extent of the wind farm controller, where the controller checks the grid at the PCC and requests from individual turbines to react and provide ancillary services to the grid.

Similar research carried out by Gevorgian *et al.* [119] developed a controller to enhance wind turbine response to system faults. This approach was focused on individual wind turbine controller development for responses to grid faults. The wind turbines react individually and not collectively to the fault, as they would under a wind farm controller. These individual controllers are only providing the system operator services for faults, and do not consider any other types of ancillary services.

6.3 Research Opportunities

Past studies and research have provided the opportunity to developed different models to investigate the performance of a wind farm controller on the power system. This work uses two different approaches to investigate the effect of the wind farm controller on the power system. These approaches have increased complexity, starting with the use of a simple model based on the work of Rakibuzzaman *et al.* [96], where a reduced dynamic equivalent of the North Scotland transmission system is created and everything south to node 4 is modelled as an external grid. The second modelling approach will be based on the RGBN model which was developed by Bell *et al.* [83], and will be used to represent the complete British transmission system.

The simulation models used in this research have been validated against published data, so the system analysis will be able to provide an accurate representation of the interaction between

the grid and the wind farm. Different frequency measurement techniques have also been examined to determine the accuracy and speed of the measurement. The IEEE 9-bus power system model consisting of three synchronous machines is created to test the different frequency measuring techniques and ensure that the best option is utilized.

Most papers encountered in literature that investigated the development of wind farm controller applications have used simple models to represent the turbine, wind field and wake interactions. Depending on the type of the research, some studies used simplified models for the wind farm representation or the simplified models for the power system representation. The representation of an accurate wind farm along with an accurate link to the power network allows for a much better understanding of the dynamic interactions between the wind farm and the grid.

The VSC-HVDC link and the network wind farm controller allow for flexible operation of the offshore wind farm. The network controller not only utilises the capability of the wind farm controller developed in Chapters 4 and 5, but also the VSC-HVDC link, as the network controller takes measures from the PCC between the HVDC and the transmission network and requests increase or decrease of power (i.e. ΔPs) from the HVDC converters and the wind farm, by maintaining a stable power transport from the wind farm to the grid.

6.4 Simulation Model Development

In this section, an overview of the power system modelling procedure is provided. The investigation of the best approach to compute the system frequency is followed by the detailed analysis of the power system modelling techniques. All the models have been developed in Simulink/Simscape Power Systems environment.

6.4.1 Grid Frequency Measurement Techniques Assessment Model Development

The system modelled to assess the frequency measurement techniques is the IEEE 9-bus power system model consisting of three generators [120]. This IEEE power system model is widely used by researchers as a test model to implement new concepts, and it is used in this work to

assess the frequency measuring techniques based on PLLs, PMUs and signals from the PSS of synchronous machines. The IEEE 9-bus power system model is shown in Figure 6-10. Three synchronous generators are connected to bus 1, 2 and 3. All the IEEE 9-bus power system model information is shown in Appendix B1, including the terminal conditions for the generators, the loads, the transmission line and the generator characteristics.

A synchronous machine is connected to bus 1, and voltage sources are connected to constant PQ busses 2 and 3 respectively. The base value for this model is assumed to be 100 MVA and the system frequency is 50Hz.

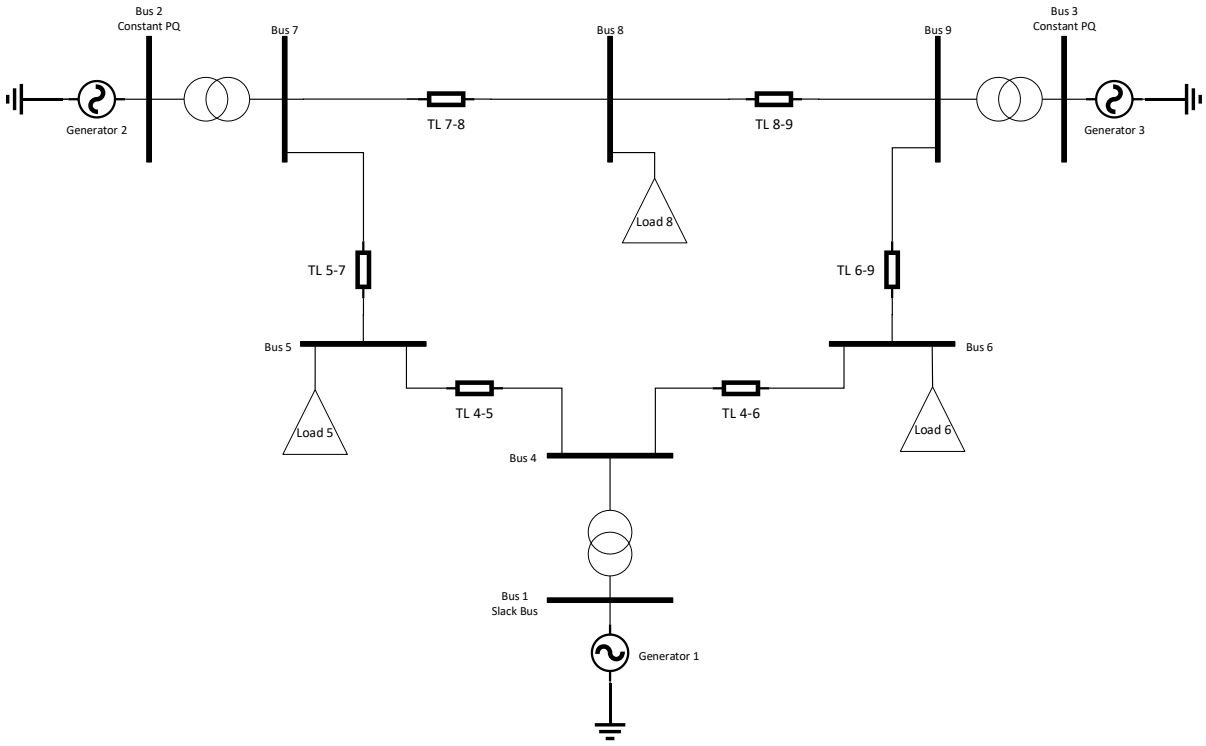

Figure 6-10: IEEE 9-bus power system model [120]

The generators provide power to three loads, which are connected to busses 5, 6 and 8. The loads are assumed to be constant PQ loads. For the 230kV transmission line representation,

typical values have been used for each segment. The power lines are represented by three-phase transmission pi sections with a line length of 100 km for each segment.

The basic model modelled the generators as simple voltage sources; however, in this work, the bus 1 generator is modelled using a complete 8th-order synchronous generator model in conjunction with a governor and excitation system. This change is essential as it allows for dynamic analysis of the power system [83] [120].

The frequency measuring techniques assessed in this research include the SRF-PLLs, the PMU and signals from the PSS of synchronous generator 1. The SRF-PLL is the standard algorithm which is used in many control systems. In this algorithm, a Park transformation (abc → dq0) is applied to the voltage input. The q component is then fed through a PI controller. The reference value of the q component is zero if the objective is to synchronise with that voltage. So, the predicted q-component is all that goes into the PI controller. The output is typically frequency, which is then integrated up to get the phase estimation. The phase estimation is then fed into the Park transformation and so the loop is closed. The SRF-PLL includes a low-pass filter to mitigate signal noise effects, while the positive and negative sequence components are used for performance improvements during faults and unbalanced operation.

The PMU is an algorithm which uses discrete Fast Fourier transforms applied to samples of the voltage. The dominant frequency calculated by the FFT is the grid frequency. The PMU model used in this research was developed by Roscoe *et al.* and has a sample rate of 10kHz [109].

The synchronous generator rotor speed signal is also used to calculate frequency. The generator frequency can be calculated by using the equation of motion of the synchronous machine [94]:

$$\Delta\bar{\omega}_r = \frac{\Delta\omega_r}{\omega_0} \qquad [6\text{-}1]$$

where $\Delta\bar{\omega}_r$ is the mean rotor angular speed deviation, $\Delta\omega_r$ is the rotor angular speed deviation and ω_0 is the rated angular velocity ($\omega_0 = 2\pi f_0$).

6.4.2 Power System Models

Two power system models with increasing complexity have been developed for the assessment of the wind farm controller effect on power system stability. The structure of both models will be thoroughly explained in the following subsections.

6.4.2.1 Reduced Great British Power System Model

The reduced GB power system model has been based on the reduced North Scotland model, developed by Rakibuzzaman *et al.* [96]. For this research, the reduced North Scotland model approach has been taken using the published data from Bell *et al.* [83] and Belivanis *et al.* [84]. The reduced GB power system model is illustrated in Figure 6-11.

The reduced GB power system model consists of 4 nodes, representing Scotland, and a connection to the remaining GB power network. Four synchronous generators are connected to nodes 1, 2, 3 and 4. Node 5 represents the remaining GB power system. The base value for this model is assumed to be 100 MVA and the system frequency is 50Hz. All the reduced GB power system model information is shown in Appendix B2, including the terminal conditions for the generators, the loads, the transmission line and the generator characteristics.

The generators provide power to five loads, which are connected to nodes 1-5. The loads are assumed to be constant PQ loads. For the transmission line representation, typical values have been used for each segment [84]. The power lines are represented by three-phase transmission pi sections with a line length of 100 km for each segment. The power line connecting node 4 to 5 is represented by three-phase transmission pi sections with a line length of 250 km.

The initial model assumed that generators are presented as voltage sources, but in this work, the all generators have been substituted by complete synchronous machine models with governor and excitation systems. This change is essential as it allows for dynamic analysis of the power system [83] [110].

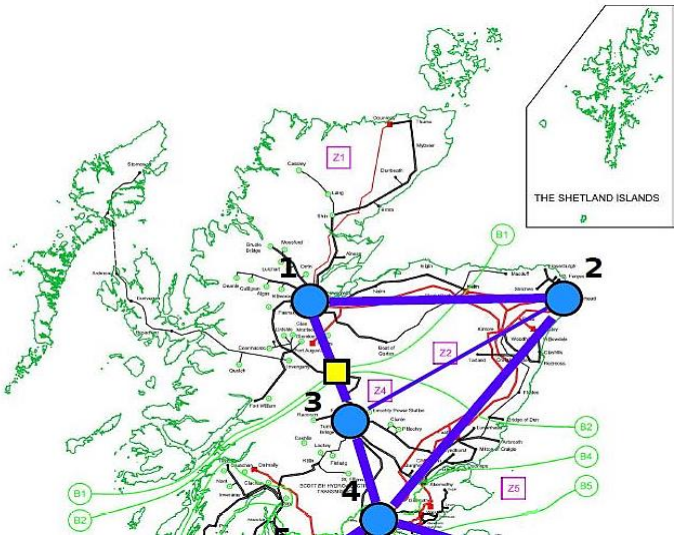

Figure 6-11: The reduced GB power system model [84]

The generation data for this model was based on the published data from Bell *et al.* [83] and Belivanis *et al.* [84]. Since these studies were based on load flow analysis, the generation units were assumed to be voltage sources. Since this research investigates the dynamic response of the power system to wind farm controllers, the change to a more sophisticated synchronous generator model was necessary [83] [120]. Since the actual generator dynamic characteristics of the representative machines to each node were not known, this work uses a single type of turbine/governor and excitation system for all the connected generators. The turbine and governor model used is the IEEE hydraulic turbine and governor model, which includes a nonlinear hydraulic turbine model, a PID governor system, and a servomotor [121]. The excitation model used is an IEEE type 1 synchronous machine voltage regulator combined with an exciter [122].

6.4.2.2 Great British Power System Model

The GB power system model has been based on the work of Bell *et al.* [83] and Belivanis *et al.* [84]. The GB power system model is illustrated in Figure 6-12 [84].

The GB power system model consists of 29 nodes, representing the GB transmission power network. Twenty-five synchronous generators are connected to nodes 1-29. All the GB power

system model information is shown in Appendix B3, including the terminal conditions for the generators, the loads, the transmission line and the generator characteristics.

The base value for this model is assumed to be 100 MVA and the system frequency is 50Hz. The generators provide power to twenty-nine loads, which are connected to nodes 1-29 respectively. The loads are assumed to be constant PQ loads [84]. For the transmission line representation, typical values have been used for each segment [84]. The power lines are represented by three-phase transmission pi sections with a line length of 100 km for each segment.

The initial model assumed that generators are presented as voltage sources, but in this work, the all generators have been substituted by complete synchronous machine models with governor and excitation systems. This is essential as it allows for dynamic analysis of the power system [83] [110]. The characteristics of the governor and excitation system of the synchronous machines used have been derived from Kundur [94] [84].

The generation data for this model is based on the published data from Bell *et al.* [83] and Belivanis *et al.* [84]. Since these studies [83] [84] were based on load flow analysis, the generation units were assumed to be voltage sources. This work is investigating the dynamic response of the power system to wind farm controllers, the change to a more sophisticated synchronous generator model was necessary [83] [120]. Since the actual generator dynamic characteristics of the representative machines to each node were not known, this research uses a single type of turbine/governor and excitation system for all the connected generators. The turbine and governor model used is the IEEE hydraulic turbine and governor model, which includes a nonlinear hydraulic turbine model, a PID governor system, and a servomotor [121]. The excitation model used is an IEEE type 1 synchronous machine voltage regulator combined with an exciter [122].

It should be noted that the developed power system does not include the interconnectors to France (i.e. Node 27 - France), Holland (i.e. Node 26 – Holland, “BRITNED”) and Northern Ireland (i.e. Node 6 - Northern Ireland).

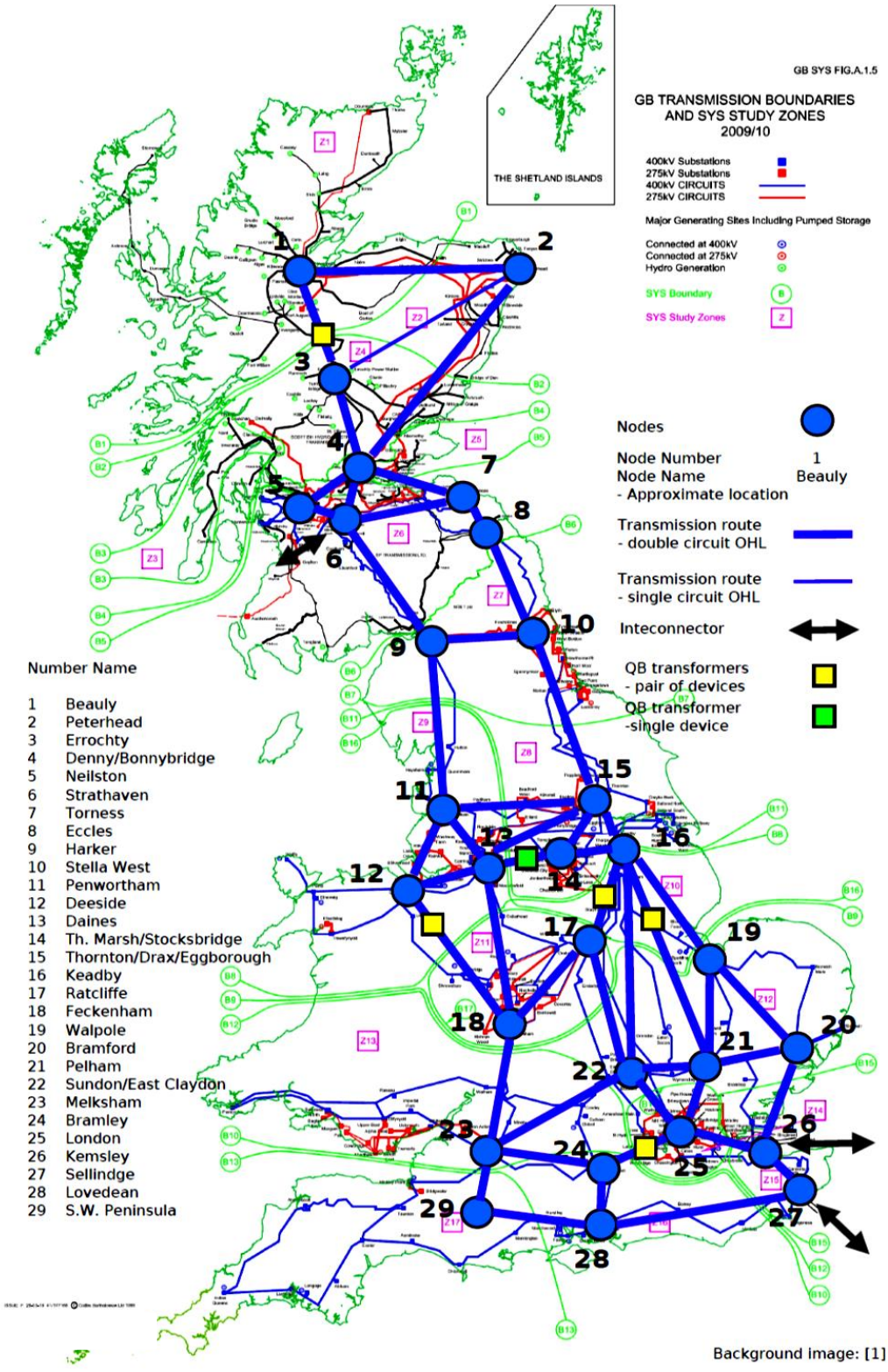

Figure 6-12: The GB power system model [84]

6.4.3 VSC-HVDC Simulation Model Development

The VSC-HVDC link connecting the offshore wind farm to the AC GB transmission network has been developed to allow increased controllability of the power transfer from the offshore wind farm to the onshore power network, as the VSC can be assumed as a controllable synchronous machine with an instantaneous phase voltage [111]. The VSC-HVDC system model information is shown in Appendix B4, including the system parameters and inner and outer loop controller development.

6.4.4 Network Wind Farm Controller Model Development

The network wind farm controller is designed to evaluate the grid measurements provided by the PMU and define the required response the wind farm controller needs to request from the turbines to provide ancillary services to the grid. The UK grid code states that all generators connected to the transmission system, depending on size and location, are requested to provide Mandatory Frequency Response (MFR) [123]. The MFR services are listed below:

- Primary response,
- Secondary response and
- High-frequency response.

Generators could offer one or combinations of different MFR services. Primary response is provided within 10 seconds of an event and can be sustained for a further 20 seconds. Secondary response is provided within 30 seconds of an event and can be sustained for a further 30 minutes. High-frequency response is provided within 10 seconds of an event and can be sustained indefinitely. The generators may also provide other balancing services to the system operator, if these additional services do not interfere with their ability to deliver MFR services.

By their definition, it is obvious that for wind farms operating below rated power the only type of MFR service that the wind farm controller can provide is the primary response. The wind farm controller can request and achieve power increase even below rated operation, but the increase is achievable for short periods of time (i.e. until the turbine reaches the PAC black limit and returns to normal operation). The wind farm controller can provide additional MFR services, such as secondary response and high-frequency response, if the wind farm has been operating under droop control.

The droop controller is a power reserve mechanism which exists in all governor controllers of synchronous generators connected to the power system. The reserved power, or curtailment, exists to provide spinning reserve relative to the rated power of the machine. The GB grid code requests a 3% - 5% droop characteristic from all connected generators which provide MFR [124].

The network wind farm controller is designed to evaluate the grid measurements provided by the PMU and define the required wind farm responses. The GB grid code defines the electricity frequency boundaries to be between 49.5Hz and 50.5Hz (i.e. 50Hz ± 1%) [125], but the normal operating limits are between 49.8Hz and 50.2Hz [126]. If the frequency is within the normal GB grid operating limits (i.e. $49.8Hz \leq frequency \leq 50.2Hz$), the network wind farm controller does not make any power change requests to the wind farm controller. If the frequency moves out of the accepted boundaries, then the controller requires a droop controller action from the wind farm controller.

The network wind farm controller request is also based on the Rate of Change of Frequency (ROCOF) measurement. If the ROCOF is within the GB grid code acceptable limits (i.e. ROCOF < 0.5 $Hz/_S$) [127], then the network wind farm controller requests the minimum droop response (i.e. 3%); however, if the ROCOF is outside the GB grid code acceptable limits (i.e. ROCOF ≥ 0.5 $Hz/_S$), then the network wind farm controller requests the maximum droop response (i.e. 5%). Figure 6-13 illustrates the flowchart of the control algorithm for the network wind farm controller.

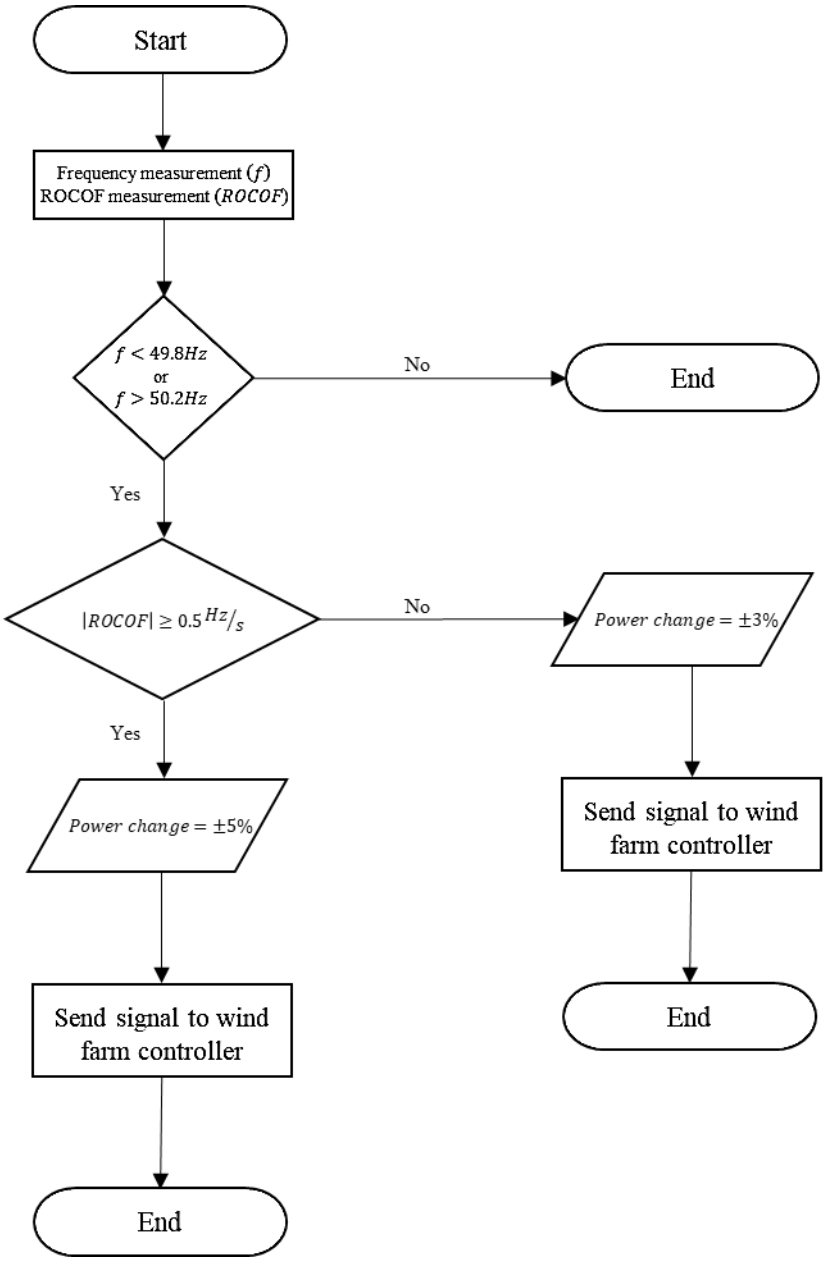

Figure 6-13: Flowchart of the control algorithm for the network wind farm controller

The duration of the signal to the wind farm controller is based on the power system frequency. The wind farm controller will continue to request the power change for the duration that the system frequency is exceeding the GB grid code acceptable range (i.e. $49.8Hz \geq frequency$, or $frequency \geq 50.2Hz$).

6.5 Simulation Models Results

In this section, the simulation results of the power system, the VSC-HVDC and network wind farm controller models are presented. The investigation of the assessment of the best approach to compute the system frequency will be followed by the analysis of the results from simulating the GB power system models. Furthermore, the investigation of the assessment of the operation of the HVDC link between the wind farm and the GB power system will be followed by the analysis of the results from the response of the network wind farm controller. All the models have been developed in Simulink/Simscape Power Systems environment.

6.5.1 Grid Frequency Measurement Techniques Assessment Simulation Results

The IEEE 9-bus power system model has been developed to assess the response of the SRF-PLL, PMU and generator rotor speed signal for power system frequency estimation. To evaluate the different measuring techniques, various scenarios have been investigated.

The first scenario assumes the loss of Bus 5 load. After 10 seconds the load is disconnected, and the frequency is measured using the three different approaches. The three-phase voltage and current measurement for the SRF-PLL and PMU is made on the PCC of the Bus 1 generator. The total simulation time is 20 seconds, and the results are depicted in Figure 6-14.

As can be seen in Figure 6-14, at 10 seconds the frequency rises due to the loss of the load, as expected, and then it fluctuates until it retains its nominal value (i.e. 50 Hz). The frequency measurements from the SRF-PLL and the PMU match up almost perfectly, while the frequency measurement from the synchronous generator shows significant overshooting with regards to the PLL and PMU measurements.

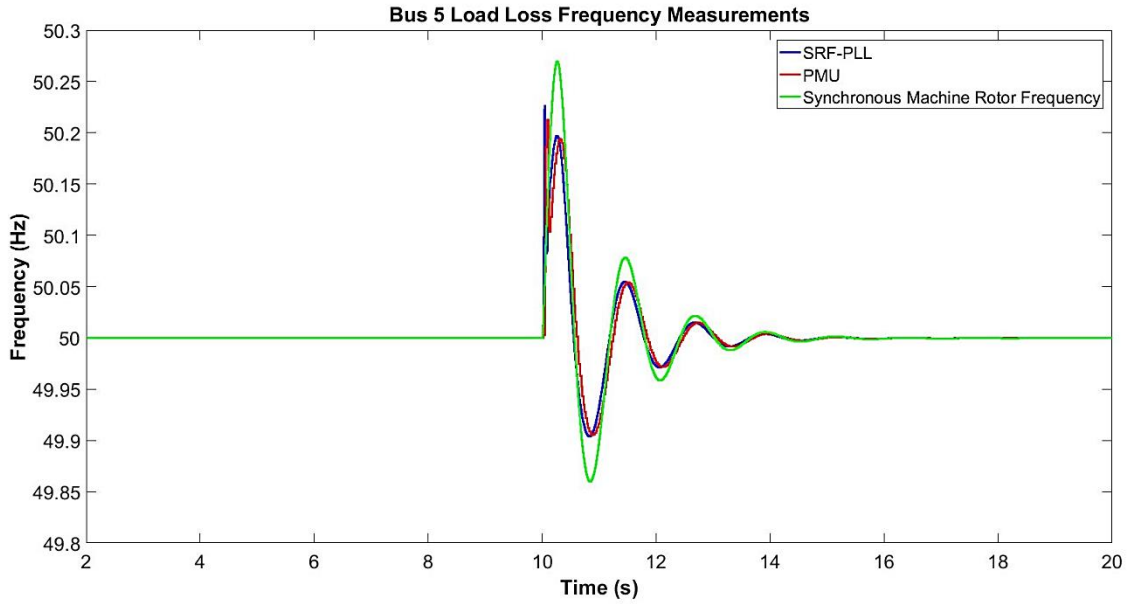

Figure 6-14: Bus 5 load loss frequency measurements

The second scenario assumes the loss of Bus 3 generator. After 10 seconds the generator is disconnected, and the frequency is measured using the three different approaches. The three-phase voltage and current measurement for the SRF-PLL and PMU is made at the PCC of the Bus 1 generator. The total simulation time is 20 seconds, and the results are shown in Figure 6-15.

As can be seen in Figure 6-15, at 10 seconds the frequency drops due to the loss of the generator, as expected, and then it fluctuates until it retains its nominal value (i.e. 50 Hz). The frequency measurements from the SRF-PLL and the PMU match up almost perfectly, but initially the SRF-PLL measurement seems to overshoot instantaneously. The frequency measurement from the synchronous generator shows significant overshooting with regards to the PLL and PMU measurements.

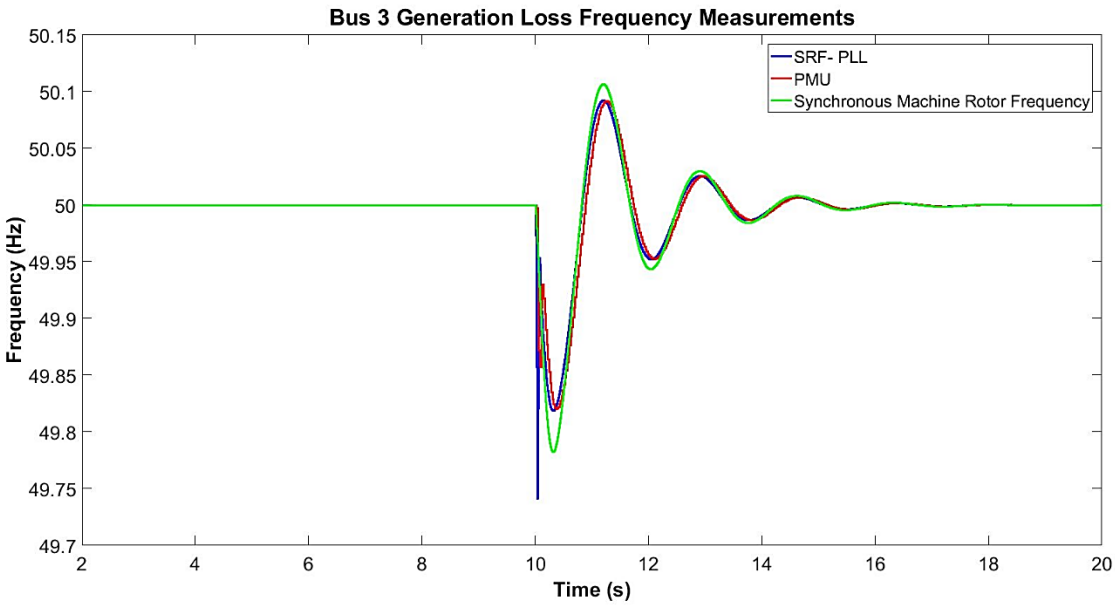

Figure 6-15: Bus 3 generator loss frequency measurements

The third and final scenario assumes the introduction of a fault on Bus 4. After 10 seconds the fault is introduced and then cleared after 300ms [128]. The frequency is measured using the three different approaches. The three-phase voltage and current measurement for the SRF-PLL and PMU is made on the PCC of the Bus 1 generator. The total simulation time is 20 seconds, and the results are shown in Figure 6-16.

As can be seen in Figure 6-16, at 10 seconds the frequency rises due to the fault and then it fluctuates until it retains its nominal value (i.e. 50 Hz). The frequency measurements from the SRF-PLL and the PMU match up almost perfectly, while the frequency measurement from the synchronous generator shows significant overshooting relative to the PLL and PMU measurements.

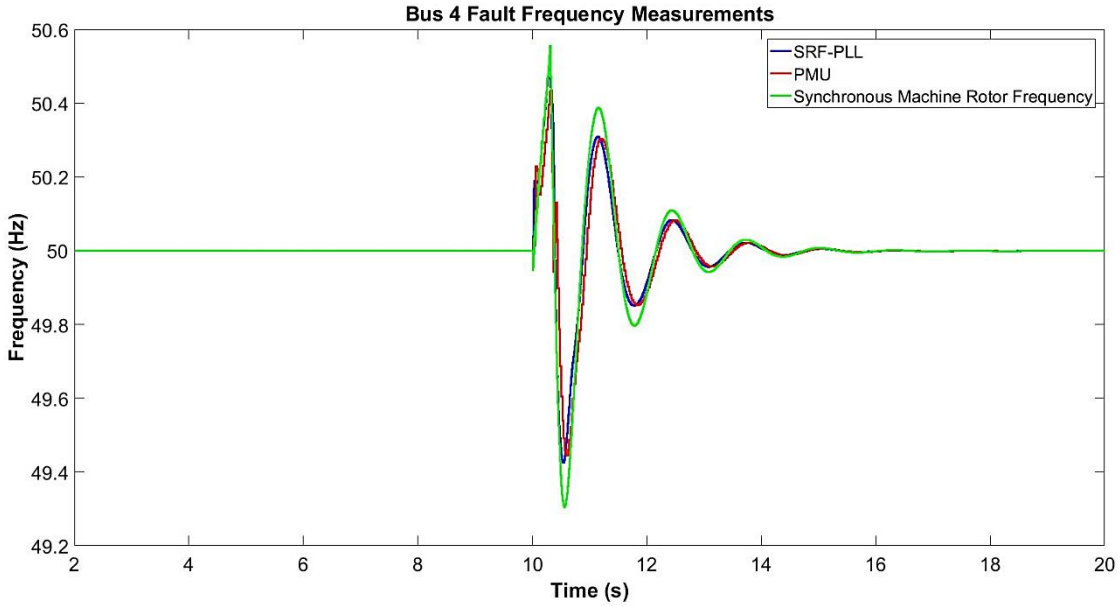

Figure 6-16: Bus 4 fault frequency measurements

6.5.2 Power System Modelling Simulation Results

The reduced GB power system model and the GB system model, with increasing complexity have been developed for the assessment of the wind farm controller effect on power system stability. These models will be simulated, evaluated and tested under different scenarios.

6.5.2.1 Reduced Great British Power System Model Simulation Results

The reduced GB power system model has been developed for the assessment of the wind farm controller effect on power system stability. To evaluate its suitability, different scenarios have been developed.

The first scenario assumes the loss of a 250MW and 50MVAr load connected on the 275kV side of Bus 3. After 10 seconds the load is suddenly disconnected, and the frequency is measured using the three different approaches. The three-phase voltage and current measurement for the SRF-PLL and PMU is made on the PCC of the Bus 2 generator, and the generator rotor

speed measurement is derived from Bus 2 generator. The simulation results are shown in Figure 6-17.

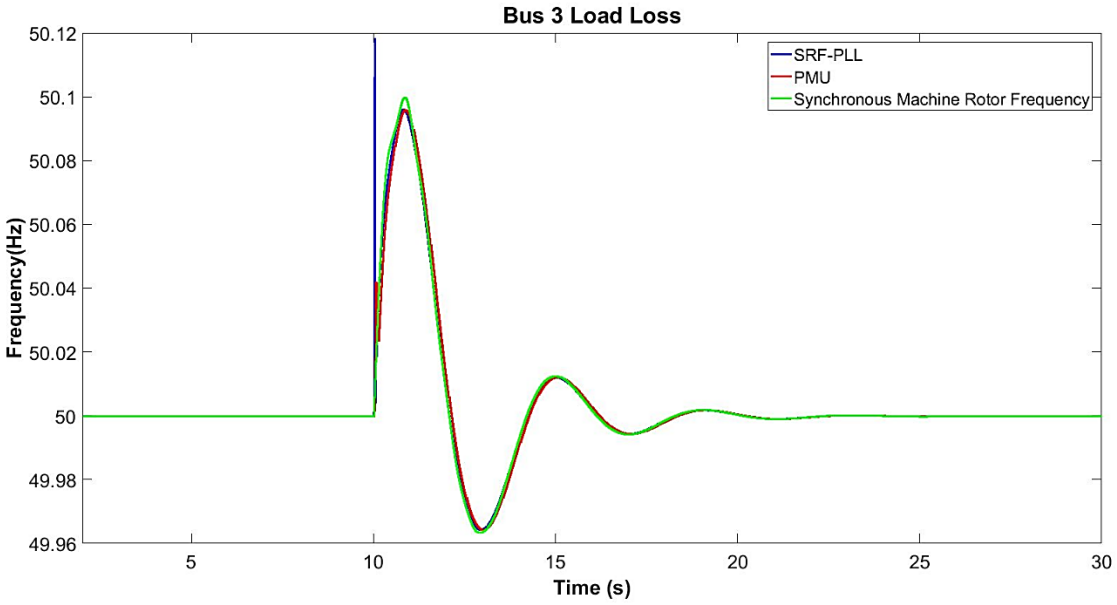

Figure 6-17: Bus 3 load loss effect

As can be seen in Figure 6-17, at 10 seconds the frequency rises due to the loss of the load, as expected, and then it gradually moves towards its nominal value (i.e. 50 Hz). The frequency measurements from the SRF-PLL shows an instantaneous initial overshoot, and then matches up with the PMU measurement almost perfectly, while the frequency measurement from the synchronous generator shows similar behaviour relative to the PMU measurement.

The second scenario assumes the introduction of a 250MW and 50MVAr load connected on the 275kV side of Bus 3. After 10 seconds the load is suddenly connected, and the frequency is measured using the three different approaches. The three-phase voltage and current measurement for the SRF-PLL and PMU is made on the PCC of the Bus 2 generator, and the generator rotor speed measurement is derived from Bus 2 generator. The total simulation time is 30 seconds, and the results are depicted in Figure 6-18.

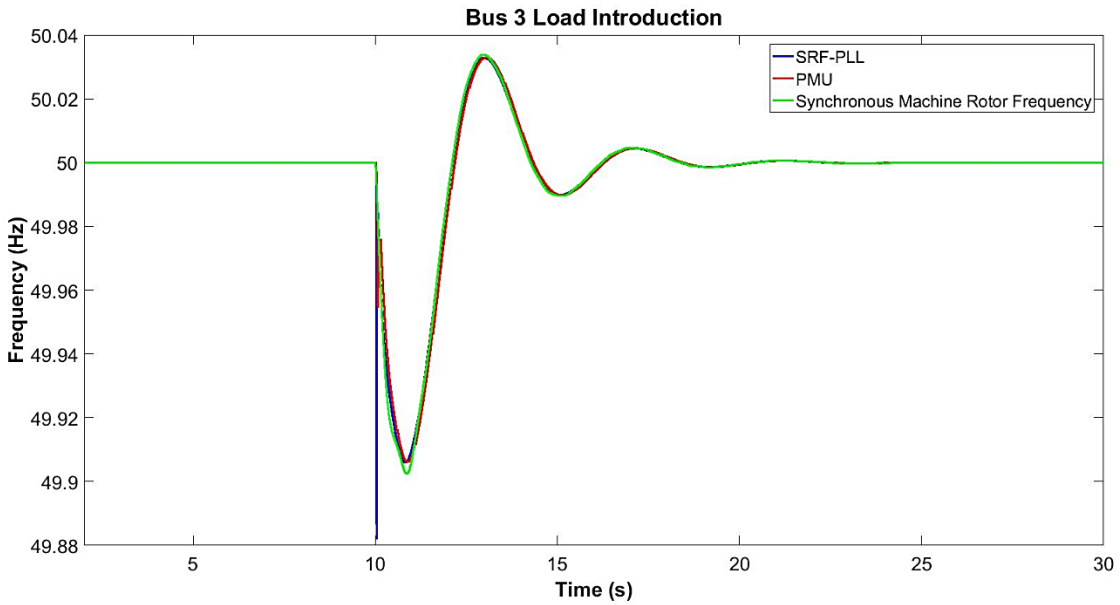

Figure 6-18: Bus 3 load introduction effect

As can be seen in Figure 6-18, at 10 seconds the frequency drops due to the introduction of the load, as expected, and then it gradually moves towards its nominal value (i.e. 50 Hz). The frequency measurements from the SRF-PLL shows an instantaneous initial overshoot, and then matches up with the PMU measurement almost perfectly, while the frequency measurement from the synchronous generator shows similar behaviour relative to the PMU measurement.

The third and final scenario assumes the introduction of a fault on Bus 4. After 10 seconds the fault is introduced and then cleared after 300ms [128]. The frequency is measured using the three different approaches. The three-phase voltage and current measurement for the SRF-PLL and PMU is made on the PCC of the Bus 2 generator, and the generator rotor speed measurement is derived from Bus 2 generator. The simulation results are shown in Figure 6-19.

As can be seen in Figure 6-19, at 10 seconds the frequency rises due to the fault and then it gradually moves towards its nominal value (i.e. 50 Hz). The frequency measurements from the SRF-PLL and the PMU match up almost perfectly, while the frequency measurement from the synchronous generator shows different behaviour relative to the PLL and PMU measurements.

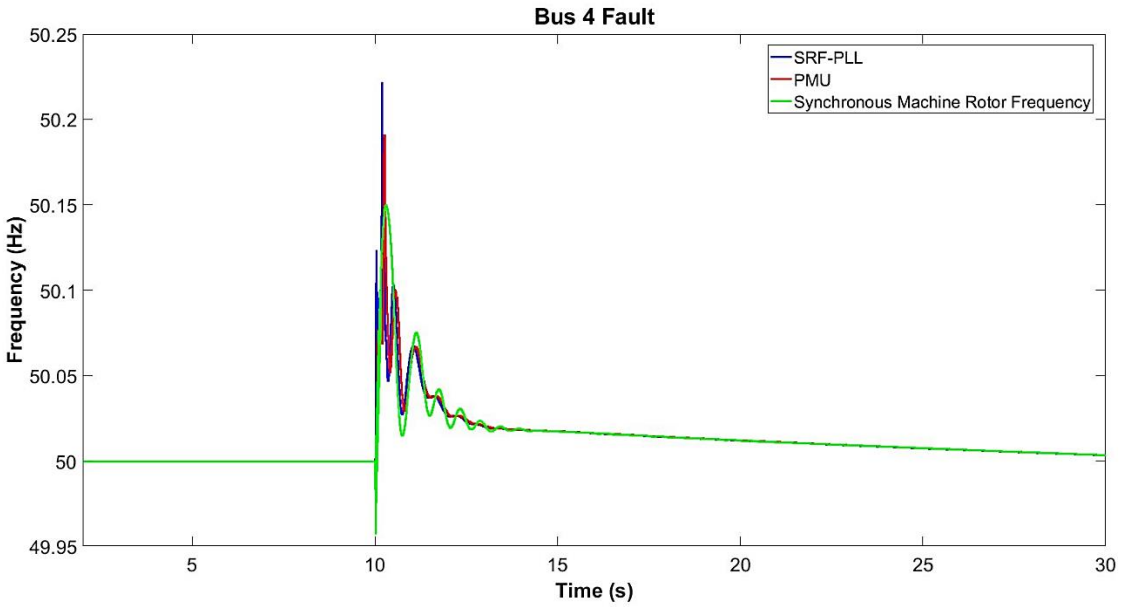

Figure 6-19: Bus 4 fault frequency effect

6.5.2.2 Great British Power System Model Simulation Results

The 29 nodes representative GB power system model has been developed for the assessment of the wind farm controller effect on power system stability. To evaluate its suitability, different scenarios have been developed.

The first scenario assumes the loss of a 250MW and 50MVAr load connected on the 275kV side of Bus 3. After 15 seconds, the load is suddenly disconnected, and the frequency is measured using the three different approaches. The three-phase voltage and current measurement for the SRF-PLL and PMU is made at the PCC of the Bus 2 generator, and the generator rotor speed measurement is derived from Bus 2 generator. The total simulation time is 30 seconds, and the results are depicted in Figure 6-20.

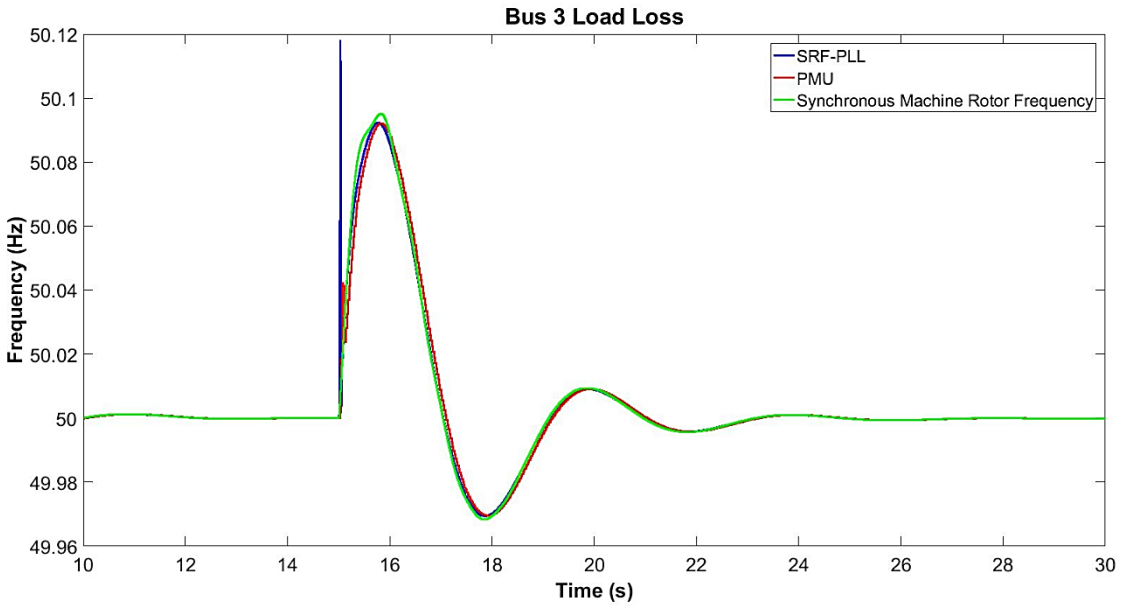

Figure 6-20: Bus 3 load loss effect

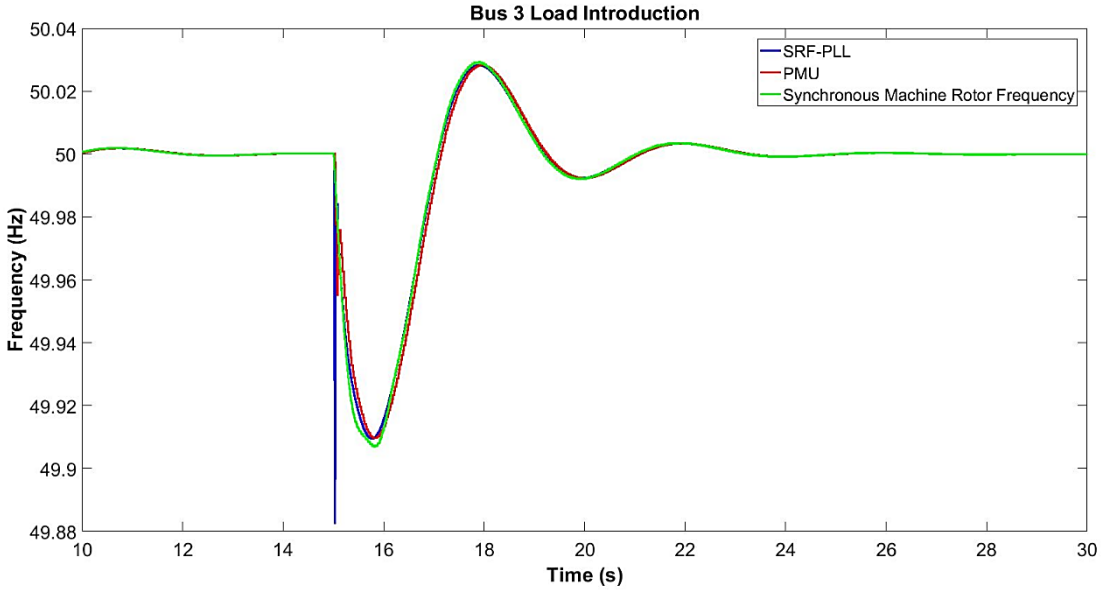

Figure 6-21: Bus 3 load introduction effect

As can be seen in Figure 6-20, at 15 seconds, the frequency rises due to the loss of the load, as expected, and then it fluctuates until reaching its nominal value (i.e. 50 Hz). The frequency measurements from the SRF-PLL shows an instantaneous initial overshoot, and then matches up with the PMU measurement almost perfectly, while the frequency measurement from the synchronous generator shows similar behaviour to the PMU measurement.

The second scenario assumes the introduction of a 250MW and 50MVAr load connected on the 275kV side of Bus 3. After 15 seconds, the load is suddenly connected, and the frequency is measured using the three different approaches. The three-phase voltage and current measurement for the SRF-PLL and PMU is made at the PCC of the Bus 2 generator, and the generator rotor speed measurement is derived from Bus 2 generator. The total simulation time is 30 seconds, and the results are shown in Figure 6-21.

As can be seen in Figure 6-21, at 15 seconds, the frequency drops due to the introduction of the load, as expected, and then it fluctuates until reaching its nominal value (i.e. 50 Hz). The frequency measurements from the SRF-PLL shows an instantaneous initial overshoot, and then matches up with the PMU measurement almost perfectly, while the frequency measurement from the synchronous generator shows similar behaviour with regards to the PMU measurement.

The third and final scenario assumes the introduction of a fault on Bus 4. After 15 seconds, the fault is introduced and then cleared after 300ms [128]. The simulation results are depicted in Figure 6-22.

As can be seen in Figure 6-22, at 15 seconds, the frequency rises due to the fault and then it gradually moves towards its nominal value (i.e. 50 Hz). The frequency measurements from the SRF-PLL and the PMU match up well, while the frequency measurement from the synchronous generator shows different behaviour in comparison to the PLL and PMU measurements.

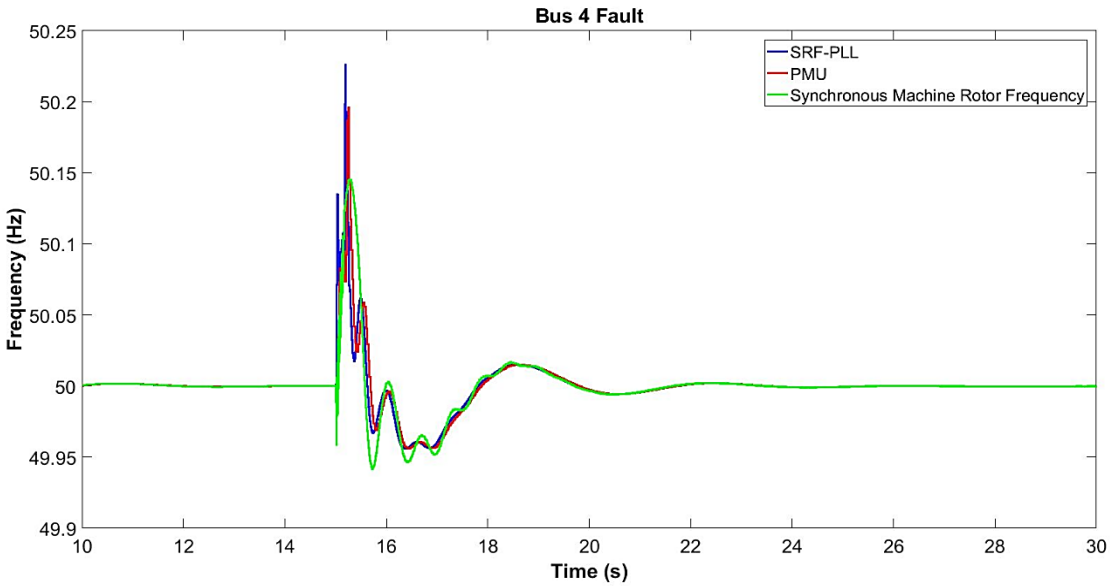

Figure 6-22: Bus 4 fault frequency effect

6.5.3 VSC-HVDC Model Simulation Results

The VSC-HVDC model has been developed to link the offshore wind farm with the power network. To evaluate the operation of the HVDC link, various scenarios have been developed. The first scenario assumes that the wind farm is producing constant active power and after 20 seconds a positive active power step change is introduced.

Figure 6-23 depicts the active power transfer between the wind fam and the power network via the HVDC link. Initially, the power from the wind farm is constant (i.e. 250MW), and at 20 seconds the power instantaneously increases by 50MW to 300MW. The DC bus power and the power injected to the network are matching up the trend of the power from the wind farm. The small variations are due to losses both in the converters and in the lines. The losses are mainly switching losses from the IGBTs and also losses in the cables of the HVDC link.

As can be seen in Figure 6-24, the DC bus voltage remains constant until the step increase in power from the wind farm. The DC controller ensures that the voltage remains constant by

increasing the current on the DC bus and transferring all the available power from the wind farm to the power network through the DC link.

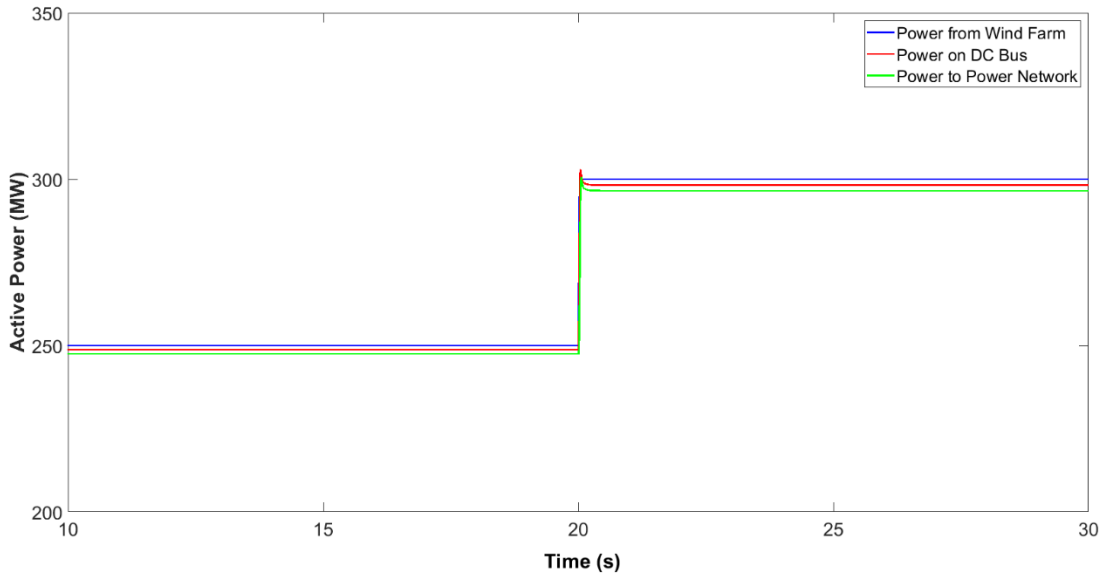

Figure 6-23: Active power transferred from the wind farm to the network via the VSC-HVDC link for positive active power step change

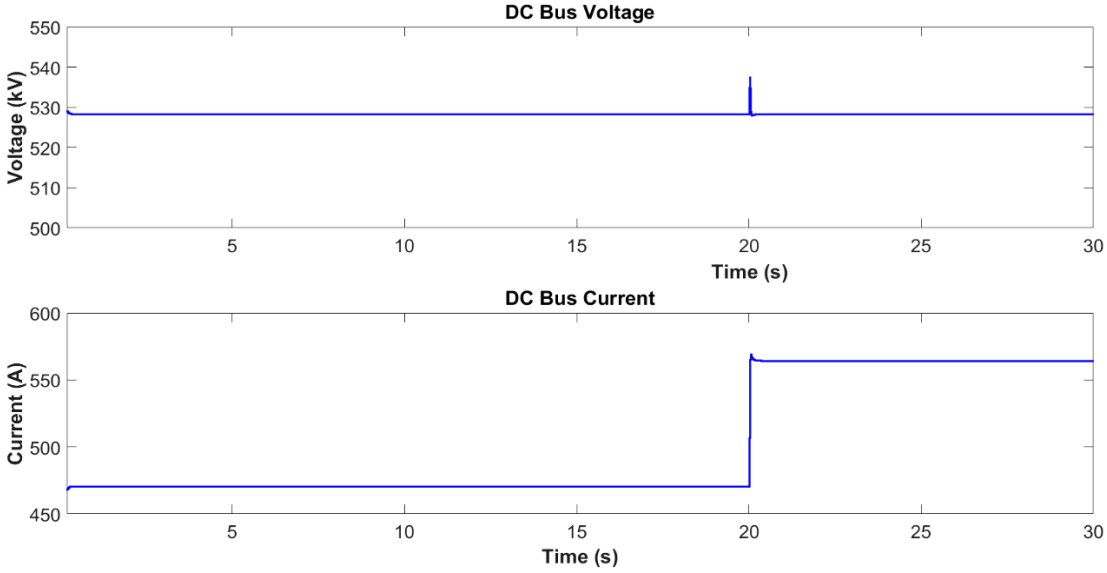

Figure 6-24: DC bus voltage and current for active power step increase

The second scenario assumes that the wind farm is producing constant active power and after 20 seconds a negative active power step change is introduced.

Figure 6-25 shows the active power transfer between the wind fam and the power network via the HVDC link. Initially, the power from the wind farm is constant (i.e. 250MW), and at 20 seconds the power instantaneously decreases by 50MW to 200MW. The DC bus power and the power injected to the network are matching up the trend of the power from the wind farm. The small variations are due to losses both in the converters and in the lines.

As can be seen in Figure 6-26, the DC bus voltage remains constant until the step increase in power from the wind farm. The DC controller ensures that the voltage remains constant by decreasing the current on the DC bus and transferring all the available power from the wind farm to the power network through the DC link.

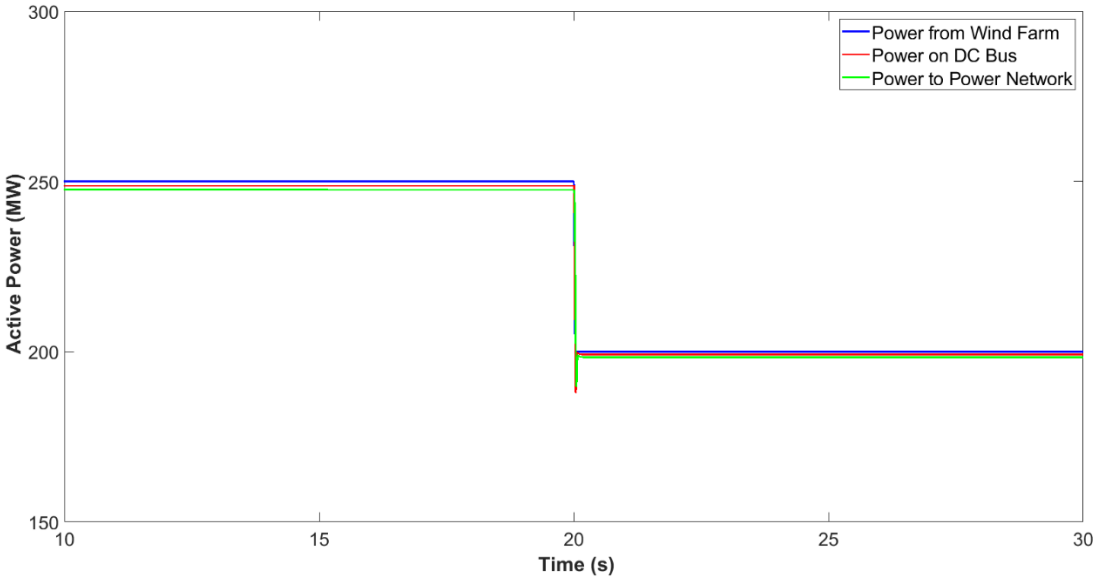

Figure 6-25: Active power transferred from the wind farm to the network via the VSC-HVDC link for negative active power step change

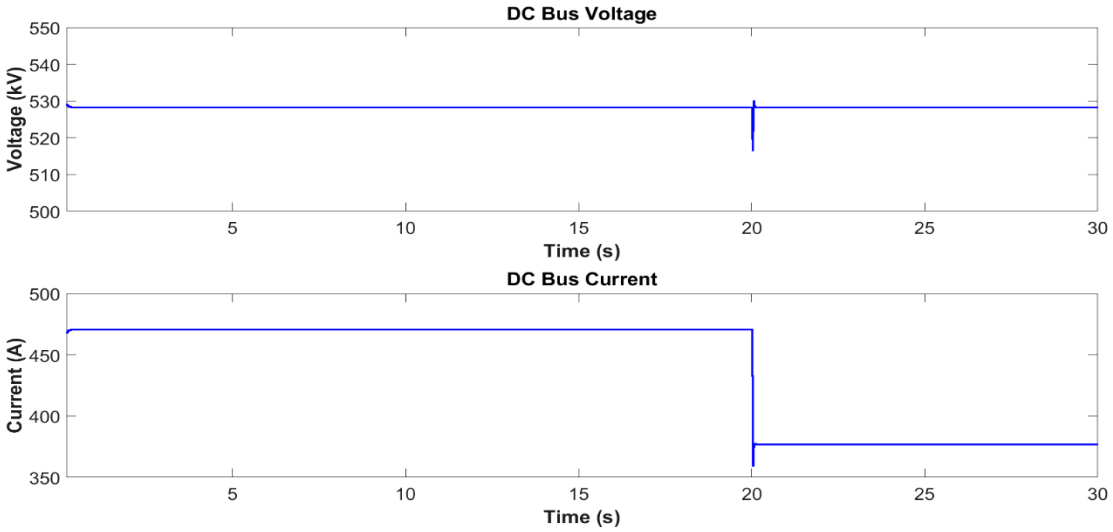

Figure 6-26: DC bus voltage and current for active power step decrease

The third scenario assumes that the wind farm outputs time-varying power. Figure 6-27 depicts the active power transfer between the wind fam and the power network via the HVDC link. The DC bus power and the power injected to the network are matching up the trend of the power from the wind farm. The small variations are due to losses both in the converters and in the lines.

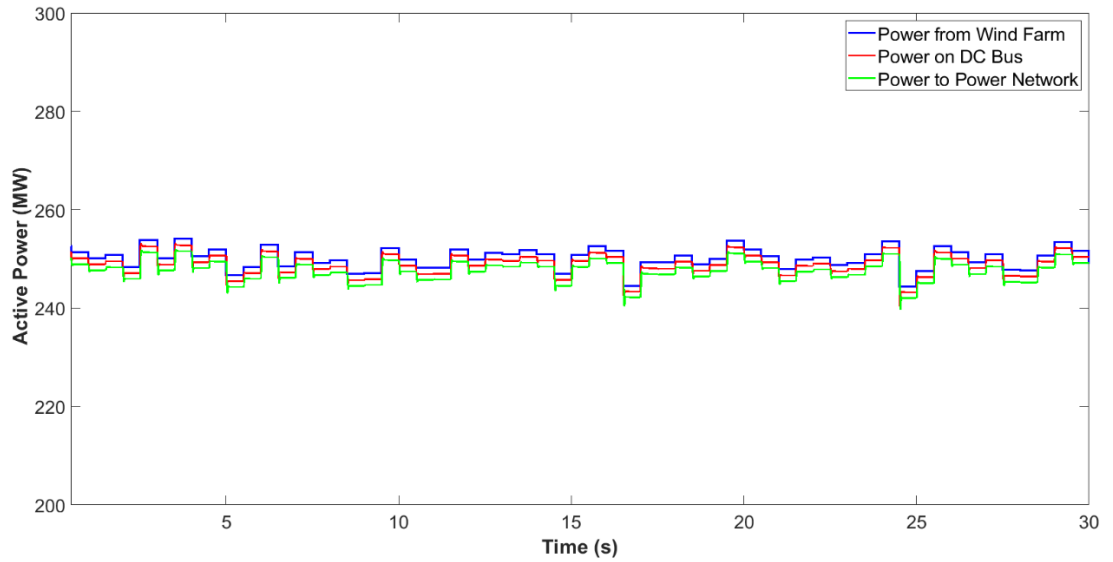

Figure 6-27: Active power transferred from the wind farm to the network via the VSC-HVDC link for time-varying active power

As can be seen in Figure 6-28, the DC bus voltage remains constant as the DC controller ensures that the voltage remains constant by altering the current on the DC bus and transferring all the available power from the wind farm to the power network through the DC link.

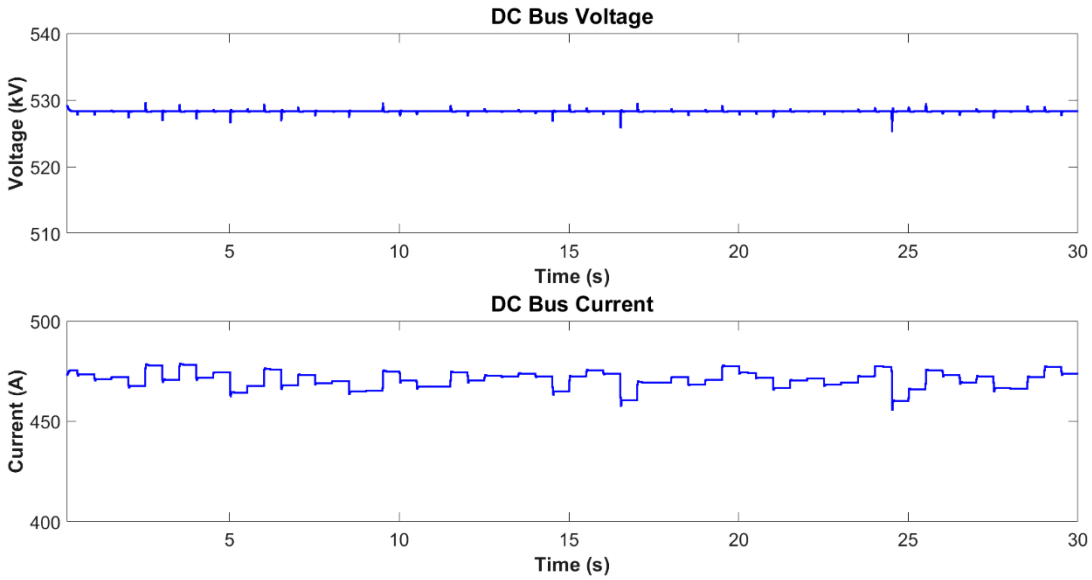

Figure 6-28: DC bus voltage and current for time-varying active power

6.5.4 Network Wind Farm Controller Simulation Results

The network wind farm model has been developed to check the power system frequency and ROCOF and send power request signals to the wind farm controller based on the operating needs of the power system. To achieve this, the network wind farm controller needs inputs from the PMU, so the controller needs to be connected to the power system. To evaluate the operation of the network wind farm model, this model is integrated into the reduced GB power system model. For the assessment of the network wind farm controller with this configuration, various scenarios have been investigated.

The first scenario assumes the loss of a 700MW and 100MVAr load connected on the 275kV side of Bus 3. After 15 seconds, the load is suddenly disconnected, and the frequency and

ROCOF are measured by the PMU. The simulation results such as the system frequency, ROCOF and network wind farm controller response are shown in Figure 6-29.

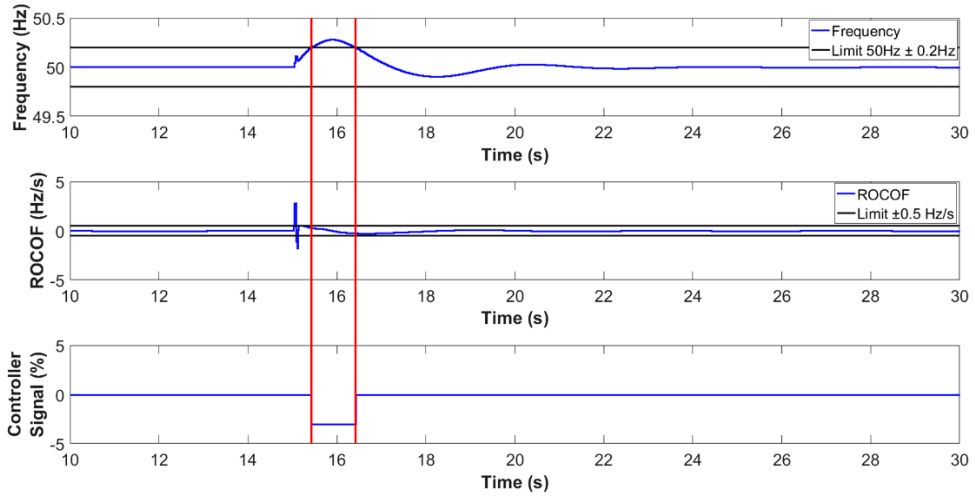

Figure 6-29: System frequency, ROCOF and network wind farm controller signal for loss of load

As can be seen in Figure 6-29, at 15 seconds the frequency rises due to the loss of the load, as expected, and then it gradually moves towards its nominal value (i.e. 50 Hz). Once the frequency moves above 50.2 Hz, the network wind farm controller requests a power decrease of 3%, based on the fact that the ROCOF is below $\pm 0.5\, {}^{Hz}/_{s}$. The controller stops the request once the frequency returns within the accepted limits (i.e. between 49.8Hz and 50.2Hz).

The second scenario assumes the introduction of a 700MW and 100MVAr load connected on the 275kV side of Bus 3. After 15 seconds the load is suddenly connected, and the frequency and ROCOF are measured by the PMU. The simulation results are depicted in Figure 6-30.

As can be seen in Figure 6-30, at 15 seconds the frequency drops due to the introduction of the load, as expected, and then it gradually moves towards its nominal value (i.e. 50 Hz). Once the frequency moves below 49.8 Hz, the network wind farm controller requests a power increase of 3%, based on the fact that the ROCOF is below $\pm 0.5\, {}^{Hz}/_{s}$. The controller stops the request once the frequency returns within the accepted limits (i.e. between 49.8Hz and 50.2Hz).

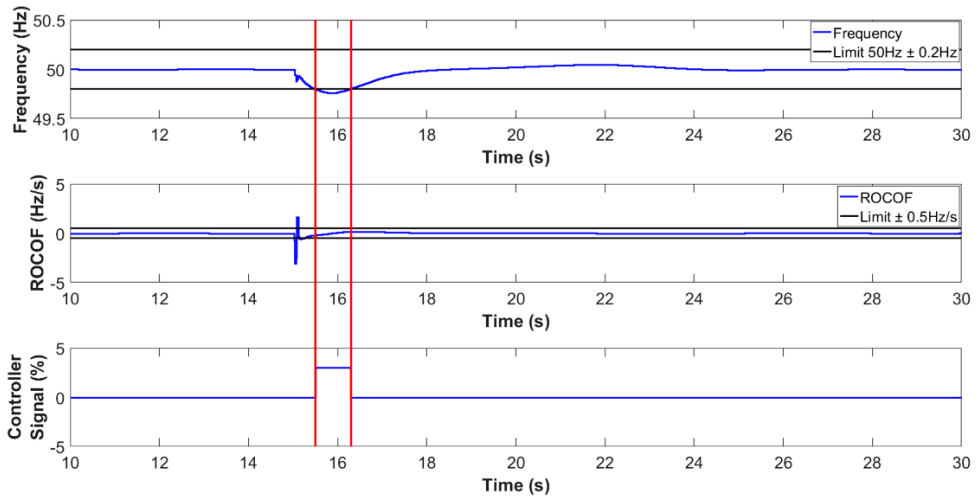

Figure 6-30: System frequency, ROCOF and network wind farm controller signal for introduction of load

The third and final scenario assumes the introduction of a fault on Bus 4. After 15 seconds the fault is introduced and then cleared after 150ms. The simulation results are shown in Figure 6-31.

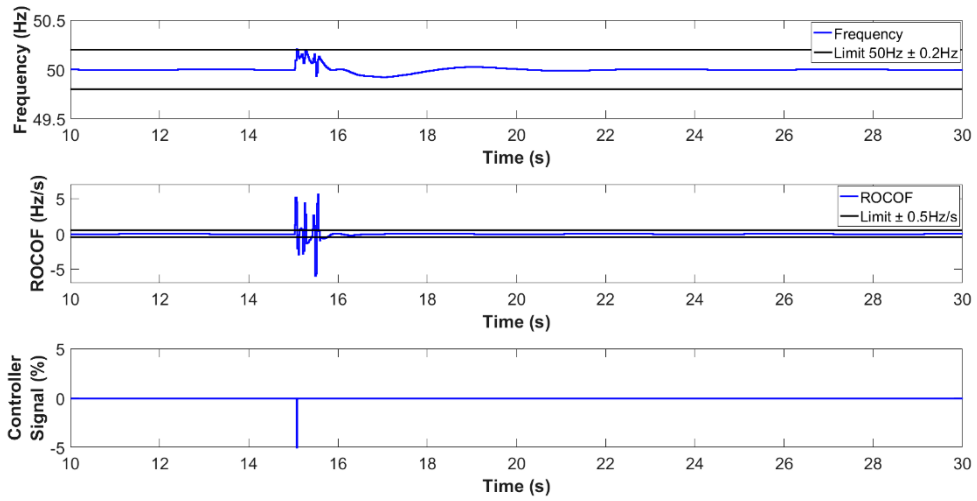

Figure 6-31: System frequency, ROCOF and network wind farm controller signal under fault conditions

As can be seen in Figure 6-31, at 15 seconds the frequency rises due to the fault and then it gradually moves towards its nominal value (i.e. 50 Hz). Once the frequency moves above 50.2 Hz, the network wind farm controller requests a power decrease of 5%, based on the fact that the ROCOF is above $\pm 0.5\,{}^{Hz}/_{S}$. The controller stops the request once the frequency returns within the accepted limits (i.e. between 49.8Hz and 50.2Hz).

6.6 Discussion and Conclusion

This chapter has focused on the assessment of different frequency measurement techniques, the development of representative GB power system models, the VSC-HVDC link between the wind farm and the power network, and the network wind farm controller. All the developed models are necessary to evaluate the capability of the wind farm controller's ability to provide ancillary services to the system operator.

The simulation results for the grid frequency measurement techniques suggest that the best measuring technique is the PMU. On the event of a loss of load, the SRF-PLL and the PMU have very similar, almost identical, measurements with the PLL initially slightly overestimating the frequency. The synchronous machine measurements show a much slower response and simultaneously fluctuates more than the PLL and PMU measurements, resulting to an overestimation of the system frequency. This occurs mainly due to the generator rotor oscillations.

For a loss of generation, the SRF-PLL and the PMU have very similar, almost identical, measurements with the PLL initially instantaneously overshooting and overestimating the frequency. The synchronous machine measurements show a much slower response and simultaneously fluctuates more than the PLL and PMU measurements, resulting to an overestimation of the system frequency, mainly due to the generator rotor oscillations.

In the event of fault, the SRF-PLL and the PMU have very similar, almost identical, measurements. The synchronous machine measurements show a much slower response and simultaneously fluctuates more than the PLL and PMU measurements, resulting in an overestimation of the system frequency. From the investigation of the different scenarios, the PMU has been evaluated as the most appropriate grid frequency measurement technique and

will be used to provide a frequency signal to the wind farm controller to alter the wind farm power output if needed.

The power system models have been created with increased complexity to allow for a representation of the British power system. The frequency measurement results during a fault do not match perfectly for the reduced GB power system model and the complete GB power system model, with the reduced GB model not capturing the total expected level of frequency oscillation, mainly due to the reduced number of synchronised generators and their interactions. In this case, the 29 node GB power system model illustrates a much better frequency measurement, as the increased number of synchronised generators allow for a much better simulation of the machine dynamics and interactions [129].

The results for load steps show very similar frequency measurements for both the reduced GB power system model and the complete GB power system model. This allows for the reduced GB power system model to be used for all load fluctuation simulation scenarios. The main advantage of the reduced GB power system is that the simulation runs much faster, with five complete synchronous machine modes representing the complete GB power network.

The VSC-HVDC link is designed to ensure the transfer of energy from the offshore wind farm to the power network. It can track the power produced by the wind farm and via the DC link synchronise and transfer all the power to the grid. The wind farm is decoupled from the grid, due to the HVDC substations, allowing for the assessment of the capability of the wind farm controller to provide synthetic inertia services to the system operator.

The network wind farm controller utilises the signal from the PMU and provides power requests to the wind farm controller. It is designed to define the requests based not only on the real-time frequency, but also on the rate of change of frequency. This defines the wind farm controller's response and sets the wind farm's behaviour to grid instabilities equivalent to the reaction of a synchronised, conventional generator. The effect of the interaction between the network wind farm controller, the HVDC link, the wind farm controller, wind farm and the power system will be thoroughly investigated and presented in Chapter 7.

Chapter 7 - Assessment of Wind Farm Controller Response on Power System Frequency Stability

In this chapter, the ability of the wind farm controller to compliment power system frequency stability is assessed. The large-scale wind farm model is equipped with a wind farm controller capable of altering the power output of the wind farm. The wind farm model is connected to the power system via a High Voltage Direct Current (HVDC) link. The network wind farm controller is located at the Point of Common Coupling (PCC) between the onshore HVDC substation and the AC grid, and uses frequency measurements to make requests for power changes to the wind farm controller. The wind farm controller is assessed under different levels of offshore wind penetration.

7.1 Introduction

The introduction of increased levels of new technologies such as large-scale renewable power plants and energy storage units is expected to affect power system stability. The development of mechanisms to improve system stability and provide ancillary services is expected to be requested in the future from all innovative power generation technologies. Given the increasing overall share of the energy market, the wind industry will be expected to introduce controllers to improve the services provided to the system operator.

Increasingly, wind turbines designs employ permanent magnet synchronous generators in tandem with fully-rated converters [130], whereas previously the typical doubly-fed induction generator concept was preferred [131]. Fully-rated converters completely decouple the generator inertia from the grid, affecting system frequency stability. With the expected reduction in rotating inertia directly connected to the grid, future wind turbine and wind farm designs may be required to incorporate mechanisms for improving power system stability. The

development of innovative controllers to improve power system frequency stability is expected to be of key importance in the future.

For completeness, it is noted that two stability issues have been highlighted for future power systems. The first is voltage stability and the second is frequency stability. Regarding the former, Zhang [132] showed that when the short-circuit ratio is low, the dynamics of the PLL negatively impact on the performance of conventional converter control algorithms, thereby introducing a voltage stability issue. Zhang also showed that replacing the conventional controller with one which mimicked aspects of a synchronous machine overcame this stability issue. Later, Ierna *et al.* [133] showed that having a small number of converters using a similar control algorithm to that of Zhang improved the performance of the remaining bulk of converters in a multi-converter system, where the remainder used the conventional control algorithm. Zhang demonstrated that the voltage stability issue was one which could be entirely handled by the converter connecting to a power system. No change would be required of, say, the rotor-side converter or the aero-mechanical control systems. This is ultimately because voltage stability does not require any change in power output; hence, frequency response studies can be carried out independently. In this thesis, focus is given to the control of the wind farm; thus, only frequency stability will be considered. In order to allow studies of frequency stability to be conducted without needing to design an unconventional converter controller, the short-circuit ratio from the perspective of the wind farm will be kept sufficiently high by placing its onshore HVDC substation in electrical proximity to a synchronous generator.

7.2 Research Opportunities

The development of innovative controllers to improve power system frequency stability is expected to be of key importance in the future. The wind farm controller developed in this work is evaluated based on its ability to improve frequency stability. The novelty of this work is the analysis of the effect of an innovative wind farm controller on the power systems model. The integrated model comprises a large wind farm model, which features the following elements: simplified representations of the complex wind and wake interactions between the wind turbines, sufficient for control system studies; an HVDC link, representing the connection between the wind farm and the power grid, whilst ensuring the decoupling of inertia between

the turbine generators and the grid; and the power system network representation with the network wind farm controller. The complete evaluation of the developed controller will facilitate understanding the effect of the introduction of novel wind farm level controllers to the power system, along with the potential benefits that can be established.

7.3 Integrated Model Simulation Results

The integrated model is based on the individual models presented in the previous chapters. The wind farm comprises 100 wind turbines which are organised in a regular lattice formation, with 800m longitudinal distance (i.e. between each row) and 400m lateral distance (i.e. between each column). For all simulated power system scenarios, the wind farm response has been simulated for three different mean wind speeds with 10% turbulence intensity: 8m/s i.e. below rated; rated, which occurs at 11m/s; and a wind speed of 15m/s i.e. above rated.

The HVDC link used to transfer the power from the wind farm to the grid is the VSC-HVDC model presented in Chapter 6. The power system models used in the integrated models are based on the reduced GB power system model. To allow for the investigation of different wind farm penetration scenarios, both the reduced GB and reduced Scottish power system models are used. The Scottish power system model is based on the GB power system model, but is designed as isolated from the rest of the GB power system. The designed Scottish power system model consists of all Scottish generators in isolation and is used to evaluate and provide a better insight to how effective the wind farm controller is in improving grid stability, especially for higher levels of wind penetration at an isolated, artificially islanded, scenario. The main difference between the GB and the Scottish power system models is that the latter does not include the generator and load representing the English power system.

Both models are simulated for 300s and have been tested for two different scenarios: the loss of load and the loss of generation. The first scenario assumes the loss of a load connected on the 275kV Bus 1. After 200 seconds, the load is suddenly disconnected, after which the network wind farm requests a response from the wind farm to provide frequency support. The second scenario assumes the loss of a generator connected on the 275kV side of Bus 3. After 200 seconds, the generator is suddenly disconnected, and the network wind farm requests a power increase response from the wind farm to provide frequency support. For both scenarios,

the communication delays between network wind farm controller and the wind farm controller have not been considered. The network wind farm controller sends its ΔP power request to the wind farm controller, while forwarding the new power setpoint to the VSC-HVDC onshore and offshore power converters ensuring rapid power change to improve system frequency stability, as depicted in Figure 7-1.

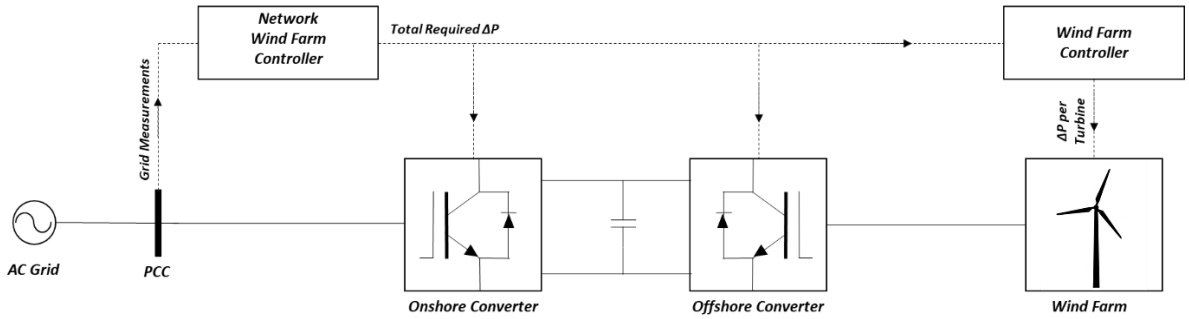

Figure 7-1: Integrated power system model overview

The wind farm power production injected to the grid has been simulated for three different mean wind speed scenarios to assess the wind farm controller response under various operating conditions. All the simulation models have been developed in Simulink/Simscape Power Systems environment.

7.3.1 GB Integrated Model Simulation Results

The reduced GB power system model, presented in Chapter 6, has been altered to evaluate the capability of the wind farm controller to provide ancillary services to the system operator. The updated reduced GB model is depicted in Figure 7-2. As can be seen from Figure 7-2, for all the nodes the respective loads and generation remains unchanged, the wind farm is connected to Bus 2 via a VSC-HVDC link (i.e. shown in red), and the newly introduced load in Bus 1 and generator in Bus 3 (i.e. shown in blue).

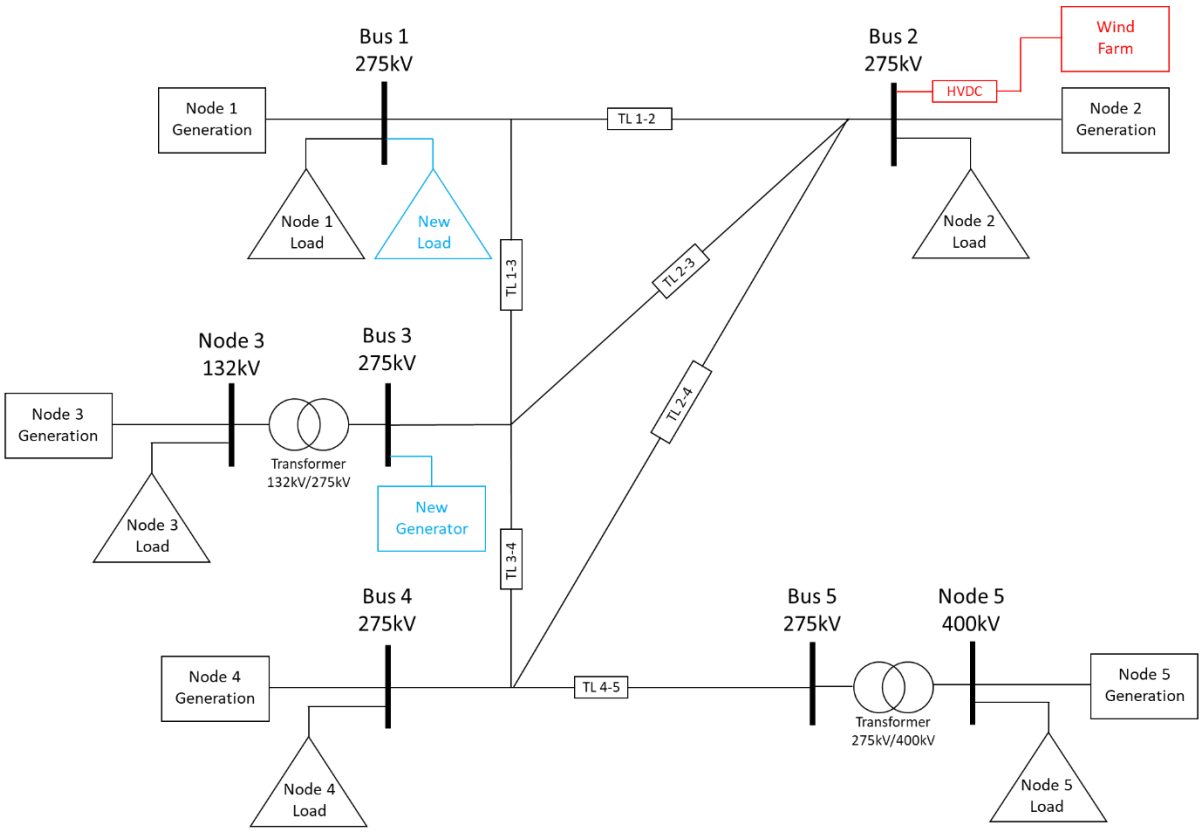

Figure 7-2: Updated reduced GB power system model

The introduced load connected to Bus 1 is defined as a 1200MW and 100MVAr load, and the introduced generator connected to Bus 3 is defined as a 1500MVA synchronous machine with the same characteristics as the Node 2 (i.e. Peterhead) synchronous generator. These values have been chosen to ensure that when the event occurs the frequency moves outside the accepted boundaries of 49.8Hz – 50.2Hz, allowing for the evaluation of the effect of the wind farm controller on power system frequency.

Table 7-1 shows the penetration of the non-synchronous wind farm in the reduced GB power system. The wind farm comprises 100 Supergen turbines with 5.2MVA rating, which corresponds to a total of 520MVA. As can be seen, the wind farm only represents 0.74% of the total grid connected generation.

Node	Generation (in MVA)
1	888
2	1691
3	827
4	2519
5	63390
Wind Farm	520
Totals	**69835**
Percentage of Wind Penetration (%)	**0.74**

Table 7-1: Generation characteristics and wind penetration

7.3.1.1 Loss of Load

The first scenario assumes the loss of a 1200MW and 100MVAr load connected on the 275kV side of Bus 1, which corresponds to 2.13% of the total connected active load, as can be seen in Table 7-2. After 200 seconds, the load is suddenly disconnected, and the simulation results are used to assess the grid frequency for two cases: the wind farm controller utilised and the controller not being utilised.

Node	Load (in MW)
1	468
2	468
3	555
4	1308
5	53482
Totals	**56281**
New Load (Bus 1)	1200
Percentage of New Load (%)	**2.13**

Table 7-2: Load characteristics

Figure 7-3 depicts the grid frequency simulation results on Bus 2 with the wind farm controller not utilised. As can be seen from Figure 7-3, for all wind speed conditions, the frequency is following an almost identical response to the loss of load. Moreover, for all the wind farm operation conditions, the frequency exceeds the 50.2Hz boundary, allowing for the assessment of the wind farm controller response.

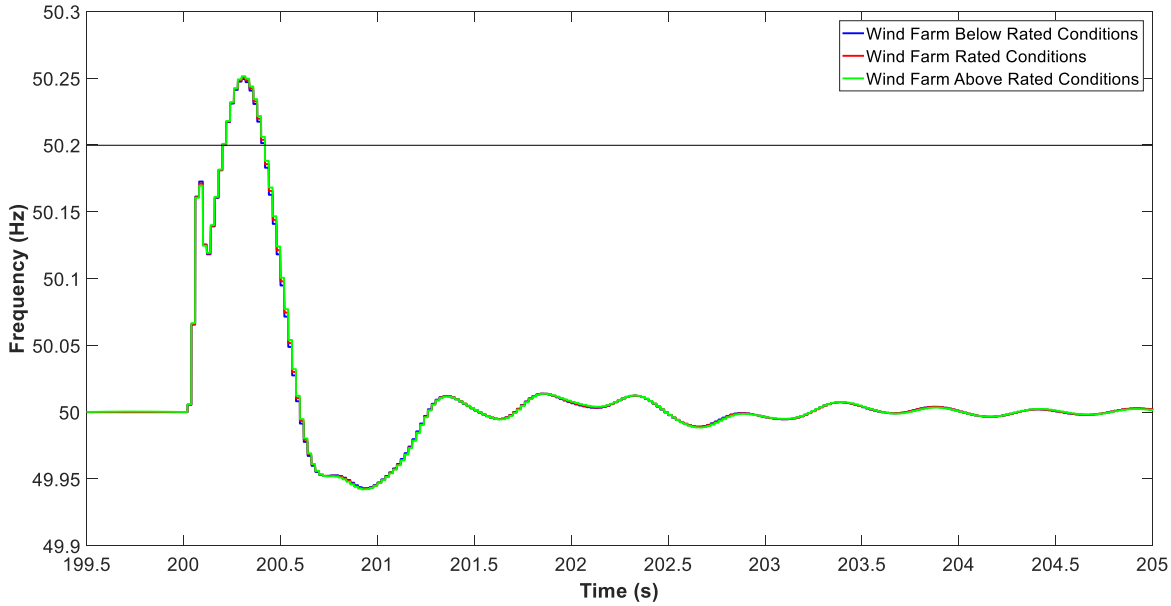

Figure 7-3: Bus 2 frequency for load loss (wind farm controller unused)

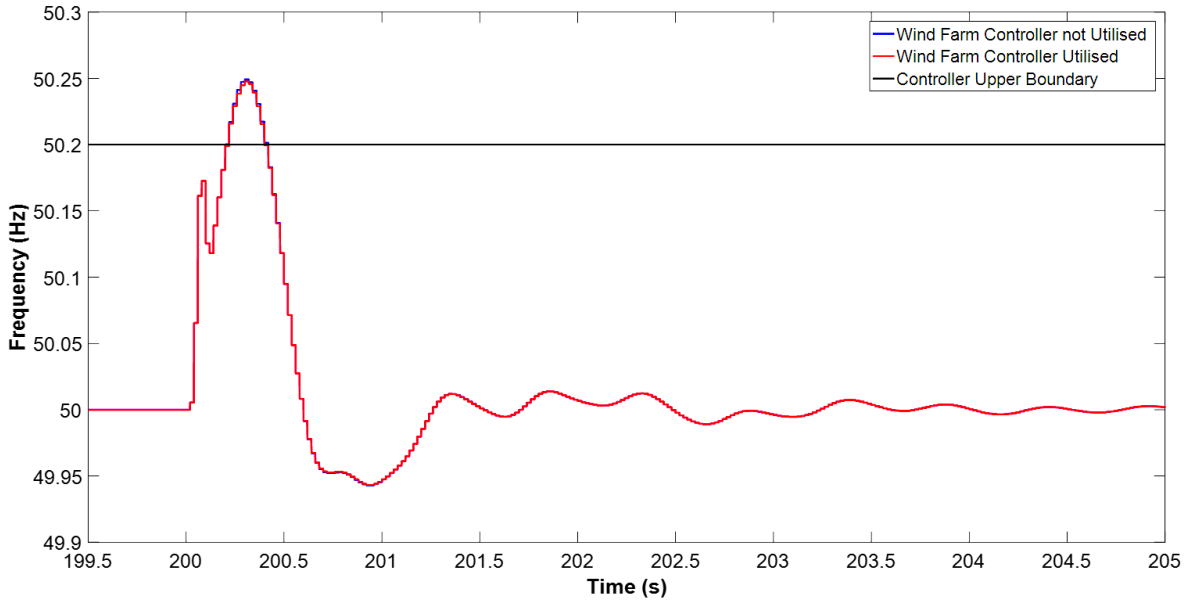

Figure 7-4(a): Comparison of Bus 2 frequency response for load loss with and without wind farm controller utilisation (below rated operation)

Figure 7-4(a) illustrates the comparison of the system frequency simulation results between the case of utilising the wind farm controller capabilities and the case of not using the wind farm controller, for below rated wind farm operating conditions. Figure 7-4(b) is used to zoom in and provide a better illustration of the effect of the wind turbine controller response.

The results show that the wind farm controller improves the frequency response of the system. The frequency deviates less with the wind farm controller being used and remains outside the accepted boundary for a smaller period of time. The results for all operating conditions and the percentage improvements can be seen in Table 7-3.

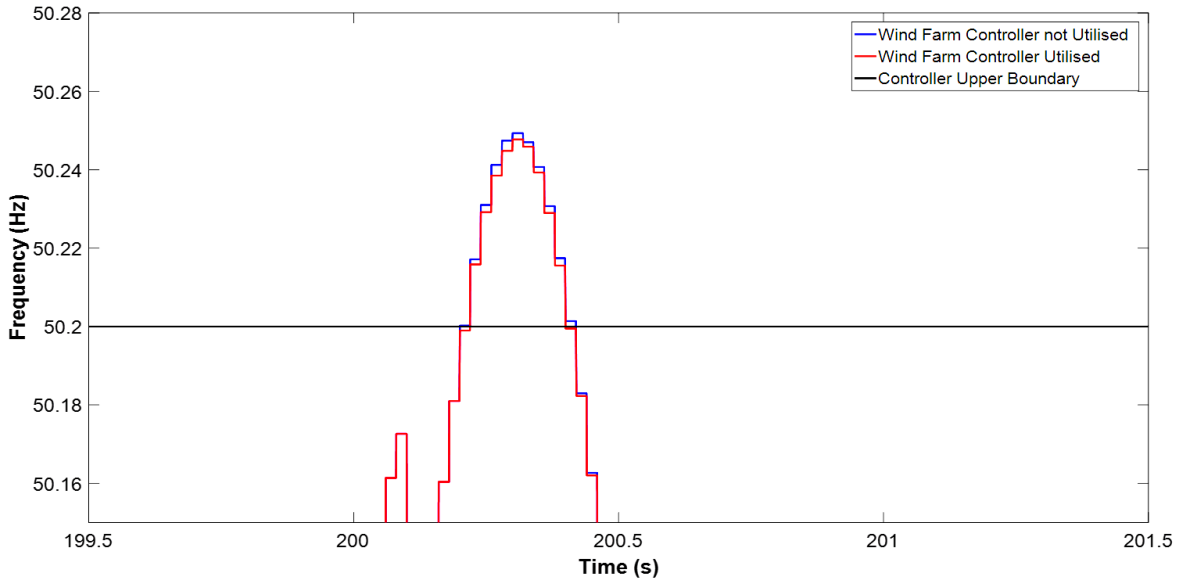

Figure 7-4(b): Zoomed in comparison of Bus 2 frequency response for load loss with and without wind farm controller utilisation (below rated operation)

Wind Farm Operational Conditions	Below Rated	Rated	Above Rated
Maximum Reached Frequency (without Wind Farm Controller Response)	50.2493	50.2505	50.2515
Maximum Reached Frequency (with Wind Farm Controller Response)	50.2477	50.2477	50.2488
Frequency Deviation Improvement (%)	**0.6418**	**1.1178**	**1.0736**
Time Outside Accepted Boundary (without Wind Farm Controller Response)	0.2200	0.2200	0.2210
Time Outside Accepted Boundary (with Wind Farm Controller Response)	0.1795	0.2000	0.2000
Time Improvement (%)	**18.4091**	**9.0909**	**9.5023**

Table 7-3: Result comparison under different operational conditions

As can be seen from Table 7-3, there is marginal improvement in the maximum reached frequency by the utilisation of the wind farm controller, but there is a significant improvement in the recovery time. The wind farm controller, by providing the required response, is capable of improving system stability, even though the wind farm only represents 0.74% of the total grid connected generation.

Figure 7-5 shows the comparison of the power produced by the wind farm for below rated operational conditions, when the wind farm controller is utilised and when the controller is not used. As can be seen from Figure 7-5, the controller requests a power decrease when the frequency exceeds 50.2Hz boundary and cancels the request once the frequency moves below the boundary. The request also changes from 5% decrease to 3% of the power produced once the ROCOF moves below 0.5.

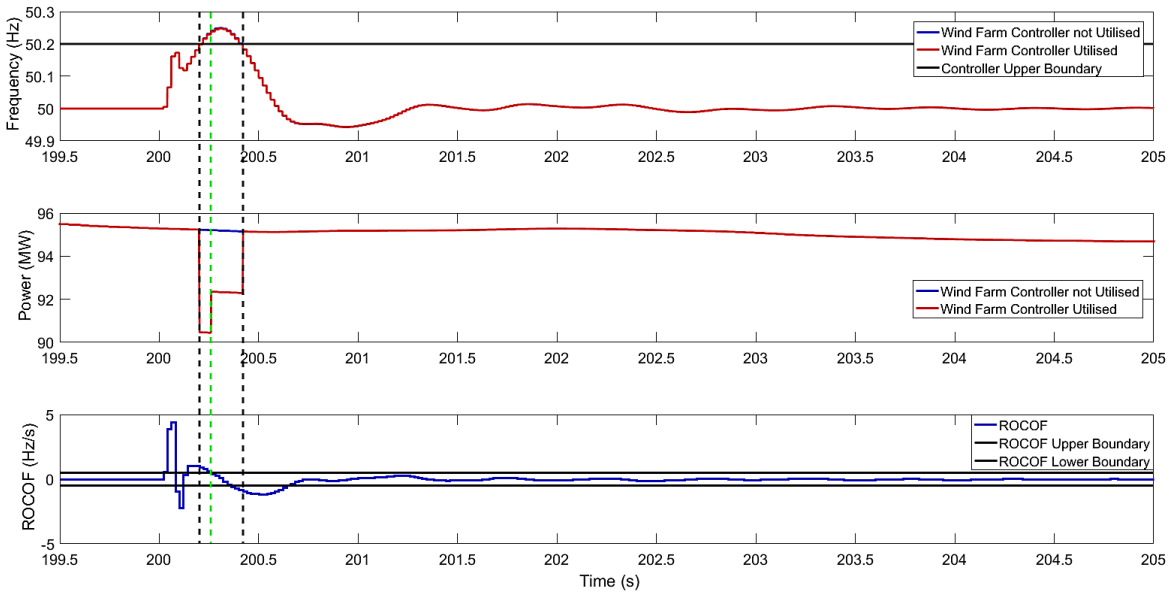

Figure 7-5: Power production from the wind farm relative to the system frequency at Bus 2 with and without wind farm controller utilisation (below rated operation)

7.3.1.2 Loss of Generation

The second scenario assumes the loss of a 1500MVA synchronous machine connected on the 275kV side of Bus 3, which corresponds to 2.15% of the total connected generation, as can be seen in Table 7-4.

The simulation results are used to evaluate the grid frequency for two cases: the wind farm controller utilised and the controller not being utilised. Figure 7-6 shows the grid frequency simulation results on Bus 2 with the wind farm controller not being utilised (i.e. OFF).

Node	Generation (in MVA)
1	888
2	2211
3	827
4	2519
5	63390
Totals	**69835**
New Generator	1500
Percentage of New Generator (%)	**2.15**

Table 7-4: Generation characteristics

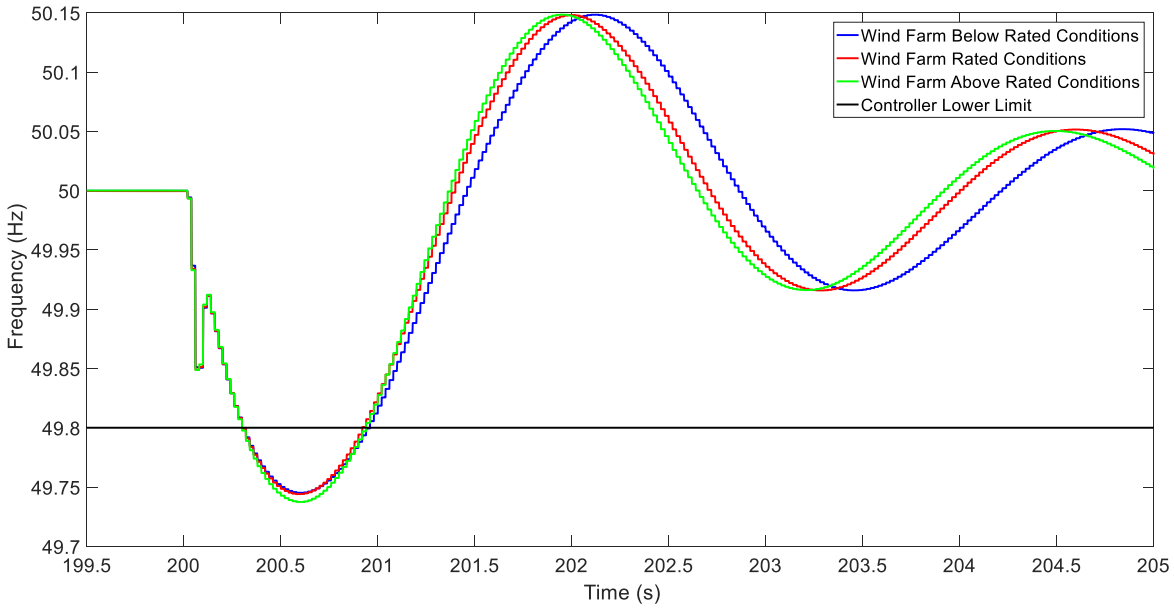

Figure 7-6: Bus 2 frequency for generation loss (wind farm controller unused)

As can be seen from Figure 7-6, at 200s the loss of the generator results to a sudden decrease in frequency. The frequency reaches a minimum value below 49.8Hz for all operating conditions before recovering to its nominal value. Figure 7-7 illustrates the comparison of the system frequency simulation results between the case of the wind farm controller being OFF and the case of the wind farm controller being ON, for rated wind farm operating conditions.

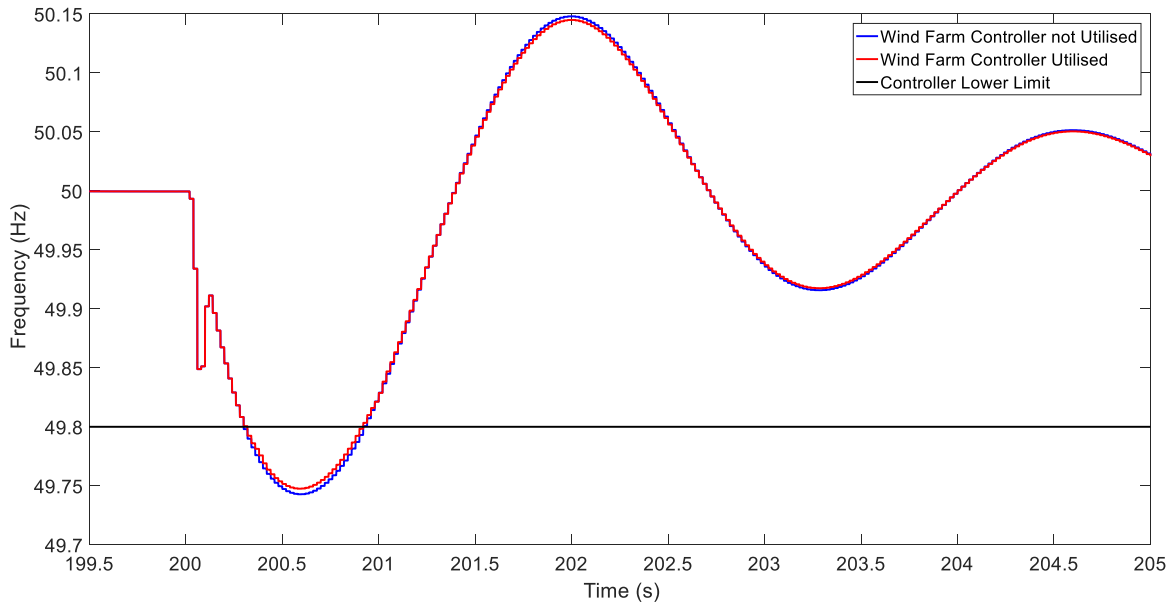

Figure 7-7: Comparison of Bus 2 frequency response for generation loss with and without wind farm controller utilisation (rated operation)

The simulation results show that the wind farm controller improves the frequency response of the system. The frequency deviates less with the wind farm controller being used and remains outside the accepted boundary for a smaller period of time. The results for all operating conditions and the corresponding percentage improvements can be seen in Table 7-5.

As can be seen from Table 7-5, there is only a marginal improvement in the minimum reached frequency by the utilisation of the wind farm controller, but there is a significant improvement in the recovery time.

Wind Farm Operational Conditions	Below Rated	Rated	Above Rated
Minimum Achieved Frequency (without Wind Farm Controller Response)	49.7439	49.7428	49.7362
Minimum Achieved Frequency (with Wind Farm Controller Response)	49.7471	49.7475	49.7425
Frequency Deviation Improvement (%)	**1.2495**	**1.8274**	**2.3882**
Time Outside Accepted Boundary (without Wind Farm Controller Response)	0.6605	0.6205	0.6410
Time Outside Accepted Boundary (with Wind Farm Controller Response)	0.6200	0.5995	0.6195
Time Improvement (%)	**6.1317**	**3.3844**	**3.3541**

Table 7-5: Result comparison under different operational conditions

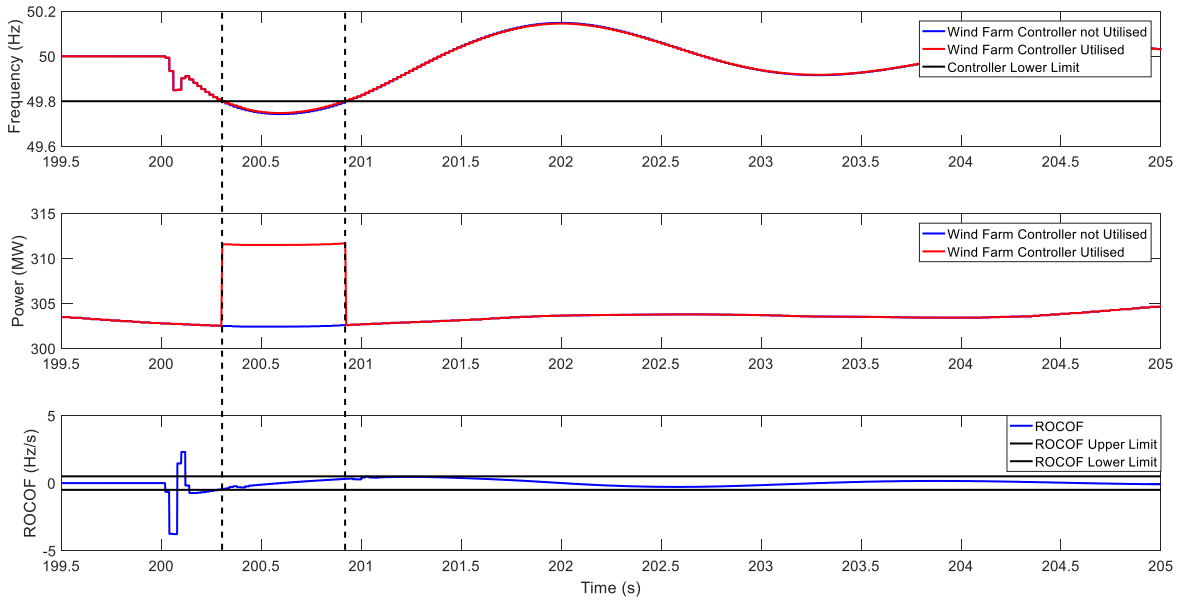

Figure 7-8: Power production from the wind farm relative to the system frequency at Bus 2 with and without wind farm controller utilisation (rated operation)

Figure 7-8 depicts the comparison of the power produced by the wind farm for rated operational conditions, when the wind farm controller is utilised and when the controller is not used. The controller requests a power increase when the frequency exceeds the 49.8Hz controller lower boundary and cancels the request once the frequency moves above the boundary. The power increase from the wind farm controller is set to 3% of the produced power while the frequency exceeds the lower limit; in so doing, the ROCOF remains within the ±0.5 range as required by the grid codes.

7.3.2 Scottish Integrated Model Simulation Results

The Scottish power system model has been developed to evaluate the capability of the wind farm controller to provide ancillary services to the system operator, as can be seen in Figure 7-9. The Scottish power system model has all the nodes the respective loads and generation remains unchanged, but the wind farm is connected to Bus 2 via a VSC-HVDC link (i.e. shown in red), and the newly introduced load in Bus 1 and generator in Bus 3 (i.e. shown in blue).

Node	**Generation (in MVA)**
1	888
2	1691
3	827
4	2519
Wind Farm	520
Totals	**6445**
Percentage of Wind Penetration (%)	**8.07**

Table 7-6: Generation characteristics and wind penetration

The introduced load connected to Bus 1 is defined as an 80MW and 10MVAr load, and the introduced generator connected to Bus 3 is defined as a 130MVA synchronous machine with the same characteristics as the Node 2 (i.e. Peterhead) synchronous generator. These values have been chosen to ensure that when the event occurs the frequency moves outside the accepted boundaries of 49.8Hz – 50.2Hz, allowing for the evaluation of the effect of the wind farm controller on power system frequency. The wind farm represents 8.07% of the total grid connected generation.

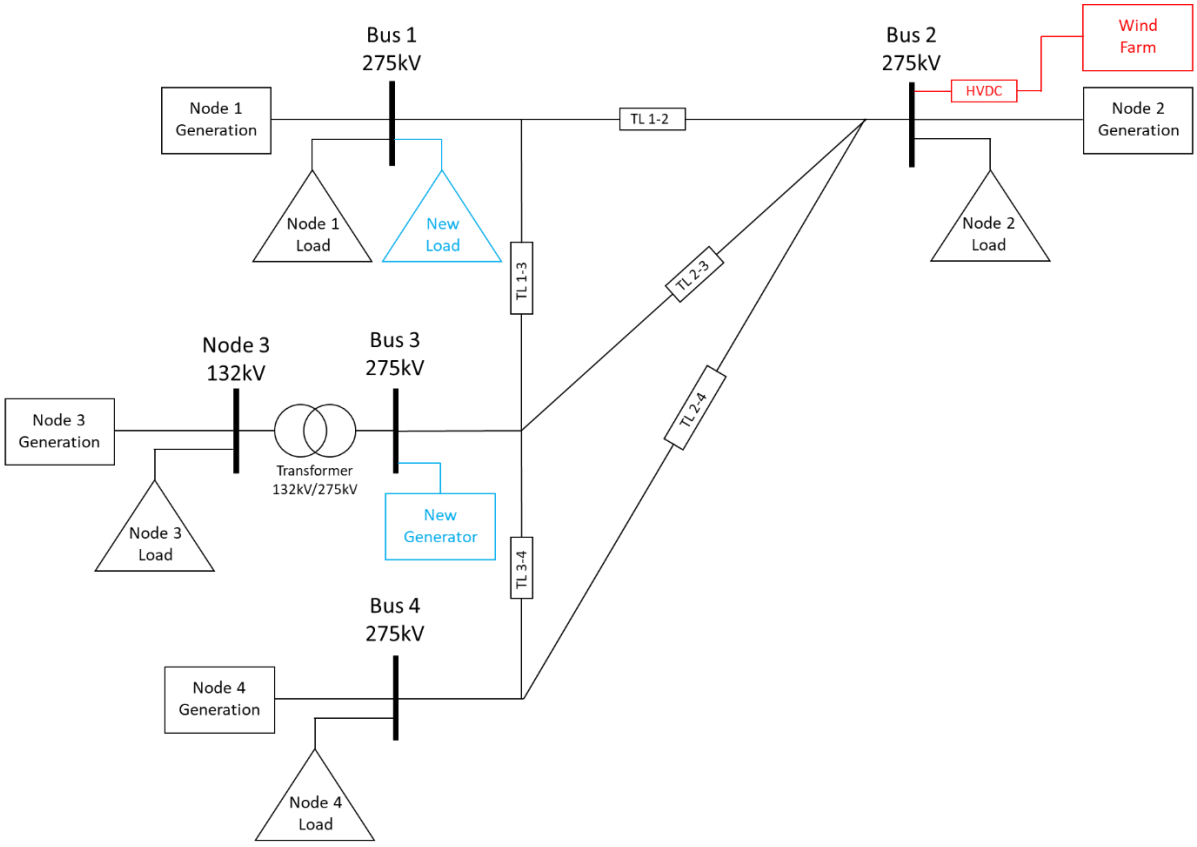

Figure 7-9: Scottish power system model

7.3.2.1 Loss of Load

The first scenario assumes the loss of an 80MW and 10MVAr load connected on the 275kV side of Bus 1, which corresponds to 2.86% of the total connected active load, as can be seen in Table 7-7. After 200 seconds, the load is suddenly disconnected, and the simulation results are used to assess the grid frequency.

Node	Load (in MW)
1	468
2	468
3	555
4	1308
Totals	**2799**
New Load	80
Percentage of New Load (%)	**2.86**

Table 7-7: Load characteristics

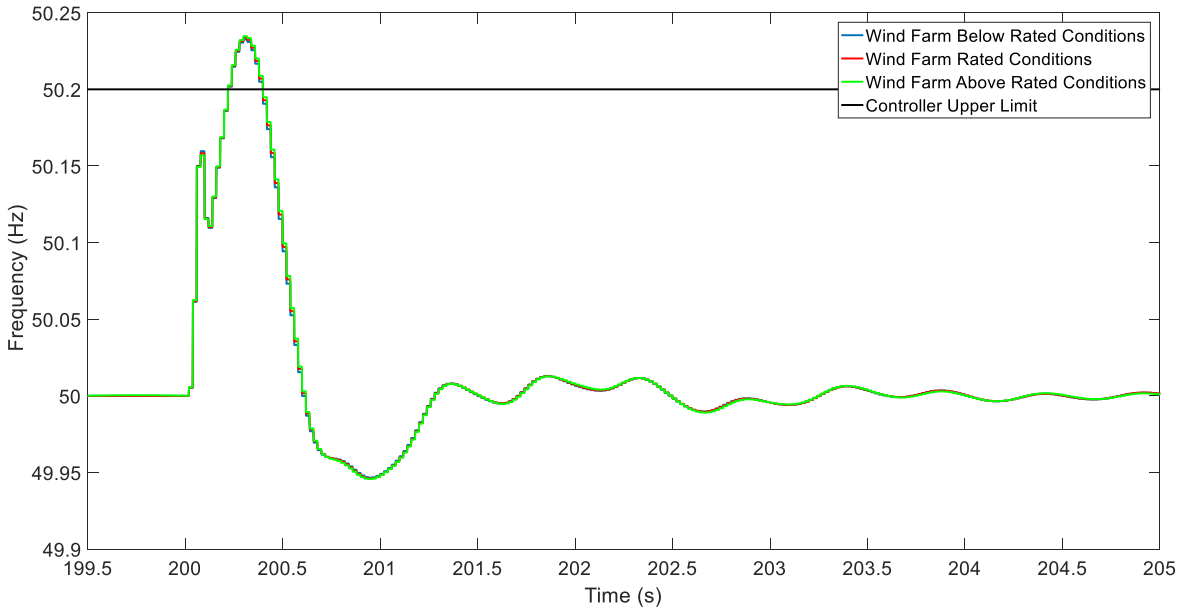

Figure 7-10: Bus 2 frequency for load loss (wind farm controller unused)

The simulation results of the system frequency, without the use of the wind farm controller, under all wind farm operational conditions are depicted in Figure 7-10. At 200s, the load gets disconnected and the frequency rises and exceeds the upper controller limit, before recovering to its nominal value.

Figure 7-11 illustrates the comparison of the system frequency simulation results between the case of the wind farm controller being OFF and the case of the wind farm controller being ON, for rated wind farm operating conditions. The wind farm controller improves the frequency recovery after the loss of load by reducing the maximum reached frequency, as well as the time the frequency remains outside the acceptable limits.

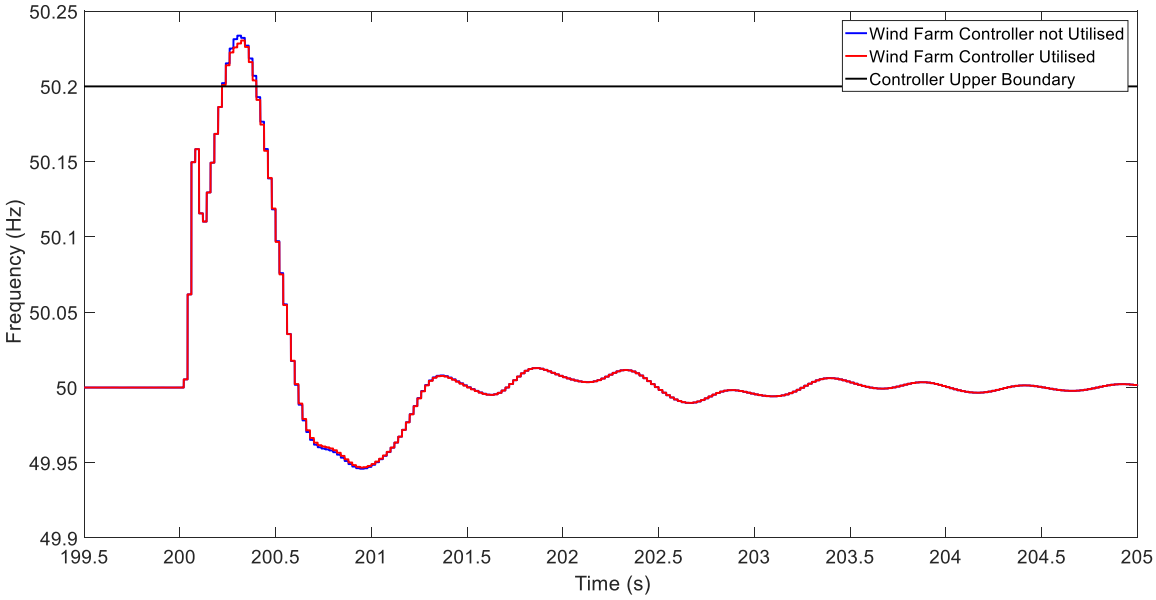

Figure 7-11: Comparison of Bus 2 frequency response for load loss with and without wind farm controller utilisation (rated operation)

The results for all operating conditions and the percentage improvements can be seen in Table 7-8. There is marginal improvement in the maximum reached frequency and recovery time by the utilisation of the wind farm controller. The wind farm controller, by providing the required response, is capable of improving system frequency stability.

Wind Farm Operational Conditions	Below Rated	Rated	Above Rated
Maximum Reached Frequency (without Wind Farm Controller Response)	50.2326	50.2337	50.2347
Maximum Reached Frequency (with Wind Farm Controller Response)	50.2302	50.2305	50.2305
Frequency Deviation Improvement (%)	**1.0318**	**1.3693**	**1.7895**
Time Outside Accepted Boundary (without Wind Farm Controller Response)	0.1805	0.1805	0.1805
Time Outside Accepted Boundary (with Wind Farm Controller Response)	0.1795	0.1795	0.1795
Time Improvement (%)	**0.5540**	**0.5540**	**0.5540**

Table 7-8: Result comparison under different operational conditions

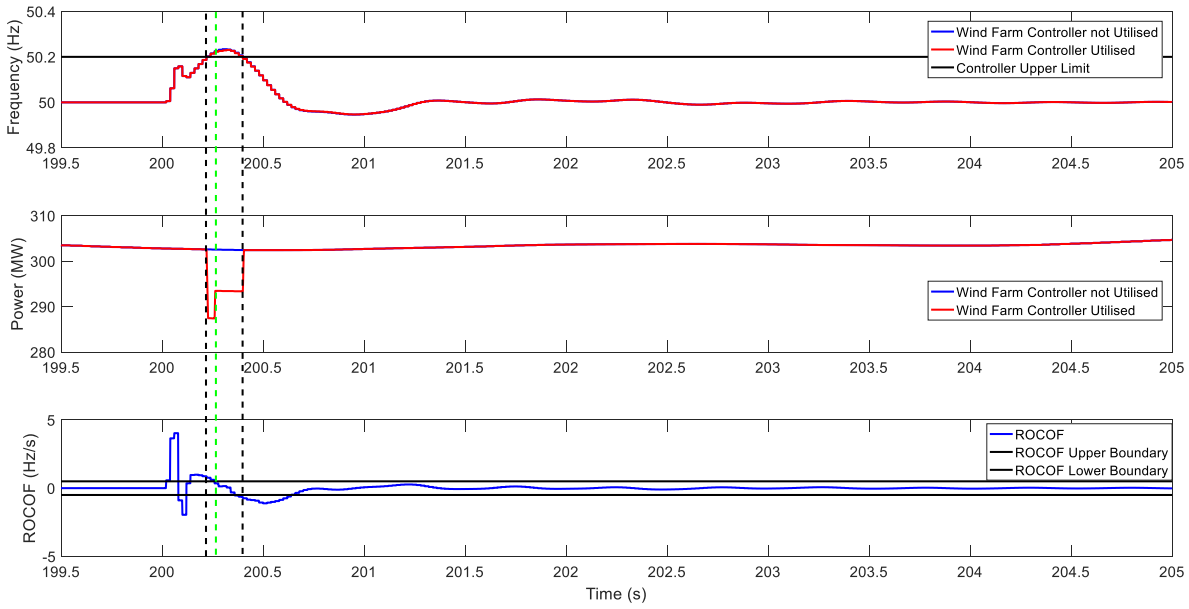

Figure 7-12: Power production from the wind farm relative to the system frequency at Bus 2 with and without wind farm controller utilisation (rated operation)

Figure 7-12 depicts the comparison of the power produced by the wind farm for rated operational conditions, when the wind farm controller ON and OFF. The controller requests a power increase when the frequency exceeds 50.2Hz boundary and cancels the request once the frequency moves below the boundary. The request also changes from 5% decrease to 3% of the power produced once the ROCOF moves below 0.5.

7.3.2.2 Loss of Generation

The second scenario assumes the loss of a 130MVA synchronous machine connected on the 275kV side of Bus 3, which corresponds to 2.02% of the total connected generation, as can be seen in Table 7-9. The simulation results are used to evaluate the grid frequency for two cases: the wind farm controller utilised and the controller not being utilised. Figure 7-13 depicts the grid frequency simulation results on Bus 2 with the wind farm controller OFF.

Node	**Generation (in MVA)**
1	888
2	2211
3	827
4	2519
Totals	**6445**
New Generator	130
Percentage of New Generator (%)	**2.02**

Table 7-9: Generation characteristics

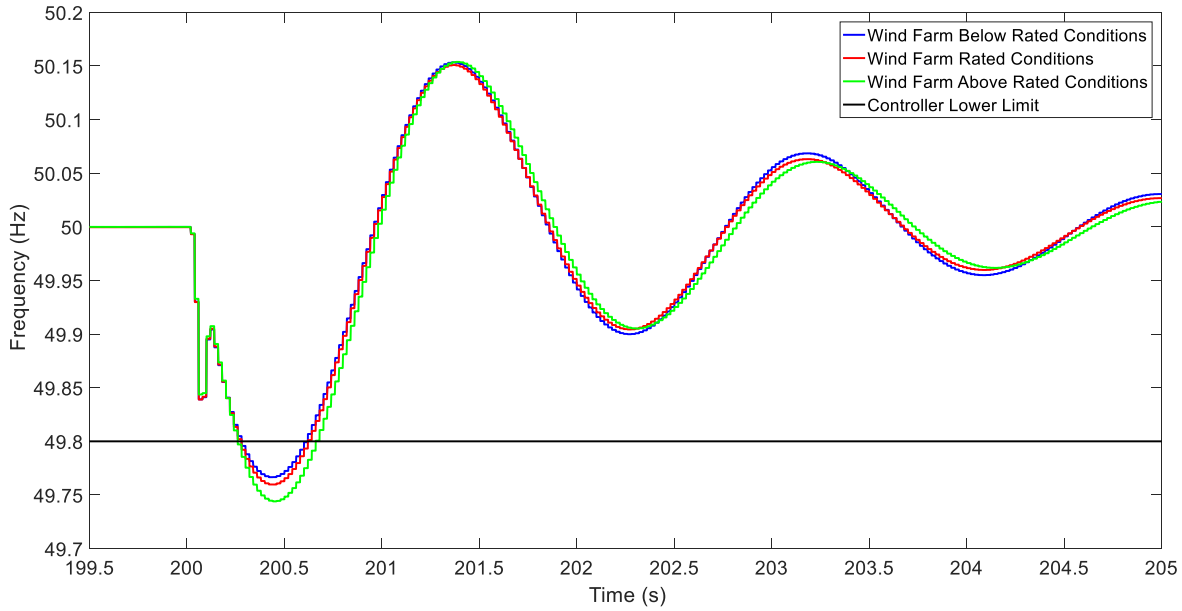

Figure 7-13: Bus 2 frequency for generation loss (wind farm controller unused)

As can be seen from Figure 7-13, at 200s the loss of the generator results in a sudden decrease in frequency. The frequency reaches a minimum value below 49.8Hz for all operating conditions before recovering to its nominal value. It should be noted that with increased wind farm power production the system frequency tends to deviate more. This is expected for the Scottish power system, as the wind farm now corresponds to 8.07% of the grid connected generation, resulting in a significant generation contribution in the power system.

Figure 7-14 illustrates the comparison of the system frequency simulation results between the case of the wind farm controller being OFF and the case of the wind farm controller being ON, for above rated wind farm operating conditions.

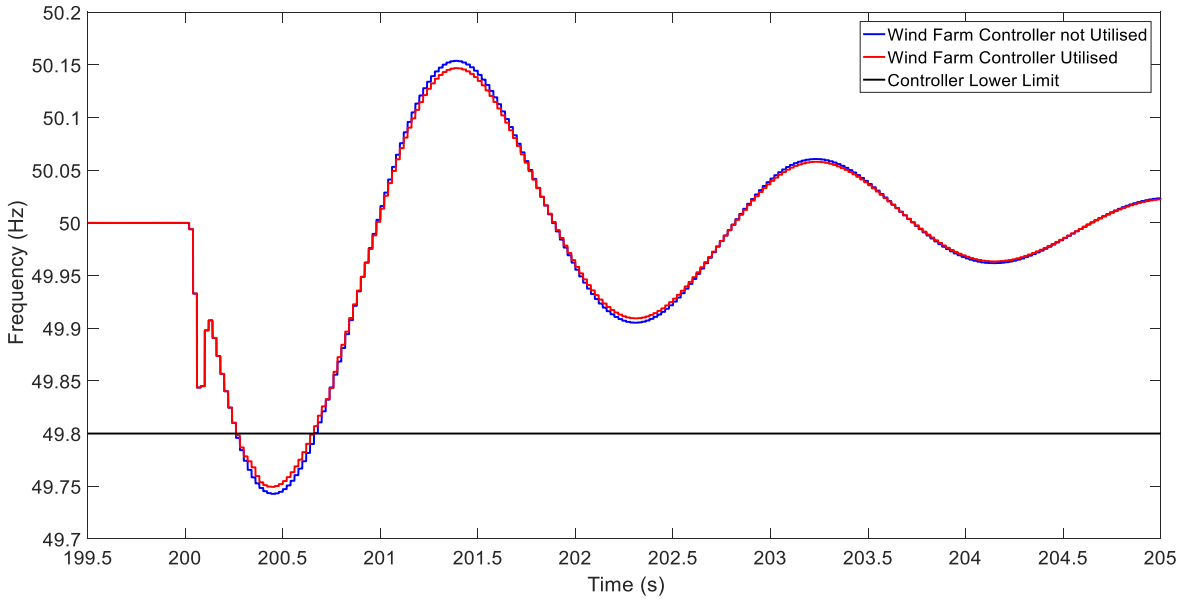

Figure 7-14: Comparison of Bus 2 frequency response for generation loss with and without wind farm controller utilisation (above rated operation)

The simulation results show that the wind farm controller improves the frequency response of the system. The frequency deviates less with the wind farm controller being used and remains outside the accepted boundary for a smaller period of time. The results for all operating conditions and the corresponding percentage improvements can be seen in Table 7-10.

Figure 7-15 depicts the comparison of the power produced by the wind farm for above rated operational conditions, when the wind farm controller is ON and OFF. The controller requests a power increase when the frequency exceeds the 49.8Hz controller lower boundary and cancels the request once the frequency moves back within the acceptable operating range. The power increase from the wind farm controller is set to 3% of the produced power while the frequency exceeds the lower limit; in so doing, the ROCOF remains within the ±0.5 range.

Wind Farm Operational Conditions	Below Rated	Rated	Above Rated
Minimum Reached Frequency (without Wind Farm Controller Response)	49.7641	49.7573	49.7415
Minimum Reached Frequency (with Wind Farm Controller Response)	49.7697	49.7641	49.7506
Frequency Deviation Improvement (%)	**2.3739**	**2.8018**	**3.5203**
Time Outside Accepted Boundary (without Wind Farm Controller Response)	0.3527	0.3805	0.4708
Time Outside Accepted Boundary (with Wind Farm Controller Response)	0.3200	0.3400	0.4000
Time Improvement (%)	**9.2713**	**10.6439**	**15.0382**

Table 7-10: Result comparison under different operational conditions

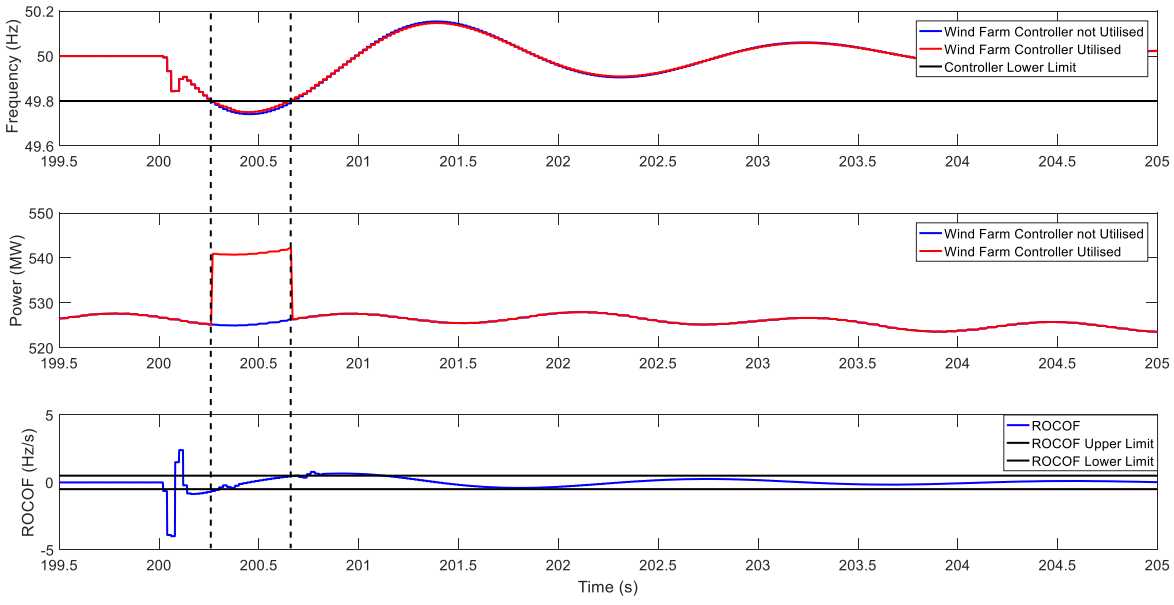

Figure 7-15: Power production from the wind farm relative to the system frequency at Bus 2 with and without wind farm controller utilisation (above rated operation)

7.4 Discussion and Conclusion

This chapter has focused on the development of integrated power system models to evaluate the effect of the use of the wind farm controller to the grid frequency stability. The models have been developed to assess the performance of the wind farm controller not only for different operational conditions but also for different levels of wind penetration. Based on the simulation results, this chapter answers the research question “can we operate (offshore) wind farms flexibly under all operational conditions to provide ancillary services to the grid operator and improve power system stability?”. This chapter concludes that the wind farm controller can be utilised to provide flexible operation of offshore wind farms, under different operating conditions, whilst improving frequency stability and allowing the wind farm operator to provide ancillary services to the power system operator.

The GB power system model is used to represent the effect of the wind farm controller on the British power system. The simulation results show that even though the wind farm corresponds to less than 1% of the total connected generation, the wind farm capabilities limit both the frequency deviation from its nominal value and the total amount of time the frequency remains out of the controller acceptable boundaries, thus improving frequency stability.

For the isolated Scottish power system model, the simulation results show even greater improvement relative to the GB power system simulation results. This is expected as for the Scottish power system model the wind farm corresponds to approximately 8% of the connected generation, and the frequency deviation is further improved with a concurrent out-of-limits period decrease.

Both power system models show the potential of the wind farm controller. With increasing levels of renewables connected to the power system and the corresponding expected rotating inertia reduction, the use of new controllers becomes essential. All simulations show that the wind farm is capable of providing synthetic inertia services under all operational conditions, as the request period is limited, allowing the controller to provide the requested power. The wind farm controller improves grid frequency stability for various levels of offshore wind integration (i.e. 0.74% and 8.07%), showing the potential of the controller even for small levels of offshore

wind integration. Future work should include the investigation of the effect of the utilisation of the wind farm controller to improve grid frequency stability at higher levels of wind integration.

This work shows that the utilisation of the wind farm controller can improve system frequency stability and provide services to the system operator. The developed wind farm is connected to the grid via a VSC-HVDC link, which decouples the wind turbines' inertia from the grid, thus decreasing system inertia. Even with decreased rotating system inertia the wind farm controller improves system frequency stability, showing the huge potential of wind farm level controllers. With more, large, offshore wind farms under development, the need for advanced wind farm flexibility is preferential/desirable. Future work should include the investigation of the effect of communication delays and how they could affect system frequency stability.

Chapter 8 – Conclusion and Future Work

In this work, a complete power system model has been developed which comprises the following elements: a wind farm model with simplified, but sufficiently accurate, representations of wind and wake effects, capable of modelling large offshore wind farms; a VSC-HVDC model; and a GB power system representative model. The thesis introduced novel approaches to wind farm modelling, including the development of two novel wind farm controllers, one designed to improve power system frequency stability, and the other designed to ameliorate offshore wind turbine reliability, taking into account O&M from real offshore wind turbines.

8.1 Thesis Conclusions

This research aims to answer the research question "Can we operate (offshore) wind farms flexibly under all operational conditions to provide ancillary services to the grid operator, thus improving power system stability whilst ensuring reduced Operation & Maintenance (O&M) costs?". This work found that the wind farm controller can be utilised to provide flexible operation of offshore wind farms while preventing wind turbine failures, under various operating conditions, whilst improving frequency stability and allowing the wind farm operator to provide ancillary services to the power system operator.

Chapter 3 is unique in providing an assessment of the effect of wind conditions on offshore wind turbine "major replacement" failures. The data used for this analysis are three-day averaged data provided directly from the turbine manufacturer of the two offshore wind farms. "Major replacement" type of failures represents approximately ~6% of the total number of failures, but corresponds to ~95% of the total cost of failures. The analysis shows that there is a relationship between the wind direction a wind turbine experiencing a failure is operating under (i.e. yaw error) relative to the other turbines in the wind farm. Mean wind speed and

turbulence intensity do not seem to have a major effect on “major replacement” wind turbine failures. This analysis allows the wind farm operator to identify and prioritise the turbines to be utilised by the wind farm controller to provide ancillary services to the grid.

In Chapter 4, the wind farm model is presented. The wind farm comprises 10 wind turbines, allowing for an in-depth review of the modelling technique and structure. The decentralised structure of the wind farm controller allows for flexible operation of the wind farm, while accepting input values from the network wind farm controller to improve grid frequency stability. This controller design approach is expected to be widely used in the future, as it is not only providing the required ancillary services to the system operator, but it does so while protecting the turbines that are more likely to experience a “major replacement” failure. This improves the operators’ ability to achieve optimal utilisation of their assets. This becomes essential for offshore wind farms, where site accessibility can be limited due to weather conditions. The wind farm model simulation results show that the wind farm controller is capable of providing primary response and, under certain operational conditions, primary and secondary response.

Chapter 5 aims to investigate the capabilities of the wind farm controller on a large wind farm. For large scale offshore wind farms, the simulation results suggest that the wind farm controller can provide power reserve services under all operational conditions when required, at the same time as ensuring increased turbine availability by following the O&M analysis presented in chapter 3. The controller is capable of providing droop control and primary response services to the system operator under all operational conditions. The simulation results also show that the aggregated power produced by large wind farms tends to be smoother compared to small wind farms, as the local wind speed fluctuations do not significantly affect the overall power production of the wind farm. As larger wind farms are connected to the power system, their ability to provide ancillary services will be desirable.

In chapter 6, the power system model is described. The power system modelling is essential for the assessment of the wind farm controller capabilities to provide ancillary services. The investigation of the best frequency measuring technique shows that the PMU is ideal for providing the network controller information about the system frequency status. The frequency measurements are then passed to the network wind farm controller, which

identifies if any events have occurred and reacts to improve the system stability. The network wind farm controller is designed to react once the frequency exceeds the pre-defined acceptable boundaries of 50±0.2Hz (i.e. between 49.8Hz and 50.2Hz) and its response is based on the ROCOF measurement. The power system model is based on representative GB power system models [84] [96], allowing for a more accurate evaluation of the effect of the introduction of the wind farm controller on the GB power system frequency stability. The developed power system models have increased complexity to allow the investigation of the effect of detailed modelling in grid frequency studies. The connection of the wind farm to the onshore transmission grid is achieved via a VSC-HVDC model. The HVDC model ensures that the wind farm is decoupled from the grid, thus the wind farm can only provide synthetic inertia services to the system operator.

Chapter 7 presents the investigation of the effect of the wind farm controller flexibility on power system frequency stability. The simulation results show that the wind farm controller can provide ancillary services to the system operator and improve frequency stability, even for low levels of wind farm controller penetration. For low wind farm penetration (i.e. complete GB model simulation), even for a modest network controller request of ±3% relative to normal operation, system frequency stability is improved. For higher wind farm penetration (i.e. isolated Scottish model simulation), the frequency stability improvements are even better. The improvements include frequency deviation decrease and limitation of the time period the frequency remains outside the accepted boundaries. All simulations suggest that the introduction of wind farm controllers on a larger scale would allow for significant improvements on power system frequency stability.

8.2 Future Work

There are various areas that have been discussed in this thesis in which improvements could be made with further work. The following paragraphs will outline what further work could be carried out to improve and build on this thesis.

As with all data analysis the quality and quantity of the inputs determine the quality of the outputs. The O&M analysis performed in this work could be improved by using more accurate data, such as 10-minute average data, which would allow to capture the effect of fast weather

condition changes on wind turbine failures, that is impossible to capture with three-day averaged values. The analysis should also be enriched by data from different types of wind turbines (e.g. direct driven machines) or turbines from different manufacturers. Future analysis should also include the investigation of correlation between independent variables of the weather conditions by using multivariate analysis.

The wind farm model could be further improved by introducing the capability to simulate the effect of turbines operating under yaw, which would allow for an assessment of the improvement to operational costs by the utilisation of the wind farm controller. In the future, it would also be advantageous to evaluate the capability of the wind farm controller to provide secondary response services to the system operator if the droop control strategy is utilised.

The network wind farm controller design strategy could be used to assess the effect of refining the build-in network controller constraints, such as allowing the network controller to request grid support not only when the frequency exceed the pre-defined boundaries, but also when the ROCOF exceed certain limits. The assessment of the frequency stability should also be evaluated for various event locations in order to investigate the effect of the distance of the event to the controller frequency stability improvement margins. Future models should also assess the effect of increased wind penetration of frequency stability and communication delays. The wind farm controller and network controller strategy could also change to allow for voltage stability improvements.

Chapter 9 – References

[1] A. Stock, *Augmented control for flexible operation of wind turbines,* Glasgow: University of Strathclyde, 2015.

[2] J. Fitzpatrick, *Smart Grids,* Dublin: Dublin City University, 2012.

[3] J. Bebic, "Power System Planning: Emerging Practices Suitable for Evaluating the Impact of High-Penetration Photovoltaics," IPCC, New York, 2008.

[4] O. Edenhofer, R. Pichs-Madruga, Y. Sokona, J. C. Minx, E. Farahani, S. Kadner, K. Seyboth, A. Adler, I. Baum, S. Brunner, P. Eickemeier, B. Kriemann, J. Savolainen, S. Schlömer, C. von Stechow and T. Zwickel, *Climate Change 2014 Mitigation of Climate Change,* New York: Cambridge University Press, 2014.

[5] UK Committee on Climate Change, *National Renewable Energy Action Plan for the United Kingdom,* London: Department of Energy and Climate Change, 2009.

[6] A. Shires, *Wind Turbine characteristics,* Cranfield: Cranfield University, 2011.

[7] F. Blaabjerg and K. Ma, "Future on Power Electronics for Wind Turbine Systems," *IEEE Journal of Emerging and Selected Topics in Power Electronics,* vol. 1, no. 3, pp. 139-152, September 2013.

[8] S. Patel, "Changing Winds: The Evolving Wind Turbine," Power Magazine, 4 January 2011. [Online]. Available: http://www.powermag.com/changing-winds-the-evolving-wind-turbine/?pagenum=3. [Accessed 14 October 2016].

[9] Wind Energy Center, "Wind Energy Center Alumni," University of Massachusetts, 24 April 2010. [Online]. Available: http://www.umass.edu/windenergy/about/history/alumni. [Accessed 14 October 2016].

[10] E. Chen, "China starts building first 10-GW mega wind farm," Reuters, 8 August 2009. [Online]. Available: http://www.reuters.com/article/us-china-wind-power-idUSTRE5771IP20090808. [Accessed 14 October 2016].

[11] D. Weston, “London Array breaks offshore production record,” Wind Power Offshore, 8 January 2016. [Online]. Available: http://www.windpoweroffshore.com/article/1378756/london-array-breaks-offshore-production-record. [Accessed 14 October 2016].

[12] J. DeCesaro and K. Porter, “Wind Energy and Power System Operations: A Review of Wind Integration Studies to Date,” National Renewable Energy Laboratory (NREL), Golden, 2009.

[13] A. Graves, K. Harman, M. Wilkinson and R. Walker, “Understanding Availability Trends of Operating Wind Farms,” in *AWEA WINDPOWER* , Houston, 2008.

[14] C. Mone, T. Stehly, B. Maples and E. Settle, “Cost of Wind Energy Review,” National Renewable Energy Laboratory, Golden, 2014.

[15] Renewables Advisory Board, “Value breakdown for the offshore wind sector,” RAB (2010) 0365, London, 2010.

[16] J. Krokstad, *Cost Reduction in Offshore Wind,* Oslo: Stakraft, 2012.

[17] B. Maples, G. Saur, M. Hand, R. van de Pietermen and T. Obdam, “Installation, Operation, and Maintenance Strategies to Reduce the Cost of Offshore Wind Energy,” National Renewable Energy Laboratory, Golden, 2013.

[18] S. Faulstich, P. Lyding and P. J. Tavner, “Effects of Wind Speed on Wind Turbine Availability,” in *EWEA*, Brussels, 2011.

[19] P. J. Tavner, R. Gindele, S. Faulstich, B. Hahn, M. W. G. Whittle and D. M. Greenwood, “Study of Effects of Weather & Location on Wind Turbine Failure Rates,” in *European Wind Energy Conference*, Warsaw, 2010.

[20] P. Tavner, C. Edwards, A. Brinkman and F. Spinato, “Influence of Wind Speed on Wind Turbine Reliability,” *WIND ENGINEERING,* vol. 30, no. 1, p. 55–72, 2006.

[21] K. Harman and B. Hendriks, “Measuring Wind Turbine Reliability - Results of the Reliawind Project,” in *EWEA*, Brussels, 2011.

[22] G. Wilson, D. McMillan and G. Ault, “Modelling the Effects of the Environment on Wind Turbine,” in *International Conference on Sustainable Power Generation and Supply (SUPERGEN 2012)*, Hangzhou, 2012.

[23] E. Wiggelinkhuizen, T. Verbruggen, H. Braam, L. Rademakers, J. Xiang, S. Watson, G. Giebel, E. Norton, M. C. Tipluica, A. MacLean, A. J. Christensen, E. Becker and D.

Scheffler, “CONMOW: Condition Monitoring for Offshore Wind Farms,” in *EWEC*, Milan, 2007.

[24] D. McMillan and G. W. Ault, “Quantification of Condition Monitoring Benefit for Offshore Wind Turbines,” *WIND ENGINEERING,* vol. 31, no. 4, p. 267–285, 2007.

[25] C. J. Crabtree, “Operational and Reliability Analysis of Offshore Wind Farms,” in *EWEA*, Copenhagen, 2012.

[26] Y. Feng, P. J. Tavner and H. Long, “Early experiences with UK round 1 offshore wind farms,” *Energy,* vol. 163, no. 4, p. 167–181, 2010.

[27] J. Carroll, A. McDonald and D. McMillan, “Failure Rate, Repair Time and Unscheduled O&M Cost Analysis of Offshore Wind Turbines,” *WIND ENERGY,* vol. 19, no. 6, pp. 1107-1119, 2016.

[28] T. Burton, D. Sharpe, N. Jenkins and E. Bossanyi, “Turbulence,” in *Wind Energy Handbook*, Chichester, John Wiley & Sons, 2001, pp. 17-18.

[29] J. Clark, “Normalising grouped data in Excel,” King's College London, 8 April 2013. [Online]. Available: https://www.youtube.com/watch?v=CSPIxFkxqcU. [Accessed 30 September 2017].

[30] B. Efron and R. Tibshirani, An Introduction to the Bootstrap, New York: Chapman & Hall/CRC, 1993.

[31] M. Rouaud, Probability, Statistics and Estimation: Propagation of Uncertainties in Experimental Measurement, Mathieu ROUAUD, 2017.

[32] M. B. Christiansen and C. B. Hasager, “Wake effects of large offshore wind farms identified from satellite SAR,” *Remote Sensing of Environment,* vol. 98, no. 2 - 3, pp. 251 - 268, 2005.

[33] N. Moskalenko, K. Rudion and A. Orths, “Study of wake effects for offshore wind farm planning,” in *IEEE Proceedings of the International Symposium of Modern Electric Power Systems (MEPS)*, Wroclaw, 2010.

[34] T. Göçmen and G. Giebel, “Estimation of turbulence intensity using rotor effective wind speed in Lillgrund and Horns Rev-I offshore wind farms,” *Renewable Energy,* vol. 99, pp. 524 - 532, 2016.

[35] J. Pierik, Y. Zhou and P. Bauer, *Wind Farm as Power Plant Dynamic modelling studies,* 2001.

[36] S. Skolthanarat, *The Modeling and Control of a Wind Farm and Grid Interconnection in a Multi-machine System The Modeling and Control of a Wind farm,* Blacksburg: Virginia Polytechnic Institute and State University, 2009.

[37] T. Petru, *Modelling of wind turbines for power system studies,* Gotenborg: Chalmers University of Technology, 2003.

[38] V. Gevorgian and E. Muljadi, "Wind Power Plant Short Circuit Current Contribution for Different Fault and Wind Turbine Topologies," in *9th Annual International Workshop on Large-Scale Integration of Wind Power into Power Systems*, Québec, 2010.

[39] M. Singh and S. Santoso, "Dynamic Models for Wind Turbines and Wind Power Plants Dynamic Models for Wind Turbines and Wind Power Plants," National Renewable Energy Laboratory, Golden, 2011.

[40] P. S. Veers, "Three-Dimensional Wind Simulation," Sandia National Laboratories, Albuquerque, 1988.

[41] M. Shinozuka and C. M. Jan, "Digital Simulation of Random Processes and Its Applications," *Journal of Sound and Vibration,* vol. 25, no. 1, pp. 111-128, 1972.

[42] D. O. Smallwood, "Random Vibration Testing of a Single Test Item with a Multiple Input Control System," in *Institute of Environmental Sciences*, 1982.

[43] J. Mann, "Wind field simulation," *Probabilistic Engineering Mechanics,* vol. 13, no. 4, pp. 269-282, 1998.

[44] N. O. Jensen, "A Note on Wind Generator Interaction," Riso National Laboratory, Roskilde, 1983.

[45] J. F. Ainslie, "Calculating the Flowfield in the Wake of Wind Turbines," *Journal of Wind Engineering and Industrial Aerodynamics,* vol. 27, pp. 213-224, 1988.

[46] M. C. Brower and N. M. Robinson, "THE OPENWIND DEEP-ARRAY WAKE MODEL: Development and Validation," in *AWS Truepower*, Albany, 2012.

[47] S. T. Frandsen, "Turbulence and Turbulence-Generated Structural Loading in Wind Turbine Clusters," Risø National Laboratory, Roskilde, 2007.

[48] W. Schlez and A. Neubert, "New Developments in Wake Models for Large Wind Farms," Garrad Hassan, Marseille, 2009.

[49] S. Frandsen, R. Barthelmie, S. Pryor, O. Rathmann, S. Larsen, J. Højstrup and M. Thøgersen, “Analytical Modelling of Wind Speed Deficit in Large Offshore Wind Farms,” *WIND ENERGY,* vol. 9, pp. 39-53, 2006.

[50] S. Ott, J. Berg and N. O. Nielsen, “Linearised CFD Models for Wakes,” Riso National Laboratory, Roskilde, 2011.

[51] C. Montavon, S. Y. Hui, J. Graham, D. Malins, P. Housley, E. Dahl, P. de Villiers and B. Gribben, “Offshore Wind Accelerator: Wake Modelling Using CFD,” EWEA OFFSHORE, Amsterdam, 2011.

[52] C. Montavon and I. Jones, *Wind Farm Flow Modelling Using CFD,* ANSYS, 2012.

[53] M. Xue, K. K. Droegemeier and V. Wong, “The Advanced Regional Prediction System (ARPS) - A multi-scale nonhydrostatic atmospheric simulation and prediction model. Part I: Model Dynamics and Verification,” Meteorology and Atmospheric Physics, Oklahoma, 2000.

[54] J. Jonkman, S. Butterfield, W. Musial and G. Scott, “Definition of a 5-MW Reference Wind Turbine for Offshore System Development,” National Renewable Energy Laboratory, Golden, 2009.

[55] F. Heer, P. M. Esfahani, M. Kamgarpour and J. Lygeros, “Model Based Power Optimisation of Wind Farms,” in *European Control Conference* , Strasbourg, 2014.

[56] V. Spudic, “Hierarchical wind farm control for power / load optimization,” in *Torque - The science of making torque from wind*, Heraklion, 2010.

[57] J. D. Grunnet, N. Soltani, T. Knudsen, M. Kragelund and T. Bak, “Aeolus Toolbox for Dynamics Wind Farm Model, Simulation and Control,” in *European Wind Energy Conference and Exhibition*, Warsaw, 2010.

[58] V. Spudic, M. Baotic and N. Peric, “Wind Farm Load Reduction via Parametric Programming Based Controller Design,” in *18th World Congress The International Federation of Automatic Control*, Milano, 2011.

[59] B. Biegel, “Distributed Control of Wind Farm,” Department of Automatic Control - Lund University , Lund, 2011.

[60] J. M. Jonkman and M. L. Buhl Jr., “FAST user’s guide,” National Renewable Energy Laboratory, Golden, 2009.

[61] P. A. Davidson, Turbulence An Introduction for Scientists and Engineers, Oxford: Oxford University Press, 2004.

[62] S. Poushpas, “Wind Farm Simulation Modelling and Control,” University of Strathclyde, Glasgow, 2016.

[63] S. Poushpas and W. Leithead, “Wind farm control through dynamic coordination of wind turbines reference power,” in *1st International Conference on Renewable Energies Offshore*, Lisbon, 2014.

[64] A. Stock, “Augmented control for flexible operation of wind turbines,” University of Strathclyde, Glasgow, 2014.

[65] V. Kourkoulis and W. Leithead, “Applying a power adjusting controller for a 2MW wind turbine,” in *EAWE 9th PhD Seminar*, Visby, 2013.

[66] D. J. Leith, “Effective wind speed models for simple wind turbine simulations,” in *Proceedings of the British Wind Energy Association Conference*, Nottingham, 1992.

[67] D. Robb and W. Leithead, “Derivation and validation of simple correlated wind speed models,” University of Strathclyde, Glasgow, 1995.

[68] M. Tsili and S. Papathanassiou, “A review of grid code technical requirements for wind farms,” *IET Renewable Power Generation,* vol. 3, no. 3, pp. 308 - 332, 2009.

[69] National Grid, “The Grid Code,” National Grid Electricity Transmission, London, 2016.

[70] National Grid, “Mandatory frequency response (MFR),” National Grid Electricity Transmission, [Online]. Available: https://www.nationalgrid.com/uk/electricity/balancing-services/frequency-response-services/mandatory-response-services?overview. [Accessed 17 December 2017].

[71] National Grid, “Security and Quality of Supply Standards,” National Grid UK, Warwick , 2004.

[72] J. Serrano-González and R. Lacal-Arántegui, “Technological evolution of onshore wind turbines - a market-based analysis,” *Wind Energy,* vol. 19, no. 1, p. 2171 – 2187, 2016.

[73] WindEurope, “Wind in power 2017 - Annual combined onshore and offshore wind energy statistics,” WindEurope, Brussels, 2017.

[74] WindEurope, “Offshore Wind - Key trends and statistics 2017,” WindEurope, Brussels, 2018.

[75] C. Vázquez Hernández, T. Telsnig and A. Villalba Pradas, “JRC Wind Energy Status Report,” JRC Science Hub, Petten, 2017.

[76] National Grid, “Security and Quality of Supply Standards,” National Grid UK, Warwick , 2004.

[77] National Grid plc, “Electricity Ten Year Statement,” National Grid, Warwick, 2016.

[78] S. Brough and S. Ashcroft, “Large Combustion Plant Directive (LCPD): Running hours during winter 2014/15 and capacity for 2015/16,” United Kingdom Energy Statistics (DUKES), London, 2015.

[79] European Parliament, “The Industrial Emissions Directive,” European Commission, Strasbourg, 2010.

[80] UK Energy Trends and Energy Prices, “UK Energy Statistics,” Department of Energy and Climate Change, London, 2016.

[81] L. P. Kunjumuhammed, B. C. Pal and N. F. Thornhill, “A Test System Model for Stability Studies of UK Power Grid,” in *IEEE PowerTech*, Grenoble , 2013.

[82] L. Shen, *Model Integration and Control Interaction Analysis of AC/VSC HVDC System,* Manchester: University of Manchester - School of Electrical and Electronic Engineering, 2015.

[83] K. R. W. Bell and A. N. D. Tleis, “Test system requirements for modelling future power systems,” in *General Meeting of the Power and Energy Society (PES)*, Minneapolis, 2010.

[84] M. Belivanis and K. R. W. Bell, “Representative GB Network Model,” Internal report in the Dep. of Electronic and Electrical Engineering - University of Strathclyde, Glasgow, 2011.

[85] W. Bukhsh, “Power Systems Test Case Archive,” The University of Edinburgh - School Of Mathematics, 31 March 2013. [Online]. Available: http://www.maths.ed.ac.uk/optenergy/NetworkData/index.html.

[86] Richard Smith, “UK Future Energy Scenarios - UK gas and electricity transmission,” National Grid, Warwick, 2012.

[87] K. C. P. Wong, H. M. Ryan and J. Tindle, *A Unified Model of the Electrical Power Network,* Sunderland: University of Sunderland, 1995.

[88] I. Graham, Object-Oriented Methods, Boston: Addison Wesley, 1991.

[89] M. Jacobson, P. Christerson and G. Jonsson, Object-Oriented Software Engineering, Boston: ACM Press/Addison-Wesley, 1992.

[90] J. Xia, A. Dyśko and J. O'Reilly, "Future stability challenges for the UK network with high wind penetration levels," *IET Generation, Transmission and Distribution,* vol. 9, no. 11, pp. 1160-1167, 2015.

[91] X. Jun and A. Dysko, "UK transmission system modelling and validation for dynamic studies," in *IEEE/PES ISGT EUROPE*, Copenhagen, 2013.

[92] Siemens, "PSS/ETM Program Application Guide," Power Technologies International, 2013.

[93] N. Martins and L. T. G. Lima, "Eigenvalue and frequency domain analysis of small-signal electromechanical stability problems," *IEEE/PES Symposium on Applications of Eigenanalysis and Frequency Domain Methods,* pp. 17-33, 1989.

[94] P. Kundur, Power System Stability and Control, New York: McGraw-Hill, 1994.

[95] W. Murrell, L. Ran and J. Wang, "Modelling UK Power System Frequency Response with Increasing Wind Penetration," in *IEEE Innovative Smart Grid Technologies - Asia (ISGT ASIA)*, Kuala Lumpur, 2014.

[96] S. Rakibuzzaman, R. Preece and M. Barnes, "Role of Multi-infeed VSC-HVDC on Dynamic Behaviour of Future North Scotland Transmission System," University of Manchester - School of Electrical and Electronic Engineering, Manchester , 2015.

[97] S. K. Chung, "A phase tracking system for three phase utility interface inverters," *IEEE Transactions on Power Electronics,* vol. 15, no. 3, pp. 431-438, 2000.

[98] V. Kaura and V. Blasko, "Operation of a phase locked loop system under distorted utility conditions," *IEEE Transactions on Industrial Informatics,* vol. 33, no. 1, pp. 58-63, 1997.

[99] W. Leonhard, Control of Electrical Drives, Berlin: Springer-Verlag, 1985.

[100] G.-C. Hsieh and J. C. Hung, "Phase-locked loop techniques – A survey," *IEEE Transactions on Industrial Electronics,* vol. 43, no. 6, pp. 609 - 615, 1996.

[101] A. Nicastri and A. Nagliero, "Comparison and evaluation of the PLL techniques for the design of the grid-connected inverter systems," in *IEEE International Symposium on Industrial Electronics*, Bari, 2010.

[102] P. Rodríguez, R. Teodorescu, I. Candela, A. V. Timbus, M. Liserre and F. Blaabjerg, "New Positive-sequence Voltage Detector for Grid Synchronization of Power Converters under Faulty Grid Conditions," in *IEEE Power Electronics Specialists Conference*, Jeju, 2006.

[103] D. W. P. Thomas and M. S. Woolfson, "Evaluation of frequency tracking methods," *IEEE Transactions on Power Delivery,* vol. 16, no. 3, pp. 367-371, 2001.

[104] M. M. Begovic, P. M. Djuric, S. Dunlap and A. G. Phadke, "Frequency Tracking In Power Networks Of Harmonics," in *ICHPS V International Conference on Harmonics in Power Systems*, Atlanta, 1992.

[105] P. J. Moore, R. D. Carranza and A. T. Johns, "A new numeric technique for high-speed evaluation of power system frequency," *IEE Proceedings - Generation, Transmission and Distribution,* vol. 141, no. 5, pp. 529-536, 1994.

[106] M. G. Adamiak, A. P. Apostolov, M. M. Begovic, C. F. Henville, K. E. Martin, G. L. Michel, A. G. Phadke and J. S. Thorp, "Wide area protection—Technology and infrastructures," *IEEE Transactions on Power Delivery,* vol. 21, no. 2, pp. 601 - 609, 2006.

[107] A. Borghetti, C. A. Nucci, M. Paolone, G. Ciappi and A. Solari, "Synchronized Phasors Monitoring During the Islanding Maneuver of an Active Distribution Network," *IEEE Transactions on Smart Grid,* vol. 2, no. 1, pp. 82 - 91, 2011.

[108] J. H. Quirós Tortós, G. Valverde and L. Ding, "Optimal placement of Phasor Measurement Units to Improve Parallel Power System Restoration," in *2nd IEEE PES International Conference and Exhibition on Innovative Smart Grid Technologies (ISGT Europe)*, Manchester, 2011.

[109] A. J. Roscoe, I. F. Abdulhadi and G. M. Burt, "P and M Class Phasor Measurement Unit Algorithms Using Adaptive Cascaded Filters," *IEEE Transactions on Power Delivery,* vol. 28, no. 3, pp. 1447 - 1459, 2013.

[110] C. Bajracharaya, "Control of VSC-HVDC for wind power," Norwegian University of Science and Technology, Trondheim, 2008.

[111] T. W. Shire, "VSC-HVDC based Network Reinforcement," Delft University of Technology, Delft, 2009.

[112] Siemens Energy Transmission, "Fact Sheet: High-voltage direct current transmission (HVDC)," Siemens , Munich, 2014.

[113] European Network of Transmission System Operators for Electricity, “Offshore Transmission Technology,” ENTSOE, Brussels, 2011.

[114] C. Du, “The control of VSC-HVDC and its use for large industrial power system,” Chalmers University of Technology, Göteborg, 2003.

[115] M. Davies, M. Dommaschk, J. Dorn, J. Lang, D. Retzmann and D. Soerangr, “HVDC Plus - Basics and Principle of Operation,” Siemens AG, Erlangen, 2011.

[116] S. Asadollah, R. Zhu, M. Liserre and C. Vournas, “Decentralized Reactive Power and Voltage Control of Wind Farms with Type-4 Generators,” in *IEEE PowerTech*, Manchester, 2017.

[117] Y. Li, L. Wei, Y. Chi, C. Liu and Z. Zhang, “RESEARCH ON REACTIVE VOLTAGE CHARACTERISTICS AND CONTROL STRATEGY OF OFFSHORE WIND FARM,” China Electric Power Research Institute, Beijing, 2013.

[118] J. T. Pierik, Y. Zhou and P. Bauer, “Windfarm as power plant; Dynamic modelling studies,” ECN Energy research Centre of the Netherlands, Amsterdam, 2008.

[119] V. Gevorgian and E. Muljadi, “Wind Power Plant Short-Circuit Current Contribution for Different Fault and Wind Turbine Topologies,” in *9th Annual International Workshop on Large-Scale Integration of Wind Power into Power Systems*, Québec, 2010.

[120] Manitoba HVDC Research Centre, *IEEE 09 Bus System,* Manitoba : Manitoba Hydro International Ltd - PSCAD, 2014.

[121] IEEE Working Group on Prime Mover and Energy Supply Models for System Dynamic Performance Studies, “Hydraulic Turbine and Turbine Control Models for Dynamic Studies,” *IEEE® Transactions on Power Systems,* vol. 7, no. 1, pp. 167-179, 1992.

[122] IEEE, *Recommended Practice for Excitation System Models for Power System Stability Studies,* IEEE® Standard 421.5, 1992.

[123] nationalgrid, “Mandatory frequency response (MFR) - Overview,” National Grid, 2017. [Online]. Available: https://www.nationalgrid.com/uk/electricity/balancing-services/frequency-response-services/mandatory-response-services?overview. [Accessed 17 December 2017].

[124] nationalgrid, “Mandatory frequency response (MFR) - Technical Requirements,” National Grid, 2017. [Online]. Available: https://www.nationalgrid.com/uk/electricity/balancing-services/frequency-response-

services/mandatory-response-services?technical-requirements. [Accessed 17 December 2017].

[125] nationalgrid, “Frequency response services,” National Grid, 2017. [Online]. Available: https://www.nationalgrid.com/uk/electricity/balancing-services/frequency-response-services. [Accessed 17 December 2017].

[126] nationalgrid, “Market, operations, and data,” National Grid, 2017. [Online]. Available: https://www.nationalgrid.com/uk/electricity/market-operations-and-data. [Accessed 17 December 2017].

[127] ofgem, “OFGEM G59, frequency changes during large distrurbances and their impact on the total system,” OFGEM, London, 2014.

[128] Office of Electricity Regulation, “Modification to the Grid Code: Protection Fault Clearance Time & Back-Up Protection (GC0023),” OFGEM, London, 2016.

[129] D. Costello and K. Zimmerman, “Frequency Tracking Fundamentals,Challenges, and Solutions,” in *IEEE - 64th Annual Conference for Protective Relay Engineers*, College Station, 2011.

[130] D. Milborrow, “Recent developments in wind turbine design - A critical review of wind turbine performance shows that outputs have steadily increased with the increases in wind turbine size,” E&T Energy and Power Hub, 26 September 2017. [Online]. Available: https://energyhub.theiet.org/users/66328-david-milborrow/posts/20629-recent-developments-in-wind-turbine-design.

[131] Power Today, “Doubly-fed induction generators in wind power generation,” Power Today, March 2013. [Online]. Available: http://www.powertoday.in/News.aspx?nId=1Ht+JZoFeuUhm2QiBNo+tw==.

[132] L. Zhang, “Modeling and Control of VSC-HVDC Links Connected to Weak AC Systems,” ROYAL INSTITUTE OF TECHNOLOGY, Stockholm, 2010.

[133] R. Ierna, A. J. Roscoe, M. Yu, J. Zhu, A. Dyśko, H. Urdal and C. Booth, “A VSM (virtual synchronous machine) convertor control model suitable for RMS studies for resolving system operator/owner challenges,” in *15th Wind Integration Workshop*, Vienna, 2016.

[134] L. Zhang, L. Harnefors and H. P. Nee, “Power-Synchronization Control of Grid-Connected Voltage-Source Converters,” *IEEE TRANSACTIONS ON POWER SYSTEMS,* vol. 25, no. 2, pp. 809 - 820, 2010.

[135] M. Liserre, F. Blaabjerg and S. Hansen, “Design and Control of an LCL-Filter-Based Three-Phase Active Rectifier,” *IEEE TRANSACTIONS ON INDUSTRY APPLICATIONS,* vol. 41, no. 5, pp. 1281 - 1291, 2005.

[136] L. Harnefors and H. P. Nee, “Model-Based Current Control of AC Machines Using the Internal Model Control Method,” *IEEE TRANSACTIONS ON INDUSTRY APPLICATIONS,* vol. 34, no. 1, pp. 133-141, 1998.

[137] A. Giles, L. Reguera and A. J. Roscoe, “Optimal controller gains for inner current controllers in VSC inverters,” in *IET International Conference on Renewable Power Generation (RPG 2015)*, Beijing, 2015.

[138] B. K. Bose, Power Electronics and Variable Frequency Drives, New York: IEEE Press Marketing, 1997.

[139] S. K. Peddapelli, Pulse Width Modulation: Analysis and Performance in Multilevel Inverters, Hyderabad: De Gruyter Oldenbourg, 2017.

[140] A. J. Roscoe, S. J. Finney and G. M. Burt, “Tradeoffs between AC power quality and DC bus ripple for 3-phase 3-wire inverter-connected devices within microgrids,” *IEEE Transactions on Power Electronics,* vol. 26, no. 3, pp. 684-688, 2011.

[141] S. Norrga, “Voltage source converters in transmission application,” in *IEEE Power Electronics Specialists Conference*, Rhodes, 2008.

[142] A. D. Hansen, F. Iov, P. E. Sørensen, N. A. Cutululis, C. Jauch and F. Blaabjerg, “Dynamic wind turbine models in power system simulation tool DIgSILENT,” Risø National Laboratory, Technical University of Denmark, Roskilde, 2007.

Appendix A

- Wind turbine location is defined by: *
- Wind turbine number is located above the wind turbine location and plotted in BLACK.
- Mean wind speed experienced by each turbine is in m/s and plotted in RED.
- Mean power produced by each turbine is in MW and plotted in BLUE.
- The wind speed direction is plotted in MAGENTA.
- X-axis corresponds to the longitudinal distance between the wind turbines.
- Y-axis corresponds to the lateral distance between the wind turbines.

Appendix A1 – Mean Wind Speed and Power Production for Below Rated Operational Conditions

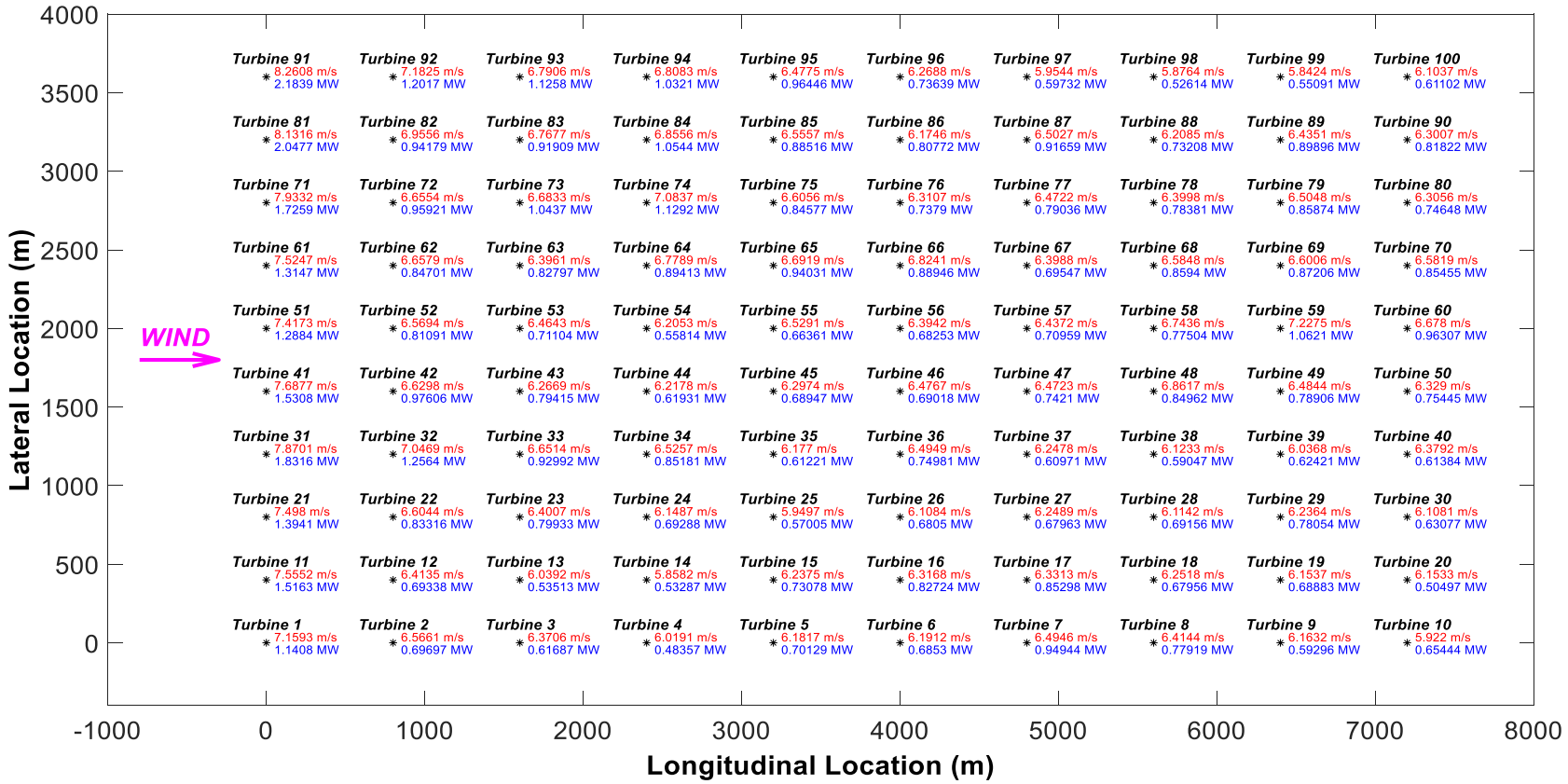

Appendix A2 – Mean Wind Speed and Power Production for Rated Operational Conditions

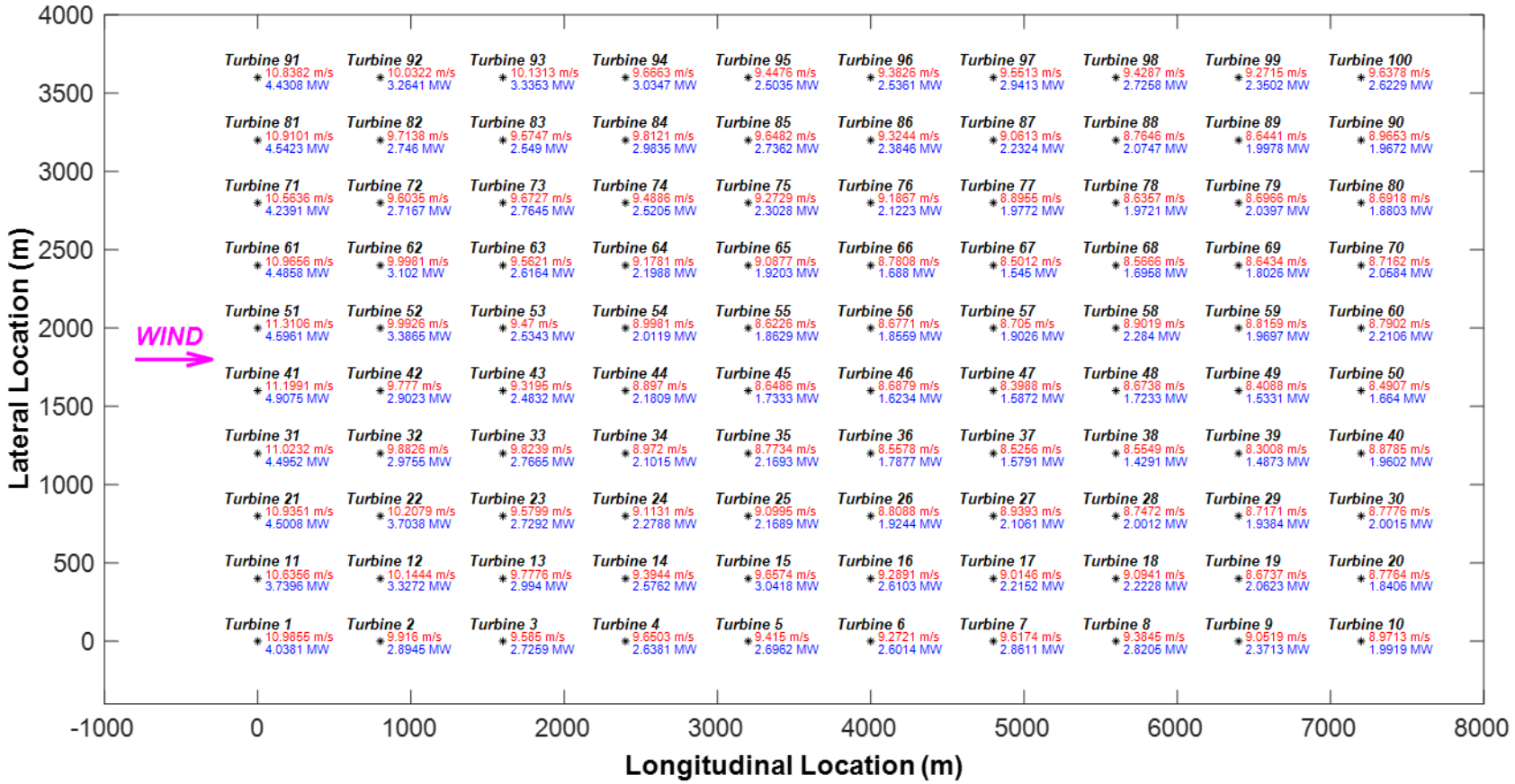

Appendix A3 – Mean Wind Speed and Power Production for Above Rated Operational Conditions

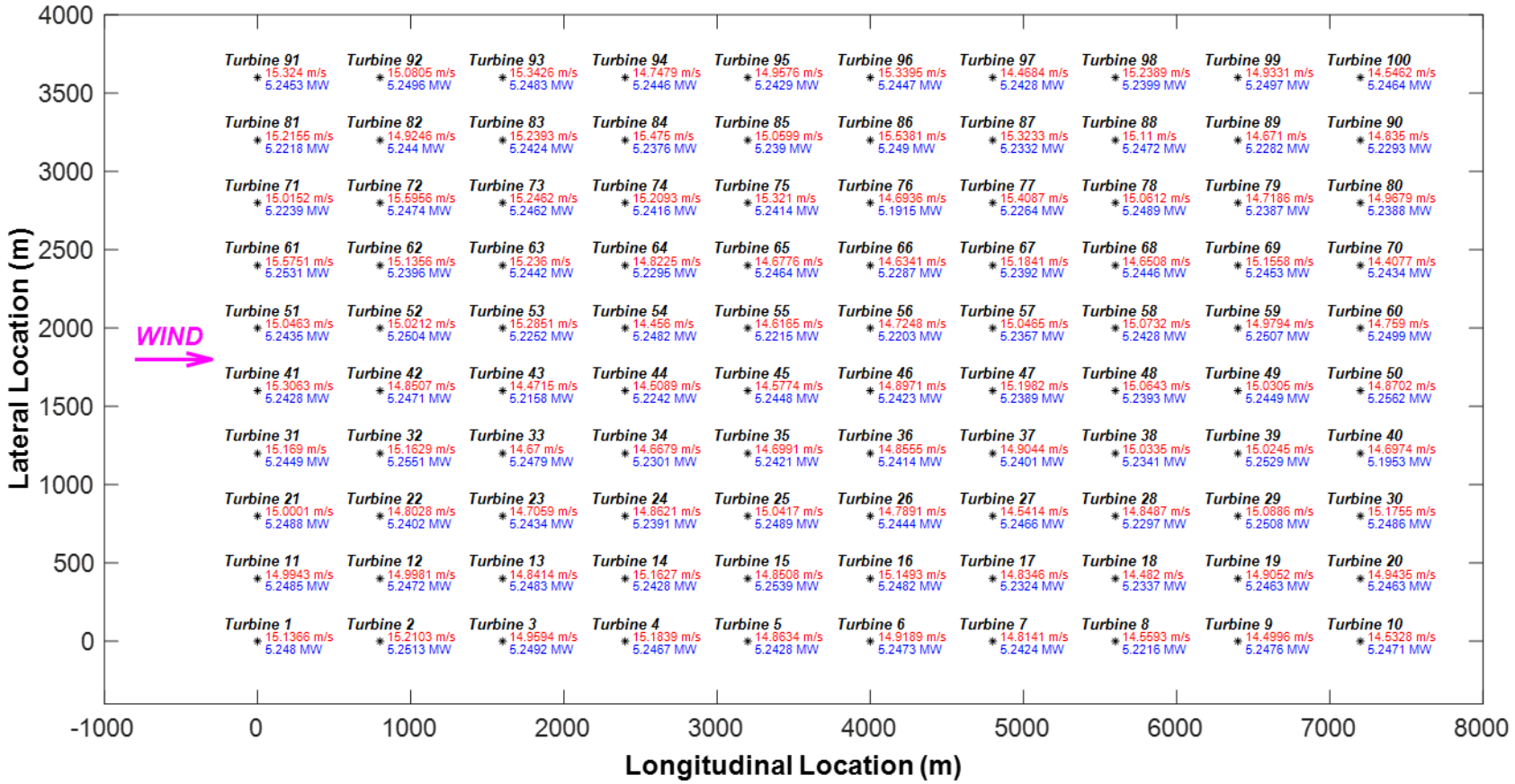

Appendix B

Appendix B1 – IEEE 9-bus Power System Information

Bus	Nominal Power (MVA)	Voltage (kV)	P (p.u.)	Q (p.u.)
1	247.5	17.16	0.76	0.185
2	192	18.45	1.63	0.371
3	128	14.145	0.85	0.181

Generator characteristics [120]

Bus	Voltage (kV)	P (p.u.)	Q (p.u.)
5	230	1.25	0.50
6	230	0.90	0.30
8	230	1.00	0.35

Load characteristics [120]

Voltage (kV)	R (Ω/km)	X (Ω/km)
72	0.41	0.5
138	0.14	0.5
230 (single)	0.09	0.5
230 (bundled)	0.04	0.4
345 (bundled)	0.03	0.3
500 (bundled)	0.02	0.3

Typical power line characteristics [120]

Generator 1			
Nominal Power (MVA)	247.5	**Voltage (kV)**	17.16
X_d (p.u.)	1.305	**X_q (p.u.)**	0.474
X_d' (p.u.)	0.296	**X_q' (p.u.)**	0.243
X_d'' (p.u.)	0.252	**X_q'' (p.u.)**	0.18
T_d' (s)	1.01	**H (s)**	3.2
T_d'' (s)	0.053	**Pole Pairs**	2

Synchronous generators characteristics (Bus 1) [120]

Appendix B2 – Reduced GB Power System Information

Node	Node Name	V (kV)	P (MW)	Q (MVAr)
1	Beauly	275	467.92	57.64
2	Peterhead	275	468.11	42.49
3	Errochty	132	468.08	98.70
4	Denny/Bonnybridge	275	1307.93	254.48
5	Remaining GB power system	400	53482.26	15467.42

Generator characteristics [84]

Node	V (kV)	P (MW)	Q (MVAr)
1	275	468	102
2	275	513	113
3	132	555	105
4	275	1308	317
5	400	53482	15613

Load characteristics [84]

Connected Nodes	Voltage (kV)	R (Ω/km)	X (Ω/km)
1-2	275	0.0122	0.02
1-3	275	0.007	0.15
2-3	275 (single)	0.03004	0.077
2-4	275	0.0004	0.065
3-4	275	0.003	0.041
4-5	400	0.001	0.024

Power line characteristics [84]

	Nominal Power	Voltage	Inertia
Generator 1	888	275	3.2
Generator 2	1691	275	3.7
Generator 3	827	132	3.2
Generator 4	2519	275	4.2
Generator 5	63390	400	4.7

Synchronous generators characteristics [84]

Appendix B3 - GB Power System Information

Node	Node Name	V (kV)	P (MW)	Q (MVAr)
1	Beauly	275	468.05	58.16
2	Peterhead	275	513.00	82.70
3	Errochty	132	555.11	101.82
4	Denny/Bonnybridge	275	1308.08	269.72
5	Neilston	400	502.11	32.88
6	Strathaven	400	1219.47	141.79
7	Torness	400	803.75	31.03
8	Eccles	400	0	0
9	Harker	400	0	0
10	Stella West	400	2663.00	341.57
11	Penwortham	400	4075.52	886.34
12	Deeside	400	1861.52	509.23
13	Daines	400	0	0
14	Th. Marsh/Stocksbridge	400	0	0
15	Thornton/Drax/Eggborough	400	4138.75	1162.71
16	Keadby	400	2441.30	821.27
17	Ratcliffe	400	1081.00	274.85
18	Feckenham	400	6034.41	2074.45
19	Walpole	400	2019.00	551.85
20	Bramford	400	1027.36	209.65
21	Pelham	400	702.00	41.95
22	Sundon/East Claydon	400	1820.00	504.75
23	Melksham	400	5206.50	1403.19
24	Bramley	400	0	0
25	London	400	10207.03	2966.89
26	Kemsley	400	1424.00	337.85
27	Sellindge	400	457.00	73.90
28	Lovedean	400	3223.79	938.52
29	S.W.Penisula	400	2577.00	291.90
Total Values		**-**	**56328.74**	**14108.96**

Generation characteristics [84]

Node	Node Name	Voltage (kV)	P (MW)	Q (MVAr)
1	Beauly	V (kV)	468.00	102.00
2	Peterhead	275	513.00	113.00
3	Errochty	275	555.00	105.00
4	Denny/Bonnybridge	132	1308.00	317.00
5	Neilston	275	502.00	128.00
6	Strathaven	400	1176.00	315.00
7	Torness	400	745.00	171.00
8	Eccles	400	117.50	37.40
9	Harker	400	130.00	53.00
10	Stella West	400	2561.00	465.00
11	Penwortham	400	3360.00	760.00
12	Deeside	400	1189.00	338.00
13	Daines	400	2524.00	766.00
14	Th. Marsh/Stocksbridge	400	1831.00	566.50
15	Thornton/Drax/Eggborough	400	2633.00	694.60
16	Keadby	400	1607.00	655.00
17	Ratcliffe	400	1081.00	371.00
18	Feckenham	400	5362.00	1935.00
19	Walpole	400	2019.00	648.00
20	Bramford	400	1027.36	305.80
21	Pelham	400	702.00	202.20
22	Sundon/East Claydon	400	1820.00	665.00
23	Melksham	400	4734.00	1337.00
24	Bramley	400	1418.00	528.00
25	London	400	9734.00	2902.00
26	Kemsley	400	1424.00	434.00
27	Sellindge	400	457.00	138.00
28	Lovedean	400	2751.00	841.00
29	S.W.Penisula	400	2577.00	356.00
Total Values			**56325.86**	**16249.50**

Load characteristics [84]

Connected Nodes	Voltage (kV)	R (Ω/km)	X (Ω/km)
1-2	275	0.0122	0.02
1-3	275	0.007	0.15
2-3	275 (single)	0.03004	0.077
2-4	275	0.0004	0.065
3-4	275	0.003	0.041
4-5	400	0.001	0.024
4-6	400	0.0013	0.023
4-7	400	0.00211	0.0135
5-6	400	0.00151	0.01613
6-7	400	0.003	0.2
6-9	400	0.00078	0.00852
7-8	400	0.0004	0.0001
8-10	400	0.00083	0.0175
9-10	400	0.00352	0.02453
9-11	400	0.00164	0.0163
10-15	400	0.00053	0.00835
11-12	400	0.0001	0.0085
11-13	400	0.0004	0.0052
11-15	400	0.00099	0.042
12-13	400	0.00096	0.01078
13-14	400	0.00082	0.01201
13-15	400	0.00137	0.023
14-15	400	0.00019	0.00222
14-16	400	0.0005	0.016
15-16	400	0.00016	0.00172
12-18	400	0.00097	0.009
13-18	400	0.00084	0.007
16-17	400	0.001	0.01072
17-18	400	0.00042	0.0018
16-19	400	0.00056	0.0141
16-21	400	0.00145	0.01824
16-22	400	0.00178	0.0172
19-20	400	0.00178	0.0213
19-21	400	0.00037	0.0059
17-22	400	0.00068	0.0097
21-22	400	0.00048	0.0061
18-23	400	0.00138	0.0096
20-21	400	0.0012	0.0048
20-26	400	0.00035	0.0023
21-25	400	0.00025	0.01
22-23	400	0.00055	0.003
22-25	400	0.00037	0.0041
23-24	400	0.00023	0.0007
23-29	400	0.00151	0.0182
24-25	400	0.00104	0.0091
24-28	400	0.00068	0.007

Connected Nodes	Voltage (kV)	R (Ω/km)	X (Ω/km)
25-26	400	0.0002	0.0057
26-27	400	0.0002	0.00503
27-28	400	0.00038	0.00711
28-29	400	0.00051	0.00796

Power line characteristics [84]

Node	Nominal Power	Voltage	Inertia
1	888	275	3.2
2	1691	275	3.7
3	827	132	3.2
4	2519	275	4.2
5	982	400	3.2
6	993	400	3.2
7	2290	400	3.7
10	3157	400	3.7
11	5363	400	4.2
12	3905	400	3.7
15	7199	400	4.2
16	11527	400	4.5
17	1802	400	3.7
18	1987	400	3.7
19	3013	400	3.7
20	1519	400	3.7
21	627	400	3.2
22	375	400	3.2
23	6956	400	4.2
25	1954	400	3.7
26	5097	400	4.2
27	1278	400	3.7
28	1424	400	3.7
29	1942	400	3.7

Synchronous generators characteristics [84] [94]

Appendix B4 - VSC-HVDC Simulation Model Development Information

The VSC-HVDC model presented in this subsection is used to connect the offshore wind farm developed in Chapter 4 to the power system. A single line representation of the VSC connected to the AC power network is illustrated in Figure B-1. The VSC can be assumed as a controllable synchronous machine with an instantaneous phase voltage described by Equation B-1 [111].

$$U = \frac{1}{2} V_{DC} M_{index} \sin(\omega_e t + \delta) + harmonics \quad \text{[B-1]}$$

where M_{index} is the modulation index, ω_e is the system radian frequency (i.e. $\omega_e = 2\pi f_0$, where f_0 is the grid nominal frequency, $f_0 = 50Hz$) and δ is the phase shift of the VSC voltage.

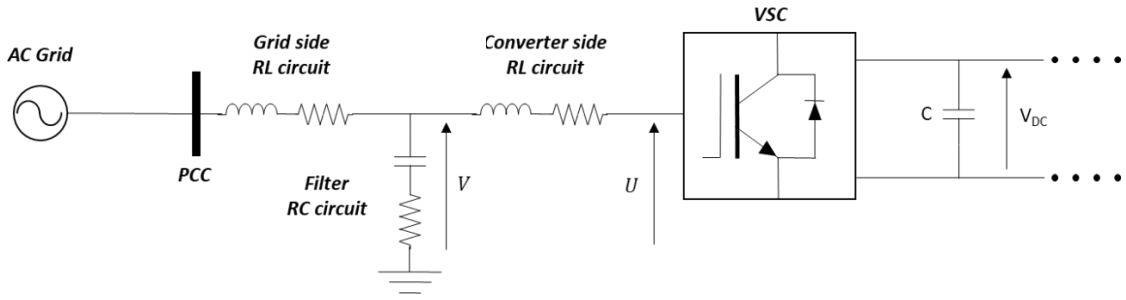

Figure B-1: Single-line representation of VSC connection to the AC grid

The harmonics are removed using filtering equipment, and the voltage at the filter bus is denoted as v. The voltage Δv across the phase reactor can be varied to control the active and reactive power flow from the VSC to the grid. The active power flow from the converter to the AC grid is described by Equation B-2 [134].

$$P = \frac{|U||V| \sin \delta}{X} \quad \text{[B-2]}$$

The reactive power flow from the converter to the AC grid is described by Equation B-3 [134].

$$Q = \frac{|V|(|V|-|U|\cos\delta)}{X} \quad \text{[B-3]}$$

The converter size is designed to be able to transfer the full capacity of 100 Supergen 5MW wind turbines, with a rated apparent power of 5.2MVA, so the base power of the HVDC-VSC link is set to 520MVA. The wind farm is assumed to be connected at Peterhead bus, which has a base voltage of 275kV. The filter base impedance (i.e. Z_{base}) has been computed to be equal to 145.43Ω by using Equation B-4 [135].

$$Z_{base} = \frac{V_{base}^2}{S_{nominal}} \quad \text{[B-4]}$$

where the base voltage (i.e. V_{base}) is 275kV and the nominal apparent power (i.e. $S_{nominal}$) is 520MVA. For the IGBT switches, the modulation ratio is computed by using Equation B-5 [136] [137].

$$M_{ratio} = \frac{f_{switching}}{f_0} \quad \text{[B-5]}$$

where M_{ratio} is the modulation ratio, $f_{switching}$ is the IGBT switching frequency and f_0 is the grid nominal frequency. Assuming switching frequency of 2kHz [138] and grid frequency is equal to 50Hz, the modulation ratio is calculated to be 40. Choosing an odd integer multiple of the fundamental frequency takes advantage of wave symmetry effects that effectively remove the even harmonics from the waveform, resulting in improved quality of the converter output [139], hence the chosen value for the modulation ratio will be 41. Then the carrier switching frequency can be computed from Equation B-5 and is equal to 2050Hz. The modulation index for the converter is set to 0.85 [111].

To obtain Sinusoidal Pulse Width Modulation (SPWM), PWM is used on the IGBTs to create the desired voltage waveform. The DC bus voltage is calculated based on the line to line voltage of the PCC between the onshore substation and the grid, using Equation B-6 [111].

$$V_{DC} = \frac{2\sqrt{2}V_{LL}}{\sqrt{3}M_{index}} \quad \text{[B-6]}$$

where the grid substation is assumed to be Peterhead, thus the line to line voltage (i.e. V_{LL}) will be 275kV and the modulation index (i.e. M_{index}) equal to 0.85. Hence, the DC bus voltage (i.e. V_{DC}) is calculated to be 528.32kV (i.e. ±264.16kV). To satisfy small ripple and avoid transient overvoltage on the DC link, the DC bus capacitor time constant, which is the time needed to charge the capacitor from zero to rated voltage, has been assumed equal to 10ms, which dictates the capacitor's size upper and lower limits as can be seen in Equations B-7 and B-8 respectively [111]. The peak percentage ripple on the DC link is assumed to be 20% [137] [140].

$$C_{upper} = \frac{2\,\tau\,S_{nominal}}{{V_{DC}}^2} \quad \text{[B-7]}$$

$$C_{lower} = \frac{S_{nominal}}{2\omega_e V_{DC} \Delta V_{DC}} \quad \text{[B-8]}$$

where C_{upper} is the DC link's capacitor upper size, C_{lower} is the DC link's capacitor lower size, τ is the capacitor time constant, $S_{nominal}$ is the nominal apparent power, V_{DC} is the nominal DC bus voltage, ΔV_{DC} is the maximum allowed ripple and ω_s is the system radian frequency (i.e. $\omega_e = 2\pi f_0$, where f_0 is the grid nominal frequency, $f_0 = 50Hz$. The calculated value for the DC link's capacitor upper size is 37.26μF and the calculated value for the DC link's capacitor lower size is 14.825μF.

The converter-side phase reactors for an IGBT based VSC converter are usually in the range of 0.1 per unit to 0.3 per unit [114] [141] [142]. Assuming a phase reactance equal to 0.2 per unit and a resistance of 0.01 per unit [132] the corresponding actual inductance and resistance values can be calculated to be equal to 92.6mH and 1.4543Ω, by using equations B-9 and B-10 respectively.

$$L_{phase} = \frac{Z_{base} X_{phase\_pu}}{\omega_e} \quad \text{[B-9]}$$

$$R_{phase} = Z_{base} R_{phase\_pu} \quad \text{[B-10]}$$

The AC filter was designed as a CR filter (i.e. capacitance-resistance) with a phase reactance equal to 5.8824 per unit and a resistance of 0.01 per unit [132]. The correspo1nding actual

capacitance and resistance values are equal to 3.72μF and 1.4543Ω, by using equations B-11 and B-12 respectively.

$$C_{filter} = {1}\Big/{\left(Z_{base}X_{filter\_pu}\right)}\Big/{\omega_e} \quad \text{[B-11]}$$

$$R_{filter} = Z_{base}R_{filter\_pu} \quad \text{[B-12]}$$

The grid-side phase reactors were designed with a phase reactance equal to 0.008 per unit and a resistance of 0.0001 per unit [132]. The corresponding actual inductance and resistance values can be calculated to be equal to 3.7mH and 0.0145Ω, by using equations B-9 and B-10 respectively.

B4.1 Inner Loop Controller Development

The standard method of controlling an IGBT-based VSC converter is by vector current control, which consists of two cascaded control loops. The outer controller is used to control the DC bus voltage, ensuring that the power taken off the DC bus is equal to the available power, thus creating a current reference. The current reference is then fed into the inner current controller. The inner current controller then regulates the current passing through the IGBT such that all the available power is dispatched onto the grid.

The most commonly implemented control system for inverters is vector current control. Using a phase-locked loop (PLL) to establish the transform for converting the three-phase voltage vector V_{abc} at the PCC to a time-independent vector in a rotating reference frame, V_{dq}. By using this transformation, and since active and reactive power can be calculated by equations B-13 and B-14 respectively, independent control of active and reactive power can be achieved.

$$P = v_d i_d \quad \text{[B-13]}$$

$$Q = -v_q i_q \quad \text{[B-14]}$$

where P is the active power, Q is the reactive power, v_d and i_d are the d-components of the voltage and current vectors in the rotating reference frame respectively, and v_q and i_q are the q-components of the voltage and current vectors in the rotating reference frame respectively.

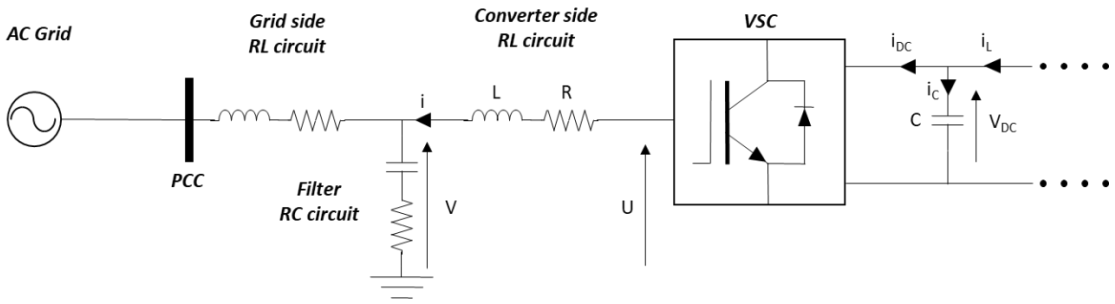

Figure B-2: Single-line representation of VSC

As illustrated in Figure B-2, the synchronous coordinates from the filter bus voltage to the VSC converter voltage, the AC-dynamics are governed by the dynamics of the converter side phase reactor, as given by Equation B-15.

$$L\frac{di_{dq}}{dt} = U_{dq} - V_{dq} - (R + j\omega_e L)i_{dq} \quad \text{[B-15]}$$

Writing the above equation component-wise gives Equations B-16 and B-17.

$$L\frac{di_d}{dt} = U_d - V_d - Ri_d + \omega_e Li_q \quad \text{[B-16]}$$

$$L\frac{di_q}{dt} = U_q - V_q - Ri_q - \omega_e Li_d \quad \text{[B-17]}$$

The dq-reference components have been chosen with the v_d aligned to the AC filter voltage; thus $v_d = V$ and $v_q = 0$. Finally, the dynamics of the DC-link are given by Equations B-18 and B-19.

$$C\frac{dV_{DC}}{dt} = i_{DC} - i_L \quad \text{[B-18]}$$

$$P_{DC} = V_{DC} i_{DC} \quad \text{[B-19]}$$

The inner current controller is based on the basic system equations of the system. It is designed to maintain active power balance in the system, ensuring that the active power taken from the network must equal the active power injected to the network, minus any losses in the DC link. Figure B-3 illustrates an overview of the block diagram of the inner current controller.

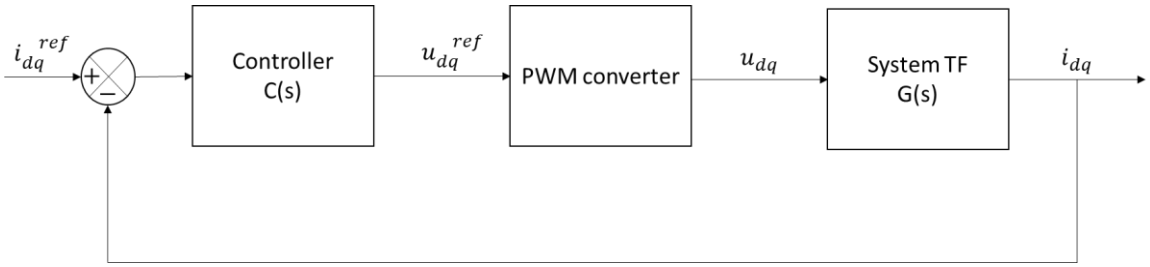

Figure B-3: Inner current controller block diagram overview

The PWM converter is used to create the desired u_{dq} voltage waveform by using the u_{dq}^{ref} reference vector input. The PWM converter will add switching harmonics to the reference voltage, but the phase reactors and the AC filtering equipment is assumed to remove the switching harmonics; hence, it is assumed that equation B-20 is valid:

$$u_{dq} = u_{dq}^{ref} \quad \text{[B-20]}$$

Equations B-16 and B-17 show that the VSC system is a strongly coupled, non-linear MIMO system. For each of the dq voltages, there are cross-coupling terms (i.e. $\omega_e L i_q$ and $\omega_e L i_d$), which can be considered as disturbances. Using Figure B-3 and taking the Laplace transform for Equation B-20 yields Equation B-21:

$$u_{dq}(s) = \left(i_{dq}^{ref}(s) - i_{dq}(s)\right) C(s) \quad \text{[B-21]}$$

where s is the complex frequency, $s = j\omega$. System inputs are modified by the introduction of feed-forward terms to eliminate the cross-coupling terms as shown in Equations B-22 and B-23.

$$u_d^{ref} = -\left(i_d^{ref}(s) - i_d(s)\right) C(s) + \omega_e L i_q(s) + u_d(s) \quad \text{[B-22]}$$

$$u_q^{ref} = -\left(i_q^{ref}(s) - i_q(s)\right) C(s) - \omega_e L i_d(s) + u_q(s) \quad \text{[B-23]}$$

Manipulating Equations B-16, B-17, B-20 and B-21 yields:

$$u_d = L\frac{di_d}{dt} + Ri_d \quad \text{[B-24]}$$

$$u_q = L\frac{di_q}{dt} + Ri_q \quad \text{[B-25]}$$

Equations B-24 and B-25 show that the cross-coupling terms are eliminated; hence, independent control for the d and q axis can be achieved. Taking the Laplace transform for Equations B-24 and B-25 yields the following result:

$$i_{dq}(s) = \frac{1}{sL+R} u_{dq}(s) \quad \text{[B-26]}$$

Hence, from Equation B-26 the system transfer function (i.e. G(s)):

$$G(s) = \frac{1}{sL+R} \quad \text{[B-27]}$$

Equations B-24 and B-25 show that the resulting system is composed by two decoupled first order systems. A PI controller is sufficient to control this system; hence, the transfer function for the controller (i.e. C(s)) is as follows:

$$C(s) = K_p + \frac{K_i}{s} = \frac{K_p s + K_i}{s} \quad \text{[B-28]}$$

where K_p is the proportional gain and K_i is the integral gain. Manipulating Equations B-27 and B-28 yields the closed-loop transfer function for the inner current controller, as shown in Equation B-29.

$$ICC\_TF_{cl}(s) = \frac{K_p s + K_i}{Ls^2 + (R + K_p)s + K_i} = \frac{\left({}^{K_p}/_{L}\right)s + {}^{K_i}/_{L}}{s^2 + \left({}^{R}/_{L} + {}^{K_p}/_{L}\right)s + {}^{K_i}/_{L}} \quad \text{[B-29]}$$

The detailed block diagram for the complete system is depicted in Figure B-4.

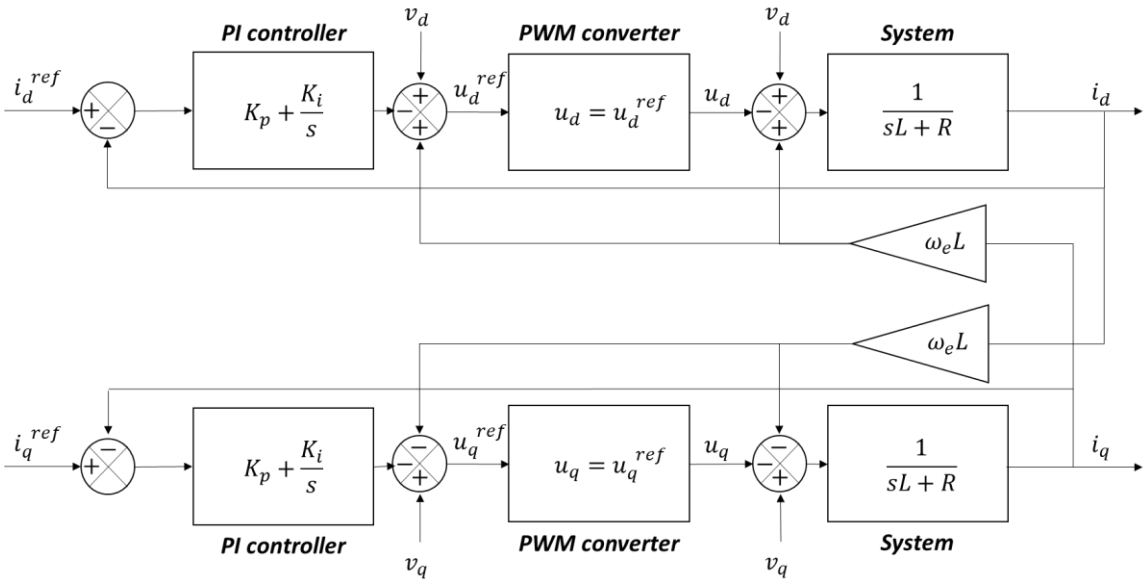

Figure B-4: System detailed block diagram

For the tuning of the controller gains, the internal model method is used [137]. The desired closed-loop bandwidth of the inner current controller is directly related to the rise time and can be calculated using Equation B-30 [136].

$$t_{rise} = {\ln(9)}\Big/{a_{cl}^{inner}} \quad \text{[B-30]}$$

where a_{cl}^{inner} is the closed-loop bandwidth of the inner current controller and t_{rise} is the rise time. The closed-loop bandwidth of the current controller for a modern transistor PWM converter with a switching frequency of 1 - 2 kHz can be chosen as somewhere between 1000 and 2500 rad/s [132]. A study by Harnefors *et al.* [136], shows that the bandwidth of most inner controllers is chosen to be less than 20% of the switching frequency. Thus, the rise time is chosen as 0.001 for a switching frequency of 2 kHz to give a closed-loop bandwidth of 2200 rad/s, well within the constraints, but also sufficiently high to have a fast rise time. The controller proportional and integral gains, K_p and K_i, can now be calculated from Equations B-31 and B-32 respectively [136].

$$K_p = a_{cl}^{inner} L \qquad \text{[B-31]}$$

$$K_i = a_{cl}^{inner} R \qquad \text{[B-32]}$$

From Equations B-31 and B-32, the proportional gain K_p has been calculated equal to 203.431 and the integral gain K_i has been calculated equal to 3195.5. The closed-loop Bode plot for the inner current controller, as defined in Equation B-29, is shown in Figure B-5.

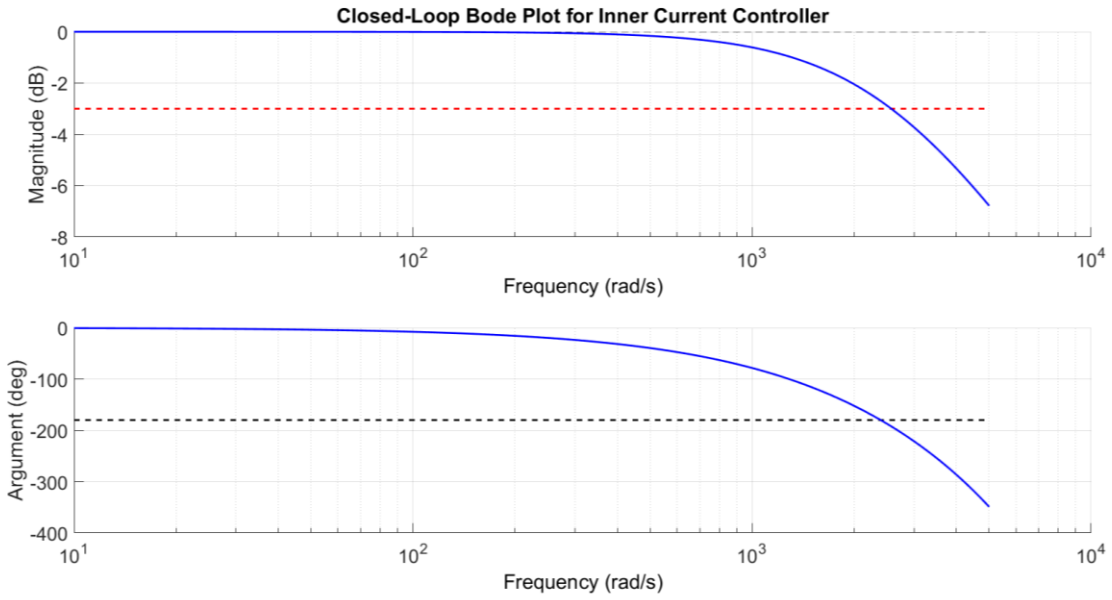

Figure B-5: Closed-loop Bode plot for the inner current controller

From Figure B-5 it can be noted that the choice of suitable controller gains was successful, and that the system is stable. The response of the system to a requested step change is illustrated in Figure B-6.

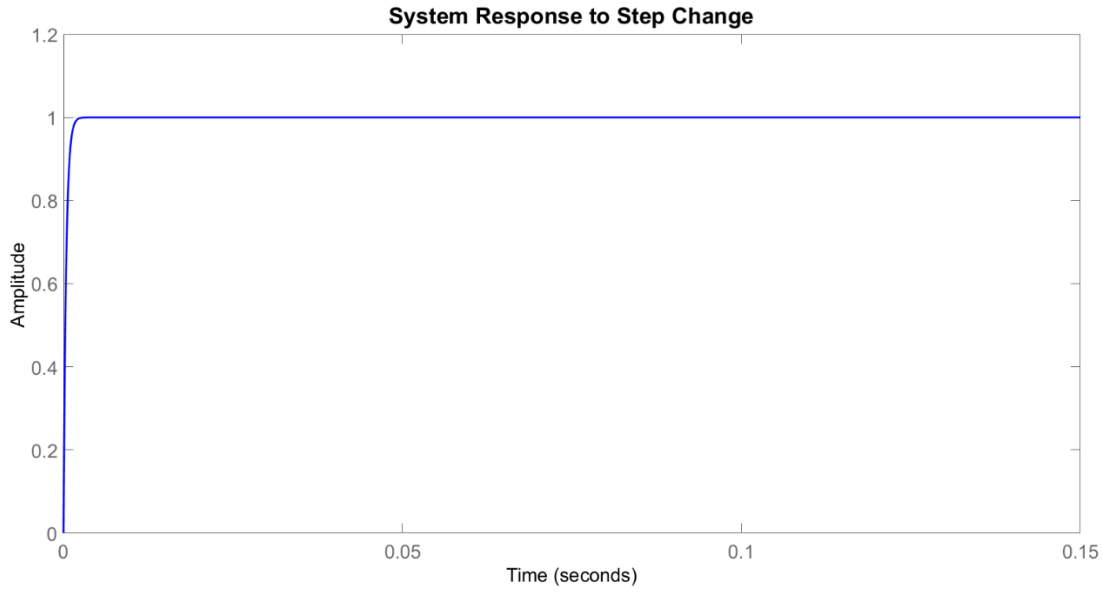

Figure B-6: System response to a step change

From Figures B-5 and B-6 it is shown that the controller gains calculated for inner current controller by using the internal control method are suitable, and the system is stable with no undesirable resonances and instabilities for the given values of phase inductance L (i.e. 0.2pu) and phase resistance R (i.e. 0.01pu).

B4.2 Outer Loop Controller Development

The outer loop controller is used to provide the current setpoints (i.e. ${i_{dq}}^{ref}$) to the inner current controller loop. The outer controller can include the controller types listed below:

- The DC voltage (i.e. V_{DC}) controller,
- The AC active power (i.e. P) controller,

- The AC reactive power (i.e. Q) controller and
- The AC voltage (i.e. V) controller.

The DC voltage controller and the AC active power controller can be used to provide the reference value for the active current (i.e. i_d^{ref}), and the AC reactive power controller and the AC voltage controller can be used to provide the reference value for the reactive current (i.e. i_q^{ref}). Figure B-7 illustrates a simplified block diagram of the outer loop controller.

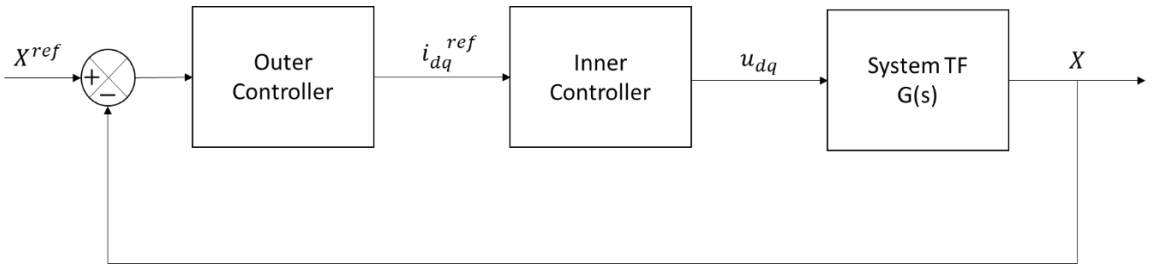

Figure B-7: Generic simplified block diagram of the outer loop controller

where X^{ref} denotes the desired setpoint of the controlled variable of the outer controller, and X denotes the actual value of the controlled variable. To ensure stability for this set of cascaded controllers, the bandwidth of the outer controller is chosen to be an order of magnitude less than that of the inner current controller, as can be seen in Equation B-33 [132] [114].

$$a_{cl}^{outer} = \frac{a_{cl}^{inner}}{10} \quad \text{[B-33]}$$

where a_{cl}^{outer} is the closed-loop bandwidth of the outer controller, and a_{cl}^{inner} is the closed-loop bandwidth of the inner current controller. The closed-loop bandwidth of the outer controller is calculated equal to 220rad/s. Since the inner loop controller reacts much faster

than the outer loop, it can be assumed that the reference current values are equal to the actual current values (i.e. $i_{dq} = {i_{dq}}^{ref}$).

For the converter on the onshore substation the reference value for the active current (i.e. ${i_d}^{ref}$) is calculated using a DC voltage (i.e. V_{DC}) controller, and the reference value for the reactive current (i.e. ${i_q}^{ref}$) is calculated using an AC voltage (i.e. V) controller. The DC voltage controller is used to ensure that the DC voltage remains constant while power is transferred thought the converters. From Equations B-13 and B-14 yields the following results:

$$P = v_d i_d = v_d {i_d}^{ref} \quad \text{[B-34]}$$

$$Q = -v_q i_q = -v_q {i_q}^{ref} \quad \text{[B-35]}$$

Manipulating Equations B-19 and B-34:

$$i_{DC} = \frac{v_d}{V_{DC}} {i_d}^{ref} = \frac{v_d}{V_{DC}} i_d \quad \text{[B-36]}$$

Coupling Equation B-18 with B-36:

$$C \frac{dV_{DC}}{dt} = \frac{v_d}{V_{DC}} i_d - i_L \quad \text{[B-37]}$$

Equation B-37 is non-linear with respect to the DC voltage (i.e. V_{DC}). To linearise Equation B-37, the Taylor series expansion of non-linear functions around a steady-state reference point has been used. For a reference point (x_0, y_0, z_0) the linear approximation will be:

$$\frac{dx}{dt} = f(x_0, y_0, z_0) \Rightarrow \frac{d\Delta x}{dt} = \frac{\partial f}{\partial x}|_{\substack{y=y_0 \\ z=z_0}} \Delta x + \frac{\partial f}{\partial y}|_{\substack{x=x_0 \\ z=z_0}} \Delta y + \frac{\partial f}{\partial z}|_{\substack{x=x_0 \\ y=y_0}} \Delta z \quad \text{[B-38]}$$

Using Equation B-38 to linearise Equation B-37 and treating i_L as a disturbance, yields the following result [110]:

$$C \frac{d\Delta V_{DC}}{dt} = \frac{v_d}{V_{DC,0}} \Delta i_d \quad \text{[B-39]}$$

where $V_{DC,0}$ is the steady state DC-link capacitor voltage. Taking the Laplace transform for Equation B-39 yields the system transfer function (i.e. $G(s)$):

$$G(s) = \frac{v_d}{V_{DC,0}} \frac{1}{sC} \quad \text{[B-40]}$$

Equation B-40 has a pole at the origin, which introduces instability to the system. A feed-forward term is used to eliminate this effect. The DC voltage controller controls the capacitor current to maintain the power transfer on the DC link. Under balance conditions the capacitor current is zero (i.e. $i_C = 0$); hence:

$$i_{DC} = i_L \quad \text{[B-41]}$$

Thus, the feed-forward term is given as follows:

$$i_d = \frac{V_{DC}}{v_d} i_L \quad \text{[B-42]}$$

A PI controller is sufficient to control this system, hence, the transfer function for the controller (i.e. $C(s)$) is similar to Equation B-28. The detailed control block diagram of the DC voltage controller is illustrated in Figure B-8.

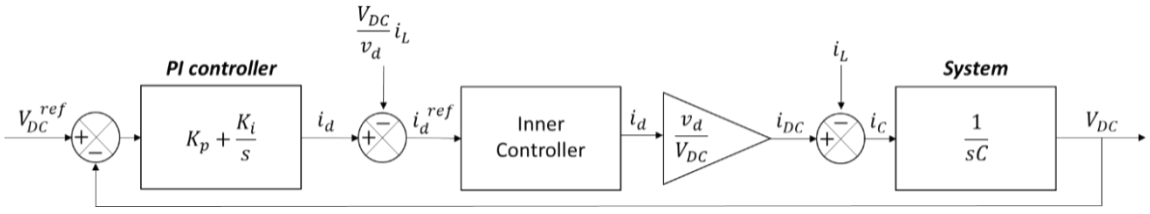

Figure B-8: Detailed control block diagram of the DC voltage controller

The DC capacitance can be calculated using Equation B-43 [132].

$$C = \frac{1}{2}\left(C_{upper} + C_{lower}\right) \quad \text{[B-43]}$$

The system DC capacitance is calculated equal to 26.04μF. The controller gains can be calculated using the internal control method, based on Equations B-44 and B-45 [132].

$$K_p = a_{cl}^{outer} C \quad \text{[B-44]}$$

$$K_i = \frac{1}{2}(a_{cl}^{outer})^2 C \quad \text{[B-45]}$$

From Equations B-44 and B-45, the proportional gain K_p of the DC voltage controller has been calculated equal to 0.0057 and the integral gain K_i has been calculated equal to 0.6302.

The AC voltage controller is used to provide the reference value for the reactive current to the onshore converter. For the AC voltage controller, the assumption is that if for the phase reactor the inductor's impedance is much larger than the resistance (i.e. $\omega_e L \gg R$) then the voltage drop depends solely on the reactive power flow over the reactor [111] [132]. For the developed system this is true (i.e. $29.1\Omega >> 1.45\Omega$). The controller can then regulate the AC voltage by controlling the q component of the current. The AC voltage drop controller transfer function is given by Equation B-46 [132].

$$\Delta V = \left(K_p + \frac{K_i}{s}\right)(V^{ref} - V) \quad \text{[B-46]}$$

where V^{ref} is the reference AC voltage at the RC filter and V is the actual voltage at the RC filter. The detailed control block diagram of the AC voltage controller is illustrated in Figure B-9.

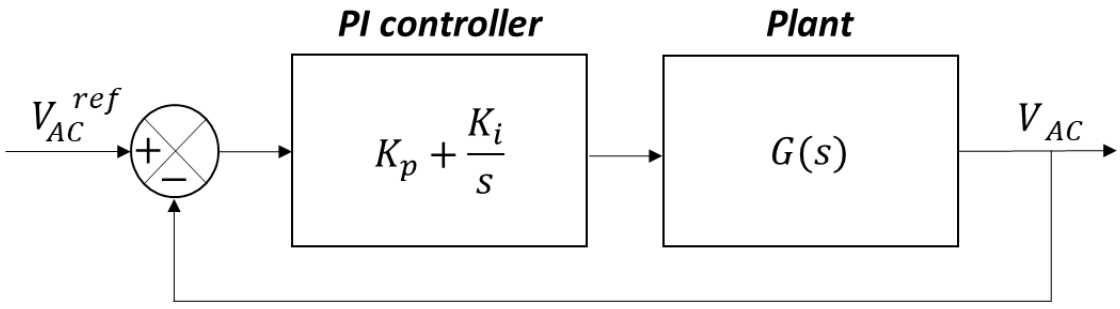

Figure B-9: Detailed control block diagram of the AC voltage controller

The controller gains for the AC voltage controller can be calculated using the internal control method, based on Equations B-47 and B-48 [132].

$$K_p = \frac{3}{2} {a_{cl}}^{outer} C \quad \text{[B-47]}$$

$$K_i = \frac{1}{30} ({a_{cl}}^{outer})^2 C \quad \text{[B-48]}$$

From Equations B-47 and B-48, the proportional gain K_p of the AC voltage controller has been calculated equal to 0.0086 and the integral gain K_i has been calculated equal to 0.042.

For the converter on the offshore substation, the reference value for the active current (i.e. ${i_d}^{ref}$) is calculated using an AC active power (i.e. P) controller, and the reference value for the reactive current (i.e. ${i_q}^{ref}$) is calculated using an AC voltage (i.e. V) controller. The AC active power of the system can be controlled using Equation B-13. The detailed control block diagram of the AC active power controller is illustrated in Figure B-10.

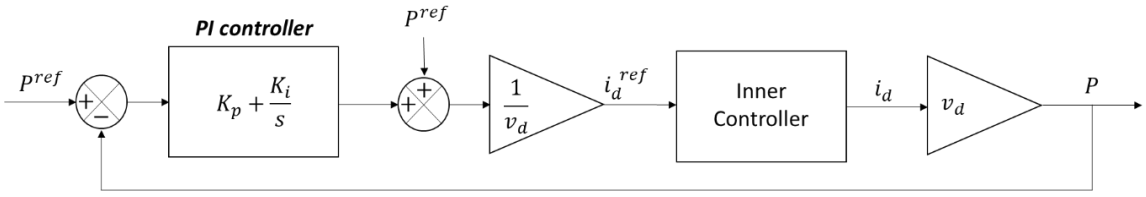

Figure B-10: Detailed control block diagram of the AC active power controller

Similar to the DC voltage controller, the proportional gain K_p of the AC active power controller has been calculated equal to 0.0057 and the integral gain K_i has been calculated to be equal to 0.6302. The controller gains for the offshore VSC AC voltage controller are equal to the gains of the onshore VSC AC voltage controller (i.e. K_p = 0.0086 and K_i = 0.042).